Author:
Boyajian, Silvia D G

Title:
Assessing modulation of the actin cytoskeleton in differing macrophage phenotypes

relevance to macrophage invasion, protease profile, and foam cell formation, during the progression of cardiovascular pathologies.

ASSESSING MODULATION OF THE ACTIN CYTOSKELETON IN DIFFERING MACROPHAGE PHENOTYPES: RELEVANCE TO MACROPHAGE INVASION, PROTEASE PROFILE, AND FOAM CELL FORMATION, DURING THE PROGRESSION OF CARDIOVASCULAR PATHOLOGIES

Silvia Dikran George Boyajian

Supervisors: Dr. Jason L. Johnson and Prof. Sarah George

A dissertation submitted to the University of Bristol in accordance with the requirements for award of the degree of Doctor of Philosophy in the Faculty of Health sciences

Bristol Medical School, March 2021

Word count: 47802

Abstract

Macrophages within atherosclerotic plaques are heterogeneous, with macrophage-colony stimulating factor (M-CSF) and granulocyte-macrophage colony-stimulating factor (GM-CSF) demonstrated to generate two different macrophage subsets (termed M-Mac and GM-Mac respectively). M-Macs display an elongated shape and are considered anti-inflammatory, due to their proposed roles in immune response suppression and induction of tissue repair. However, GM-Macs exhibit a rounded morphology and are regarded as pro-inflammatory. The actin cytoskeleton modulates cell shape and regulates cellular functions, which in macrophages includes the engulfment of apoptotic cells (efferocytosis), and phagocytosis of modified lipoproteins and subsequent foam cell formation, a hallmark of advanced atherosclerosis.

The key findings within this thesis demonstrate that the actin-perturbing drugs fasudil and pravastatin reduced the F-actin content of human M-Macs and GM-Macs, which was associated with shifting macrophages towards an anti-inflammatory phenotype (increased TGFBI and decreased MMP-12), suggesting actin cytoskeleton remodelling regulates macrophage polarisation. In addition, fasudil or pravastatin decreased oxLDL-induced foam cell formation in human GM-Macs, which was associated with decreased protein expression of the scavenger receptors OLR1 and CD36, alongside increased levels of the cholesterol efflux molecules NCOR1, NCOR2, and PPARα suggesting actin cytoskeleton remodelling regulates foam cell formation. Relatedly, human GM-Macs displayed impaired efferocytosis capacity compared to human M-Macs, which could be restored to M-Mac levels through the addition of fasudil or pravastatin. However, discrepancies were observed between mRNA and protein levels of some key molecules, suggesting the involvement of a post-transcriptional regulatory mechanism, such as SUMOylation. Analysis of advanced human atherosclerotic plaques revealed increased pSTAT5 expression and decreased SUMO protein levels within foam cell macrophage-rich regions, suggesting reduced STAT5 SUMOylation in advanced plaques. Confirmatory in vitro studies showed that blocking STAT5 SUMOylation augmented foam cell formation and efferocytosis capacity in human GM-Mac foam cells while reducing their F-actin content. Preliminary mechanistic studies suggest that sustained STAT5 activation (afforded by blocking its SUMOylation) within human GM-Macs upregulated OLR1 expression and its accumulation at the cell membrane, permitting enhanced efferocytosis effects dependent on actin cytoskeleton remodelling.

Taken together, our results imply an essential role for the actin cytoskeleton in regulating the inflammatory phenotype of macrophages, including the novel regulation by STAT5 SUMOylation, suggesting that targeting actin cytoskeleton remodelling in GM-Macs, may have therapeutic potential for reducing plaque progression and improving stability.

Acknowledgments

First and foremost, I would like to thank my supervisor Dr. Jason Johnson, for his genuine guidance, and support at every step on my PhD. I am honoured to be part of his team and work under his supervision which I benefitted hugely from his immense knowledge. I also want to thank Professor Sarah George for her continuous advice which helped me throughout the research.

I would like to thank Professor Saadeh Suleiman, for his cherished encouragement, support, and kindness, and helping me to get over difficulties.

I would like to thank my colleagues and everyone one on level seven for offering me a warm and welcoming environment, as well as for training me new techniques and helping me with my experiments during the past 4 years. I am really grateful.

Special thanks to my friends, Lujain Alsadder, for her kindness and support to get over difficulties, as well as all the laughs we had together, and sharing unforgettable memories. Lien Mari Reolizo for all the laughs, jokes, and experiences we shared. Aleksandra Frankow, for her kindness and nice gestures, really appreciated.

Special thanks to my beloved husband Tarek Rabadi, for his great support, understanding, and believing in me and encouraging me to reach my goals. To my beautiful children Sama and Murad, for tolerating all the times I have been away and busy with my work and study for long hours. You will always be the source of my inspiration.

Special thanks to my loving parents Dikran and Natalia Boyajian, for teaching me to be strong, and to fight for my goals, and never give up. Believing in me and giving me all the support, love, and care all the time. Thanks to my sisters Maria and Lena Boyajian for making me cheerful, and optimistic all the time. Thanks to my mother in law Siham Tadros, for her continuous support.

Finally, I would like to thank Al-Balqaa' Applied university in Jordan for offering me this opportunity and awarding me this scholarship.

Thank you all.

I dedicate this thesis to my children Sama and Murad

Author's declaration

I declare that the work in this dissertation was carried out in accordance with the requirements of the University's *Regulations and Code of Practice for Research Degree Programmes* and that it has not been submitted for any other academic award. Except where indicated by specific reference in the text, the work is the candidate's own work. Work done in collaboration with, or with the assistance of, others, is indicated as such. Any views expressed in the dissertation are those of the author.

SIGNED: ..... DATE:...14/03/2021.....

Contents

List of Abbreviations

3'UTR	Three prime un-translated regions
A	
AB	Antibody
ABCA1	ATP-binding cassette subfamily A member 1
ABCG1	ATP-binding cassette subfamily G member 1
ABP	Actin binding protein
ACAT	Acyl coenzyme A: cholesterol acyl transferase
ACTA 2	Actin alpha 2
ADP	Adenosine diphosphate
ALS	Amyotrophic lateral sclerosis
ANOVA	Analysis of variance
ApoB	Apolipoprotein B
Apoe	Apolipoprotein E
ARG1	arginase 1
ATP	Adenosine triphosphate
B	
BCA	Bicinchoninic acid
BSA	Bovine serum albumin
C	
CCL2	C-C motif ligand 2
CCR5	C-C chemokine receptor type 5
CD36	Cluster of differentiation 36
Cdc42	Cell division control protein 42
cDNA	Complementary DNA
CHD	Coronary heart disease
CHIP	Chromatin immunoprecipitation
CR	Complement receptor
CRP	C-reactive protein
CSF	Colony stimulating factor
CSF1R	Colony stimulating factor-1 receptor
CSF2RA	colony stimulating factor 2 receptor subunit alpha
CT	Cycles of threshold
CVD	Cardiovascular disease
CX3CL1	C-X3-C motif ligand 1
CX3CR1	C-X3-C motif chemokine receptor 1
D	
DAB	3,3’-Diaminobenzidine

DAPI	4’,6-diamidino-2-phenylindole
DES	Drug-eluting stents
DMSO	Dimethyl sulfoxide
DNA	Deoxyribonucleic acid
DPBS	Dulbecco’s phosphate-buffered saline

E

ECFC	Endothelial colony-forming cell
ECM	Extra cellular matrix
EDTA	Ethylenediaminetetraacetic acid
EEL	External elastic lamina
eNOS	Endothelial nitric oxide synthase
ERK5	Extracellular signal regulated kinase 5

F

F-actin	Filamentous actin
FBS	Foetal bovine serum
FcR	Fc Fragment Of IgG receptor
FDA	Food and drug administration
FGF2	Fibroblast growth factor 2
FIM	Factor increasing monocytopoiesis
Folr2	Folate receptor beta
FPP	Farnesyl pyrophosphate
FSCN1	Fascin-1

G

G-actin	Monomeric globular actin
GBD	Global Burden of Disease
GDP	Guanosine diphosphate
GEF	Guanine nucleotide exchange factor
GGPP	Geranyl-geranyl pyrophosphate
GM-CSF	Granulocyte-macrophage colony-stimulating factor
GPCR	G-protein-coupled receptor
GTP	Guanosine triphosphate

H

HB	Haemoglobin
HBSS	Hank's balanced salt solution
HCL	Hydrochloric acid
HDL	High-density lipoprotein
HIF-1α	Hypoxia inducible factor alpha
HMG-CoA	3-hydroxy-3-methylglutaryl-coenzyme A
HODHBt	3-hydroxy-1, 2, 3-benzotriazin-4(3H)-one
HPLC	High performance liquid chromatography

HRP	Horseradish Peroxidase
HRP	Horseradish peroxidase
I	
ICAM-1	Intercellular adhesion molecule 1
ICC	Immunocytochemistry
IEL	Internal elastic lamina
IgG	Immunoglobulin-G
IHC	Immunohistochemistry
IL	Interleukin
INFγ	Interferon γ
iNOS	Inducible nitric oxide synthase
ITAM	Immunoreceptor tyrosine-based activation motif
J	
JAK	Janus kinase
K	
kDa	Kilodaltons
KO	Knockout
L	
LAP	LC3-associated phagocytosis
LC3	microtubule-associated protein 1A/1B-light chain 3
LC3	microtubule-associated protein 1A/1B-light chain 3
LDL	Low density lipoprotein
LDL-C	LDL-cholesterol
LIMK1	LIM kinase 1
LO	Lipoxygenase
LOX-1	Lectin-like ox-LDL receptor-1
LPS	Lipopolysaccharide
LXRα	Liver X receptor alpha
Ly6C	lymphocyte antigen 6C
Lyve1	Lymphatic vessel endothelial hyaluronan receptor 1
M	
MAPK1	Mitogen-activated protein kinase 1
MCP-1	Monocyte chemoattractant protein 1
M-CSF	Macrophage colony-stimulating factor
MHC	Major histocompatibility complex
MI	Myocardial infarction
miR	microRNA
MLC	Myosin light chain

MMP	Matrix metalloproteinase
MPO	Myeloperoxidase
MPS	Mononuclear phagocyte system
MR	Mannose receptor
MRC1	Mannose receptor C type 1
mRNA	Messenger ribonucleic acid
MSRI	Macrophage scavenger receptor 1

N

NAB	Neutralizing antibody
NADPH	Nicotinamide adenine dinucleotide phosphate hydrogen
NCOR	Nuclear receptor corepressor
NFκB	Nuclear factor kappa-light-chain-enhancer of activated B cells
NFκBIA	Nuclear factor-kappa-B-inhibitor alpha
NKT	Natural killer
NO	Nitric oxide
NOX	NADPH oxidase
NPF	Nucleation promoting factor

O

OCT1	Octamer binding transcription factor 1
OLR1	Oxidized low-density lipoprotein receptor 1
oxLDL	Oxidized low-density lipoprotein

P

PAGE	Polyacrylamide gel electrophoresis
PBMCs	Peripheral blood mononuclear cells
PBS	Phosphate-buffered saline
Pc2	Polycomb protein 2
PDGF	Platelet-derived growth factor
PH	Power of hydrogen
PI-3K	Phosphatidylinositol-3 kinase
PIAS	Protein inhibitor of activated STAT
PIT	Pathological intimal thickening
PKB	Protein kinase B
PKC	Protein kinase C
PLA	Polyactic acid
PMA	Phorbol 12-myristate 13-actetae
POU2F1	POU domain transcription factor OCT-1
PPARA	Peroxisome proliferator-activated receptor Alpha (gene)
PPARα	Peroxisome proliferator-activated receptor Alpha (protein)
PRINCE	Pravastatin inflammation/CRP evaluation
PS	Phosphatidylserine

pSMAD	phosphorylated SMAD
pSTAT	Phosphorylated signal transducer and activator of transcription

Q

qPCR	Quantitative polymerase chain reaction

R

RanBP2	Ran-binding protein 2
RDX	Radixin
RhoA	Ras homolog family member A
RhoGDI	Rho GDP-dissociation inhibitors
RNA	Ribonucleic acid
ROCK	Rho-associated kinase
ROS	Reactive oxygen species
RPM	Revolution per minute
RPMI-1640	Roswell Park Memorial Institute-1640
RT	Room temperature
RT-qPCR	Reverse transcription quantitative polymerase chain reaction

S

SAE	SUMO-Activating Enzyme
SDS	Sodium dodecyl sulphate
SELE	Selectin-E
SEM	Standard error of the mean
SENP	Sentrin-specific protease
SEPP1	Selenoprotein-1
SHIP	SH2 domain-containing inositol phosphates
SM22-α	Smooth muscle protein 22-alpha
SM-MHC	Smooth muscle cell myosin heavy chain
Sn2	Substitution Nucleophilic Bimolecular
SPARC	Secreted protein acidic and cysteine rich
SR-A	Scavenger receptor A
STAT	Signal transducer and activator of transcription
SUMO	Small ubiquitin-like modifier
SYBR	Synergy Brands, Inc.

T

TBS-T	Tris buffered solution containing tween
TF	Tissue factor
TFPI-2	Tissue-factor pathway inhibitor-2
TGFBI	Transforming growth factor-beta induced (gene)
TGFβI	Transforming growth factor-beta induced (protein)
TGFBR	Transforming growth factor-beta receptor
TGFβ	Transforming growth factor β

TGS	Tris/Glycine/SDS
TH	T helper
TIMP	Tissue inhibitor of metalloproteinase
TLR	Toll-like receptor
TNFα	Tumour necrosis factor α
U	
Ubc9	Ubiquitin carrier protein 9
UV	Ultraviolet
V	
VCAM-1	Vascular cell adhesion protein 1
VCL	Vinculin
vD3	1α,25-Dihydroxyvitamin D3
VEGF	Vascular endothelial growth factor
VLDL	Very low-density lipoprotein
VSMCs	Vascular smooth muscle cells
W	
WAVE	WASP/WASP-family verprolin-homologous protein
WB	Western Blotting
WBC	White blood cell
α - SMA	Alpha-smooth muscle actin

List of Figures

List of Tables

1 GENERAL INTRODUCTION

1.1 Epidemiology and aetiology of atherosclerosis

Atherosclerosis is the major cause for the development of multiple cardiovascular diseases (CVD), such as coronary heart disease (CHD) and stroke. Although studies from the Global Burden of Disease (GBD) show a significant reduction in CVD mortality rates comparing the period from 1990 to 2013, it is still considered as a primary cause of fatality in the UK and worldwide with approximately 17 million deaths throughout the world, and 233,000 deaths in the UK yearly (Bhatnagar, Wickramasinghe et al. 2016). The rate of development of atherosclerosis depends on different factors increasing its risk in certain patient groups more than others. The typical risk factors can be divided into two groups. The first group are non-modifiable risk factors including increasing age, male gender, genetic abnormalities for example, genetic defects that affects the plasma lipoprotein levels in the body (such as, familiar hypercholesterolemia), and family history of previous coronary artery disease (Kim and Han 2013). The second group are modifiable risk factors including cigarette smoking (Doll, Peto et al. 2005), hypertension, diabetes mellitus, hyperlipidaemia, and obesity (Guilbert 2003, Insull 2009)

Atherosclerosis is now considered a chronic inflammatory disease, precipitated by endothelial cell dysfunction, which is focal and gradually develops over decades. It occurs at susceptible areas of large arteries (Insull 2009) and medium-sized arteries (Ross 1999), especially at curvatures or bifurcations. Atherosclerosis is characterised by the accumulation of extracellular lipid within the arterial wall accompanied by inflammatory cells (Libby, Ridker et al. 2002). The initial steps in the development of atherosclerosis can regress spontaneously while the later stages will progress continuously (Insull 2009). The structure of a normal blood vessel consists of three layers, the intima, media, and the adventitia (as illustrated in Figure 1.1). The first layer that abuts the lumen of the vessel is called the tunica intima. The tunica intima (or intimal layer) is the thinnest layer consisting of one layer of endothelial cells located upon a basement membrane. Following the intimal layer is a dense elastic sheet called the internal elastic lamina (IEL) that separates the tunica intima from tunica media. The tunica media (or medial layer) is the thickest layer of all. The tunica media has an essential role in providing elasticity and to support the function of the vessel due to its composition of elastic fibres, vascular smooth muscle cells (VSMCs), and connective tissue. Beneath the medial layer is the external elastic lamina (EEL). Finally, the outermost layer is the tunica adventitia (or adventitial layer), which predominantly consists of connective tissue, fibroblasts, small vessels, and nerves.

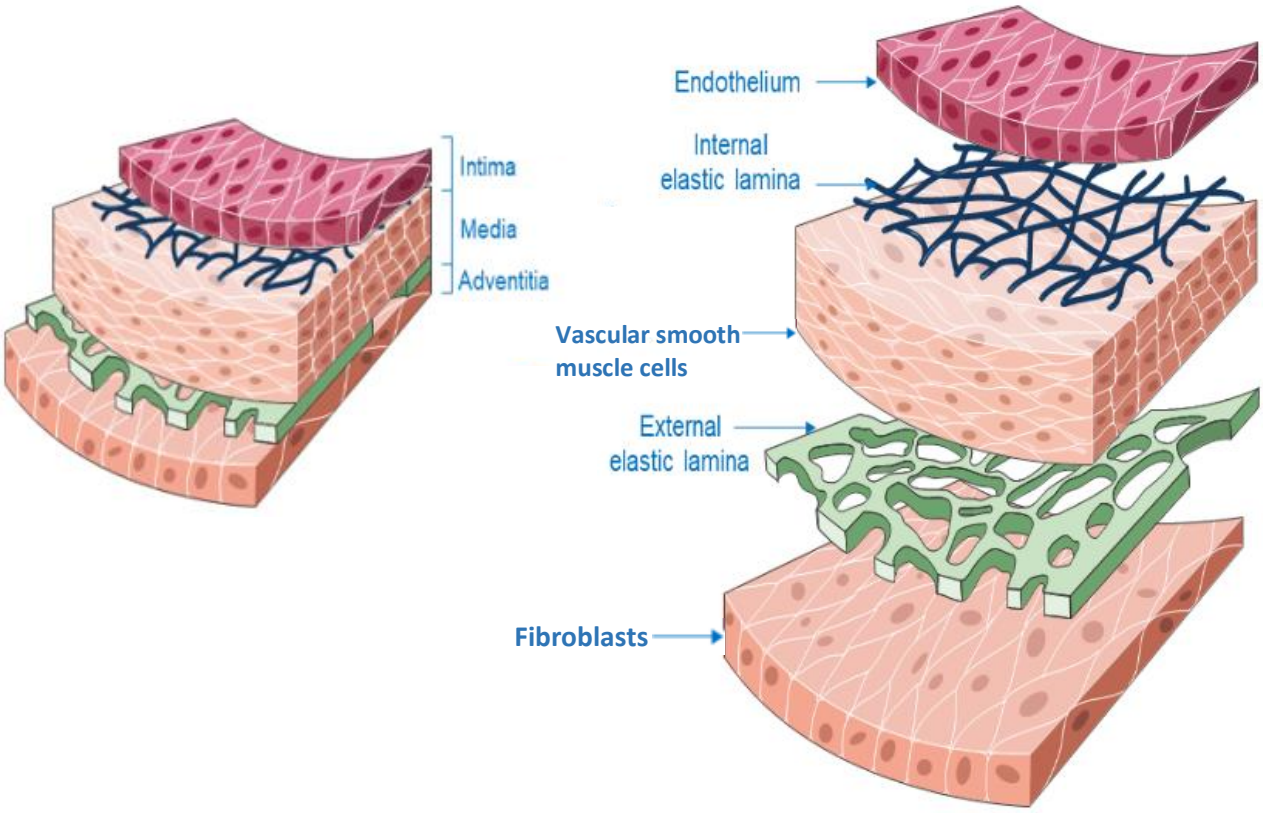

Figure 1.1 Organisation of normal blood vessel

Histology of a normal blood vessel composed of three layers. The innermost layer abutting the lumen is the tunica intima that consists of a monolayer of endothelial cells. Beneath it is the internal elastic lamina separating the intima from the media. The tunica media, which is the thickest layer consisting of vascular smooth muscle cells. And finally, Tunica adventitia that is separated from the media by the external elastic lamina and is composed of fibroblasts, vessels, and nerves. Figure made using elements from https://smart.servier.com/

1.2 Pathogenesis of atherosclerosis

Atherosclerosis is a disease that primarily affects the coronary and carotid arteries to precipitate myocardial infarction and stroke, respectively. During its inception, pre-atherosclerotic arteries are characterised by the presence of intimal thickenings accompanied by the accumulation of extracellular lipids. The lipoproteins which initially accumulate within the arterial wall (such as low-density lipoprotein (LDL)) become modified and finally oxidized. Oxidized LDL (oxLDL) can provoke an inflammatory reaction that triggers the recruitment of inflammatory cells and the development of atherosclerosis (Insull 2009).

In 1990, Russel Ross proposed that the pathogenesis of atherosclerosis is initiated due to increased cholesterol concentrations within the plasma, predominantly LDL (Ross 1999). With the prolonged exposure to other risk factors that were mentioned earlier, such as smoking, hypertension, and diabetes mellitus, endothelial cells become dysfunctional at atherosclerosis-prone areas, a hypothesis referred to as response to injury (Ross 1999). These athero-prone sites are located mainly at branch points or curvatures within the arterial tree, where blood flow is disturbed and oscillatory in nature and accompanied by low shear stress (VanderLaan Paul, Reardon Catherine et al. 2004). Endothelial cells are able to sense changes in blood flow, and are relatedly termed as mechanosensitive and therefore play a major role in blood flow regulation through the release of different mediators such as endothelin (Chiu and Chien 2011). Endothelial cells also produce nitric oxide (NO) in an endothelial nitric oxide synthase (eNOS)-dependent manner and is a powerful oxidant that has athero-protective properties. NO exerts essential homeostatic actions that include vasodilation, decreasing the adhesion of leukocytes (Singh, Mengi et al. 2002), inhibiting the uptake of lipids, suppressing the proliferation of VSMCs (Ross 1999), and reducing platelet aggregation (Cooke and Tsao 1994). Disturbed low shear stress leads to the activation of different signalling pathways and causes widening of the junctions between the cells that resulting in increased permeability of endothelial cells (Li, Haga et al. 2005). Therefore, dysfunctional endothelial cells decrease their production of eNOS and increase their permeability (Smith, Trogan et al. 1995). Firstly, reduced eNOS levels permit medial VSMC migration and proliferation within the intimal area, fostering the development of an adaptive intimal thickening, the precursor to atherosclerotic plaque formation in humans. Therefore, these newly recruited VSMCs secrete and lay down specific extracellular matrix (ECM) proteins which have an increased affinity for the binding and retention of LDL (Stary , Nakashima, Fujii et al. 2007). Secondly, this causes increased insudation and accumulation of LDL within the adaptive intimal thickening of the arterial wall (Smith, Trogan et al. 1995).

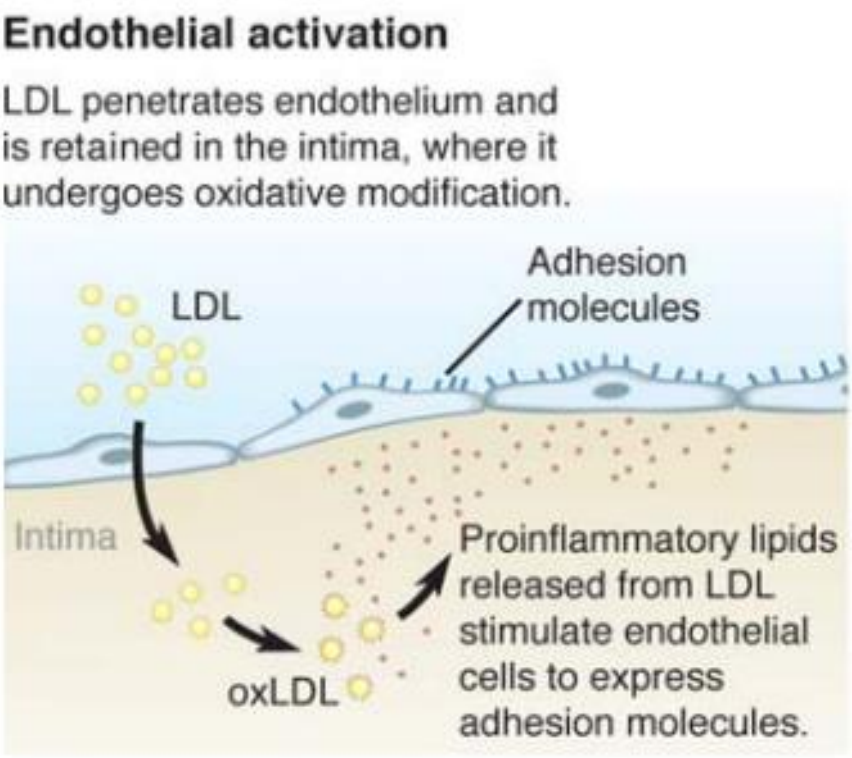

Figure 1.2 Endothelial dysfunction in the arterial wall

Endothelial dysfunction due to different risk factors including hyperlipidaemia, cigarette smoking, and hypertension, alongside alterations in shear stress, permits the accumulation and modification of LDL via oxidation. OxLDL activates endothelial cells and increases the expression of adhesion molecules such as vascular adhesion molecule-1 (VCAM-1). Figure is taken from (Hansson, Robertson et al. 2006)

Atherosclerosis develops gradually over decades. Each stage of atherosclerotic development is characterised by specific pathological changes which permits the differentiation of each stage in pathogenesis from the other (Insull 2009).

1.2.1 Fatty streaks/pathological intimal thickening

As mentioned above, adaptive intimal thickenings at athero-prone sites serve as a soil-bed for the accumulation of lipids and ensuing inflammatory cell recruitment. This transition into an early pre-atherosclerotic lesion is historically termed as a fatty streak, and more recently pathological intimal thickening (PIT) (Kolodgie Frank, Burke Allen et al. 2007). PIT is defined as an early stage of atherosclerosis, PIT identifies a lesion formed by extracellular accumulation of lipids with VSMCs are abundantly present in the thickened tunica intima and macrophages are infiltrated and become foam cells (Nakagawa and Nakashima 2018). Fatty streaks/PITs are the initial step in the development of atherosclerosis (Glass and Witztum 2001). The development of fatty streaks begins in early years of life (Insull 2009) and can be visible microscopically (Stary, Chandler et al. 1994, Insull 2009) due to streaks or patches that appear yellow in colour (Stary, Chandler et al. 1994). Even though fatty streaks can be visible grossly, not all initial lesions of atherosclerosis show changes in their appearance. On the other hand, all early lesions display similar histological changes within the intimal region of the arterial wall (Stary, Chandler et al. 1994). Microscopically, fatty streaks consist of droplets of lipid accumulated within a VSMC and ECM-rich intimal thickening, alongside accumulation of T cells, mast cells, and most dominantly macrophages, most of which exist as foam cell macrophages (lipid-laden macrophages) and are responsible for the yellow appearance on the vessel luminal surface (Hansson, Robertson et al. 2006) (as illustrated in Figure 1.3). Although within fatty streaks most of the accumulated lipids are engulfed by macrophages, recent evidence has proposed that VSMCs can also accrue modified lipoproteins and therefore contribute to foam cell numbers (Allahverdian, Chehroudi Ali et al. 2014, Maguire, Pearce et al. 2019). Demonstrating the efficient clearance of modified lipoproteins within these early lesions, only small amounts of lipids accumulate within the extracellular area which mainly consists of cholesterol esters (Stary, Chandler et al. 1994).

Fatty streak development has multiple steps. It starts with increased levels of LDL-cholesterol (LDL-C) within the blood alongside the presence of different risk factors such as hypertension and smoking, facilitating the accumulation and subsequent trapping of LDL-C within the adaptive intimal thickenings located at athero-prone areas. At the lesion site, the homeostatic balance between different matrix components will be altered, increasing the content of proteoglycans such as heparan sulphate. As proteoglycans have a high affinity for lipoproteins, they will bind and become trapped within the

proteoglycan-rich adaptive intimal thickenings (Tavafi 2013). As a result of its accumulation alongside the prevalence of reactive oxygen species (ROS), LDL can be modified by oxidation (Glass and Witztum 2001). OxLDL induces an inflammatory reaction through the activation of endothelial cells which subsequently upregulate and express cell adhesion molecules such as vascular cell adhesion protein-1 (VCAM-1), intercellular adhesion molecule-1 (ICAM-1), P-selectin, and E-selectin (Cybulsky and Gimbrone 1991). P-selectin and E-selectin have a pivotal role in the development of atherosclerosis since the deletion of both genes in Apolipoprotein E (Apoe)-deficient mice inhibited monocyte entry into athero-susceptible regions and decreased the formation of atherosclerosis by 60% (Dong, Chapman et al. 1998). Moreover, studies showed that Apoe-deficient mice lacking the ICAM-1 gene had significantly reduced formation of atherosclerosis (Collins, Velji et al. 2000). Subsequently, cell adhesion molecules have an important role in the recruitment of inflammatory cells to athero-prone areas during atherogenesis. Additionally, oxLDL can provoke the recruitment of monocytes to early atherosclerotic lesions by increasing the expression of monocyte chemoattractant protein-1 (MCP-1) (Navab, Berliner et al. 1996). Studies showed that deletion of MCP-1 gene or its receptor C-C Chemokine receptor 2 (CCR2) leads to a decrease in the development of atherosclerosis (Boring, Gosling et al. 1998). Monocytes within intimal thickenings are exposed to growth factors such as macrophage-colony stimulating factor (M-CSF) which will induce their differentiation into macrophages (Hansson, Robertson et al. 2006). Differentiation of monocytes into macrophages has an essential role in atherogenesis (Smith, Trogan et al. 1995). Macrophages upregulate the expression of different cell-surface receptors such as scavenger receptors (Hansson, Robertson et al. 2006). Scavenger receptors are important for the engulfment of oxLDL by phagocytosis and the formation of foam cell macrophages (Yamada, Doi et al. 1998).

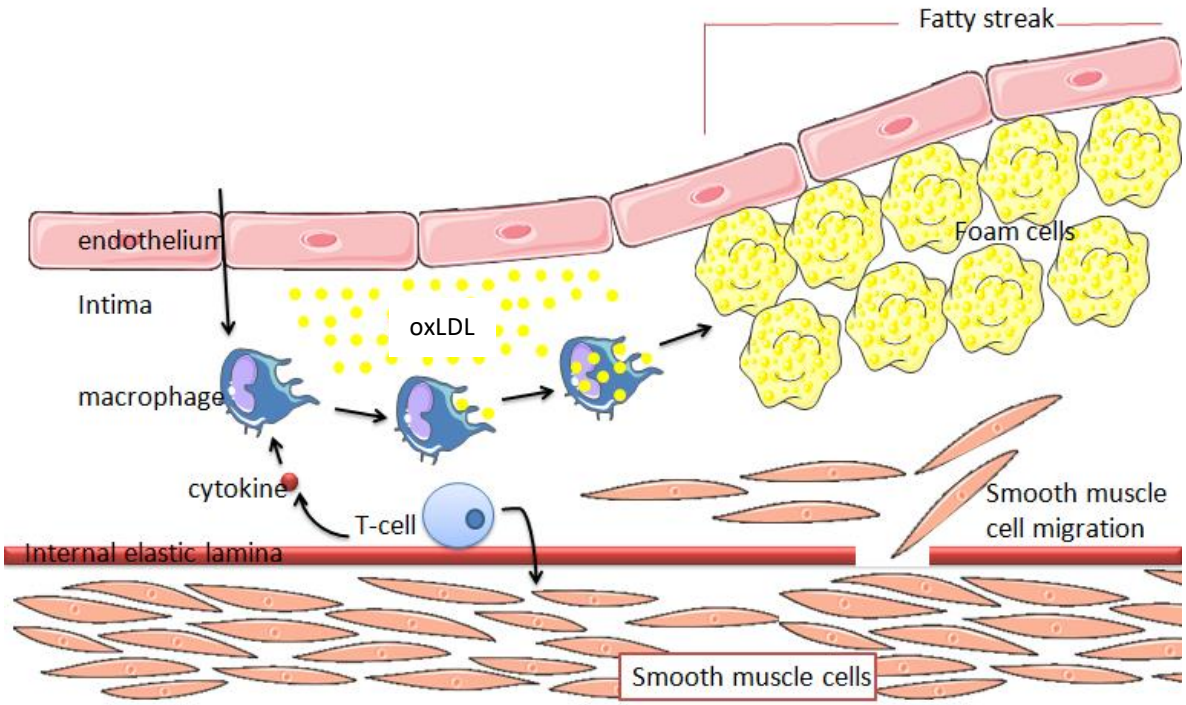

Figure 1.3 Development of fatty streaks/PITs

Fatty streaks/PITs within the arterial wall consists mainly of foam cell macrophages that give the yellow appearance of the affected area, as well as small amounts of extracellular lipid and T cells, within a VSMC and ECM-rich thickening. Figure made using elements from https://smart.servier.com/

1.2.2 Formation of atherosclerotic plaque

Mature atherosclerotic plaques display distinct pathological characteristics. This includes the formation of a necrotic/lipid-rich core with a thick VSMC and ECM-rich fibrous cap, as a result of the core forming within a pre-existing intimal thickening (Stary, Chandler et al. 1994, Virmani, Kolodgie et al. 2000, Insull 2009, Bentzon, Otsuka et al. 2014). If the necrotic/lipid-rich core is extensive, it can force the fibrous cap to protrude into the vessel lumen affecting the normal blood flow within the vessel and down-stream organs, such as the heart and brain (Insull 2009) (as illustrated in figure 1.4).

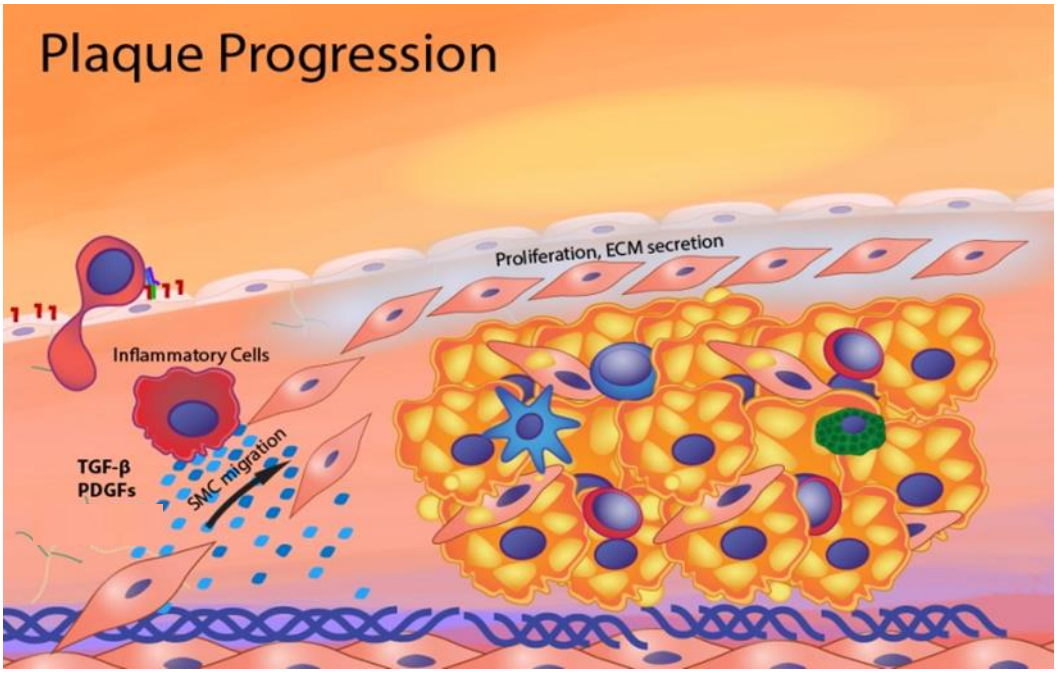

Figure 1.4 Pathological changes associated with established atherosclerotic plaque formation. *Established atherosclerotic plaques are characterised by the presence of a necrotic/lipid-rich core formed from cell debris, extracellular lipid, and cholesterol crystals, overlain by a VSMC and ECM-rich fibrous cap. Inflammatory cells, including foam cell macrophages and occasional T lymphocytes are located around the core, particularly between the core periphery and the fibrous cap. In the absence of expansive remodelling, established atherosclerotic plaques can markedly protrude into the vessel lumen and compromise blood flow. SMC, smooth muscle cell; ECM, extracellular matrix; TGFβ, transforming growth factor β; PDGF, platelet-derived growth factor Figure is taken from (Linton, Yancey et al. 2000)*

 Foam cell formation

 Macrophage

 T-regulatory cell

 Monocytes

 Mast cell

 T helper cell type 1

 Vascular smooth muscle cell

 Dendritic cell

 oxLDL

Under physiological conditions and in the presence of high-density lipoprotein (HDL), macrophages efflux lipoproteins to extracellular HDL through reverse cholesterol transport, preventing foam cell formation (Nissen, Tsunoda et al. 2003). During atherosclerosis, foam cell macrophages continue to accrue modified lipoproteins which ultimately results in their death (Falk 2006). Mechanistically, foam cell macrophages do not downregulate scavenger receptor expression and therefore, continually accumulate lipoproteins (Falk 2006), resulting in lysosomal dysfunction due to decreased levels of lysosomal acid lipase (Jerome 2006). Lysosomal acid lipase is an enzyme essential for the destruction of cholesterol within lysosomes (Griffin, Ullery et al. 2005). Accordingly, cholesterol esters amass within lysosomes and induce apoptosis of foam cell macrophages (Linton, Yancey et al. 2000). In addition, adjacent foam cell macrophages become defective in their efferocytosis capacity (engulfment and clearance of apoptotic cells), causing apoptotic foam cell macrophages to undergo secondary necrosis further perpetuating inflammation alongside the release of modified cholesterol (Badimon and Vilahur 2014). Consequently, death of foam cell macrophages leads to the formation of a lipid-rich necrotic core, that is characterized by being soft (gruel-like), lacking collagen support, avascular, and containing minimal cell numbers (Falk 2006). Unlike macrophages, VSMCs have incompetent functional lysosomes (which are necessary for the hydrolysis of cholesterol) (Jerome, Minor et al. 1991) along with low expression of ATP-binding cassette transporter (ABCA1), leading to the accumulation of lipids within the cells, and eventually death of VSMCs (Allahverdian, Chehroudi et al. 2014). Death of VSMCs has a destructive effect on atherosclerotic plaques, since VSMCs are the main source for the production of collagens, which are important for the stability of the fibrous cap (van der Wal and Becker 1999). Moreover, death of foam cell macrophages increases the expression and activity of matrix metalloproteinases (MMPs) (Libby, Ridker et al. 2002). Altogether, this causes destruction and weakening of the fibrous cap, and the development of a vulnerable plaque (van der Wal and Becker 1999).

Advanced atherosclerotic plaques are classified into stable and unstable phenotypes according to their composition (van der Wal and Becker 1999). Stable plaques are featured by the presence of a thick fibrous cap composed of multi-layered VSMCs embedded within abundant fibrillar collagens. The thick fibrous cap forms a protective barrier between flowing blood and the highly-thrombogenic necrotic/lipid-rich core, and prevents bio-mechanical rupture of the plaque, and subsequent clinical consequences (Linton, Yancey et al. 2000). The fibrous cap is preserved by the regulation of athero-protective growth factors and cytokines such as, transforming growth factor β (TGFβ) and interleukin 10 (IL-10). Both TGFβ and IL-10 are released from anti-inflammatory cells including protective macrophage subsets and T-regulatory cells (Letterio and Roberts 1998). In support, studies showed that Apoe-deficient mice lacking TGFβ receptor II on T cells show a significant increase in the

development of advanced atherosclerotic plaques (Robertson, Rudling et al. 2003). Other studies showed that global deficiency of IL-10 in Apoe-deficient mice increases plaque development (Mallat, Besnard et al. 1999). IL-10 has also been proposed to enhance the stability of plaques by reducing the activation of MMPs and inhibiting thrombogenicity. It has been reported that IL-10 promotes the release of TGFβ and vice versa (Potteaux, Esposito et al. 2004). Alongside, T-regulatory cells inhibit the release of interferon γ (IFNγ) from pro-inflammatory macrophage subsets (Linton, Yancey et al. 2000).

Accordingly, in the presence of sufficient efferocytosis capacity, inhibition of IFNγ, and the secretion of athero-protective cytokines (IL-10, and TGFβ) plaques are maintained as a stable phenotype and less prone to rupture. It has also been reported that stable plaques can undergo expansive/adaptive remodelling of their vessel wall to compensate for plaque volume, and therefore limit the encroachment into the lumen and prevent deleterious effects on blood flow and potential occlusion of the vessel (Falk 2006) (as illustrated in Figure 1.5). As such, stable plaques within coronary arteries are usually asymptomatic, but in the long-term can cause some clinical symptoms such as stable angina pectoris (van der Wal and Becker 1999).

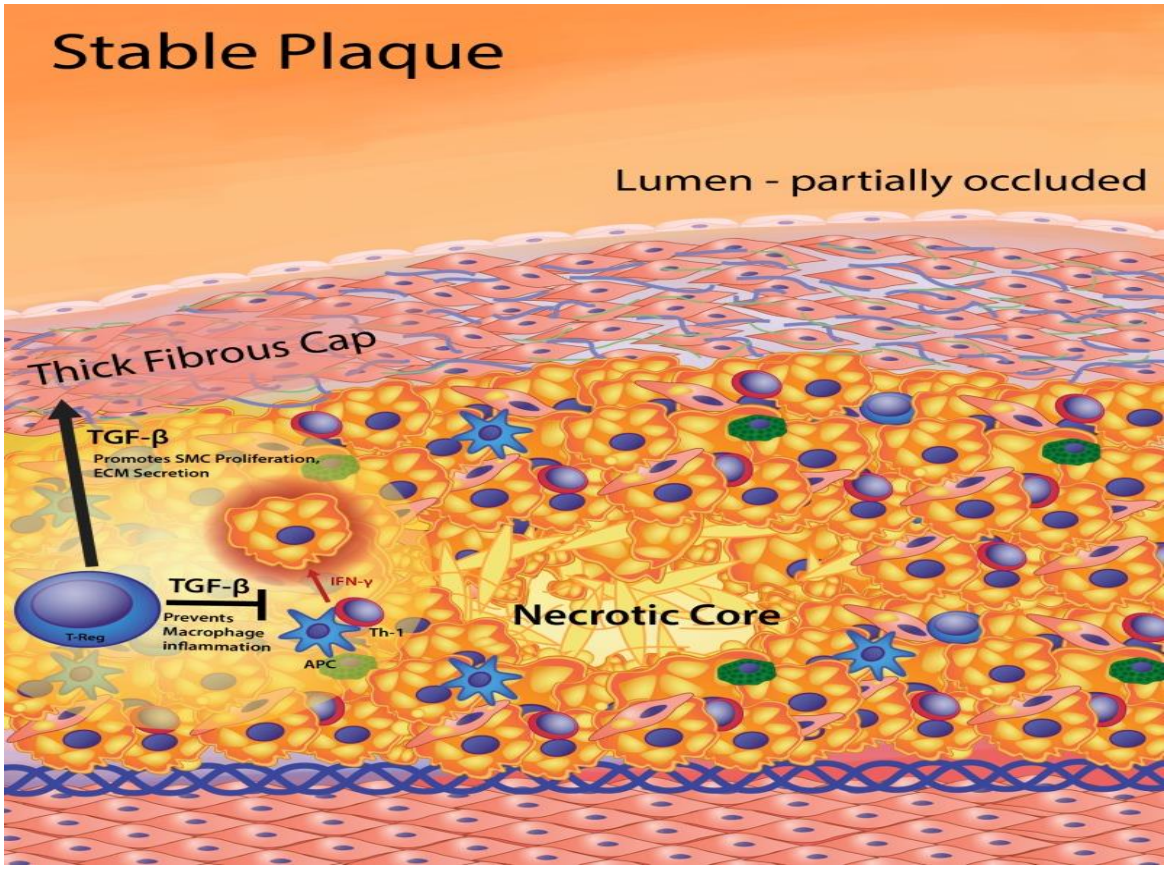

Figure 1.5 Pathological changes associated with the development of stable plaques.

Stable plaques are characterised by the presence of a thick fibrous cap composed of several layers of vascular smooth muscle cells within collagenous extracellular matrix, small necrotic core containing cell debris, droplets of lipid and sparse cholesterol crystals. The stability of the plaque is preserved by increased secretion of TGFβ and IL-10 from T-regulatory cells and macrophages. A partially-occluded lumen can be seen due to the increase in the cellular contents within the vessel wall. TGFβ, transforming growth factor β; T-reg, T regulatory cell; IFNγ, interferon-γ; Th1, T helper cell type 1. Figure is taken from (Linton, Yancey et al. 2000).


Foam cell formation


Macrophage


T-regulatory cell


oxLDL


Mast cell


T helper cell type 1


Vascular smooth muscle cell


Dendritic cell

Conversely, unstable plaques (also termed vulnerable plaques) are the plaques with highest risk to rupture. They are characterised by the presence of an enlarged necrotic core (Rauch, Osende et al. 2001). Enlargement of necrotic core is associated with increasing accumulation of extra-cellular lipids and free cholesterol. It has been reported that T cells within vulnerable plaques release IFNγ, which can polarise macrophages towards a pro-inflammatory phenotype (Linton, Yancey et al. 2000). Pro-inflammatory macrophages increase the release of inflammatory chemokines, MMPs, and inhibit the release of anti-atherogenic cytokines including TGFβ and IL-10 (Linton, Yancey et al. 2000). Moreover, pro-inflammatory macrophages have inefficient efferocytosis capacity that will lead to the inability for these macrophages to engulf apoptotic macrophages (Dickhout, Basseri et al. 2008). The inability to eliminate the apoptotic macrophages leads to secondary necrosis of apoptotic macrophages and subsequent release of all their cellular contents, which will cause further enlargement of the necrotic core and perpetuate the inflammatory response (Thorp, Li et al. 2009). Necrotic core enlargement is also associated with intra-plaque haemorrhage (Rauch, Osende et al. 2001), and most importantly, with increased VSMC death (Badimon and Vilahur 2014). The death of VSMCs leads to decreased support within the fibrous cap due to the reduced collagen production and diminished cellular content (Felton, Crook et al. 1997). Indeed, it has been demonstrated that patients suffering from symptomatic unstable angina have a higher percentage of apoptotic VSMCs compared to patients with stable angina (Bauriedel, Hutter et al. 1999). Furthermore, the increased expression of MMPs (predominantly from focal aggregates of foam cell macrophage) leads to further fibrous cap destruction (Hansson, Robertson et al. 2006). Pathological studies of human ruptured coronary plaques showed that the main characteristics for a vulnerable plaque include a thin fibrous cap (<65 μM), presence of haemorrhage, hyper-cellular content of foam cell macrophages and T cells within the plaque, as well as hypo-cellular content of VSMCs within the fibrous cap, and finally, an enlarged necrotic core accounting for more than 30% of atherosclerotic plaque area (Virmani, Burke et al. 2006) (as illustrated in Figure 1.6). Lipidomic studies demonstrated that the lipid fractions within plaques are different between stable and unstable lesions, indicating that stable plaques have more cholesterol esters, whereas unstable plaques have increased lysophosphatidylcholine content, indicative of increased oxidation levels within unstable plaques (Stegemann, Drozdov et al. 2011). Rupture of the plaque causes the release of pro-thrombotic factors and pro-coagulant factors, especially the release of tissue factor (TF), which is abundant within the necrotic core (Toschi, Gallo et al. 1997). TF is affiliated with the activated macrophages and initiates the coagulation process and thrombin formation (Toschi, Gallo et al. 1997). When TF is exposed to blood flow in the lumen, it interacts with factor VII which causes the activation of factor X. Factor X is important in the conversion of prothrombin to thrombin, an enzyme important for the coagulation of the blood, and subsequently,

increasing the risk for thrombus formation (Gentry, Ye et al. 1995). Consequently, the formation of a thrombus at the site of plaque rupture is responsible for most of the related clinical events in CVD patients such as sudden cardiac death, myocardial infarction (MI), and strokes.

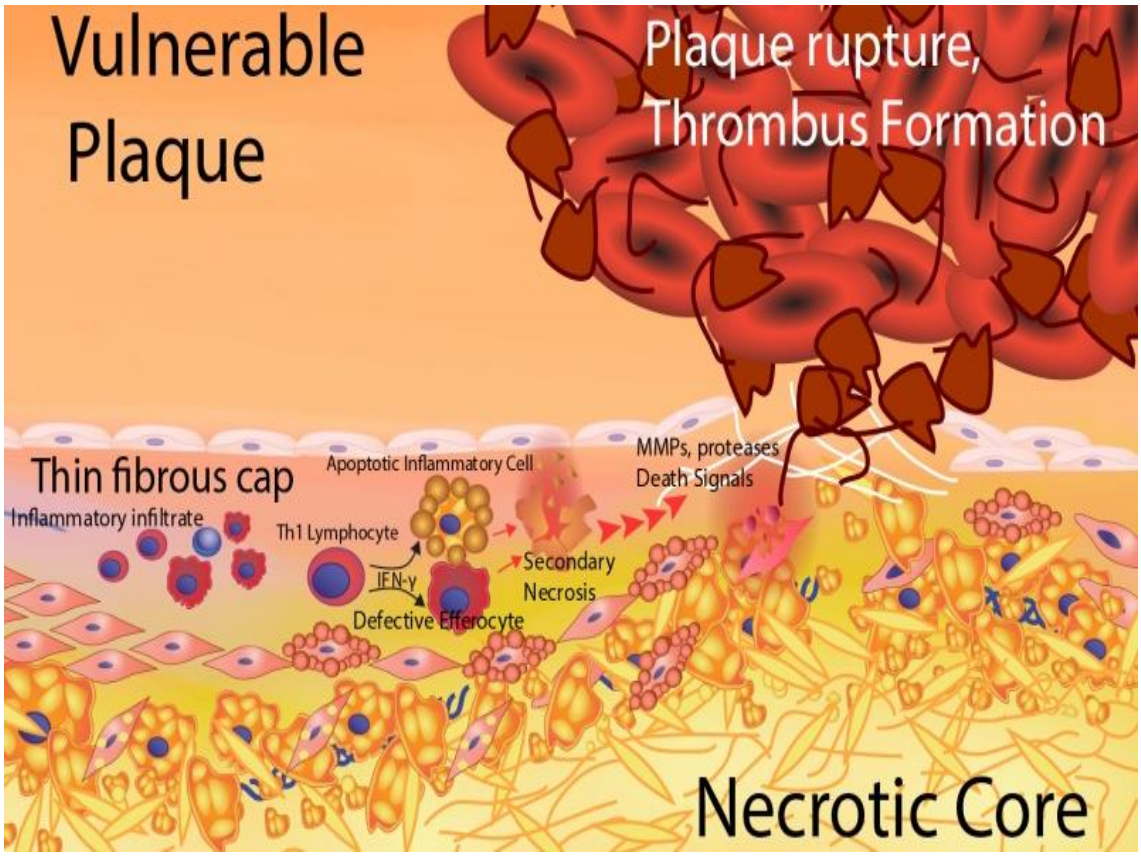

Figure 1.6 Pathological changes associated with the development of unstable plaques.

Unstable plaques are characterised by the presence of a thin fibrous cap, enlarged necrotic core with abundant extra-cellular lipid and cholesterol crystals, focal accumulations of foam cell macrophages at the shoulder regions, and diminished fibrous cap, VSMC, and collagen content. T cells within the vulnerable plaque release IFNγ generating pro-inflammatory macrophages. Pro-inflammatory macrophages inhibit the secretion of TGFβ and IL-10 and increase the release of MMPs, precipitating fibrous cap degradation and thinning. In addition, pro-inflammatory macrophages display inefficient efferocytosis, resulting in secondary necrosis. Altogether, these processes increase the susceptibility of plaque rupture and succeeding potential of thrombus formation. IFNγ, interferon-γ; MMP, matrix metalloproteinases; Th1, T helper cell type 1. Figure is taken from (Linton, Yancey et al. 2000).


Foam cell formation


Macrophage


T-regulatory cell


oxLDL


T helper cell type 1


Vascular smooth muscle cell

1.3 Monocytes

Monocytes are the largest cell-type within the leukocyte/white blood cells (WBC) class. They display an amoeboid morphology with a unilobed nucleus and a non-granulated cytoplasm (Nichols, Bainton et al. 1971). Monocytes are the main effector cells during innate immune responses in the body (Nikiforov, Wetzker et al. 2019). Monocytes originate from pluripotent stem cells within the bone marrow. The monoblasts form pro-monocytes that are the direct progenitor cells of monocytes (Figure 1.7) (van Furth and Beekhuizen 1998). Within the bone marrow, monoblasts divide to form monocytes that remain within the bone marrow for around a day before entering the circulation. Within the circulation, monocytes' half-life is up to 71 hours in humans (van Furth and Beekhuizen 1998). Several factors and cytokines determine the formation of monocytes such as M-CSF, granulocyte-macrophage colony-stimulating factor (GM-CSF), and IL-3, as well as inflammatory factors such as factor increasing monocytopoiesis (FIM), which can double the number of circulating monocytes compared to under normal conditions, with the majority of them migrating toward the source of inflammation (van Furth and Beekhuizen 1998). Circulating monocytes in the blood do not proliferate, their role involves the removal of toxic substances and cellular debris (Auffray, Sieweke et al. 2009). It has been postulated that circulating monocytes can facilitate the renewal of tissue-resident macrophages, such as Kupfer cells within the liver (Geissmann, Auffray et al. 2008).

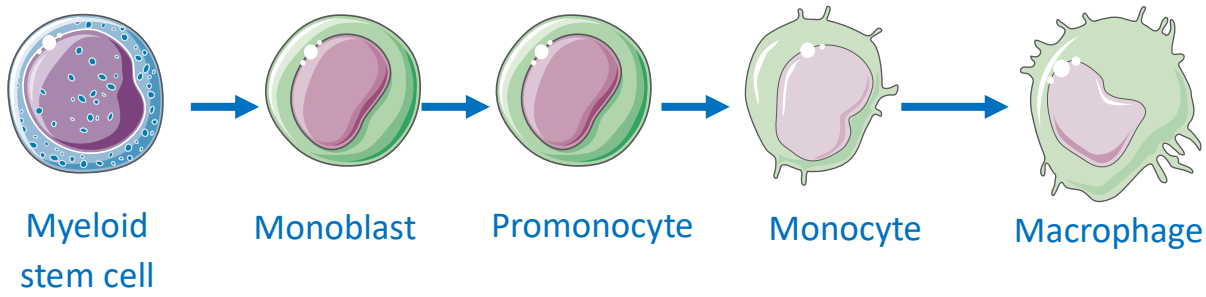

Figure 1.7 Origin of monocytes

Monocytes originate from myeloid stem cells within the bone marrow. Pro-monocytes originate from monoblasts and are the direct precursor for monocyte production. Monocytes most commonly differentiate into macrophages once within tissues. Figure made using elements from https://smart.servier.com/

Flow cytometry and microscopy analysis of mouse monocytes have demonstrated the existence of different subsets that can be delineated according to their expression of different cell-surface markers (Johnson and Newby 2009). Monocytes which display high levels of lymphocyte antigen 6C, high levels of C-C chemokine receptor 2, and low levels of CX3C chemokine receptor 1 ($Ly6C^{high}CCR2^{+}CX3CR1^{low}$) expression are known as inflammatory monocytes, and can differentiate into dendritic cells and inflammatory macrophages (Kratofil Rachel, Kubes et al. 2017). Conversely, $Ly6C^{low}CCR2^{-}CX3CR1^{high}$ monocytes are termed as patrolling monocytes, and are thought to survey the endothelium and underlying tissues for signs of damage. This action is mediated by binding of C-X3-C motif chemokine receptor 1 (CX3CR1) on the monocyte surface with β_2-integrins on endothelial cells within small arteries, therefore, their role is associated with the processes of wound repair (Audoy-Rémus, Richard et al. 2008, Woollard and Geissmann 2010). Underlying their patrolling function, $Ly6C^{low}$ monocytes stay for a longer time in the circulation compared to $Ly6C^{high}$ monocytes. On the other hand, their recruitment to inflammatory sites such as atherosclerosis is delayed and depends on the expression of C-X3-C motif ligand 1 (CX3CL1) (Johnson and Newby 2009). In contrast, although $Ly6C^{high}$ monocytes reside for a shorter time in the circulation, they can move to the inflammation site rapidly (Johnson and Newby 2009). Accordingly, studies showed the presence of $Ly6C^{high}$monocytes within early atherosclerotic plaque lesions in mice (Swirski, Libby et al. 2007). The chemokines responsible for the recruitment of $Ly6C^{high}$ monocytes into atherosclerotic plaques are CX_3CL1 and C-C motif ligand 2 (CCL2). Indeed, it has been reported that the gene-deletion of CX_3CL1 and CCL2 has an anti-atherosclerotic effect on lesions in mouse models (Johnson and Newby 2009). Studies showed that the involvement of C-C chemokine receptor type 5 (CCR5) is also important for the migration of $Ly6C^{high}$ monocytes (Tacke, Alvarez et al. 2007). Therefore, these three chemokines and their receptors (CX_3CL1/CX3CR1, CCL2/CCR2, and CCL5/CCR5) have a pivotal role in the recruitment and the entry of monocytes into mouse atherosclerotic plaques (Johnson and Newby 2009). While monocyte subsets have also been identified in humans, they are differentiated according to their cell-surface expression of Fc Fragment Of IgG IIIA (FCGR3A) which is more commonly termed CD16, and CD14 (Ziegler-Heitbrock, Ancuta et al. 2010). Accordingly, three monocyte subsets have been identified in humans termed classical (CD14++CD16-), intermediate (CD14++CD16+), and non-classical (CD14+CD16++) (Thomas, Hamers et al. 2017). The $Ly6C^{high}$ monocytes in mice are considered the equivalent to CD14++CD16-population, while $Ly6C^{low}$ monocytes in mice are thought similar to the CD14+CD16++ population in humans, based upon similar expression patterns of CCR2 (Johnson and Newby 2009). The CD14++CD16- population are more abundant compared to the CD14+CD16++ population and are considered anti-inflammatory due their production of anti-inflammatory cytokines such as IL-10 in response to pathogens. On the other hand, the CD14+CD16++ population are less abundant and

deemed to have a pro-inflammatory effect as their numbers are increased during inflammatory responses and they are able to release pro-inflammatory cytokines and chemokines such as IL-8, IL-6, and CCL2 (Schlitt, Heine et al. 2004). However, the circulating numbers of classical CD14++CD16- monocyte subset have been shown to predict future cardiovascular risk, independent of their expression of chemokine receptors (Berg Katarina, Ljungcrantz et al. 2012). A study showed that primary human monocytes, isolated from the blood of patients suffering from atherosclerosis, can react to the presence of lipopolysaccharide (LPS) in a stronger manner which was demonstrated by the increase in the expression and the release of pro-inflammatory cytokines. This finding may suggest that monocytes in atherosclerotic patients obtained trained immunity (Bekkering, Blok et al. 2016). Furthermore, human monocytes subsets display differences in their responses to oxLDL, as CD14++CD16+ monocytes more readily phagocytose modified lipoproteins compared to CD14++CD16−monocytes (Mosig, Rennert et al. 2009). Moreover, the intermediate CD14++ CD16+ monocytes also show differences in their phagocytic capacity, while also displaying reduced ability to adhere to the substratum, alongside increased release of IL-12 compared to the CD14++CD16- population (Kapellos, Bonaguro et al. 2019).

1.4 Macrophages

1.4.1 Macrophage subsets in atherosclerosis.

Macrophages within atherosclerotic plaques can originate from different sources, with some macrophages already residing in the adventitia and therefore called resident macrophages (Nagenborg, Goossens et al. 2017). Such macrophages are activated in the presence of inflammation and are considered as the first line of protection within tissues. Study in mice showed that adventitial resident-macrophages are embryonically originated from CX3CR1 positive precursors which express lymphatic vessel endothelial hyaluronan receptor 1 (Lyve1) (Ensan, Li et al. 2016). It has been reported that resident macrophages also express mannose receptor 1 (MRC1) known as CD206 alongside folate receptor β (Folr2) similar to anti-inflammatory macrophages, suggesting that the resident macrophages exert anti-inflammatory effects in the tissue (Kim, Shim et al. 2018).

In addition to bone marrow-derived monocytes giving rise to macrophages, monocytes can originate from spleen, and together with bone marrow-derived monocytes, are known as the mononuclear phagocyte system (MPS). Monocytes from both reservoirs are released into the circulation and are recruited to tissues such as atherosclerotic plaques, during an inflammatory response (Xu, Jiang et al. 2019). Within the same atherosclerotic plaque, it has been demonstrated that macrophages are heterogeneous and exist as different phenotypes. Macrophage subsets are highly dependent on the stimuli from the microenvironment such as cytokines, lipids, and haemorrhage (Xu, Jiang et al. 2019), and can be classified into anti-inflammatory and pro-inflammatory macrophage subsets (Mantovani, Sica et al. 2004). The pro-atherogenic stimuli such as oxLDL, not only effects macrophage polarisation, but also stimulates monocytes and precursor cells within the bone marrow (Murphy, Akhtari et al. 2011). Recent controversial mouse studies have postulated that VSMCs can differentiate into macrophage-like foam cells in the atherosclerotic plaques due to their high proliferative capacity (Chappell, Harman et al. 2016). However, studies in human showed that these VSMC-derived macrophage-like cells are different from classical macrophages in salient functions such as efferocytosis and phagocytosis, as well as their transcriptional profile (Vengrenyuk, Nishi et al. 2015).

The classically activated M1 and alternatively activated M2 macrophage subsets (and others) have been identified predominantly through in vitro studies. M1 macrophages are polarised in response to interferons, toll-like receptor ligand, lipoproteins, and lipopolysaccharides (Barrett Tessa 2020). They secrete pro-inflammatory mediators such tumour necrosis factor α (TNFα), IL-1β, and IL-6, contributing to tissue destruction (Martinez, Gordon et al. 2006, Wolfs, Donners et al. 2011). Pro-inflammatory transcription factors are expressed by M1 macrophages such as nuclear factor-kappa-

light-chain-enhancer of activated B cells (NFκB) and signal transducer and activator of transcription (STAT) (Barrett Tessa 2020). On the other hand, M2 macrophages display anti-inflammatory properties, they are polarised in response to IL-4, IL-10 and IL-13 (Wolfs, Donners et al. 2011). M2 macrophages secrete anti-inflammatory mediators such as collagen and IL-10, and they are characterised by expressing high levels of arginase-1, and MRC1 (Barrett Tessa 2020).

Colony stimulating factors (CSFs) are secreted glycoproteins that attach to receptors on the cell surface of hemopoietic stem cells, and have also been assigned an essential role in the regulation of macrophage heterogeneity (Di Gregoli and Johnson 2012). It has been reported that M-CSF and GM-CSF can generate two different macrophage phenotypes in vitro, referred from hereon as M-Mac and GM-Mac, respectively. M-Mac and GM-Mac differ in their morphology, function, phagocytic capacity, and transcriptome (Di Gregoli and Johnson 2012). Under physiological conditions, M-CSF is expressed by numerous cell types including macrophages, VSMCs, and endothelial cells. On the other hand, GM-CSF is weakly expressed by these cell types and requires stimulation by inflammatory cytokines such as TNFα or exposure to modified lipoproteins, in order to be upregulated (Di Gregoli and Johnson 2012). During pathological conditions such as atherosclerosis, the expression of GM-CSF and the polarisation of macrophages toward a pro-inflammatory macrophages become dominant (Di Gregoli, Jenkins et al. 2014). Advanced human plaque is associated with high expression of GM-CSF, while cell surface expression of the M-CSF receptor is compromised, favouring macrophage polarisation to a GM-Mac phenotype (Di Gregoli, Jenkins et al. 2014). This can be reversed during the resolution of an inflammatory response where GM-CSF concentrations diminish (Hamilton 2008), suggesting that polarisation of macrophages is not terminal in the presence of a single CSF (Hamilton 2008) and there is a competition between different CSFs in macrophage differentiation and polarisation (Di Gregoli and Johnson 2012). Regarding cell morphology, M-Macs display an elongated shape compared to GM-Macs which have a more rounded shape (Waldo, Li et al. 2008). During inflammation, GM-Macs release pro-inflammatory cytokines and proteases such as IL-23, TNFα, MMP-12, and MMP-14. In contrast, M-Macs secrete anti-inflammatory cytokines and factors such as, CD206, IL-10, arginase 1 (ARG1), and selenoprotein 1 (SEPP1) (Verreck, de Boer et al. 2004). Accordingly, M-Macs are considered as anti-inflammatory macrophages, where GM-Macs are reported as pro-inflammatory macrophages.

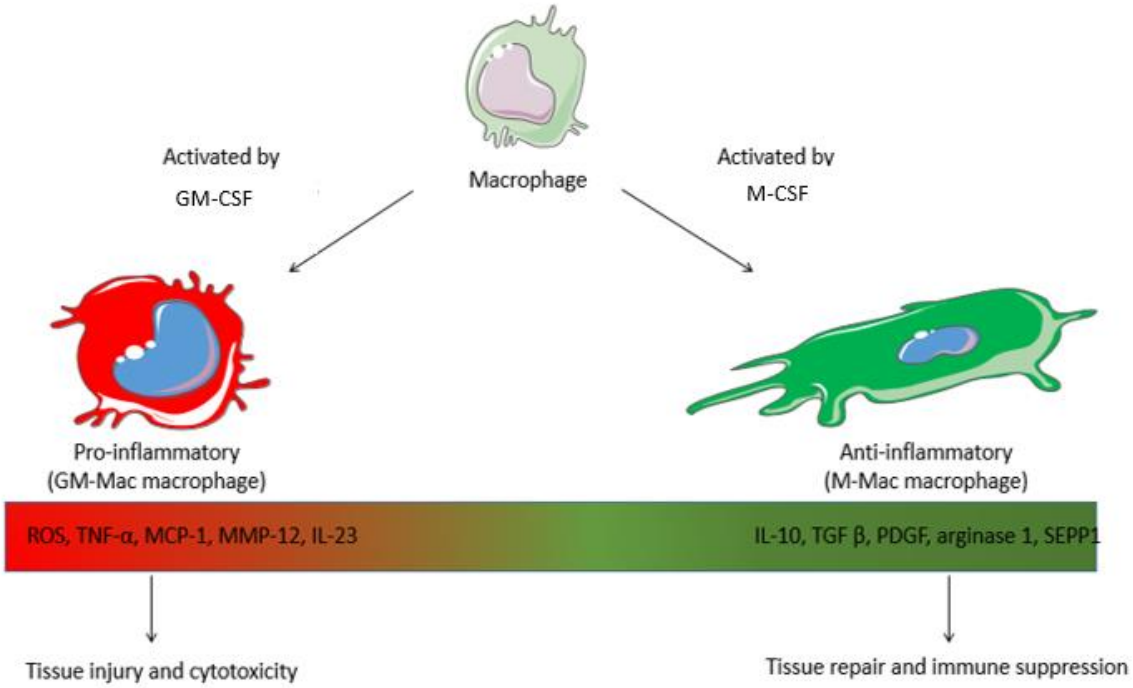

Figure1.8 Macrophage heterogeneity

Macrophages can be differentiated into different subsets by stimulation with distinct colony stimulating factors (CSFs). The pro-inflammatory macrophages (on the left-hand side) are polarised by GM-CSF, giving rise to a phenotype displaying a rounded shape, and responds to tissue injury and cytotoxicity through the release of ROS, TNFα, MCP-1, MMP-12, and IL-23.

Anti-inflammatory macrophages (on the right-hand side) are polarised by the presence of M-CSF, are elongated in shape, and proposed to play an essential role in the suppression of immune responses and induce tissue repair during healing, by the release of IL-10, TGFβ, PDGF, arginase 1, and SEPP1.

GM-CSF, granulocyte macrophage colony-stimulating factor; INFγ, interferon gamma; TNFα, tumour necrosis factor alpha; M-CSF, macrophage colony-stimulating factor; IL, interlukein; TGFβ, transforming growth factor β; ROS, reactive oxygen species; MCP-1, monocyte chemoattractant protein-1; MMP, matrix metalloproteinase; PDGF, platelet-derived growth factor; SEPP1, selenoprotein 1. Figure made using elements from https://smart.servier.com/

1.4.2 Foam cell formation in macrophages

Macrophages are well known for their ability to uptake oxLDL and transform into foam cell macrophages during atherogenesis and plaque progression. Unchecked uptake of oxLDL increases the esterification of cholesterol, while suppressed efflux of cholesterol leads to its accumulation within the cytoplasm as droplets, giving rise to foam cell formation and their distinguishable appearance under the microscope (Yu, Fu et al. 2013). The uptake of oxLDL is mediated by specific receptors known as scavenger receptors such as CD36 and macrophage scavenger receptor-1 (MSR1, also known as SR-AI).It has been reported in mice that the inhibition of MSR1 decreases the ability of macrophages to engulf modified lipoproteins and transform into foam cells, subsequently preventing the further accumulation of macrophages within atherosclerotic lesions (Robbins, Hilgendorf et al. 2013). Studies in primary human macrophages showed that M-Mac and GM-Mac subsets differentially express genes related to cholesterol homeostasis (Waldo, Li et al. 2008). Both M-Mac and GM-Mac subsets are able to uptake lipids and form foam cells, but M-Macs capability to accumulate oxLDL is more rapid compared to GM-Macs, attributed to their increased expression of scavenger receptors (Irvine, Andrews et al. 2009). In addition, the M-Mac subsets have markedly lower expression of mediators for reverse cholesterol transport such as ABCG1, in comparison to GM-Macs (Irvine, Andrews et al. 2009). Furthermore, the increased uptake of lipids by M-Macs causes changes in their behaviour, indicating a shift towards a pro-inflammatory phenotype as evidenced by reduced IL-10 expression and increased levels of MCP-1 and IL-6 (Di Gregoli and Johnson 2012). It has been postulated that this phenotypic change in M-Mac occurs in order for them to increase their ability to efflux cholesterol and lessen the formation of foam cells (Di Gregoli and Johnson 2012). Foam cell macrophages release several pro-inflammatory mediators inducing further recruitment of monocytes and associated accumulation of macrophages.

1.4.2.1 *Scavenger receptors and toll-like receptors in macrophages*

CD36 and MSR1 are the most prevalent macrophage scavenger receptors and are responsible for 75-90% of macrophage oxLDL internalisation (Kunjathoor, Febbraio et al. 2002). CD36 is a cell surface glycoprotein that is 88 kDa in size, and is expressed by multiple cell types other than macrophages, including VSMCs, platelets, and endothelial cells (Collot-Teixeira, Martin et al. 2007). CD36 was first discovered as a glycoprotein III b/IV in platelets (Yu, Fu et al. 2013), but subsequent studies with MSR1-specific monoclonal antibody, identified its expression by monocytes (Talle, Rao et al. 1983). According to its structure and function, CD36 was classified as a member of class B scavenger receptor family. It is composed of two transmembrane extracellular regions and two cytoplasmic areas and has high-affinity ligand binding for oxLDL. Oxidation of LDL incorporates substitution nucleophilic bimolecular

(sn-2 acyl group) forming a specific characteristic in its structure that is essential for its high-affinity binding to CD36 (Kunjathoor, Febbraio et al. 2002). The expression of CD36 by macrophages is upregulated by the endocytosis of oxLDL and subsequent signalling through protein kinase C (PKC)- or PKB-dependent activation of the peroxisome proliferator-activated receptor gamma (PPARγ) pathway (Feng, Han et al. 2000, Munteanu, Taddei et al. 2006). It has been reported that deficiency in the expression of CD36 in old and young Apoe-deficient knockout mice leads to a decrease in the size of atherosclerotic plaques (Collot-Teixeira, Martin et al. 2007). On the other hand, studies showed that mice deficient for Apoe and CD36 showed increased atherosclerosis with heightened foam cells formation within aortic sinus lesions, suggesting that lipid uptake by plaque macrophages occurs in the absence of CD36 (Moore, Kunjathoor et al. 2005). Another study showed that patients with CD36 deficiency are more prone to develop advanced atherosclerosis (Yuasa-Kawase, Masuda et al. 2012).Taken together, the role of CD36 in the development of foam cell macrophages and atherosclerotic plaques requires further elucidation.

MSR1 is a membrane glycoprotein that is about 77 kDa in size and represents another major macrophage scavenger receptor that has a vital role in the uptake of oxLDL. While under physiological conditions MSR1 expression is predominantly restricted to macrophages, specific growth factors and oxidative stress, can induce MSR1 expression by VSMCs and endothelial cells (Linton, Yancey et al. 2000). Studies in Apoe knockout mice which were also deficient in MSR1 showed a significant reduction in the size of atherosclerotic plaques as alongside a 60% inhibition in macrophage foam cell formation (Babaev, Patel et al. 2000), supporting a pro-atherosclerotic role for MSR1. However, and similar to CD36, contrasting results have been reported with mice deficient for Apoe and CD36 demonstrating increased atherosclerosis and macrophage foam cell formation within aortic sinus lesions, implicating alternative receptors can mediate lipid uptake by plaque macrophages in the absence of MSR1 and CD36 (Moore, Kunjathoor et al. 2005). Furthermore, it has been reported that MSR1 has other functions in macrophages such as mediating cell adhesion to ECM (Fraser, Hughes et al. 1993).

The oxidized low-density lipoprotein receptor 1 (OLR-1), which is also known as lectin-like oxLDL receptor-1 (LOX-1), is a 50-kDa glycoprotein member of SR family class E. OLR1 was first identified in endothelial cells (Sawamura, Kume et al. 1997), but was later detected in several other cell types including macrophages, platelets, VSMCs, and fibroblasts (Kattoor, Goel et al. 2019). In addition to its role in oxLDL uptake, studies showed that OLR1 has an essential role in apoptosis, contribution to endothelial dysfunction, and macrophage foam cell formation (Kattoor, Goel et al. 2019). Expression of OLR1 is regulated by different mediators which includes oxLDL, TNFα, IFNγ, and IL-1 (Kattoor, Goel et al. 2019). Under physiological conditions, the expression of OLR1 is low. However, inflammatory

responses and conditions such as hypertension and diabetes mellitus upregulate the expression of OLR1 (Xu, Ogura et al. 2013). Studies in endothelial cells demonstrated that when bound to oxLDL, OLR1 induces an increase in the expression of MCP-1 and VCAM-1 (Aoyama, Sawamura et al. 1999). which in turn further increases OLR1 levels, revealing self-cycle activation between OLR1 and oxLDL (Feng, Cai et al. 2014). It has been demonstrated that OLR1 is able to bind MMP-14, triggering activation of Rac1 and Ras homolog family member A (RhoA) (Kattoor, Goel et al. 2019). Subsequently, RhoA reduces the production of eNOS while Rac1 increases the activity of nicotinamide adenine dinucleotide phosphate hydrogen (NADPH) oxidase, resulting in heightened production of oxidative stress and ROS (Sugimoto, Ishibashi et al. 2009).

In addition to the scavenger receptor family, other types of receptor have the ability to identify and uptake oxLDL such as Toll-like receptors (TLRs) especially TLR2 (Kadl, Sharma et al. 2011), TLR4 (Choi, Harkewicz et al. 2009), and TLR9 (Karper, Ewing et al. 2012). TLRs are a family of proteins that have an essential role in the innate immune system and are expressed by multiple cell types including dendritic cells and macrophages. In mammals, 13 members of TLR family have been recognised and they are recognised as specialised receptors which identify pathogen-associated molecular patterns (PAMPs) (Cole, Georgiou et al. 2010). It has been demonstrated that TLRs and scavenger receptors can interact during atherosclerosis, resulting in activation of NFκβ signalling pathway (Stewart, Stuart et al. 2010). Such activation leads to the release of pro-inflammatory mediators including TNFα and IL-12 (Cole, Georgiou et al. 2010). Studies showed that during atherosclerosis, the expression of TLRs especially TLR1, TLR2, and TLR4 is upregulated within inflammatory cells such as T and B lymphocytes, macrophages, VSMCs and endothelial cells (Xu, Shah et al. 2001).

1.4.2.2 *Reverse cholesterol transport*

The removal of accumulated lipids within macrophages after the process of phagocytosis is known as cholesterol efflux. Cholesterol efflux is considered as the initial step of reverse cholesterol transport, which is the process where the cholesterol particles are transferred from peripheral tissues to the liver for biliary elimination (Yu, Fu et al. 2013). Lipids can be diffused passively through cell membranes or via an active mechanism through specific transporters such as SR-BI, ABCA1, and ABCG1 and then lipids are collected by ApoA1 and HDL (Yu, Fu et al. 2013). Mature HDL as well as lipid poor ApoA1 are considered as the main contributors in preventing the formation of foam cells by regulating the removal of cholesterol from macrophages. HDL transports cholesterol back to the liver via two different routes, either by binding to SR-BI (Acton, Rigotti et al. 1996) or through LDL and its receptors (Lewis and Rader 2005). In addition to reverse cholesterol transport, HDL has been shown to have an

anti-atherogenic effect within atherosclerotic plaques (Nofer, Kehrel et al. 2002). Studies showed that injection of ApoA1 results in reduced expression of adhesion molecules on activated endothelial cells (Shaw, Bobik et al. 2008), through inactivation of the NFκβ signalling pathway (Park, Park et al. 2003). Accordingly, HDL suppresses the recruitment of monocytes, the activation, proliferation, and accumulation of macrophages within atherosclerotic plaques by suppressing the expression of adhesion molecules in monocytes (Murphy, Woollard et al. 2008) through the inhibition of the PPARγ and NFκβ signalling pathways (Bursill, Castro et al. 2010).

ABCA1 is a member of the superfamily of ABC transporters which are expressed by macrophages and responsible for mediating cholesterol efflux via ApoA1 or Apoe (Fielding and Fielding 1995). It has been reported that ABCA1 has an essential role in the prevention of macrophage foam cell formation within atherosclerotic plaques. Studies showed that patients who carry a loss-of-function ABCA1 mutation display low HDL-cholesterol levels accompanied with advanced atherosclerotic lesions when compared to controls (Bochem, van Wijk et al. 2013). Multiple pathways have been implicated in the regulation of ABCA1, with studies in THP-1 macrophages showing that agonism of the PPARγ and liver X receptor alpha (LXRα) signalling pathways increased ABCA1 expression, resulting in the enhanced cholesterol efflux (Lee, Moon et al. 2013). A further study noted that activation of the PKCα pathway enhanced expression of ABCA1 in macrophage foam cells differentiated from THP-1 cells (Liu, Lu et al. 2013). Opposingly, it has been demonstrated that unsaturated fatty acids can inhibit the expression of ABCA1 in macrophages (Ku, Park et al. 2012). Furthermore, stimulation of THP-1 derived macrophages with IL-12 and IL-18 downregulated ABCA1 levels (Yu, Jiang et al. 2012).

ABCG1 is another transporter that mediates the removal of cholesterol from macrophages through HDL particles via ApoA1. Supporting an athero-protective role for ABCG1 through facilitating macrophage cholesterol efflux, mice with bone marrow-restricted deficiency of ABCG1 expression displayed a significant increase in aortic root atherosclerotic plaque size (Out, Hoekstra et al. 2006). Regulation of the expression of ABCG1 is similar to ABCA1 since the activation of LXRα increases ABCG1 levels (Jun, Hoang et al. 2013). SR-BI also mediates the efflux of cholesterol via HDL, inferring an anti-atherosclerotic role. Indeed, bone marrow-restricted loss of SR-BI increased the development of atherosclerotic lesions in Apoe-deficient mice (Zhang, Yancey et al. 2003). However, although patients with deficiency in the expression of SR-BI suffer from blunted cholesterol efflux, they are at no greater risk of developing clinically-relevant atherosclerosis (Yu, Fu et al. 2013).

1.4.3 Efferocytosis in macrophages

The process of efficient apoptotic cell removal is termed as efferocytosis (Yurdagul, Doran et al. 2018). Efferocytosis is important in maintaining homeostatic balance, resolution of inflammation, and allowing development of organs in the body (Arandjelovic and Ravichandran 2015). Efferocytosis is performed by professional cells (macrophages) and non-professional cells (neighbouring cells) depending on the setting. Macrophages rapidly migrate toward apoptotic cells and clear them through efferocytosis; accordingly, it is very rare to detect apoptotic cells in tissues (Hochreiter-Hufford and Ravichandran 2013). The migration of macrophages towards dying cells is regulated by specific mediators released from the apoptotic cells themselves such as 'find me' signals which includes chemokines such as CX3CL1, adenosine triphosphate (ATP) nucleotides, and lysophosphatidylcholine (Elliott, Chekeni et al. 2009). Accordingly, recruited macrophages are able to recognise specific signals known as 'eat-me' signals that are located on the surface of apoptotic cells and bind to specific macrophage receptors either directly or indirectly using bridging molecules (Yurdagul, Doran et al. 2018). Internalisation of dead cells occurs in multiple steps. Initially, binding of dead cells to receptors. Therefore, after a proper binding between signals and receptors occur, reorganisation of the macrophage actin cytoskeleton takes place, which permits engulfment of dead cells to begin alongside triggering internalization of apoptotic cells in a process termed as 'tether and tickle' (Hoffmann , deCathelineau et al. 2001). It has been reported that the formation of F-actin filaments within the phagocytic cup is promoted and regulated by Rho family of small GTPases such as RhoA, Cdc42, and Rac1 (Nakaya, Kitano et al. 2008). Internalised apoptotic cells are conjugated with microtubule-associated protein 1A/1B-light chain 3 (LC3)-family of proteins that are specific autophagy proteins via a process known as LC3-associated phagocytosis (LAP) (Martinez, Malireddi et al. 2015). LAP enhances the fusion of phagosomes to lysosomes leading to degradation of the apoptotic cell via hydrolysis. Cholesterol particles resulting from the degradation process activates members of the PPAR and LXR signalling families, leading to upregulated expression of ABCG1 and ABCA1 in order to stimulate cholesterol efflux from macrophages (Kidani and Bensinger 2012).

Efficient efferocytosis within the body is dependent on its rapidity and competence (Brown, Heinisch et al. 2002), with the recognition and targeting of apoptotic cells for efferocytosis occurring within minutes, explaining the low probability of detecting apoptotic cells in healthy and normal tissues (Ravichandran 2010). However, within advanced atherosclerotic plaques apoptotic corpses are readily detected, suggesting that the efferocytosis capacity in atherosclerotic lesions is markedly dysregulated in comparison to normal tissues (Schrijvers, De Meyer et al. 2005). Furthermore, impaired efferocytosis in macrophages is associated with suppression of reverse cholesterol transport (which is usually activated during efferocytosis, as mentioned earlier), leading to enhanced foam cell formation

- a key driver of atherosclerotic plaque progression (Kojima, Downing et al. 2019). Whereas efficient efferocytosis suppresses pro-inflammatory responses by enhancing the release of anti-inflammatory mediators such as TGFβ and IL-10 from macrophages (Fadok, Bratton et al. 1998), impaired efferocytosis of apoptotic cells stimulates pro-inflammatory macrophage polarisation and propagates inflammation (Kojima, Downing et al. 2019). Finally, non-removed apoptotic cells undergo secondary necrosis (Ravichandran and Lorenz 2007), a process that involves the degradation of dead cell membranes and subsequent release of their contents, including multiple cytokines and chemokines, leading to enhanced inflammation and neovascularisation within the plaques, increasing their vulnerability to rupture (Mallat, Hugel et al. 1999). The mechanisms leading to impaired efferocytosis within atherosclerosis are poorly described (Schrijvers, De Meyer et al. 2005). It has been proposed that the marked increase in apoptosis overwhelms the efferocytosis capacity within advanced plaques (Thorp and Tabas 2009). However, a deficiency in efferocytosis is not exhibited during the early stages of atherosclerosis and data from studies suggested that the capacity of the efferocytosis system is sufficient to cope with the increased numbers of apoptotic cells seen in early plaques (Tabas 2010). It has also been suggested that during atherosclerosis, macrophage efferocytosis capacity is less efficient due to the number of efferocytosis-poor pro-inflammatory phenotypes outnumbering the content of efferocytosis-competent anti-inflammatory macrophages (Yamamoto, Yancey et al. 2011). Moreover, the increasing presence of ROS during plaque progression reduces the phagocytic capacity of macrophages (Schrijvers, De Meyer et al. 2005). Other studies noted that VSMCs, considered to display non-professional phagocytic capacity, lose their ability to uptake apoptotic cells when exposed to oxLDL (Clarke, Talib et al. 2010). Most importantly, it has been demonstrated that apoptotic cells within plaques are less 'edible' to macrophages compared to apoptotic cells in other parts of the body (Kojima, Weissman et al. 2017). Supportingly, it has been reported that expression of the 'eat-me' molecule calreticulin is decreased in dead intra-plaque cells making them more resistant for clearance by efferocytosis (Leeper, Raiesdana et al. 2013). Moreover, it has been reported that TNFα (which is upregulated in advanced atherosclerotic lesions) stimulates the expression of 'don't eat me' molecules including CD47 on the membrane of apoptotic VSMCs (Kojima, Volkmer et al. 2016). This finding suggests the presence of a deleterious feedback loop where impaired efferocytosis stimulates the release of TNFα (Martinet, Schrijvers et al. 2011) and TNFα perpetuates the ineffective clearance of apoptotic cells by suppressing efferocytosis. Finally, oxLDL can trigger the generation of autoantibodies which mask the eat-me ligands upon the surface of apoptotic cells, preventing their recognition and clearance by macrophages (Shaw, Hörkkö et al. 2001). Furthermore, abundant oxLDL will compete with apoptotic corpses for the same scavenger receptors, further preventing the clearance of apoptotic cells in atherosclerotic plaques (Schrijvers, De Meyer et al. 2007).

1.5 Actin cytoskeleton

The cytoskeleton of eukaryotic cells has an essential role in maintaining and providing support to the intracellular components. The actin cytoskeleton is composed of three families of filamentous proteins which are subdivided according to their size; microtubules (which are the largest type of filaments); intermediate filaments; and the smaller actin filaments (Karp 2010). The actin cytoskeleton is a fundamental structure during biological functions such as morphogenesis during development, wound healing, and in immune defence (Dominguez 2014). It is well known that the actin cytoskeleton regulates cell shape and motility of cells through its ability to mediate the production of different cellular components such as filopodia, lamellipodia, and focal adhesions (Dominguez 2014). These elements have pivotal roles in maintaining the function of different cells, including immune cells such as macrophages, neutrophils, and monocytes. Pertinent to atherosclerosis (and as briefly mentioned in the previous section), reorganisation of the macrophage actin cytoskeleton facilitates their clearance of apoptotic cells (Hoffmann , deCathelineau et al. 2001, Nakaya, Kitano et al. 2008).

1.5.1 Structure of actin cytoskeleton

The actin cytoskeleton of cells exists in two isoforms; polymeric filamentous actin (F-actin); and monomeric globular actin (G-actin). Actin is an ATP-ase and the hydrolysis of this nucleotide is crucial for the transition between filamentous and globular actin forms. The importance of the two actin isoforms arises from the fact that there must be a homeostatic balance between them for the stability of actin filaments (Hall 1994). As illustrated in Figure1.9, ATP-bound G-actin attaches to filaments at its so-called barbed (+) end, while the release of G-actin occurs from the pointed (-) end when in an adenosine diphosphate (ADP) bound state, a process that is known as actin filament treadmilling (Dominguez 2014). The polarity mentioned above controls the directional growth of actin filaments. The regulation of this procedure is tightly controlled by a family of proteins called actin binding proteins (ABP). It has been demonstrated that polymerisation of actin occurs at specific areas known as actin nucleation sites, which are located at the plasma membrane (Hall 1994). It has also been reported that the plasma membrane at these sites has numerous ABP located at the tips of lamellipodia and microspikes, for example, α-actinin, fimbrin, and talin. Other sites in the plasma membrane invested with actin filaments are focal adhesions alongside aggregations of integrins, and the adherens junctions together with clusters of cadherins (Hall 1994).

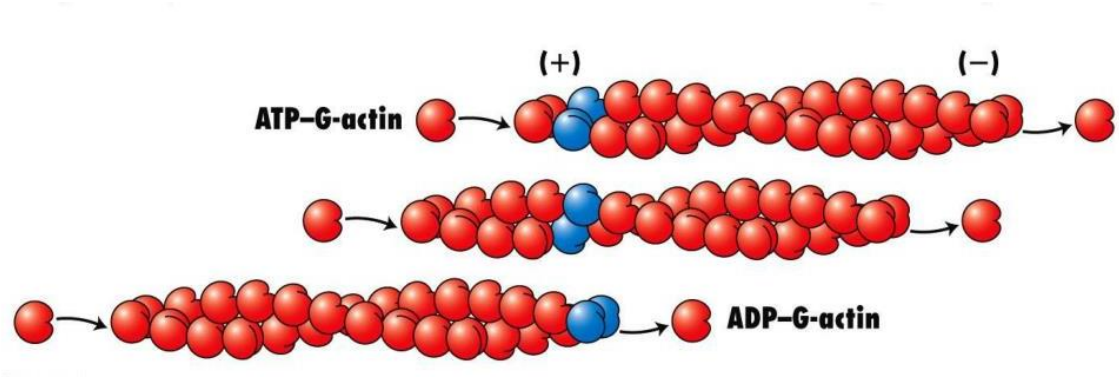

Figure 1.9-Actin filament treadmilling

Monomeric (globular) actin in an ATP-bound state attaches to the barbed (+) end of filaments while it is released from the pointed (-) end in ADP bound state. Figure is taken from (Lodish, Berk et al. 2008)

The organisation of the actin cytoskeleton is controlled by a number of extracellular factors such as cytokines, chemokines and growth factors (Hall 1994). Signals received by the cell activate different types of receptors. For example, M-CSF stimulates the M-CSF receptors on macrophages and can lead to actin cytoskeleton remodelling (Pixley and Stanley 2004). Furthermore, signals transmitted through activated receptors trigger an arm of the Ras superfamily, the Rho family of small GTPases, including Rho, Rac, and Cdc42 (Hall 1994). Recent studies have identified a number of cytoskeleton effector proteins which interact with Rho GTPase family members. For example, Rho-associated kinase (ROCK) is activated by the small GTP-binding protein RhoA. ROCK exists in two isoforms, ROCK1 and ROCK2, which share 90% similarity in their kinase domains, and have vital roles in controlling functions of the cell such as regulating cell shape, migration, and proliferation (Zanin-Zhorov, Flynn et al. 2016)

Another example of cytoskeleton effector proteins which can interact with Rho family of small GTPases (including Cdc42 and Rac) are the Cdc42/Rac interactive binding (CRIB) motif-containing proteins such as Wiskott-Aldrich syndrome Protein (WASP), and formins (Dominguez 2014). Moreover, these proteins are usually auto-inhibited by internal interactions, and can be activated by Rho family of small GTPases (Dominguez 2014). WASP is one of the most studied ABPs (Hall 1994) and is considered a nucleation promoting factor (NPF) as it attaches directly to the Actin related protein 2/3 (Arp2/3) complex, an actin filament nucleation factor which promotes the assembly of new actin filaments (Jones 2000). The attachment between WASP and the Arp2/3 complex leads to activation of Arp2/3 protein and initiates nucleation of actin as both Arp2 and Arp3 form the initial subunits of new actin filament branches (Dominguez 2014).

1.5.2 Role of the actin cytoskeleton in monocyte/macrophage migration and invasion

During inflammatory responses, at the site of inflammation multiple pro-inflammatory and chemotactic mediators are released which are responsible for the recruitment of monocyte/macrophages (Iijima, Huang et al. 2002). The migration cycle of macrophages occurs in multiple steps that include briefly the protrusion of the plasma membrane due to actin cytoskeleton remodelling, attachment of integrins to adhesion sites, and finally the contraction of the cell toward the inflammatory site by actomyosin contraction (Lauffenburger and Horwitz 1996). Migration is initiated when macrophages sense pro-inflammatory chemokines and cytokines via specific receptors, this stimulates both Rho GTPase and phosphoinositide 3-kinase (PI3K) signalling pathways (Fukata, Nakagawa et al. 2003). These signalling pathways lead to rearrangement and remodelling of the macrophage actin cytoskeleton, forming cell protrusions at the leading edge toward the source of inflammation (Petrie, Doyle et al. 2009).

It has been reported that polymerisation of the actin cytoskeleton leads to the formation of different types of protrusions depending on the type of migration needed for the cell such as, microspikes or filopodia (Ridley 2011). Microspikes are precursors of filopodia and are characterised as short in length (up to 20 µm) with a diameter around 0.1-0.2 µm and consist of bundles of F-actin. Filopodia are finger-like slender, tapering cytoplasmic projections that extend beyond the leading edge of lamellipodia in migrating cells (Jones 2000). It has been reported that filopodia have the ability to sense the external cytokines to provide the exact direction of migration for the cell (Yamaguchi and Condeelis 2007). The most common type of protrusions is pseudopodia and lamellipodia. Lamellipodia are characterised as flat, thin veil-like protrusions, which extend directly from the cell membrane, do not contain any organelles, and consists of networks of myosin II and F-actin filaments. Lamella, is a thick area located in between the cell and lamellipodia, which is described to have strong attachments to underlying substrates, and has organelles and networks of F-actin filaments (Chhabra and Higgs 2007). The initiation of lamellipodia occurs through three different mechanisms that are responsible for the polymerisation of the actin filaments; the first mechanism is the generation of a new free positive end at the leading edge of an actin filament; second, is the uncapping of an actin filament that has a cap on it; and the third mechanism involves severing (and depolymerisation) of F-actin filament at the leading edge, by the ABP cofilin (Zigmond 2004).

It has been reported that Arp 2/3 has pivotal role in mediating remodelling of the actin cytoskeleton and the formation of cell protrusions at the cell leading edge, in addition to its role in directing macrophage migration towards the site of inflammation (Suraneni, Rubinstein et al. 2012). Different cytokines and growth factors can stimulate chemotaxis in macrophages. M-CSF is the main growth factor responsible for the proliferation and differentiation of monocytes to macrophages (Sasaki,

Ohsawa et al. 2001). M-CSF is also considered as a chemoattractant for macrophages, at sites of infection and during atherosclerosis (Pixley 2012). Binding of M-CSF to its receptor leads to phosphorylation of this receptor tyrosine kinase and during downstream signalling, activates NPFs such as members of the WASP/WASP-family verprolin-homologous protein (WAVE) family via interaction with Rac and Cdc42, and eventually inducing actin cytoskeleton rearrangement (Mouchemore and Pixley 2012). Signalling through PI3K has an important role in chemotaxis, and can also stimulate Rho-GTPases, important regulators of the actin cytoskeleton. Moreover, it has been reported that there is an interaction between PI3K and CSF1R signalling via p85, and that CSF1R ligation with M-CSF interacts with multiple signalling pathways and complexes, which succeed in mediating cytoskeletal changes. SH2 domain-containing inositol phosphatase (SHIP) is an inhibitor of PI3K and bone marrow macrophages from SHIP-deficient mice show increased migratory capacity to M-CSF, and elevated levels of F-actin relative to wild-type control macrophages (Vedham, Phee et al. 2005).

The WASP family consists of five in members including WAVE1, WAVE2, WAVE3, N-WASP, and WASP. Members of the WAVE1-3 play an essential role in the formation of membrane ruffles and lamellipodia through the regulation of Rho-GTPase family members such as, Rac (Suetsugu, Kurisu et al. 2006), while N-WASP has a vital role in the formation of filopodia by the regulation of Cdc42 (Miki, Sasaki et al. 1998). It has been reported that WASP has an important role in guiding macrophages chemotaxis. Additionally, WASP has a pivotal role in the formation of podosomes in macrophages (Calle, Chou et al. 2004), which is a dynamic cell-ECM adhesive structures formed at the ventral surface of different cells such as macrophages, and composed of an actin rich core surrounded by adhesion proteins . Accordingly, WASP provides stability and support for lamellipodia by providing sufficient adhesion to the underlying substrate (Rougerie, Miskolci et al. 2013). Studies showed that the insufficient adhesion of lamellipodia causes the protrusion area to fold back, a process known as ruffling (Borm, Requardt et al. 2005). Forms of cell attachment to substrates are different, for example, focal adhesions use large contacts or attachments to the underlying substrate. On the other hand, macrophages use small point contacts to the substratum that are rich in phosphopaxillin, termed as focal complexes (Linder and Aepfelbacher 2003). Macrophages also use podosomes for their adhesion to ECM, and podosomes have larger contact surfaces than focal complexes. Podosomes are dynamic, located at the cell leading edge, and have a core rich with actin filaments mediated by the activation of Arp 2/3 and WASP family members. It has been demonstrated that podosomes have a ring of integrin receptors such as vinculin and talin that provide a link between the actin cytoskeleton (actin filaments and bundles of myosin II) and focal adhesions enriched with integrins (a large family of type-

1 transmembrane heterodimeric glycoprotein receptors that mediate cell adhesion (Hood and Cheresh 2002).

It has been demonstrated that during migration, cells are continuously breaking and forming contacts between integrins and ECM proteins. Integrins are able to stimulate intracellular signalling pathways to activate the Rho family of small GTPases (Rac and Cdc42) to control actin cytoskeleton reorganisation (Hood and Cheresh 2002). On the other hand, it has been reported that integrins may have a role in the release of MMPs such as MMP-2 and MMP-9, which can degrade and remodel the ECM (Mignatti and Rifkin 1993). Similar to other cytoskeletal characteristics, podosome formation is in part regulated by M-CSF via the PI3K signalling pathway (Wheeler, Smith et al. 2006). Moreover, podosomes are associated with remodelling of the ECM through the localised degradation of ECM proteins by matrix degrading enzymes (Burgstaller and Gimona 2005).

It has been demonstrated that activation of Rac and Rho stimulates the formation of lamellipodia and stress fibres (Ridley and Hall 1992). Stress fibres are a cytoskeleton network consisting of F-actin bundles and myosin II, and are important for cell migration and adhesion due to their association with integrins and focal adhesions (Jones 2000). On the other hand, activation of Cdc42 stimulates the formation of filopodia, with a study revealing that Cdc42, Rho, and Rac can stimulate and activate each other to form different cellular protrusions (Ridley and Hall 1992). Another role for Rho family of small GTPases is to provide stability for cellular protrusions by regulating the formation of cell adhesion contacts. It has been reported that Cdc42 and Rac have key roles in the regulation of focal complexes while Rho is important for the regulation of focal adhesions (Jones 2000).

For a cell to migrate it needs a specific level of force generated by the exterior adhesion and the interior tension (Palecek, Loftus et al. 1997). A study showed that the Rho family of small GTPases has an essential role in mediating the contractility of the cell. RhoB is important for the adhesion of the cell to the ECM via the regulation of integrin expression, and macrophages lacking RhoB have limited migratory capacity (Wheeler and Ridley 2007). On the other hand, RhoA mediates the retraction of the cell 'tail' during macrophage migration, through the regulation of myosin activity (Rougerie, Miskolci et al. 2013). Accordingly, the activity of myosin is connected to actin cytoskeleton dynamics.

Interestingly, in order for migratory cells to reach their maximum velocity, adhesion levels of integrins to the ECM should be at intermediate levels. This is important as high levels of contact will make it hard for a cell to break the contacts, leading to immobilisation of the cell, while low levels of contact decrease the traction necessary for movement (Hood and Cheresh 2002). It is worth mentioning that there are other proteins involved in cell migration such as cortactin, an actin binding protein that has a vital role in the regulation of the actin cytoskeleton (Yamaguchi and Condeelis 2007).

1.5.3 Role of the actin cytoskeleton in macrophage phagocytosis

Phagocytosis can be defined as the uptake of cells and particles that are more than 0.05 µm in diameter (Aderem and Underhill 1999). Phagocytosis is dependent on cellular organisation of the actin cytoskeleton. Indeed, mouse macrophages are unable to uptake IgG-coated erythrocytes after treatment with the actin-perturbing drug cytochalasin B (Kaplan 1977). It has been reported that cells with a high rate of phagocytosis such as macrophages are characterised by the presence of specific phagocytic receptors such as Fc Fragment Of IgG receptors (FcRs) (Aderem and Underhill 1999). Demonstrating the importance of FcRs to phagocytosis, endothelial cells and fibroblasts transfected with cDNA encoding FcRs displayed significantly increased phagocytic capacity (Indik, Park et al. 1995). The most prevalent FcRs associated with the induction of innate immune responses in human macrophages are FcγRI (also known as CD64), FcγRIIA (also known as CD32), and FcγRIII (also known as CD16) (Ravetch 1997). FcγRIIA is composed of immunoreceptor tyrosine-based activation motif (ITAM) located in the cytoplasm, a transmembrane region, and Fc binding site located extracellularly. Binding of a ligand to the Fc receptor causes activation of the ITAM motif via phosphorylation. FcγRI and FcγRIII (CD16) share a similar structure with FcγRIIA (CD32) but lack the presence of ITAM within their cytoplasm (Ravetch 1997). Accordingly, FcγRI and FcγRIII bind to specific transmembrane proteins that display ITAM motif (Sanchez Mejorada and Rosales 1998). The initial phosphorylation of ITAM is mediated by the Src family of tyrosine kinases (Greenberg 1995); this triggers sequential activation of Syk kinase family members , leading to rearrangement and reorganisation of the actin cytoskeleton within the cell and eventually the formation of phagosomes (Ghazizadeh, Bolen et al. 1995).

Alternative downstream effectors of actin cytoskeleton reorganisation and phagosome formation have been proposed during Fc-mediated responses. First, PI3-kinase may contribute to Syk-dependent signalling necessary for FcγR-mediated phagocytosis, as mouse macrophages lacking Syk or exposed to a PI3-kinase inhibitor are still able to polymerise actin during FcγR-mediated phagocytosis of latex beads, but unable to internalise them (Crowley, Costello et al. 1997). The Rho family of small GTPases are also important regulators of the actin cytoskeleton (Caron and Hall 1998). Relatedly, the Rho family of small GTPases can regulate phagocytosis, as Rho inhibition in a mouse macrophage cell line suppressed FcγR aggregation, an initial step during phagocytosis (Hackam, Rotstein et al. 1997). Similarly, the downregulation of Cdc42 and Rac1 (with dominant-negative constructs) in a mouse macrophages cell line prevented the accumulation of actin filaments at the phagocytic cup, leading to the inhibition of phagocytosis (Cox, Chang et al. 1997). Finally, myosins (a family of motor proteins) participate in phagocytic cup development, as myosin II accumulates around the phagocytic cup in macrophages and is therefore thought to impart a mechanical route for the internalisation of modified

lipoprotein (Stendahl, Hartwig et al. 1980). Other myosin family members including myosin IX and myosin V may also participate in macrophage phagocytic cup formation due to their co-localisation with actin filaments during FcγR-mediated phagocytosis (Swanson, Johnson et al. 1999).

Complement-receptors (CR) are also expressed by macrophages which can mediate phagocytosis. including CR1, CR3, and CR4 (Brown 1991). The mechanism of phagocytosis differs between CRs and FcRs. Although, both are dependent on reorganisation of the actin cytoskeleton. While FcγRs engulf material which has been coated with IgG antibodies, CRs bind material covered by complement. The relation of both receptor families to RhoA is considered another important difference between them, as CR-triggered phagocytosis requires the involvement of RhoA, whereas during FcγR-mediated phagocytosis the role of RhoA is controversial (Rougerie, Miskolci et al. 2013). FcR-mediated phagocytosis involves extensive remodelling of the actin cytoskeleton, requiring extensions from the plasma membrane to reach the surface of the material/particle until covering it completely, and the formation of an invagination pushes the particle toward the cell body in order to engulf it (Qualmann and Mellor 2003). Conversely, CRs opsonise material targeted for phagocytosis with minimal changes to their cell membrane, with the material sinking within the cells into the phagosomes, the contact areas are considered loose but rich with different cytoskeletal proteins such as, vinculin, paxillin, α-actinin, and F-actin (Allen and Aderem 1996). Moreover, CRs require additional stimulation in order to opsonise material such as, GM-CSF and TNFα (Aderem and Underhill 1999). It has also been revealed that internalisation of particles via CRs does not induce oxidative burst or pro-inflammatory responses compared to phagocytosis via FcRs (Aderem and Underhill 1999).

Macrophages can also utilise MRC1 for the phagocytosis of pathogens that express fucose or mannose on their surface (Stahl and Ezekowitz 1998). During MRC1-mediated phagosome formation, actin cytoskeleton modifications are required similar to CRs and FcRs, which includes different cytoskeletal proteins such as, talin and F-actin. However, unlike CRs and FcRs, paxillin and vinculin are not involved in MRC1-mediated phagosome formation (Allen and Aderem 1996). MRC1 ligation with pathogens induces a pro-inflammatory response including the release of GM-CSF, IL-6, IL-12, and TNFα.

1.5.4 Role of actin cytoskeleton in foam cell formation

Macrophages are the major inflammatory cell type involved in the progression of atherosclerosis; macrophages readily internalise oxLDL. Excess free cholesterol (unesterified cholesterol) within macrophages is converted via acyl coenzyme A: cholesterol acyl transferase (ACAT) into cholesterol ester within the endoplasmic reticulum, which is subsequently stored as lipid droplets within the cytoplasm of macrophages (Martin and Parton 2006, Weibel, Joshi et al. 2012). It has been reported that cholesterol esters accumulate within the endoplasmic reticulum bilayer until the lipid droplets develop and bud off. Recent evidence has highlighted the potential participation of the cytoskeleton to macrophage foam cell formation. Microtubules are polymers of tubulin which form part of the cytoskeleton and facilitate the movement of lipid droplets within cells (Robenek, Hofnagel et al. 2006). Cytoskeletal proteins such as actin and tubulin have been identified bound to lipid droplets, potentially aiding their movement and storage alongside provision of stability and support to the droplets (Cermelli, Guo et al. 2006). Further support for an association between actin cytoskeleton reorganisation and foam cell formation is provided by the evidence that numerous cytoskeletal proteins are upregulated when macrophages accumulate modified lipoproteins (Becker, Gharib et al. 2010). Furthermore, disruption of the actin cytoskeleton can inhibit the conversion of free cholesterol into cholesterol esters in macrophages (Tabas, Zha et al. 1994). In addition, the interaction between lipid droplets and cytosolic neutral cholesterol ester hydrolase is facilitated by cytoskeletal proteins, which is important for the formation of foam cells (Weibel, Joshi et al. 2012). Accordingly, cytoskeletal proteins appear to contribute to determining the size and composition of lipid droplets. Studies showed that disruption of the actin cytoskeleton of macrophages using actin perturbing drugs results in the formation of smaller lipid droplets with reduced cholesterol ester content, but enriched in triglycerides (Weibel, Joshi et al. 2012). More recent evidence demonstrated that macrophage foam cell formation in mouse atherosclerotic plaques is associated with depolymerisation and subsequent repolymerisation of F-actin via the activation of the Rho family of small GTPases Cdc42 and Rho, but not Rac1 (Singh, Haka et al. 2019).

Accordingly, in this study we aim to modulate the actin cytoskeleton in two divergent macrophage subsets, M-Mac and GM-Mac, and assess effects on their phagocytosis, and foam cell formation, the key mechanisms involved in the progression of atherosclerotic plaques. As such, the findings should provide therapeutic insight into how strategies to modulate the macrophage actin cytoskeleton globally or within specific subsets, may influence the progression of cardiovascular diseases such as atherosclerosis.

1.6 Hypothesis

The actin cytoskeleton is differentially regulated in macrophage subsets and subsequently dictates their function and contribution to atherosclerosis.

1.7 Aim

To address the above hypothesis, the aims of this study are to:

- Assess the effect of actin-perturbing drugs on macrophage polarisation.
- Assess the effect of actin-perturbing drugs on foam cell formation in macrophage subsets.
- Determine the effects of SUMOylation on differing modes of macrophage polarisation and its relation to actin cytoskeleton rearrangements in macrophages.

2 MATERIALS AND METHODS

2.1 Cell culture of THP-1 cells and primary human macrophages

2.1.1 Dulbecco's Phosphate Buffered Saline (DPBS)

Dulbecco's Phosphate Buffered Saline free from magnesium and calcium (Themo Fisher Scientific; catalogue number: 14190), was used and stored at room temperature.

2.1.2 Hank's Balanced Salt Solution (HBSS)

Hank's Balanced Salt Solution with Phenol Red without calcium and magnesium (Lonza; catalogue number: BE10-543F), was used and stored at room temperature.

2.1.3 Serum-free Roswell Park Memorial Institute 1640 (RPMI-1640) Medium

RPMI 1640 without L-glutamine was purchased from Thermo Fisher Scientific (catalogue number: 21870076) and supplemented as in Table 2.1. All supplements were filtered by using a syringe filter to prevent infection, mixed and finally stored at 4°C.

Table 1: Media composition for RPMI Reagent

Reagent	Final Concentration	Supplier
Gentamycin	400 µl/500 ml	PAA (P11-040)
Penicillin and Streptomycin	100 lU/ml & 100 µl/ml	PAA (P11-010)
L-glutamine	2 mM	PAA (M11-004)

2.1.4 10% FBS/RPMI 1640 culture media

Serum-free RPMI 1640 without L-glutamine (Thermo Fisher Scientific; catalogue number: 21870076) was supplemented with foetal bovine serum (FBS) gold to obtain 10% FBS/RPMI. All the components of 10% FBS/RPMI are listed in Table 2.2. FBS was added using a syringe filter to prevent infection, mixed well and finally stored at 4°C.

Table 2: Media composition for 10% FBS/RPMI Reagent

Reagent	Final Concentration	Supplier
Foetal Bovine Serum	10%	PAA (A11-151)
Gentamycin	400 µl/500 ml	PAA (P11-040)
Penicillin and Streptomycin	100 lU/ml & 100 µl/ml	PAA (P11-010)
L-glutamine	2 mM	PAA (M11-004)

2.2 Culture of THP-1 cells

THP-1 cells, which are a human monocytic cell line derived from an acute monocytic leukaemia patient, were obtained from ATCC (catalogue number: TIB-202). Cells were thawed using hot tap water, then 10 ml of 10% FBS/RPMI media was added. Cells were centrifuged at 1500 rpm for 5 minutes. After discarding the supernatant, the cell pellet was resuspended in 10 ml 10% FBS/RPMI media. Cells were then transferred to a flask containing 30 ml of 10% FBS/RPMI media and incubated at 37 ^{o}C in 5% CO_2.

2.2.1 Subculturing of THP-1 cells

To maintain cultures, the cell suspension was centrifuged at 1500 rpm for 5 minutes. After discarding the supernatant, the cell pellet was resuspended in 10% FBS/RPMI media. Cells were then added to a fresh flask at $1x10^5$ per ml in 10% FBS/RPMI media. In order to maintain cells between $5x10^4$ cells per ml and $8x10^5$ cells per ml, medium was renewed, and cells density checked by counting every 3 days.

2.2.2 Counting of THP-1 cells

To maintain cultures, the THP-1 cells were counted using a Neubauer Chamber (Haemocytometer). To calculate the concentration of the cells, the following formula was applied:

$$\text{Concentration} = \frac{\text{Number of cells x } 10^4}{\text{Number of large corner squares (i.e up to 4)}}$$

2.2.3 THP-1 cell seeding and differentiation into macrophages

Counted cells were seeded at $1x10^5$ cells/ml in fresh 10% FBS/RPMI media. To differentiate THP-1 cells into macrophages, cells were treated with 8.1 µM of Phorbol 12-myristate 13-acetate (PMA) (Sigma; catalogue number: P1585) for 72 hours prior to use. THP-1 cells differentiated into macrophages were treated with 20 ng/ml of either M-CSF (Miltenyi Biotec; catalogue number: 130-093-963), or GM-CSF (Miltenyi Biotec; catalogue number: 130-093-862) for 7 days by changing the media every 3 days to obtain different macrophage subsets (anti- or pro-inflammatory macrophages respectively).

2.2.4 THP-1 cells storage

Confluent cell suspension was centrifuged at 1500 rpm for 5 minutes. After discarding the supernatant, the cell pellet was resuspended in 1 ml of Cell Banker II cell freezing media (Amsbio; catalogue number: 11891) and then transferred to cryovials. Cryovials were placed at -80 ºC freezer for 24 hours then stored under liquid nitrogen.

2.3 Human monocyte isolation from fresh blood with SepMate-50 tubes

Human peripheral blood mononuclear cells (PBMCs) were isolated from the whole blood of healthy donors, (which were collected under South West 4 Research Ethics Committee reference 09/H0107/22) and diluted in PBS without calcium and magnesium (Themo Fisher Scientific) 1× (ratio 1:1). Diluted samples were subjected to density gradient separation on 15 ml of Ficoll-Paque (Sigma; catalogue number: GE17-1440-02) within SepMate-50 tubes (Stem cell technologies; catalogue number: 85450). Keeping the tube vertical, diluted blood was added down the side of the tube, then the tube centrifuged for 10 minutes at 2,500 rpm at room temperature. After centrifugation, the top layer which contains the peripheral blood mononuclear cells (PBMCs) was tranferred (by pouring) into a Falcon tube. PBMCs were then washed three times using sterile HBSS (5-7 ml of buffer if 2-3 ml of blood was used) under centrifugation of 10 minutes at 1600 rpm for each wash. To isolate monocytes by adhesion, the cell pellet was resuspended in 10% FBS/RPMI media and 1 x 10^6 of cells (PBMCs)/well were added to 6-well tissue culture plate for two hours at 37 ºC. After two hourss, the non-adherent cells were removed by washing 3 times with sterile DPBS. To mature freshly isolated monocytes into macrophages, fresh 10% FBS/RPMI media supplemented with 20ng/ml of M-CSF (Miltenyi Biotec; catalogue number: 130-096-491) or GM-CSF (Miltenyi Biotec; catalogue number: 130-095-372) were added and cells were cultured for 7 days by changing 10% FBS/RPMI media supplemented with 20 ng/ml of M-CSF or GM-CSF every 3 days.

2.4 Molecular biology

2.4.1 Cell lysis

Cells were washed twice with DPBS and lysed in 350 µl of Buffer RLT obtained from RNeasy Plus Mini Kit (Qiagen; catalogue number: 74136). Before use, 10% β-mercaptoethanol was added to the buffer RLT to inactivate endogenous RNases. To facilitate lysis of cells, wells were scraped with a rubber plunger from a 1 ml syringe. Lysates were transferred to DNAse/RNAse-free eppendorf tubes and stored at -20 ºC freezer.

2.4.2 RNA extraction and purification

RNA isolation and purification were performed using the Qiagen RNeasy Plus Mini Kit (Qiagen; catalogue number: 74136). Cell lysates were transported to gDNA eliminator spin columns to shear genomic DNA and reduce viscosity of lysates, then centrifuged at 10,000 rpm for 30 seconds. To adjust binding conditions, 350 µl of 70% ethanol was added to each sample. Samples were then applied to RNeasy spin columns for the adsorption of RNA to the membrane and centrifuged at 10,000 rpm for 15 seconds. Contaminants were removed with simple wash spins (700 µl of buffer RW1, and twice with 500 µl of buffer RPE). Finally, to elute the RNA, 30 µl of RNAse-free water was added and centrifuged at 10,000 rpm for 1 minute. Columns were discarded, and the RNA was stored at -20°C if not used immediately.

2.4.3 RNA quantification

The concentration of total RNA was assessed using a NanoDrop spectrophotometer (LabTech; model number: ND-1000). RNA samples (1.5 µl) were added to the NanoDrop to quantify the RNA concentration (ng/ml) by measuring the absorbance at 230 nm, 260 nm, and 280 nm. Samples with a 260/280 ratio = 2.0 indicates pure nucleic acid content, whereas samples with 260/230 ratio ≤ 1.8 (indicates the presence of contaminants such as proteins, ethanol or phenol) or a 260/230 ratio >2.2 were excluded from further analysis.

2.4.4 Reverse transcription polymerase chain reaction (RT-PCR)

Reverse transcription of RNA to generate cDNA was performed using the QuantiTect Reverse transcription kit (Qiagen; catalogue number: 205311). Firstly, 2 µl of genomic DNA wipeout buffer was applied to each RNA sample to remove RNA secondary structure, then the sample was denatured at 42 ºC for 2 minutes in a thermal block cycler (Bio-Rad; model number: C1000). Samples were

immediately cooled on ice. Subsequently, 6 µl of master mix was added to each sample, (composed of Quantiscript Reverse Transcriptase, Quantiscript RT Buffer, and RT Primer Mix) and incubated at 42 ºC for 30 minutes, then at 95 ºC for 3 minutes. Finally, samples were cooled to 4 ºC and cDNA was stored at -20 ^{o}C.

2.4.5 Quantitative PCR (qPCR)

A LightCycler 480 SYBR Green I Master kit (Roche; catalogue number: 04707516001) was used to perform quantitative PCR (qPCR). Firstly, a SYBR Green Mastermix was added to each well of a 96 well plate (Greiner Bio-one; catalogue number: 669 285) and composed of 5 µl SYBR green, 3 µl PCR grade water and 1 µl primers. Secondly, 1 µl of cDNA was added to the Mastermix within each well. Samples of cDNA were previously normalised to the same concentration, were tested as duplicates, and a blank RT reaction sample was used as a negative control for each primer. Plastic plate sealers (Greiner Bio-one; catalogue number: 676040) were used to seal the plates. The plates were then centrifuged at 2,500 rpm for 30 seconds using an MPS-1000 mini-plate spinner (Labnet). The plates were then loaded onto a LightCycler 480 real-time PCR System (Roche) to detect cDNA sequences under the following conditions:

Table 3: Program used qPCR on the LightCycler 480 system

STEP	TEMPERATURES (ºC)	TIME
Pre-Incubation	95	5 minutes
Amplification (x45 cycles)		
Denaturation	95	10sec
Annealing	60	10sec
Elongation	72	10sec
Final elongation	72	10sec
Melting curve	95	5sec
	65	1min
	97	Continuous
Cooling	40	-1.5 ºC/sec

Individual genes within a sample generate a specific expression intensity which is presented as Cycles to Threshold (CT), this value indicates the cycle number whereby the amplified cDNA reaches a linear threshold of detection. The CT value is used to calculate the fold change in mRNA expression using the following equation:

$$fold\ change = 2^{-\Delta CT}$$
$$where\ \Delta C_T = C_{T,\,\text{experimental}} - C_{T,\,control}$$

Considering all cDNA samples were run in duplicate, two C_T values were generated per sample. These values were averaged to give a mean C_T value for each sample.

2.4.6 Primer design

Primers for the analysis of qPCR were designed using the Primer Blast software available on the Sigma-Aldrich website and purchased from Sigma. Additional pre-designed and validated QuantiTect primer assays were purchased from Qiagen if the Sigma primers proved problematic. The table below displays the characteristics of the primers used for qPCR analysis:

Table 4: List of primers used for qPCR

GENE	FORWARD/REVERSE	PRIMER SEQUENCE
ABCA1	REVERSE	CCTATGTGCTGCCATATGAAGCTG
	FORWARD	CTGGCAAGGTACCATCTGAGGTCT
ABCG1	REVERSE	CTGCACTGTGACATCGACGAGA
	FORWARD	CTCTGCCCGGATTTTGTACCTG
CD36	REVERSE	GTGAAGTTGTCAGCCTCTGTTCCA
	FORWARD	GTGCAAAATCCACAGGAAGTGATC
CSF1	REVERSE	TTGGGGTACAGGCAGTTGCAATCA
	FORWARD	CAAGGCCTGCGTCCGAACTTTCTA
CSF1R	REVERSE	AGCTCAAGTTCAAGTAGGCACTCT
	FORWARD	TCCCTCAACAATCTGACTTTCATA
CSF2	REVERSE	AATATTCCCATTCTTCTGCCATGC
	FORWARD	ACTTTCTGCTTGTCATCCCCTTTG
CSF2RA	REVERSE	ATGACATTTGGGGCCAGGCG
	FORWARD	CCGCCGTGCCTGGGTAAATT
FSCN1	REVERSE	CCTTGTTATAGTCGCAGAAC
	FORWARD	CAACATCAAAGACTCCACAG
IL-10	REVERSE	TCTATAGAGTCGCCACCCTGATGTC
	FORWARD	TCTTCCCTGTGAAAACAAGAGCAAG
LOX-1 (OLR1)	REVERSE	GACAGCGCCTCGGACTCTAAATAA
	FORWARD	TGTTACCTATTTTCCTCGGGCTCA
MMP12	FORWARD	TTACCCCCTTGAAATTCAGCAAGA
	REVERSE	CGTGAACAGCAGTGAGGAACAAGT
MRC1	REVERSE	ATCCGTCCAAAGGAACGTGTGT
	FORWARD	AAATTGGCAAGAGGCACGAAAA
MSR1	REVERSE	GCCAGGGTTTGAGACAGAAAGTGT
	FORWARD	GGTAGACTCACAGCCGTCCAACTT

NCOR1	REVERSE	ACGGCCCTCTTCAGTCTCCTCT
	FORWARD	GTTGGTGAGGAGCTGCTTGGTT
PPARA	REVERSE	GGACTCAACAGTTTGTGGCAAG
	FORWARD	CCGAGCTCCAAGCTACTCTT
RDX	REVERSE	TCGAGTCTGTTCTTCTAGTTC
	FORWARD	CATCAGAAGCAGTTGGAAAG
SPARC	REVERSE	AAAGGGTTAAACCACAGGTCATTA
	FORWARD	GACACAAAAACACATGAGCATACA
TGFBI	REVERSE	GTTGGTGGCTAGGATGTCTTTATT
	FORWARD	CCCTAGTGAGACTTTGAACCGTAT
TGFBR1	REVERSE	CCATTGATATTGCTCCAAACCACA
	FORWARD	ATCGTCGAGCAATTTCCCAGAATA
TGFBR2	REVERSE	CGAAAGCATGAAGGACAACGTG
	FORWARD	ACTGAAGCGTTCTGCCACACAC
TGFBR3	REVERSE	AGTGTGTGCCTCCTGACGAAGC
	FORWARD	TGCTCCGATCACAAAGGCTGCA
TIMP3	REVERSE	CTCGTTCTTGGAAGTCACAAAGCA
	FORWARD	CTTCCGAGAGTCTCTGTGGCCTTA
VCL	REVERSE	GATTTATTAGCAGTACCAACCG
	FORWARD	AGAGGTATTTGATGAGAGGG

2.5 Western blotting

2.5.1 Protein extraction by sodium dodecyl sulphate (SDS) lysis

Cells were washed twice with DPBS and subsequently lysed using 100 µl of SDS lysis buffer (5% SDS, 50 mm Tris hydrochloric acid (HCL) (pH 6.8), 10% glycerol). To facilitate lysis of cells, wells were scraped with a rubber plunger from a 1 ml syringe. Lysates were transferred to 0.5 ml eppendorf tubes and stored within a -20 ºC freezer until further anlaysis.

2.5.2 Protein assay

To calculate the protein concentration of samples, the colorimetric Bicinchoninic Acid (BCA) Assay kit (Thermo Scientific; catalogue number: 23235) was used in accordance with the manufacturer's instructions. Using a 96-well plate, 140 µl of High-Performance Liquid Chromatography water (HPLC) grade water was added to the appropriate wells. To construct a standard curve, 0, 0.1, 0.25, 0.5, 1.0, 2.5, 5.0 and 10 mg/ml of bovine serum albumin were used. Then, 1 µl of the sample was added to the appropriate wells, with all samples and standards analysed in duplicate. Next, 150 µl of BCA reaction mix solution (prepared from 50% of reagent A, 48% of reagent B, and 2% of reagent C) was added to the respective wells, and the plate was incubated at 37 ºC for 1 hour. The plate was then read at 560

nm in a GloMax plate reader (Promega). Finally, a standard curve was plotted, and the protein concentration of the samples calculated.

2.5.3 Gel electrophoresis

To ensure equal volume and protein concentration of each sample, the approrpaite volume of HPLC water was added to cell lysates. Before heating samples to 95 ºC for 5 minutes, 1.5 µl of Bromothenol blue and 1.5 µl of β-mercaptoethanol were added to each sample, to break all the disulfide bonds and denature the protein of interest, then, a BLUeye Prestained Protein Ladder (Geneflow; catalogue number: S6-0024) was prepared as a molecular weight marker. Samples were loaded into 7.5% Mini-PROTEAN® TGX™ Stain-Free Gels (Bio-Rad; catalogue number: 456-8024) and subjected to electrophoresis through a 10% running buffer containing 1X Tris/ Glycine/ SDS (TGS) (Bio-Rad; catalogue number: 161-0732) in a Mini-PROTEAN® Tetra Cell (Bio-Rad; catalogue number: 165-8004) at 200 V for 35 minutes.

After 35 minutes of electrophoresis, the precast gel packs were opened and placed within a ChemiDoc MP System and exposed to ultraviolet (UV) light for 5 minutes. The principle of stain-free gels is based on the interaction between tri-halo compounds (present in the precast gel) and tryptophan residues (present in proteins). This interaction produces a fluorescent signal which is activated and detectable under UV light. The images produced were used to both control and calculate the total protein amount loaded.

2.5.4 Protein transfer

Following electrophoresis and imaging under UV light, the Trans-Blot Turbo Transfer Starter System (Bio-Rad; catalogue number: 170-4155) was used to transfer seperated proteins within the gels onto a 0.2 µM mini nitrocellulose membrane (Bio-Rad; catalogue number: 170-4158) or 0.2 µM midi nitrocellulose membrane (Bio-Rad; catalogue number: 170-4159).

2.5.5 Immunodetection

After protein transfer, in order to avoid non-specific binding of subsequently deployed antibodies to the surface of the membrane, the membrane was incubated with a blocking solution consisitng of 5% skimmed milk powder in Tris-Buffered Saline-Tween (TBS-T) (20 mM Tris, 137 mM NaCl, 0.1% (v/v) Tween; pH:7.6) for one hour. Then, membranes were incubated with the relevant primary antibody diluted in SignalBoost Immunoreaction Enhancer Kit A (Merck Milipore; catalogue number: 407207-1kit) at room temperature for 1 hour or 4 ºC overnight (Table 5 shows the details of antibodies used).

Subsequently, membranes were washed with 5% skimmed milk powder/TBS-T (twice briefly and once for 60 minutes), then incubated with the relevant horseradish peroxidase (HRP)-conjugated secondary antibody (as detailed in Table 6) diluted in SignalBoost Immunoreaction Enhancer Kit B (Merck Millipore; catalogue number: 407207-1kit) for 1 hour at room temperature. The membrane was then subjected to multiple washes with TBS-T (twice briefly, twice for 30 minutes, and once for 5 minutes). Finally, any positive immuno-labelling was detected using a ChemiDoc MP Imaging System (Bio-Rad) after incubating the membrane with Luminate Forte Western HRP substrate (Merk Millipore; catalogue number: WBLUF0100).

2.5.6 Densitometry

To determine the density of detected bands (densitometry), Image Lab software (Bio-Rad) was used. In order to analyse and assess the differences between band densities, stain free gels were used to normalise the data obtained.

Table 5: List of primary antibodies used for Western blotting

Antibody	Species	Dilution used	Molecular weight	Catalogue number	Company
TGFβI	Goat	1/250	64 kDa	Sc14741	Santa cruz
OLR1	Mouse	1/500	31 kDa	MABS186	Merck Millipore
CD36	Rabbit	1/1000	90 kDa	D8L9T	Cell Signaling Technology
NCOR2	Rabbit	1/500	220 kDa	NB120-2781	Novus Biologicals
MSR1	Goat	1/1000	80 kDa	AF2708	R&D systems
pSTAT5A	Rabbit	1/1000	90 kDa	PA5-37744	Invitrogen
TGFβR1	Rabbit	1/500	56 kDa	AB135814	abcam
TGFβR2	Rabbit	1/1000	65 kDa	AB186838	abcam
TGFβR3	Rabbit	1/1000	110 kDa	2519S	Cell Signaling Technology

Table 6: List of secondary antibodies used for Western blotting

Antibody	Species	Dilution used	Catalogue number	Company
Anti-Goat	Rabbit	1/1000	P0449	Dako
Anti-Rabbit	Goat	1/1000	P0448	Dako
Anti-Mouse	Goat	1/1000	P0447	Dako

2.6 Immunocytochemistry on cell cultures

2.6.1 Immunocytochemistry for F-actin using phalloidin

Cells were seeded at $1x10^5$ cells/well on 13mm circular glass coverslips in a 24 well plate. Cells were then fixed using 500 µl/well of 3% paraformaldehyde in DPBS for 10 minutes. Subsequently, wells were washed twice with DPBS. To permit permeabilisation of the cells and permit access to the F-actin filaments, cells were incubated with 0.2 % Triton/DPBS (500 µl/well) for 15 minutes, followed by three washes with DPBS (500 µl/well) for 3 minutes. Cells were then incubated with 400 µl of Image-iT™ FX fluorescence signal enhancer (Thermo Fisher Scientific; catalogue number: I36933) for 30 minutes to prevent non-specific binding of antibodies to cells. Cells were then incubated with (300 units/ml) AlexaFluor 594-phalloidin (Thermo Fisher Scientific; catalogue number: 21836) in DPBS (400 µl/well for 30 minutes in the dark). Cells were subsequently washed 3 times for 3 minutes with 500 µl/well of DPBS then coverslips were removed and mounted upon glass microscope slides with Prolong gold mounting medium containing DAPI (4',6-diamindino-2-phenylindole) (Molecular Probes; catalogue number: P36931) for labelling of nuclei. Finally, a fluorescent microscope was used to visualise F-actin filaments (red) and nuclei (blue), and the percentage of nucleated cells positive for F-actin, or the F-actin content within nucleated cells were assessed in six random x20 magnification fields per coverslip, with average number of cells in x20 magnification was approximately 200 cells/image, while average number of cells in x40 magnification was approximately 20 cells/image.

2.6.2 Fluorescent immunocytochemistry (ICC)

Cells were seeded at $1x10^5$ cells/well on 13mm circular glass coverslips in a 24 well plate. All volumes used for the 24 well plates were between 250 and 500 µl per well. Cells were then fixed using 3% paraformaldehyde in DPBS for 10 minutes. Subsequently, wells were washed twice with DPBS and subjected to permeabilisation through incubation with 0.2 % Triton/DPBS for 15 minutes, followed by washing with DPBS for 2 minutes. Next, cells were incubated in Image-iT™ FX fluorescence signal enhancer (Thermo Fisher Scientific; catalogue number: I36933) for 30 minutes to prevent non-specific binding of antibodies to cells. Liquid was carefully removed, and cells were incubated with relevant primary antibody diluted in DPBS at 4 ºC overnight (see Table 7). The next day, cells were washed 3 times for 2 minutes with DPBS and then incubated with relevant fluorescently-conjugated secondary antibody for 1 hour at room temperature in the dark (see Table 8). Cells were washed 3 times for 3 minutes with DPBS, then coverslips were removed and mounted upon glass microscope slides with Prolong gold mounting medium containing DAPI (4',6-diamindino-2-phenylindole) (Molecular Probes;

catalogue number: P36931) for labelling of the nuclei. Finally, a fluorescent microscope was used to image and count cells within ten random x 40 magnification fields. Data is presented as percentage of nucleated cells (blue) immune-labelled positive (green or red). Quantification was done blinding using manual counting.

Table 7: List of primary antibodies used for ICC

Antibody	Species	Dilution used	Catalogue number	Company
TGFβI	Goat	1/250	Sc14741	Santa cruz
MMP-12	Mouse	1/500	ab56305	Abcam
PPARα	Rabbit	1/500	NBP1-03288	Novus Biologicals
NCOR1	Rabbit	1/800	E4S4N	Cell Signaling Technology
POU2F1	Rabbit	1/1000	GTX105202	GeneTex
SPARC	Mouse	1/500	MAB941	R&D systems
pSMAD3	Rabbit	1/250	44-246G	Invitrogen
NCOR2	Rabbit	1/500	HPA001928	Sigma
pSTAT5A	Rabbit	1/200	C71E5	Cell Signaling Technology
OLR1	Mouse	1/250	MABS186	Merck Millipore

Table 8: List of secondary antibodies used for ICC

Antibody	Species	Dilution used	Catalogue number	Company
Anti-Goat-DyLight 488	Horse	1/200	DI-3088	Vector laboratories
Anti-Rabbit-DyLight 488	Horse	1/200	DI-1088	Vector laboratories
Anti-Mouse-DyLight 488	Horse	1/200	DI-2488	Vector laboratories
Anti-Rabbit-DyLight 594	Goat	1/200	A11012	Invitrogen

2.6.3 Live/dead assay

To assess the incidence of cell death, a Ready Probes cell viability imaging kit (blue/green) (Thermo Fisher Scientific; catalogue number: R37609) was used. Cells were seeded at $1x10^5$ cells/well in a 24 well plate. After the appropriate experimental conditions, two drops each of NucBlue Live and NucGreen Dead reagents/ml were added to each well and incubated for 20 minutes. An inverted fluorescence microscope was used to image and count the number of dead (green labelled) and live (blue labelled) cells. Data is presented as percentage of dead cells.

2.7 Oil red O histochemistry on cells

Cells were seeded at $1x10^5$ cells/well on 13mm circular glass coverslips in a 24 well plate and co-incubated with 10 µg/ml Dil-conjugated human oxidized low-density lipoprotein (Dil-oxLDL) (Thermo Scientific Fisher; catalogue number: L34358) for 24 hours to assess lipid accumulation and subsequent foam cell formation. The next day, cells were fixed with 3% paraformaldehyde in DPBS and rinsed in DPBS. Afterwards, cells were rinsed in 60% isopropanol for approximately 20 seconds to permeabilise the cells, then stained wih Oil red O which is a fat soluble dye that is used for staining neutral triglycerides and lipids, for 15 minutes at room temperature. Oil red O was removed carefully, and cells were rinsed in 60% isopropanol for approximately 20 seconds. For brightfield microscopy assessment, cells were washed in distilled water and subsequently stained for 3 minutes with Mayer's haematoxylin (Merck; catalogue number: 100579). Cells were then incubated in tap water for 5 minutes to aid 'blueing' of the nuclei. Coverslips were removed and mounted upon glass microscope slides with VectaMount AQ Aqueous Mounting Medium (VectorLabs; catalogue number: H-5501-60). For Fluorescence microscopy assessment, cells were washed in distilled water, coverslips removed, and mounted with ProLong gold mounting medium containing DAPI (Molecular Probes; catalogue number: P36931) for labelling the nuclei. Finally, cells were analysed with a brightfield or fluorescent microscope respectively, to visualise lipid accumulation (red). Data is presented as percentage of nucleated cells (blue) with lipid accumulation (red) and termed as foam cell macrophages.

2.8 Efferocytosis assay

Recipient PBMC monocyte-derived monocytes macrophages were seeded at $1x10^5$ cells/well in a 24 well plate. To produce apoptotic labelled macrophages, THP-1 cells were differentiated into macrophages and seeded at $1x10^5$ cells/well in a 24 well plate, and labelled with 5µM Vybrant® CFDA SE (carboxyfluorescein diacetate, succinimidyl ester) Cell Tracer Kit (Invitrogen; catalogue number: V12883) in DPBS for 15 min at room temperature. The cells were then placed in fresh 10% FBS/RPMI media for six hours. To induce apoptosis, cells were washed twice with DPBS and then 2.5 ng/ml of Super-Fas-Ligand (Enzo; catalogue number: ALX-522-020-C005) in serum free medium was added and cells incubated for 24 hours. For assessment of efferocytosis, the labelled apoptotic THP-1 macrophages which were in suspension (which have therefore undergone apoptosis and detached) were collected, vortexed and resuspended in 10% FBS/RPMI medium. At the same time the recipient cells were washed twice with DPBS and then co-incubated with the 10% FBS/RPMI media containing the labelled apoptotic THP-1 cells for 24 hours. Finally, images were acquired under phase-contrast

and the green fluorescence channel using an inverted fluorescence microscope, within six random x20 magnification fields per well. Data was presented as the percentage of macrophages containing fluorescently-labelled apoptotic cells.

2.9 Cell Fractionation assay

To permit the assessment of protein expression within cell membrane fractions alone, a Cell Fractionation kit (Cell Signaling Technologies; catalogue number: 9038) was used. Cells were seeded at $1x10^5$ cells/well in a 24 well plate and exposed to the appropriate experimental conditions. All subsequent steps were perfomred on ice or at 4 °C, with the exception for the addition and sonication of the CyNIB buffer. Cells were washed with cold PBS once, and then trypsinised through incubation with 0.5% Trypsin-EDTA (Thermo Fisher Scientific; catalogue number: 15400054) at 37°C, 5% CO_2 for 5 minutes until cells were detached from the plate. Cold 10% FBS/RPMI media was then added to deactivate the trypsin. Next, cells were collected and centrifuged at 1,000 rpm for 5 minutes. The supernatant was then discarded, and the cell pellet was washed with cold PBS. To separate the cytoplasmic fraction, cells were centrifuged at 1,400 rpm at 4 °C for 5 minutes and the supernatant discarded. The remaining cell pellet was resuspended in cytoplasm isolation buffer, vortexed for 5 seconds and incubated on ice for 5 minutes, then centrifuged for 5 minutes at 1,400 rpm. The supernatant was saved which represents the cytoplasmic fraction. To separate the membrane fraction, the cell pellet was resuspended in membrane isolation buffer, vortexed for 15 seconds, then incubated on ice for 5 minutes. Cells were then centrifuged at 10,000 rpm for 5 minutes and the supernatant was saved, which represents the membrane fraction. To separate the cytoskeletal and nuclear fraction, the cell pellet was resuspended in cytoskeleton/nucleus isolation buffer, sonicated for 5 seconds at 20% power for 3 times and saved. This represents the cytoskeletal and nuclear fraction. All lysates were stored within a -20 °C freezer.

2.10 Immunohistochemistry of human coronary atherosclerotic plaques

2.10.1 Human coronary samples

Coronary artery segments were collected from cadaveric heart donors from the Bristol Valve Bank and incorporated into the Bristol Coronary Artery Biobank under National Research Ethics Service approval

(08/H0107/48). The patients with coronary arteries histologically defined as non-diseased, harbouring stable, or unstable plaques (n=10/group) were of similar age and gender ratio, as described previously (Di Gregoli, Somerville et al. 2020). Coronary artery plaques were histologically classified as stable or unstable through evaluation of intraplaque cellular content, lipid/necrotic core size, and collagen amount, as shown to be effective delineators in human coronary plaque phenotyping (Davies, Richardson et al. 1993, Falk, Nakano et al. 2013), and as described previously (Di Gregoli, Jenkins et al. 2014, Di Gregoli, Mohamad Anuar Nur et al. 2017).

2.10.2 Immunohistochemistry (IHC)

Serial paraffin sections were deparaffinised through incubation with Clearene (Surgipath) for three periods of 5 minutes. Afterwards, sections were rehydrated with incubation in 100% ethanol twice for 5 minutes, once in 90% (v/v) ethanol for 5 minutes, once in 70% (v/v) ethanol for 5 minutes, and finally 5 minutes in HPLC water. To ensure efficient antigen retrieval, sections were microwaved for 2 x 6 minutes in 10 mM citrate buffer (pH 6.0). Slides were left for 30 minutes at room temperature to cool, and then transferred for 5 minutes under running tap water. Slides were then washed 3 x 5 minutes with PBS, and then the tissue sections delineated using a hydrophobic wax pen (ImmEdge Pen; Vector Labs; catalogue number: H-4000). In order to inhibit endogenous peroxidase activity, slides were incubated with BLOXALL Blocking Solution (Vector laboratories; catalogue number: SP-6000) for 10 minutes. Slides were then incubated with 10% (v/v) horse serum/PBS for 30 minutes at room temperature. This was followed by 3 washes in PBS and incubation with 50 µl of appropriate primary antibody (see Table 9 for details) diluted in PBS, overnight at 4 °C. A negative control was included using the same species IgG diluted to the same IgG concentration as the primary antibody that was used. Next day, sections were washed 3 times in PBS then incubated with 50 µl of relevant biotinylated secondary antibody (see Table 10 for details) diluted in PBS, for 30 minutes at room temperature. Again, sections were washed 3 times with PBS then incubated with 50 µl of Extravidin-horseradish peroxidase (Sigma; catalogue number: E2886) diluted 1:200 in PBS, for 30 minutes at room temperature, followed by 3 washes with PBS. To detect antibody labelling, 250 µl of SIGMA*FAST* 3,3'-Diaminobenzidine (DAB) Peroxidase Substrate (Sigma; catalogue number: D4293) was added to sections for 10 minutes at room temperature and then sections were washed in tap water. To visualise cell nuclei, sections were subsequently stained for 3 minutes with Mayer's haematoxylin (Merck; catalogue number: 100579). Slides were then washed in tap water for 5 minutes to remove haematoxylin and aid 'blueing' of the nuclei. Sections were then dehydrated through 5-minute incubations in a graduated ethanol series (once in 70% ethanol, once in 90% ethanol, and twice in 100% ethanol). To remove ethanol, sections were incubated 3 x 5 minutes with Clearene. Slides were finally

mounted with coverslips in DPX mountant (Merck; catalogue number: 109249). Cells with both blue and brown staining were detected as positive nucleated cells, where cells with only blue nuclei were considered as negative cells. Ten fields at x40 magnification were acquired per section using a computerised image analysis program (Image Pro Plus; DataCell, Maidenhead, United Kingdom). The percentage of positive cells was quantified using ImageJ.

Table 9: List of primary antibodies used for IHC

Antibody	Species	Dilution used	Catalogue number	Company
SENP1	Rabbit	1/100	HPA011765	Sigma
pSTAT5A	Rabbit	1/100	PA5-37744	Invitrogen
SUMO1	Rabbit	1/50	4930S	Cell Signaling Technology
SUMO2/3	Rabbit	1/100	NBP1-95473	Novus biologicals

Table 10: List of secondary antibodies used for IHC

Antibody	Species	Dilution used	Catalogue number	Company
Anti-Rabbit IgG-Biotin	Goat	1/200	B7389	Sigma

2.11 Statistical analysis

Values are expressed as mean ± standard error of the mean (SEM). Group values were compared using Graphpad Instat. Data from THP-1 cell and monocyte/macrophage experiments comparing two groups was analysed using a two-tailed, paired t-test. An analysis of variance (ANOVA) multiple comparison test with Student-Newman-Keuls Multiple Comparisons tests was used for experiments with greater than two comparison groups. In all cases, statistical significance was concluded when the two-tailed probability was less than 0.05. N-values in macrophages differentiated from THP-1 cells represent number of replicates, while n-values in Human peripheral blood mononuclear cells (PBMCs) represent the number of healthy donors and n-values in plaque samples represent number of patients with coronary arteries histologically defined as non-diseased, harbouring stable, or unstable plaques (n=10/group) were of similar age and gender ratio.

3 EFFECT OF ACTIN-PERTURBING DRUGS ON THE POLARISATION OF DIVERGENT MACROPHAGE SUBSETS

3.1 Introduction

3.1.1 THP-1 as a model for human macrophages

THP-1, which is a cell line, originated from a child patient suffering from acute monocytic leukaemia, and were established first by Tsuchiya et al in 1980 (Tsuchiya, Yamabe et al. 1980). This cell line is universally used as a model to study the behaviour and function of macrophages (Chanput, Mes et al. 2014). THP-1 cells display as round single nucleated cells in suspension and express specific monocytic markers (Qin 2012). It has been reported that differentiation of THP-1 cells into macrophage-like cells can be achieved either by incubation with phorbol-12-myristate-13-acetate (PMA), or 1 α,25-dihydroxy vitamin D3 (vD3) for 72 hours (Chanput, Mes et al. 2014). It has been shown that the majority of THP-1 cells treated with PMA stick to tissue culture surfaces and change their morphology to a flatter shape (Qin 2012).

Macrophages differentiated from THP-1 cells with PMA for 72 hours show more similarities to PBMC monocyte-derived macrophages compared to macrophages originated from THP-1 cells exposed to vD3 for 72 hours (Qin 2012, Chanput, Mes et al. 2014). THP-1 derived macrophages incubated with PMA for 72 hours differentiate into more mature cells, with low proliferation rates, and high phagocytic capacity (Qin 2012). THP-1 derived macrophages show marked expression of macrophage-associated cell surface markers including CD11b and CD14, similar to PBMC monocyte-derived macrophages.

The use of THP-1 cells has lots of advantages. First, the proliferation rates of THP-1 monocytes compared to primary human macrophages is significantly higher, with THP-1 numbers able to quadruple in less than four days. Second, THP-1 cells are easy to handle and are safe to use in tissue culture since there is no evidence of any viruses or toxins within the cells (Chanput, Mes et al. 2014). Third, due to their immortalised property, THP-1 cells can be cultured for up to 25 passages without change in their activity or sensitivity. It has been demonstrated that THP-1 cells can be preserved in liquid nitrogen for many years and remain viable after thawing (Mangan and Wahl 1991). Finally, compared to the inherent heterogeneity observed in PBMC monocyte-derived macrophages between different donors, THP-1 cells decrease this variability making reproducibility of results easier. This property is important when studying chemicals/molecules with high variability in their biological functions such as ox-LDL (Rogers, Thornton et al. 2003). However, this can also be considered as a weakness, when considering therapeutics will need to be applicable to heterogeneous populations. Other limitations have been reported for THP-1 cells including the demonstration that the reduced expression of LDL receptors in THP-1 cells requires higher doses of ox-LDL compared to their primary PBMC-derived counterparts (Chanput, Mes et al. 2014). In addition to THP-1 cells, there are other

immortalised human-monocyte macrophage cell lines, for example, U937, ML-2, and MMO MAC6 cells. Results showed that the monocytic properties for these cells were weaker when compared to THP-1 cells (Chanput, Mes et al. 2014).

3.1.2 Role of fasudil and pravastatin as actin perturbing drugs

Rho-associated protein kinases (ROCK), serine/ threonine kinases with a molecular weight of 160 kDa, consist of a middle coiled-coil domain, an amino-terminal kinase domain, a Rho-binding domain, and a carboxy-terminal cysteine-rich region. The carboxy-terminal region has a power of hydrogen (PH) domain which is important for the auto inhibition of the amino-terminal region of ROCK (Julian and Olson 2014). ROCKs were the first identified down-stream kinases of the small family GTPases, such as RhoA which is a well-characterised regulator of the cell cytoskeleton. RhoA is usually located in the cytosol of the cell in an inactive form. When a stimulator affects the cell (such as growth factor activation of Guanine nucleotide exchange factors (GEFs)), the inactive RhoA in a Rho-GDP form is changed to Rho-GTP form by Rho-GEF. This activation leads to the translocation of activated RhoA to the cell membrane. On the cell membrane, activated RhoA can bind and activate a number of kinases including ROCKs (Liu, Li et al. 2013).

Studies showed that humans have two ROCK isoforms: ROCK1 and ROCK2. They are located on different chromosomes, with ROCK1 located on chromosome 18 while ROCK2 is located on chromosome 2 (Dong, Yan et al. 2010). ROCK1 and ROCK2 share 65% homology of their amino acid sequence and 90% of their kinase domain (Dong, Yan et al. 2010). It has been reported that the two isoforms are differentially expressed throughout the body, for example ROCK2 is expressed within the brain and heart, while ROCK1 is predominantly expressed within the liver, kidney, and lung (Dong, Yan et al. 2010).

ROCK1 and 2 have been proposed to play contributory roles in atherogenesis, as deployment of a ROCK1/2 inhibitor (Y-27632) in mice decreased early atherosclerotic lesion formation which was associated with blunted Rho-kinase activity (Mallat, Gojova et al. 2003). It is postulated that the RhoA/ROCK pathway effects on atherosclerosis are related to the dysfunction of endothelial cells, immune response and inflammation (Dong, Yan et al. 2010), leading to augmented expression of pro-inflammatory cytokines and associated recruitment of monocytes and subsequent macrophage accumulation.

Further insights have suggested ROCK activation plays roles throughout the different stages of atherosclerotic plaque formation. First, ROCK activation is involved in the downregulation of eNOS expression (Takemoto, M. et al 2002) resulting in increased endothelial cell permeability alongside

facilitating vascular smooth muscle cell (VSMC) growth (Yamakawa, T et al 2000), effects which promote atherogenesis (Wang, H.W. et al 2008). Second, ROCK activation has been associated with monocyte recruitment and related macrophage accumulation in developing atherosclerotic lesions, where their uptake of ox-LDL induces their transformation into foam cells, the hallmark of atherosclerosis (Dong, Yan et al. 2010). Relatedly, it has recently been shown that ROCKs increase the phagocytic capacity of macrophages via regulation of their actin cytoskeleton (Julian and Olson 2014). Rac activation increases the formation of spikes and lamellipodia, while Cdc42 regulates the formation of cell membrane protrusions such as filopodia. Principally, ROCKs promote the stability of actin filaments via phosphorylation of LIM kinase-1 (LIMK1) and subsequent down-stream activation of effector proteins, for example myosin and resultant generation of actin-myosin contraction. ROCKs can also phosphorylate myosin light chain (MLC) which thereafter increases actin stress fibre and focal adhesion formation (Julian and Olson 2014). It has been reported that polarisation of macrophages towards different macrophage subsets involves Rho/ROCK signalling. Studies showed that inhibiting the ROCK2 signalling pathway shifted anti-inflammatory M2 macrophages towards a pro-inflammatory M1 phenotype, as evidenced by increased expression of pro-inflammatory macrophage markers (Zandi, Nakao et al. 2015), demonstrating ROCK signalling regulates macrophage plasticity. Accordingly, modulation of the ROCK signalling pathway may represent an attractive therapeutic avenue for inflammatory cardiovascular diseases such as atherosclerosis.

Fasudil (1-(5-isoquinolinesulfonyl)-homo-piperazine) is a ROCK inhibitor that is clinically approved for the treatment of patients with cerebral vasospasm after subarachnoid haemorrhage surgery (in Japan), and recently approved for use in clinical trials for Raynaud's disease, atherosclerosis and amyotrophic lateral sclerosis (ALS) (Shi and Wei 2013). Fasudil competes with ATP binding to the kinase domain of ROCK, the prevention of ATP attachment leads to inhibition of the RhoA/ Rho kinase (ROCK) signalling pathway. Studies showed that inhibition of the RhoA/ROCK signalling pathway by fasudil enhances the expression of eNOS, which decreases endothelial dysfunction, the contraction of VSMCs, and monocyte/macrophage recruitment and their polarisation to different phenotypes. However, in contrast to the aforementioned study by Zandi and colleagues (Zandi, Nakao et al. 2015), ROCK inhibition with fasudil was able to significantly decrease the expression of pro-inflammatory M1 macrophage markers such as CD40, and iNOS, while significantly increasing the levels of anti-inflammatory M2 markers including CD206, suggesting fasudil shifts macrophage polarisation towards an anti-inflammatory phenotype (Liu, Li et al. 2013). A comparison of the two studies (Liu, Li et al. 2013, Zandi, Nakao et al. 2015) reveals some differences which may explain the divergent effects on macrophage polarisation, including the use of monocytes isolated from different sites (spleen verses

bone-marrow). More importantly, fasudil inhibits both ROCK1 and 2, while the study from Zandi and colleagues (Zandi, Nakao et al. 2015) deployed a ROCK2-specific inhibitor, suggesting that targeting of both ROCK isoforms is necessary to shift macrophages towards an anti-inflammatory phenotype.
The recruitment and infiltration of monocytes through the endothelial layer during atherogenesis is regulated by different adhesion molecules and chemokines such as ICAM-1 and MCP-1, which have an essential role for the localised accumulation of monocyte/macrophages. Fasudil treatment has been shown to decrease the infiltration of monocyte/macrophages through suppression of MCP-1 and the inflammatory cytokine TNF-α, while enhancing the production of anti-inflammatory cytokines such as IL-10, in part supporting the anti-inflammatory actions of ROCK1/2 inhibition. Furthermore, with actin cytoskeleton remodelling a major downstream consequence of ROCK signalling, these findings support a fundamental role for ROCK signalling and associated reorganisation of the actin cytoskeleton on macrophage behaviour including their migration, proliferation, adhesion, and polarisation (Liu, Li et al. 2013, Rao, Ye et al. 2017). Accordingly, a reduced chemotactic response alongside shifting of macrophage polarisation towards an anti-inflammatory phenotype afforded with fasudil treatment, would be expected to affect the phagocytic capacity of macrophages and their subsequent transformation into foam cells, which are considered as critical steps for the formation of atherosclerosis. Indeed, two independent studies have shown that administration of ROCK1/2 inhibitors (either Y-27632 or fasudil) are able to blunt the formation and progression of atherosclerotic plaques in mice (Mallat, Gojova et al. 2003, Wu, Xu et al. 2009)

Statins (3-hydroxy-3-methylglutaryl-coenyme A reductase inhibitors) are a family of drugs used to effectively reduce circulating LDL-cholesterol levels in clinical practices (Byrne, Cullinan et al. 2019). Moreover, statins are administered to patients as primary or secondary prevention of cardiovascular disorders. Primary prevention involves treating patients who do not have clinical cardiovascular indications but are predicted to be of future high risk, while secondary prevention comprises treating patients suffering from CVD to limit the occurrence of an adverse cardiovascular event (Perk, De Backer et al. 2012). Statins are termed pleiotropic compounds as alongside their ability to lower LDL-cholesterol levels, they can exert additional athero-protective effects through modulation of inflammatory and vascular cells (Sawada and Liao 2013). Statins prevent the synthesis of isoprenoid intermediates that are essential for the biosynthesis of the cholesterol pathway, such as farnesylpyrophosphate (FPP) and geranyl-geranylpyrophosphate (GGPP), which are downstream effectors of L-mevalonic acid (Sawada and Liao 2013). Additionally, FPP and GGPP regulate post-translational modification (isoprenylation) of GTP-ase family members, such as Rho, Ras, and Rac (Van Aelst and D'Souza-Schorey 1997). Isoprenylation has a vital role in the functional activity of multiple proteins that are associated in the proliferation of the cell, cell transformation, and cell growth-

signaling pathways such as Rho-GTPases (Van Aelst and D'Souza-Schorey 1997). Accordingly, inhibiting isoprenylation of GTP-ase family members with statins, blunts the activity of Rho, Ras, and Rac (Sawada and Liao 2013). As such, in addition to perturbing cholesterol synthesis, a key mechanism of statin action in regulating CVD is considered to be through the inhibition of Rho or its kinase ROCK (Takemoto, Sun et al. 2002). Mechanistically, statins can improve the function of endothelial cells through increasing the levels of eNOS (Essig, Nguyen et al. 1998), by enhancing mRNA stability of eNOS via inhibition of the Rho/ROCK pathway (Laufs, La Fata et al. 1998). Moreover, administration of statins to patients suffering from stable atherosclerosis lead to an improvement of endothelial dysfunction through the inhibition of ROCK activity (Dong, Yan et al. 2010). Furthermore, studies reported that the anti-inflammatory effects of statins involve the inhibition of inflammatory chemokines and cytokines such as MCP-1, IL-6, and IL-8 (Oesterle, Laufs et al. 2017). Additionally, by inhibiting the activity of Rac1, statins reduce the production of ROS and downregulate the inflammatory pathways (Dichtl, Dulak et al. 2003). Studies in a rabbit model showed that statins inhibited the release of MMP-1, MMP-3, and MMP-9 by macrophages and VSMCs (Luan, Chase Alex et al. 2003). MMPs have an essential role in the degradation of ECM proteins, especially elastin, and subsequent remodelling of the arterial wall (Harris, Smith et al. 2010, Myasoedova, Chistiakov et al. 2018). Supporting a direct anti-inflammatory effect of statins upon atherosclerosis, either pravastatin or simvastatin administration to hypercholesteroleamic mice significantly retarded atherogenesis and improved the stability of established atherosclerotic lesions, without affecting plasma LDL-cholesterol levels (Bea, Blessing et al. 2002, Johnson, Carson et al. 2005).

3.1.3 Aim of this Chapter

In this chapter, I attempt to ascertain whether THP-1 derived macrophages represent a realistic model for mimicking the properties of two recently-characterised macrophage subsets proposed to play opposing roles in atherosclerosis. In addition, the effect of actin perturbing drugs (fasudil and pravastatin) on the behaviour and function of macrophages including their polarisation, are assessed in relation to atherogenesis and the progression of atherosclerotic plaques.

3.2 Results

3.2.1 Macrophages differentiated from THP-1 cells mirror the morphological divergency of human PBMC-derived macrophages in response to GM-CSF or M-CSF

To assess whether macrophages obtained from THP-1 cells acquire a similar morphology as human PBMC derived macrophages after polarisation with GM-CSF or M-CSF, THP-1 cells were incubated with PMA for 72 hours to induce their adherence then differentiated through incubation with 20 ng/ml of granulocyte-macrophage colony-stimulating factor (GM-CSF), or macrophage colony-stimulating factor (M-CSF) for 6 days to obtain two distinct macrophage subsets (GM-Mac and M-Mac respectively). This protocol was used throughout this chapter to generate the GM-Mac and M-Mac subsets from THP-1 cells.

As has been reported for human PBMC-derived macrophages (Waldo, Li et al. 2008), morphological differences were observed between the GM-CSF and M-CSF polarised THP-1 macrophage subsets. Macrophages incubated with GM-CSF exhibited a rounded shape in contrast to macrophages incubated with M-CSF which displayed a mixture of rounded and elongated morphology (Figure 3.1). This data confirms the results observed in human PBMC derived macrophages.

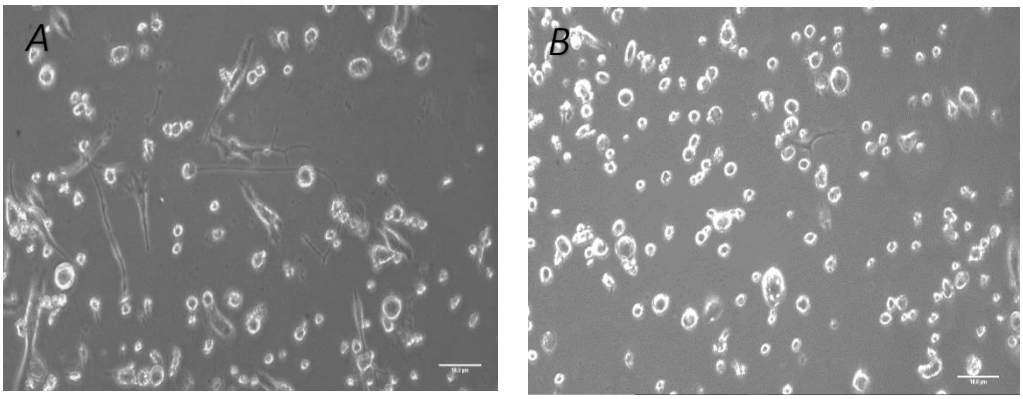

Figure 3.1 Effect of M-CSF and GM-CSF maturation on the morphology of THP-1 macrophages.

Representative phase contrast microscopy images of (A) six-day M-CSF (20 ng/ml) directed THP-1 macrophages (M-Mac), and (B) six-day GM-CSF (20 ng/ml) directed macrophages (GM-Mac). Scale bars represent 10 μm.

3.2.2 GM-CSF polarised macrophages differentiated from THP-1 cells have reduced F-actin accumulation compared to M-CSF polarised macrophages

With alterations in macrophage morphology and function associated with changes in F-actin content (Grosheva, Haka et al. 2009), GM-CSF (GM-Mac) and M-CSF (M-Mac) polarised THP-1 macrophages were stained with AlexaFluor 594-conjugated phalloidin to enable the visualisation and quantification of cellular F-actin content. The average accumulation of F-actin was significantly reduced within GM-CSF polarised macrophages (44%; $p<0.01$) compared to their M-Mac counterparts (Figure 3.2).

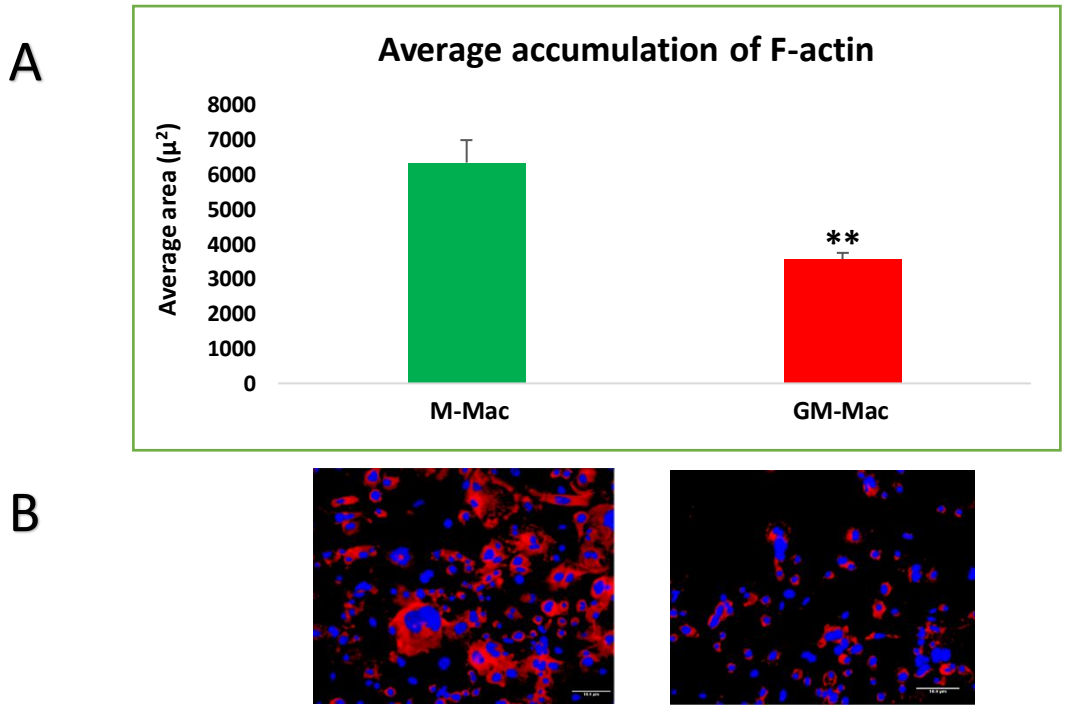

Figure 3.2 GM-CSF polarised THP-1 macrophages (GM-Mac) display reduced F-actin accumulation compared to M-Macs.

A: Quantification of F-actin content within M-Mac and GM-Mac subsets, measured within six random x 20 magnification fields. ** indicates $p<0.01$; two tailed, paired t-test, n=4.

B: Representative images of F-actin within M-Mac and GM-Mac subsets, stained with AlexaFluor 594-conjugated phalloidin (red) alongside a DAPI nuclear counterstain (blue).

Scale bar represents 10 µm and applies to both panels. N-values in macrophages differentiated from THP-1 cells represent number of replicates.

3.2.3 Addition of M-CSF to GM-Macs does not rescue their decreased F-actin content

To assess the plasticity of GM-Macs differentiated from THP-1 cells by assessing the effect of M-CSF addition on pro-inflammatory GM-Mac F-actin content, six-day GM-CSF polarised THP-1 macrophages were incubated with M-CSF (20 ng/ml) for 24 hours. Analysis of AlexaFluor 594-conjugated phalloidin-labelled images showed that 24-hour addition of M-CSF to GM-Macs did not influence F-actin content within the GM-Mac subset (Figure 3.3). Our finding suggests that GM-Macs (differentiated from THP-1 cells) require higher concentrations of M-CSF and/or longer incubation periods to revert back to an anti-inflammatory phenotype.

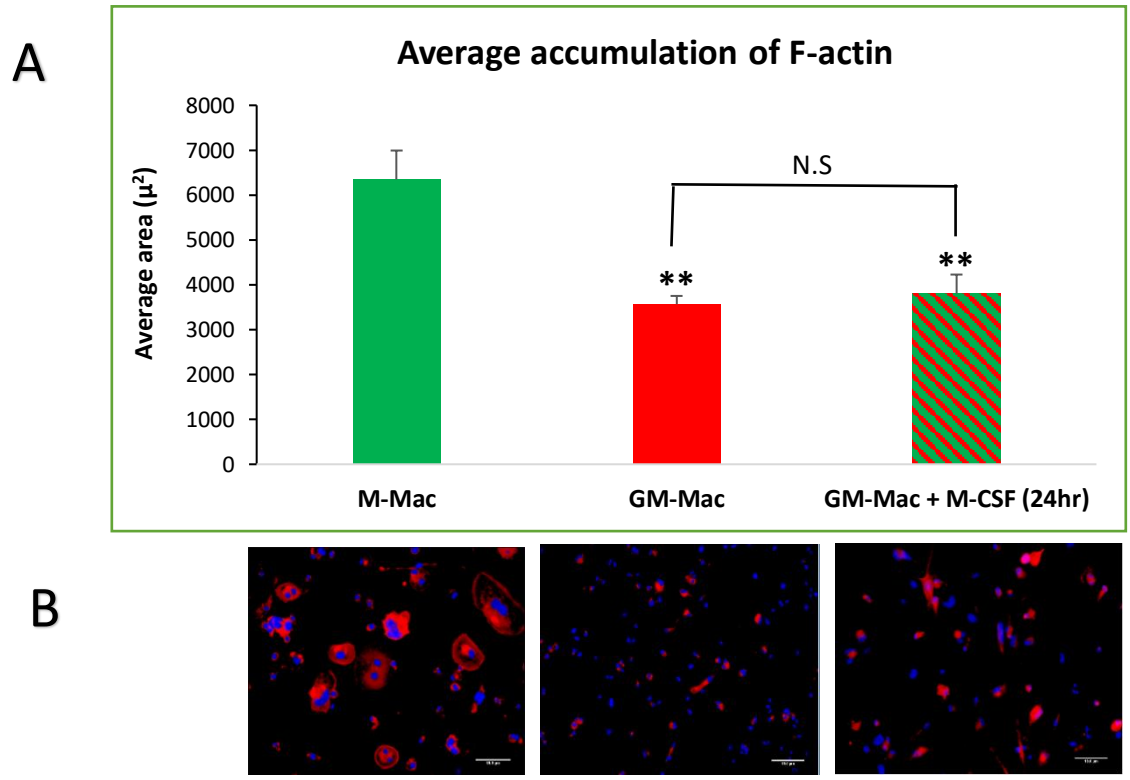

Figure 3.3 M-CSF addition does not affect F-actin content in GM-Macs.

A: Quantification of F-actin content within M-Mac, GM-Mac, and GM-Mac treated with M-CSF, measured within six random x 20 magnification field. ** indicates $p<0.01$ and N.S denotes not significant vs GM-Mac; ANOVA, Student-Newman-Keuls Multiple Comparisons Test, n=4.

B: Representative images of F-actin within M-Mac, GM-Mac, and GM-Mac treated with M-CSF, stained with AlexaFluor 594-conjugated phalloidin (red) alongside a DAPI nuclear counterstain (blue). Scale bar represents 10 μm and applies to all panels. N-values in macrophages differentiated from THP-1 cells represent number of replicates.

3.2.4 Addition of GM-CSF to M-Mac subsets significantly reduced F-actin content and changed cell morphology to GM-Mac phenotype, which was associated with increased expression of MMP-12 and colony stimulating factor 2 receptor subunit alpha (CSF2RA)

To assess the effect of GM-CSF addition on anti-inflammatory M-Mac F-actin content, six-day M-CSF polarised THP-1 macrophages were incubated with GM-CSF (20 ng/ml) for 24 hours. Quantification of AlexaFluor 594-conjugated phalloidin labelling revealed that GM-CSF addition to M-Macs significantly reduced F-actin content (25%; $p<0.01$; n=4; Figure 3.4) which was associated with a shift in cell morphology towards a rounded GM-Mac phenotype.

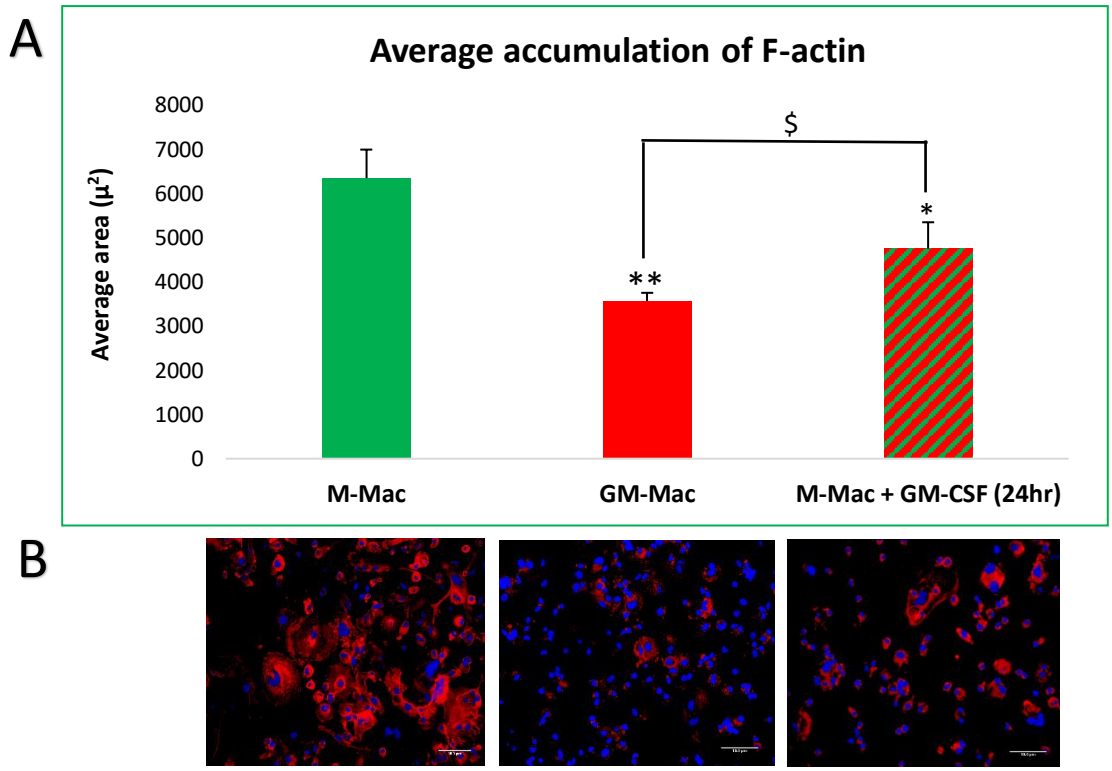

Figure 3.4 GM-CSF addition reduced M-Mac F-actin content.

A: Quantification of F-actin content within M-Mac, GM-Mac, and M-Macs treated with GM-CSF, measured within six random x 20 magnification field. ** indicates $p<0.01$, * indiates $p<0.05$ vs M-Mac and $ indiates $p<0.05$ vs GM-Mac; ANOVA, Student-Newman-Keuls Multiple Comparisons Test, n=4.

B: Representative images of F-actin within M-Mac, GM-Mac, and M-Macs treated with GM-CSF, stained with AlexaFluor 594-conjugated phalloidin (red) alongside a DAPI nuclear counterstain (blue). Scale bar represents 10 μm and applies to all panels. N-values in macrophages differentiated from THP-1 cells represent number of replicates.

To examine whether the morphological changes exerted on the anti-inflammatory M-Mac subset by GM-CSF stimulation was associated with a shift towards a GM-Mac phenotype, mRNA expression for M-Mac markers and regulators (TGFBI, CSF1, and CSF1R) and GM-Mac indicators (MMP12, CSF2, and CSF2RA) were assessed. Q-PCR analysis showed GM-CSF addition to M-Macs induced a significant increase in MMP12 and CSF2RA mRNA expression (5-fold; $p<0.05$, and 1.4-fold; $p<0.01$ respectively; n=4; Figure 3.5).

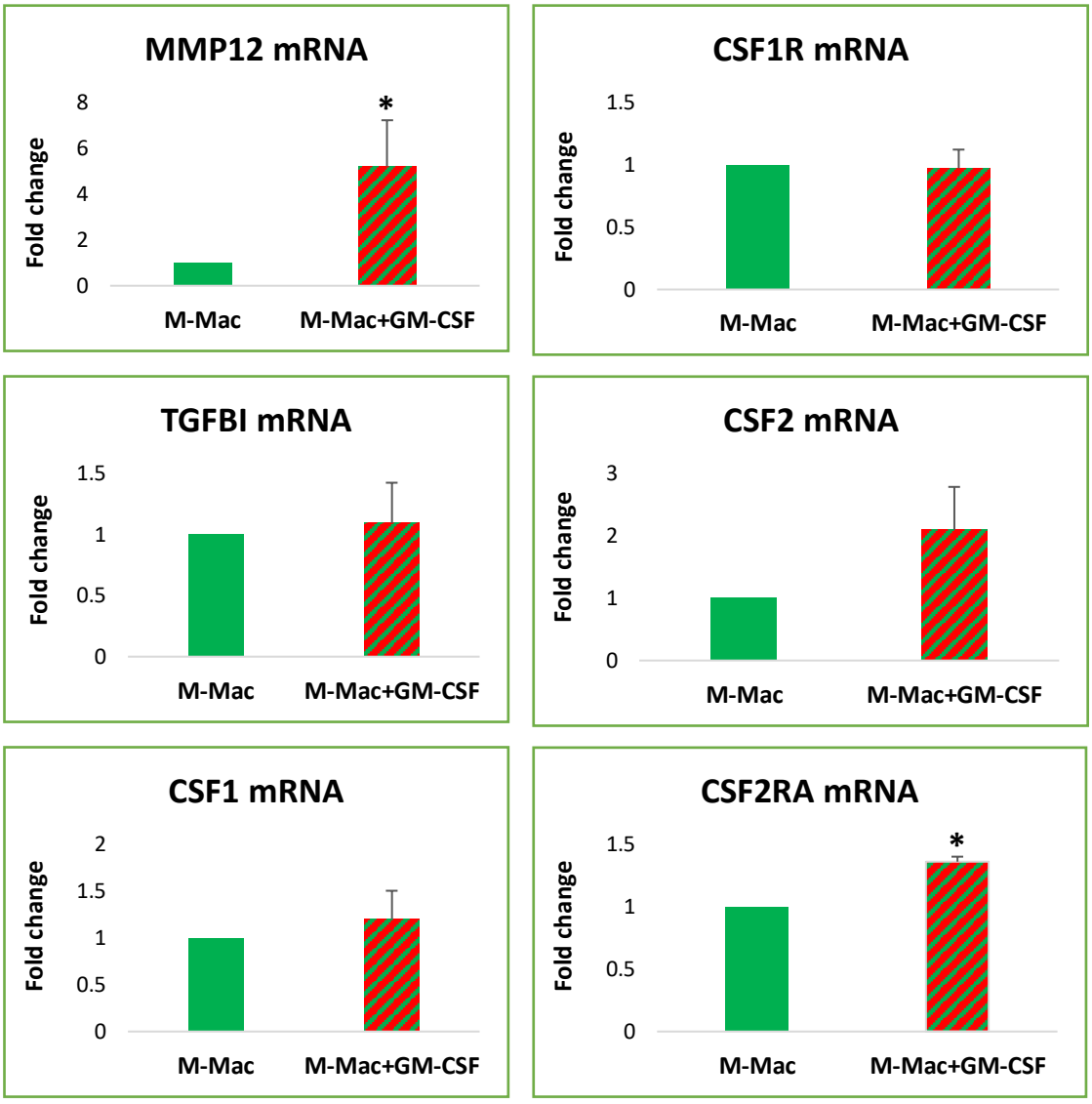

Figure 3.5 GM-CSF addition increased M-Mac MMP12 and CSF2RA mRNA expression.

Quantification of MMP12, CSF1R, TGFBI, CSF2, CSF1, and CSF2RA mRNA expression in M-Mac and M-Mac macrophages treated with 20 ng/ml of GM-CSF for 24 hours, assessed by RT-qPCR. Data presented as fold change against unstimulated M-CSF matured (M-Mac) macrophages (mean ± SEM; *indicates $p<0.05$; two tailed, paired t-test, n=4). N-values in macrophages differentiated from THP-1 cells represent number of replicates.

3.2.5 M-Mac and GM-Mac subsets derived from THP-1 cells regulate mRNA expression of select MMPs, CSFRs, and scavenger receptor markers in the same manner as primary human macrophages

To ascertain whether macrophage subsets differentiated from THP-1 cells display the same patterns of gene expression as primary human macrophages, six-day M-Mac and GM-Mac derived from THP-1 cells were assessed for mRNA expression of markers deemed characteristic of the GM-Mac subset (MMP12 and SPARC) or M-Macs (TIMP3 and TGFBI).

Results showed that GM-Mac derived from THP-1 cells exhibited significantly increased mRNA expression of MMP12, SPARC and TIMP3 compared to M-Macs (4-fold; P< 0.001, 3-fold; P< 0.01, and 3.5-fold; P< 0.01 respectively; n=10; Figure 3.6), whereas expression of TGFBI mRNA levels were signficantly decreased (30%; P< 0.05; n=10; Figure 3.6). These findings are in line with observations from human primary PBMC-derived macrophages (JLJ unpublished study and (Waldo, Li et al. 2008)), and support the proposition that GM-Mac have a pro-inflammatory phentoype (Di Gregoli and Johnson 2012)

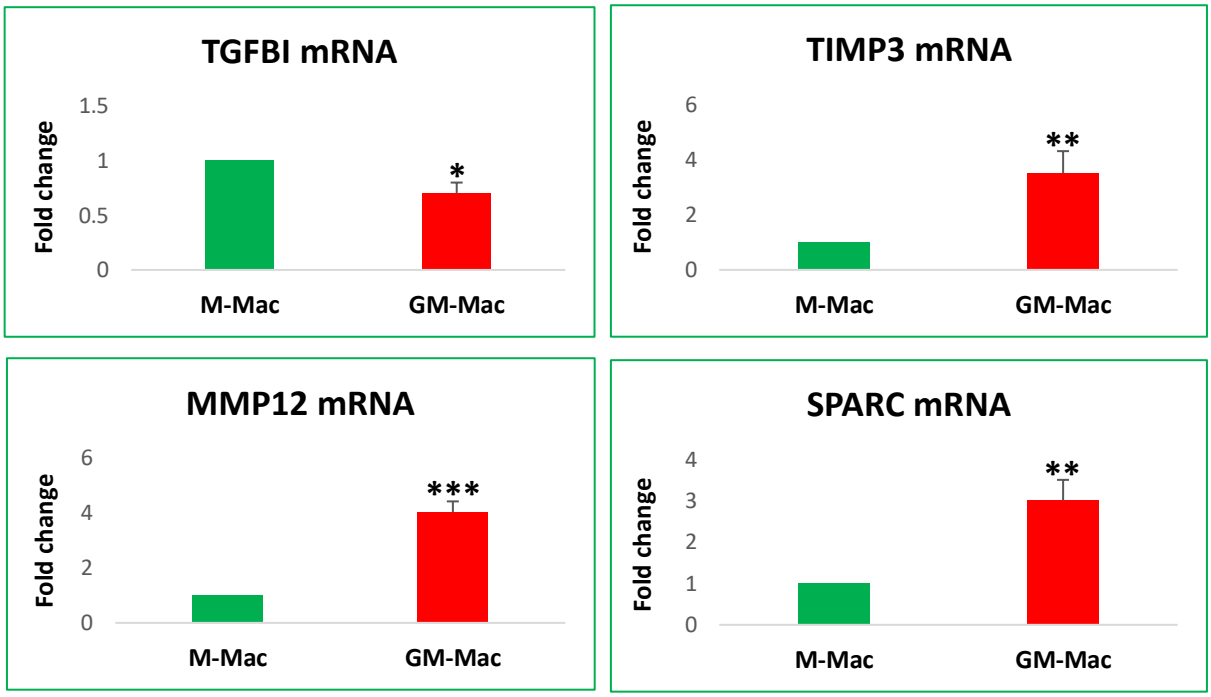

Figure 3.6 M-Mac and GM-Mac subsets derived from THP-1 cells display similar mRNA expression patterns of specific cell markers as primary human macrophages.

Quantification of TGFBI, TIMP3, MMP12, and SPARC mRNA expression in M-Mac and GM-Mac subsets derived from THP-1 cells, assessed by RT-qPCR. Data presented as fold change against M-CSF matured (M-Mac) macrophages (mean ± SEM; *indicates p<0.05, ** indicates p<0.01, *** indicates p<0.001; two tailed, paired t-test, n=10). N-values in macrophages differentiated from THP-1 cells represent number of replicates.

Next, the mRNA expression of genes associated with phagocytosis and macrophage polarisation were assessed between M-Mac and GM-Mac subsets differentiated from THP-1 cells, including numerous pivotal scavenger receptors MSR1, OLR1 (LOX-1), CD36, and MRC1 alongside different CSF receptors. Q-PCR results revealed significantly increased mRNA expression of the scavenger receptors MRC1, CD36, and MSR1 in the anti-inflammatory M-Mac subset compared to pro-inflammatory GM-Macs (2.5-fold; $p<0.05$, 4.7-fold; $p<0.01$, and 25-fold; $p<0.001$ respectively; n=4; Table 3.1). Moreover, analysis showed levels of the anti-inflammatory cytokine IL10 and the receptor for M-CSF, CSF1R, were also significantly increased in the M-Mac subset (3.2-fold; $p<0.05$, and 2.2-fold; $p<0.05$ respectively; n=4; Table 3.1). In contrast, the scavenger receptor OLR1 (LOX-1) and the GM-CSF receptor CSF2RA were significantly increased in the GM-Mac subset when compared to M-Macs (1.5-fold; $p<0.05$, and 5-fold; $p<0.001$ respectively; n=4; Table 3.1).

These findings further support the notion that M-Macs represent an anti-inflammatory macrophage subset, through increased expression of IL10 and MSR1 (CD206), which are well-characterised markers of the anti-inflammatory M2 macrophage phenotype (Johnson and Newby 2009). Additionally, M-Mac and GM-Mac display distinct sets of scavenger receptors suggesting different mechanisms for the uptake of modified lipoproteins, with the M-Mac subset favouring CD36 and MSR1, while OLR1 is increased in GM-Macs. Furthermore, there appears to be positive feedback mechanisms for polarisation in both subsets, with M-Macs increasing expression of CSF1R (the receptor for M-CSF) and GM-Macs exhibiting elevated CSF2RA expression (the specific receptor for GM-CSF). Finally, the results from THP-1-derived M-Mac and GM-Mac subsets are similar to those observed in M-CSF and GM-CSF polarised macrophages derived from human primary monocytes (Di Gregoli and Johnson 2012).

Gene	Macrophage subsets differentiated from THP-1 cells
	M/GM fold change ± SEM
OLR1 (LOX-1)	0.19 ± 0.06
CD36	4.76 ± 0.02
MSR1	25 ± 0.005
MRC1	2.5 ± 0.08
IL10	3.2 ± 0.03
CSF1R	2.21 ± 0.05
CSF2RA	0.63 ± 0.063

Table 3.1: Table summarising mRNA expression changes between THP-1-derived M-Mac and GM-Mac subsets

Quantification of key lipoprotein-related scavenger receptors (OLR1, CD36, MSR1, and MRC1) and anti-inflammatory cytokine IL10, the receptor for M-CSF, CSF1R, and the receptor for GM-CSF, CSF2RA, assessed by RT-qPCR. Data presented as fold change compared to M-CSF matured (M-Mac) macrophages (mean ± SEM; green filled-box indicates significantly decreased compared to M-CSF matured (M-Mac) macrophages ($p<0.05$); red filled-box indicates significantly increased compared to M-CSF matured (M-Mac) macrophages ($p<0.05$); two tailed, paired t-test, n=4). N-values in macrophages differentiated from THP-1 cells represent number of replicates.

3.2.6 M-Mac and GM-Mac subsets derived from THP-1 cells regulate protein expression of MMP-12, SPARC, and TGFβI similar to primary human macrophages

To validate the findings observed at the mRNA level, ICC was performed to assess the protein expression of MMP-12, SPARC, and TGFβ-induced in M-Mac and GM-Mac subsets. In line with the q-PCR data, significantly increased protein expression of MMP-12 and SPARC (3-fold; $p<0.001$, and 2-fold; $p<0.05$ respectively; n=6; Figure 3.7 and 3.8 respectively) was observed in the GM-Mac subset compared to M-Macs, while TGFβ-induced levels were significantly decreased (2-fold; $p<0.05$; n=6; Figure 3.9).

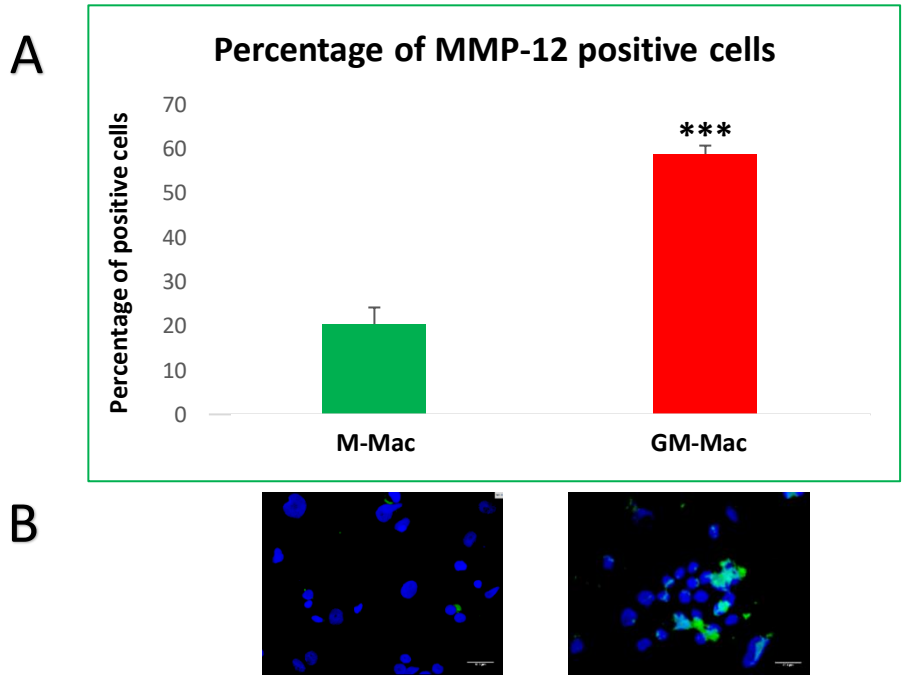

Figure 3.7 MMP-12 protein expression is increased in THP-1-derived GM-Macs.

A: Quantification of cellular MMP-12 protein expression in M-Mac and GM-Mac subsets derived from THP-1 cells, assessed by immunocytochemistry. Data presented as percentage of positive cells calculated within 10 random x 40 magnification fields. *** indicates $p<0.001$; two tailed, paired t-test, n=6. N-values in macrophages differentiated from THP-1 cells represent number of replicates.

B: Representative images of immunocytochemistry for MMP-12 within M-Mac and GM-Mac subsets. Positive cells are shown as green and all nuclei are stained blue with DAPI. Scale bar represents 10 µm and applies to both panels.

A

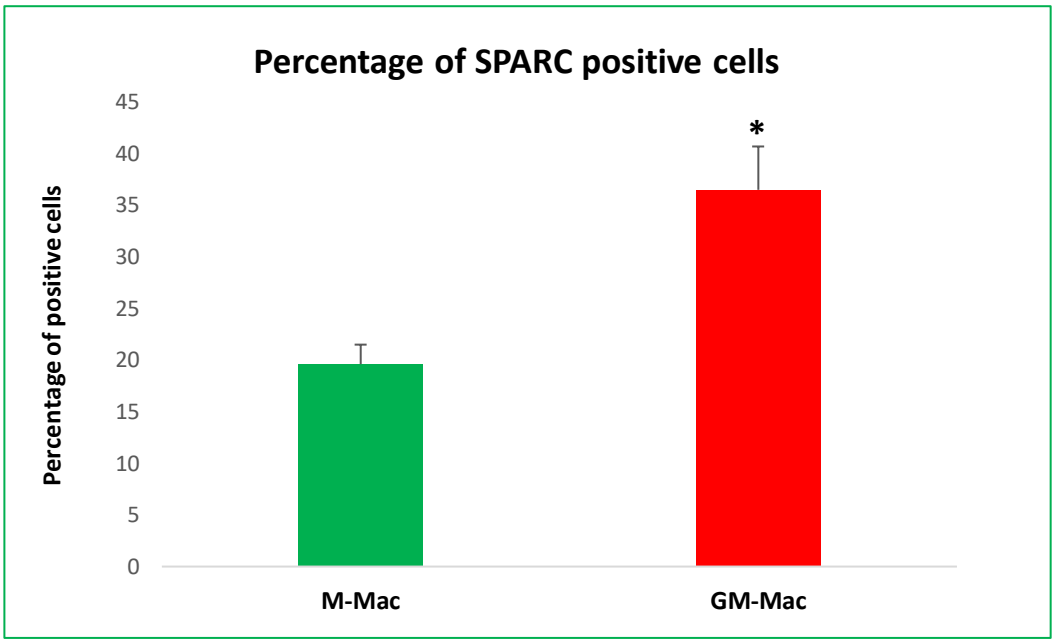

B

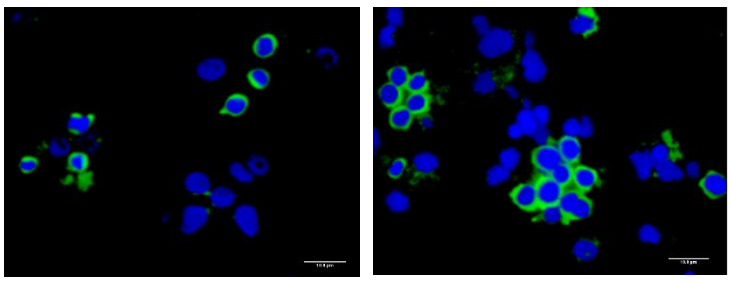

Figure 3.8 SPARC protein expression is increased in THP-1-derived GM-Macs.

A: Quantification of cellular SPARC protein expression in M-Mac and GM-Mac subsets derived from THP-1 cells, assessed by immunocytochemistry. Data presented as percentage of positive cells calculated within 10 random x 40 magnification fields. *indicates $p<0.05$; two tailed, paired t-test, n=6. N-values in macrophages differentiated from THP-1 cells represent number of replicates.

B: Representative images of immunocytochemistry for SPARC within M-Mac and GM-Mac subsets. Positive cells are shown as green and all nuclei are stained blue with DAPI. Scale bar represents 10 µm and applies to both panels.

A

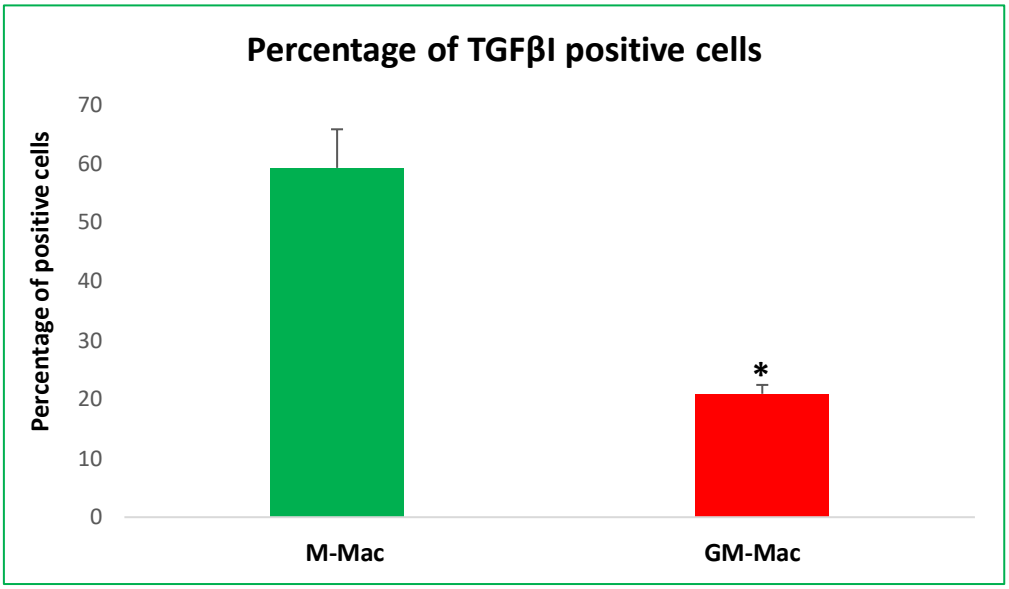

B

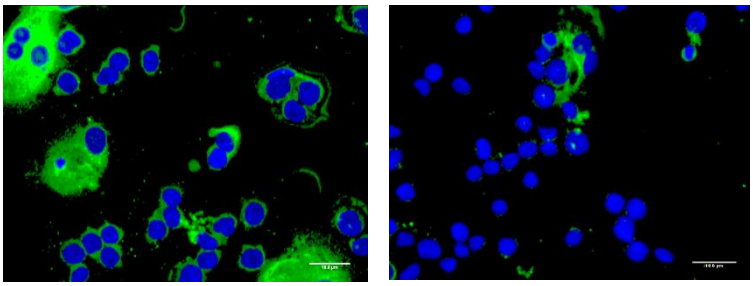

Figure 3.9 TGFβ-induced protein expression is decreased in THP-1-derived GM-Macs.

A: Quantification of cellular TGFβ-induced protein expression in M-Mac and GM-Mac subsets derived from THP-1 cells, assessed by immunocytochemistry. Data presented as percentage of positive cells calculated within 10 random x 40 magnification field. *indicates $p<0.05$; two tailed, paired t-test, n=6. N-values in macrophages differentiated from THP-1 cells represent number of replicates.

B: Representative images of immunocytochemistry for TGFβI within M-Mac and GM-Mac subsets. Positive cells are shown as green and all nuclei are stained blue with DAPI. Scale bar represents 10 µm and applies to both panels.

3.2.7 Actin perturbing drugs (fasudil and pravastatin) cause a reduction in F-actin content within M-Mac and GM-Mac subsets

Due to the differential accumulation of F-actin within M-Mac and GM-Mac subsets, the effect of the actin-perturbing drugs fasudil and pravastatin on cytoskeleton rearrangement were explored. However, in the first instance a range of different doses of fasudil and pravastatin were administrated to macrophages in order to identify the appropriate concentration of fasudil and pravastatin that modulates F-actin content within macrophage subsets without affecting cell viability.

Results with fasudil treatment showed that 100 µM of fasudil caused a significant increase in the percentage of cell death for M-Mac and GM-Mac subsets (39.1% and 31.3% respectively; Figure 3.10) and therefore deemed toxic at this dose. In contrast, the 1 µM and 10 µM doses of fasudil did not significantly induce cell death in either macrophage subset (Figure 3.10). However, further analysis revealed that 10 µM of fasudil exerted a greater effect on F-actin content compared to the 1 µM dose, therefore the 10 µM dose of fasudil was deployed in subsequent experiments. Similarly for pravastatin, the highest dose (10 µM) significantly induced cell death in both M-Mac and GM-Mac subsets (11.2% and 14.0%; Figure 3.11), and was therefore considered toxic, while both 1 µM and 5 µM doses of pravastatin were not overtly harmful to either macrophage subset (Figure 3.11). As the 5 µM dose of pravastatin was more effective at modulating macrophage F-actin content, this dose was used for all subsequent experiments.

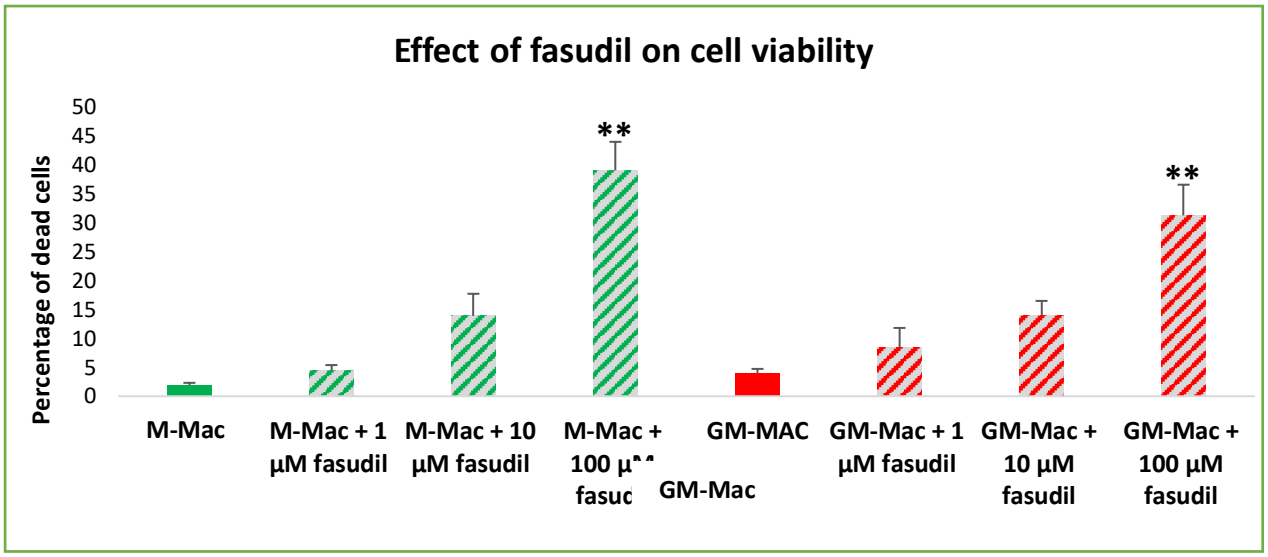

Figure 3.10 Effect of Fasudil on M-Mac and GM-Mac cell viability

Quantification of cell death in M-Mac and GM-Mac subsets derived from THP-1 cells and treated for 24 hours with increasing doses of Fasudil, assessed by immunocytochemistry. Data presented as percentage of dead cells calculated within six random x 20 magnification fields. ** indicates $p<0.01$; ANOVA, Student-Newman-Keuls Multiple Comparisons Test, n=4 N-values in macrophages differentiated from THP-1 cells represent number of replicates.

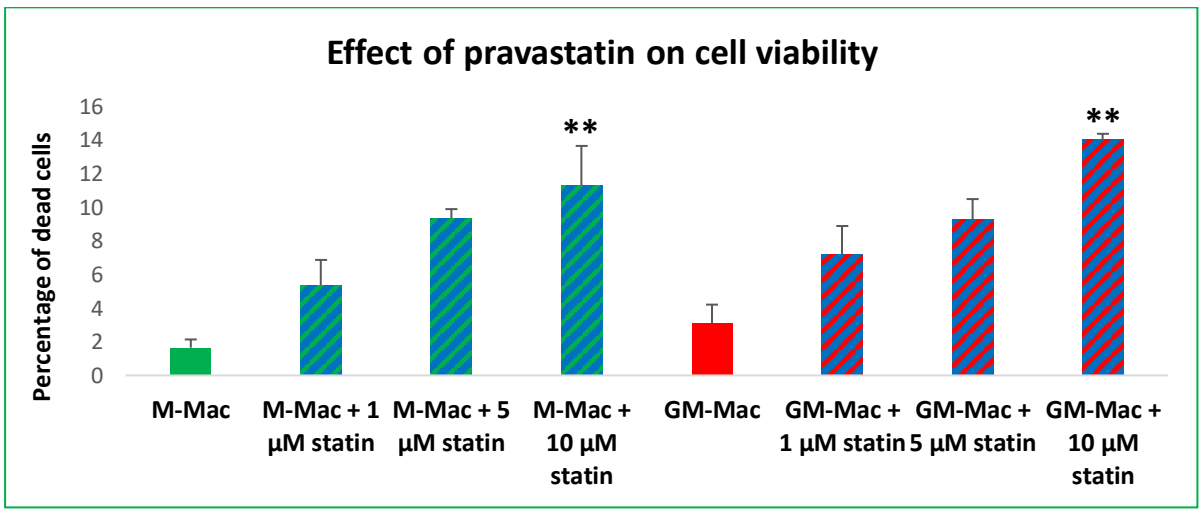

Figure 3.11 Effect of pravastatin on M-Mac and GM-Mac cell viability.

Quantification of cell death in M-Mac and GM-Mac subsets derived from THP-1 cells and treated for 24 hours with increasing doses of pravastatin (statin), assessed by immunocytochemistry. Data presented as percentage of dead cells calculated within six random x 20 magnification fields. ** indicates $p<0.01$; ANOVA, Student-Newman-Keuls Multiple Comparisons Test, n=4. N-values in macrophages differentiated from THP-1 cells represent number of replicates.

Next, the selected doses of the two actin perturbing drugs were assessed and validated for their ability to alter F-actin content in the two different macrophage subsets. Image analysis demonstrated that the M-Mac subset treated with either 10 µM of fasudil or 5 µM of pravastatin showed a significant reduction in the accumulation of F-actin (74%; $p<0.001$, and 63%; $p<0.001$ respectively; n=5; Figure 3.12). Similarly, GM-Macs treated with either 10 µM of fasudil or 5 µM of pravastatin showed a significant reduction in the accumulation of F-actin (62%; $p<0.001$, and 61%; $p<0.001$ respectively; n=5; Figure 3.13)

A

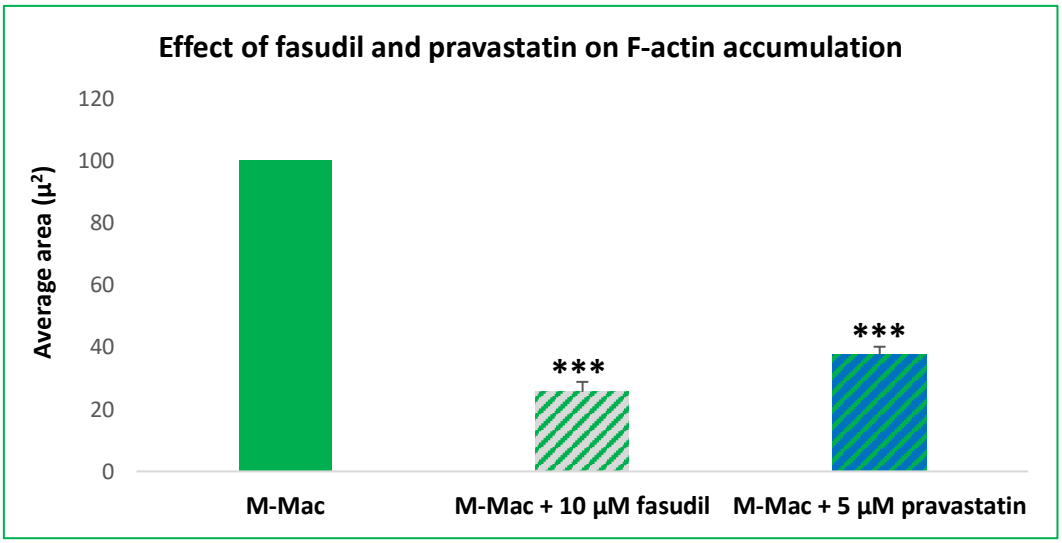

B

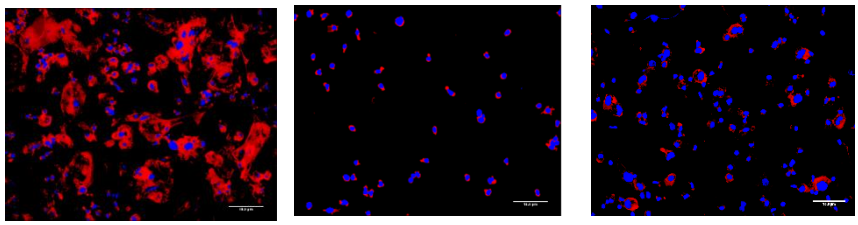

Figure 3.12 Fasudil or pravastatin addition reduced M-Mac F-actin content.

A: Quantification of F-actin content within M-Macs treated with fasudil (10 µM) or pravastatin (5 µM) for 24 hours, measured within six random x 20 magnification fields. Data presented as fold change in average cell area positive for F-actin; *** indicates $p<0.001$; two tailed, paired t-test, n=5. N-values in macrophages differentiated from THP-1 cells represent number of replicates.

B: Representative images of F-actin within M-Macs treated with fasudil (10 µM) or pravastatin (5 µM) for 24 hours, stained with AlexaFluor 594-conjugated phalloidin (red) alongside a DAPI nuclear counterstain (blue). Scale bar represents 10 µm and applies to all panels.

A

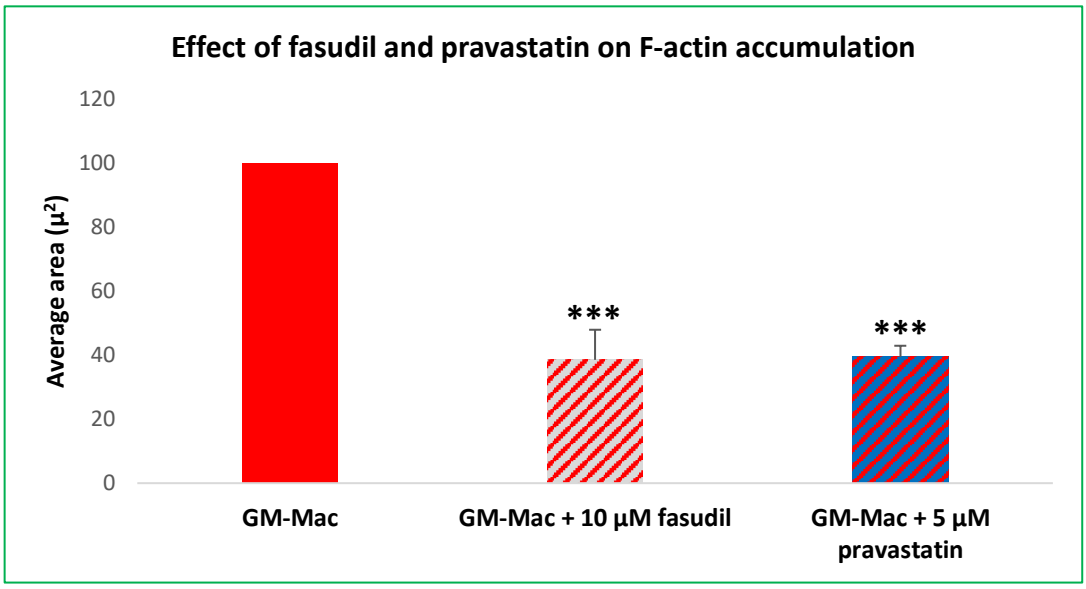

B

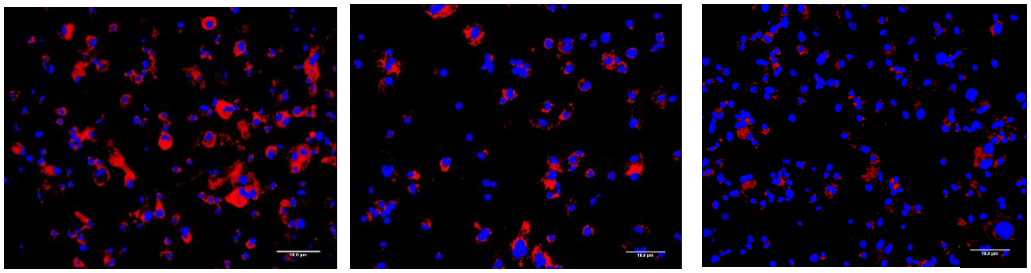

Figure 3.13 Fasudil or pravastatin addition reduced GM-Mac F-actin content.

A: Quantification of F-actin content within GM-Macs treated with fasudil (10 µM) or pravastatin (5 µM) for 24 hours, measured within six random x 20 magnification fields. Data presented as fold change in average cell area positive for F-actin; *** indicates $p<0.001$; two tailed, paired t-test, n=5. N-values in macrophages differentiated from THP-1 cells represent number of replicates.

B: Representative images of F-actin within GM-Macs treated with fasudil (10 µM) or pravastatin (5 µM) for 24 hours, stained with AlexaFluor 594-conjugated phalloidin (red) alongside a DAPI nuclear counterstain (blue). Scale bar represents 10 µm and applies to all panels.

3.2.8 Actin perturbing drugs (fasudil and pravastatin) regulate the mRNA expression of TGFBI, MMP12, and TIMP3 in M-Mac and GM-Mac subsets

The previous results showed that fasudil (10 μM) or pravastatin (5 μM) were able to regulate the accumulation of F-actin within both M-Mac and GM-Mac subsets derived from THP-1 cells. As such, qPCR was preformed to assess whether alterations in F-actin content was associated with changes in mRNA expression of the macrophage subset markers TGFBI, MMP12, and TIMP3. Results showed that pravastatin (5 μM) significantly increased mRNA expression of TGFBI, MMP12, and TIMP3 in the anti-inflammatory M-Mac subset (1.9-fold, 4.7-fold, and 1.5-fold respectively; $p<0.05$; n=5; Figure 3.14), while fasudil (10 μM) only increased TGFBI levels (2.7-fold; $p<0.05$; n=5; Figure 3.14), with MMP12 and TIMP3 expression unaffected (Figure 3.14). In regard to the pro-inflammatory GM-Mac subset, pravastatin similarly increased TGFBI and TIMP3 mRNA expression (1.9-fold and 2-fold respectively; $p<0.05$; n=5; Figure 3.14), with no effect upon MMP12 levels (Figure 3.14). Fasudil administration also had no effect on GM-Mac MMP12 levels or TGFBI expression, although TIMP3 mRNA expression was significantly elevated (2.8-fold; $p<0.05$; n=5; Figure 3.14). These findings suggest that F-actin perturbation with pravastatin, and to a lesser degree fasudil, shifts macrophages towards an anti-inflammatory phenotype.

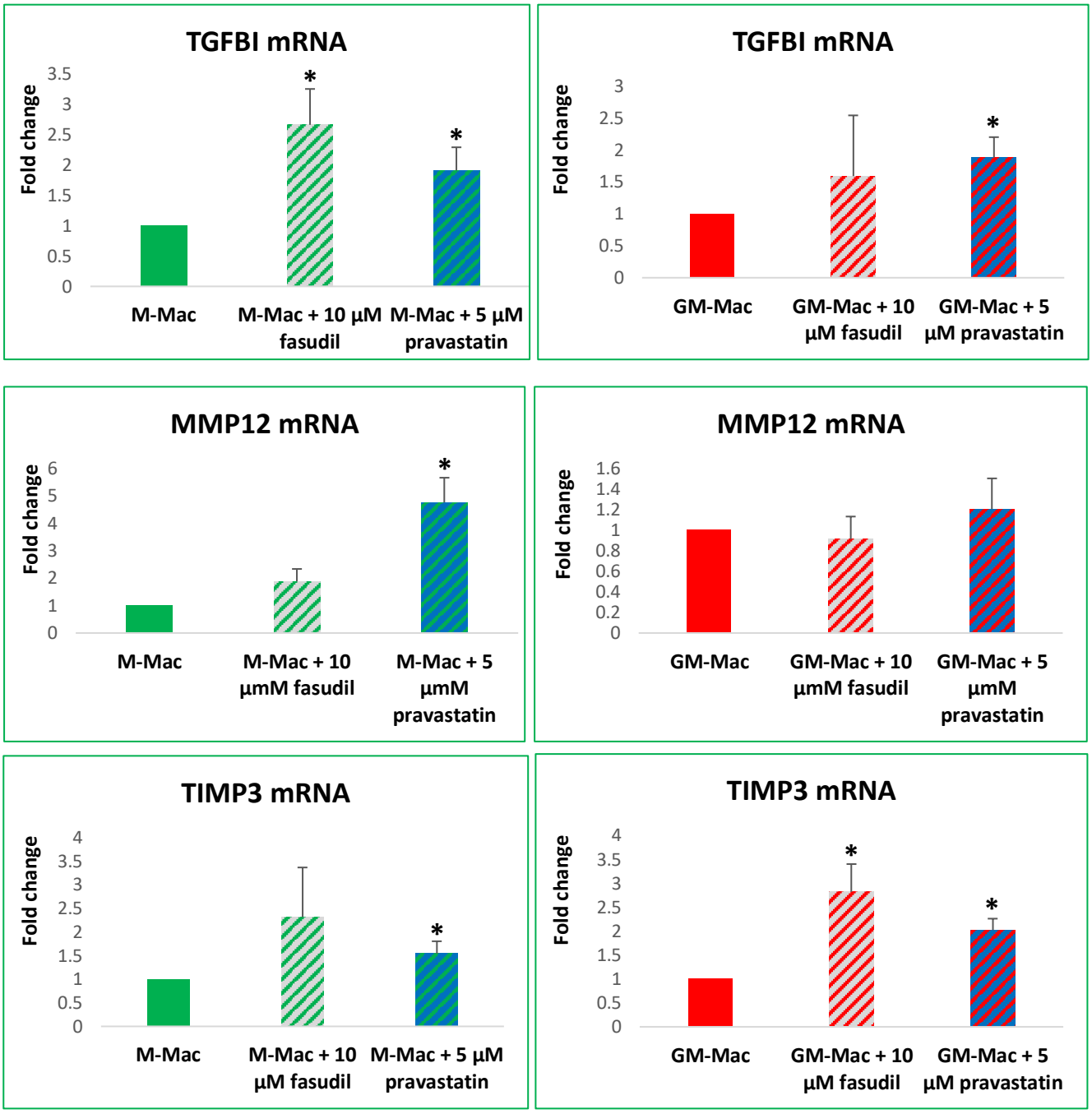

Figure 3.14 Fasudil or pravastatin addition regulates TGFBI, MMP12, and TIMP3 mRNA expression in M-Mac and GM-Mac subsets.

Quantification of TGFBI, MMP12, and TIMP3 mRNA expression in M-Mac and GM-Mac subsets derived from THP-1 cells, treated for 24 hours with fasudil (10 µM) or pravastatin (5 µM) and assessed by RT-qPCR. Data presented as fold change against untreated M-Macs or untreated GM-Macs (mean ± SEM, *indicates $p<0.05$; two tailed, paired t-test, n=5). N-values in macrophages differentiated from THP-1 cells represent number of replicates.

3.2.9 Pravastatin regulates mRNA expression of genes associated with F-actin dependent cytoskeleton rearrangement in M-Mac and GM-Mac subsets

Fascin, an actin-bundling protein, has an essential role in regulating and maintaining the stability of actin filament bundles which is important for the adhesion and migration of cells (Jayo A 2010). Another actin-binding protein, Radixin, has an essential role in forming a link between plasma membrane proteins and the actin cytoskeleton (Ivetic 2004). While vinculin, a cytoskeletal protein, is involved in linkage of the actin cytoskeleton to focal adhesions, particularly at cell-matrix and cell-cell junctions (Mierke 2009).

As either fasudil or pravastatin altered the F-actin content within both M-Mac and GM-Mac subsets, changes in the mRNA expression of genes associated with F-actin regulated cytoskeleton rearrangement were assessed. QPCR analysis revealed fasudil addition did not significantly change the mRNA expression of Fascin 1 (FSCN1), Vinculin (VCL), or Radixin (RDX) in either macrophage subset (Figure 3.15). However, pravastatin significantly increased the mRNA expression of FSCN1, VCL, and RDX (40%; $p< 0.05$, 17%; $p< 0.01$, and 54%, $p< 0.05$; respectively; n=5; Figure 3.15) within the M-Mac subset, alongside elevated levels of FSCN1, and VCL in GM-Macs (20%; $p< 0.01$, and 30%, $p< 0.05$; respectively; n=5; Figure 3.15).

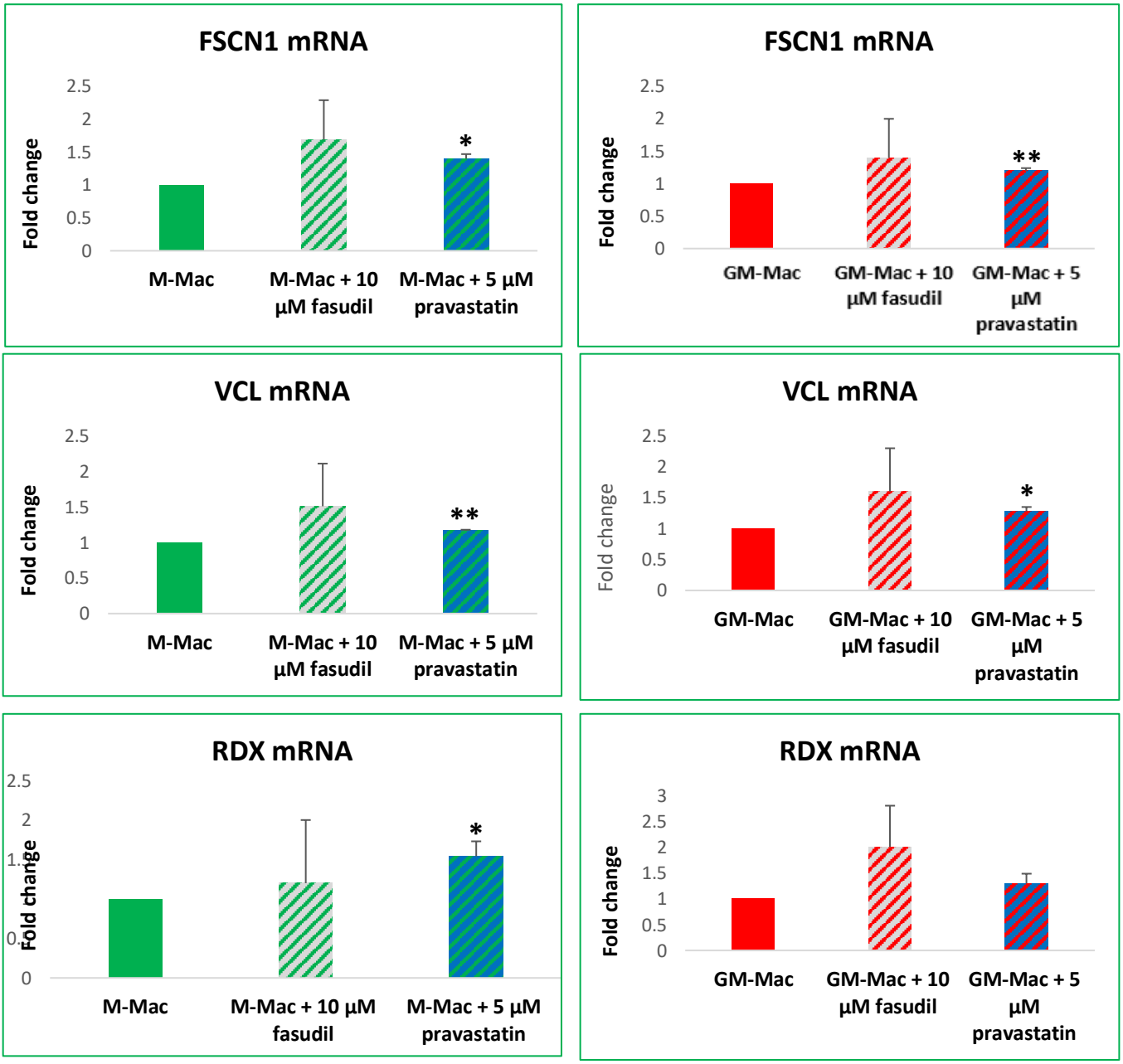

Figure 3.15 Pravastatin addition regulates FSCN1, VCL, and RDX mRNA expression in M-Mac and GM-Mac subsets.

Quantification of FSCN1, VCL, and RDX mRNA expression in M-Mac and GM-Mac subsets derived from THP-1 cells, treated for 24 hours with fasudil (10 µM) or pravastatin (5 µM) and assessed by RT-qPCR. Data presented as fold change against untreated M-Macs or untreated GM-Macs (mean ± SEM, *indicates $p<0.05$, ** indicates $p<0.01$; two tailed, paired t-test, n=5). N-values in macrophages differentiated from THP-1 cells represent number of replicates.

3.2.10 Pravastatin regulates TGFβI and MMP-12 protein expression in M-Mac and GM-Mac subsets

To validate the effects of pravastatin on TGFBI and MMP12 mRNA expression in the M-Mac and GM-Mac subsets translated to the protein level, fluorescent immunocytochemistry (ICC) was performed. Results showed pravastatin administration significantly increased protein expression of the anti-inflammatory marker TGFβI in both the M-Mac and GM-Mac subsets (1.5-fold; $p<0.05$, and 2-fold; $p<0.05$; n=4; Figure 3.16 and 3.17 respectively). In line with pravastatin exerting anti-inflammatory effects, the protein expression of MMP-12 was significantly reduced in GM-Macs treated with pravastatin (20%; $p<0.05$; n=4; Figure 3.18).

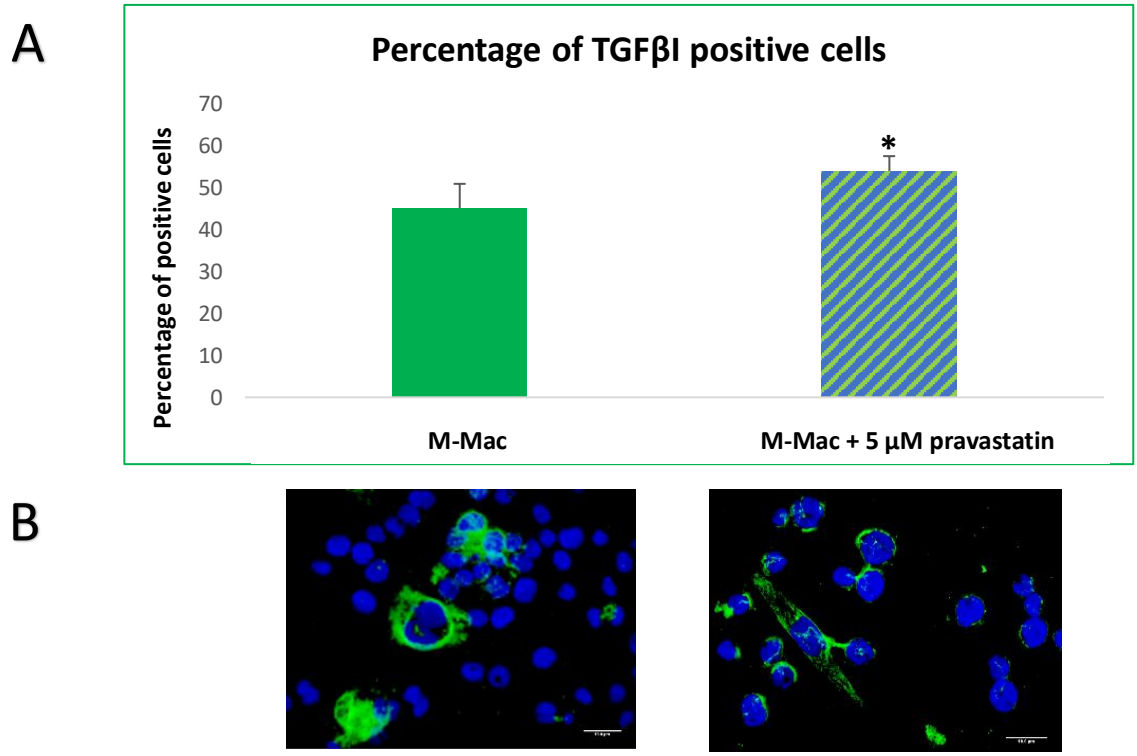

Figure 3.16 Pravastatin increased TGFβI protein expression in M-Macs.

A: Quantification of cellular TGFβI protein expression in M-Mac subset derived from THP-1 cells after 24 hour pravastatin adminstration, assessed by immunocytochemistry. Data presented as percentage of TGFβI positive cells calculated within 10 random x 40 magnification fields. *indicates $p<0.05$; two tailed, paired t-test, n=4. N-values in macrophages differentiated from THP-1 cells represent number of replicates.

B: Representative images of immunocytochemistry for TGFβI within M-Macs treated with pravastatin for 24 hours. Positive cells are shown as green and all nuclei are stained blue with DAPI. Scale bar represents 10 µm and applies to both panels.

A

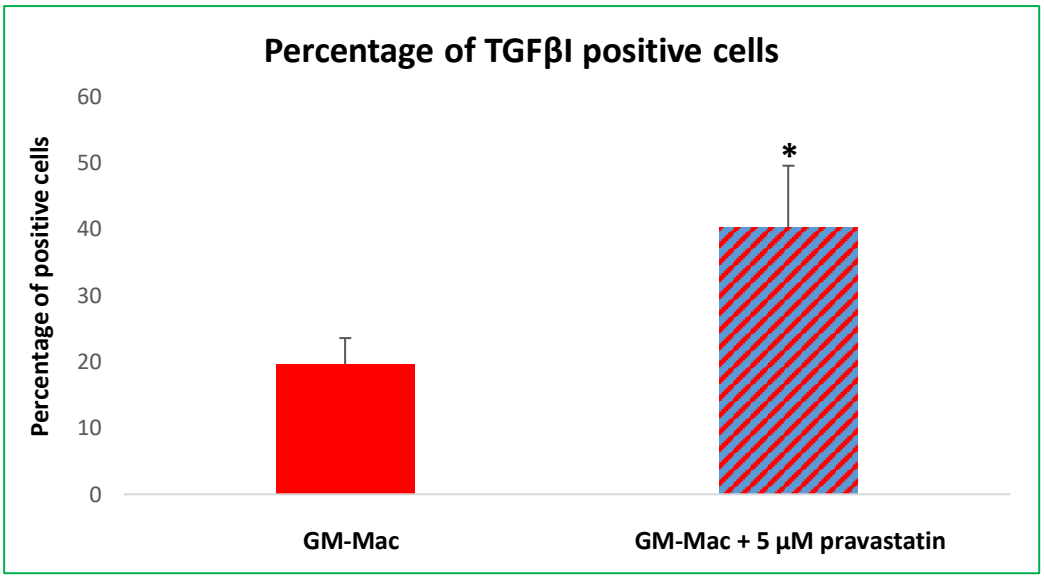

B

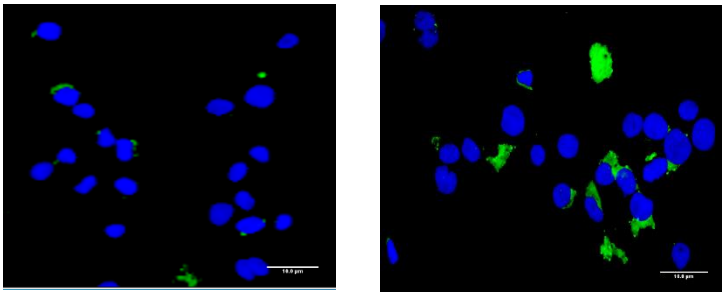

Figure 3.17 Pravastatin increased TGFβI protein expression in GM-Macs.

A: Quantification of cellular TGFβI protein expression in GM-Mac subset derived from THP-1 cells after 24 hour pravastatin adminstration, assessed by immunocytochemistry. Data presented as percentage of TGFβI positive cells calculated within 10 random x 40 magnification fields. *indicates $p<0.05$; two tailed, paired t-test, n=4. N-values in macrophages differentiated from THP-1 cells represent number of replicates.

B: Representative images of immunocytochemistry for TGFβI within GM-Macs treated with pravastatin for 24 hours. Positive cells are shown as green and all nuclei are stained blue with DAPI. Scale bar represents 10 µm and applies to both panels.

A

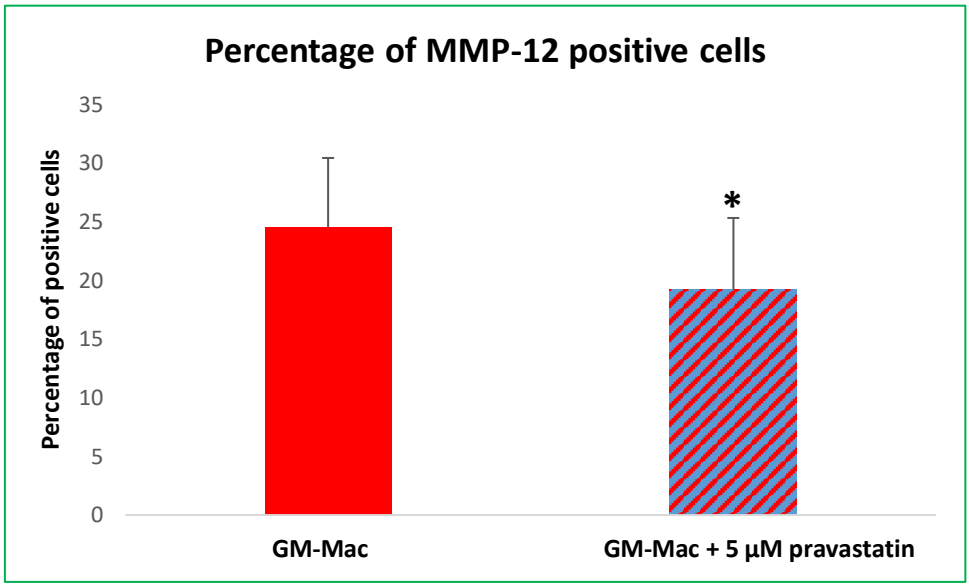

B

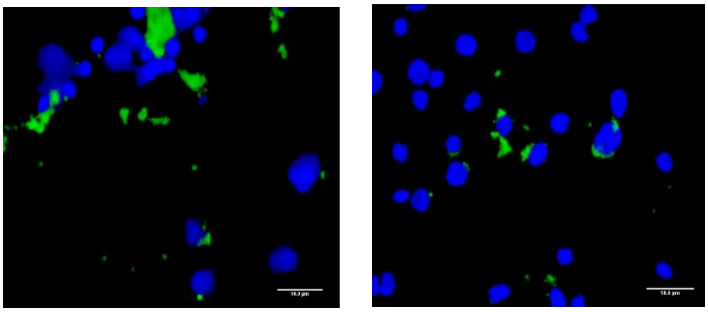

Figure 3.18 Pravastatin reduced MMP-12 protein expression in GM-Macs.

A: Quantification of cellular MMP-12 protein expression in GM-Mac subset derived from THP-1 cells after 24 hour pravastatin adminstration, assessed by immunocytochemistry. Data presented as percentage of MMP-12 positive cells calculated within 10 random x 40 magnification fields. *indicates $p<0.05$; two tailed, paired t-test, n=4. N-values in macrophages differentiated from THP-1 cells represent number of replicates.

B: Representative images of immunocytochemistry for MMP-12 within GM-Macs treated with pravastatin for 24 hours. Positive cells are shown as green and all nuclei are stained blue with DAPI. Scale bar represents 10 µm and applies to both panels.

3.2.11 Fasudil regulates TGFβI and MMP-12 protein expression in M-Mac and GM-Mac subsets

To validate the findings observed in macrophage subsets treated with fasudil regarding the reduction in F-actin content in both M-Mac and GM-Mac subsets, alongside increased mRNA expression of TGFBI in M-Macs, western blotting and fluorescent immunocytochemistry (ICC) were performed. Results showed that despite no effect at the mRNA level, fasudil administration induced a significant reduction in the protein expression of MMP-12 in the GM-Mac subset (3-fold; $p<0.01$; n=4; Figure 3.19), suggesting a shift towards an anti-inflammatory phenotype through as yet unidentified post-transcriptional mechanism with no significant change in the protein expression of MMP-12 in the M-Mac subsets. A similar discrepancy was observed for TGFβI expression, with fasudil-treated M-Macs showing a significant reduction in TGFβI protein expression (2-fold; $p<0.01$; n=5; Figure 3.20), whereas mRNA levels were increased (Figure 3.14), while no effect on the protein expression of TGFβI in the GM-Mac subsets was detected. A reduction in TGFβI would suggest ROCK inhibition and associated F-actin perturbation with fasudil, drives the M-Mac subset towards a more GM-Mac phenotype through a post-transcriptional regulatory pathway, such as the involvement of microRNAs which will need further investigation.

A

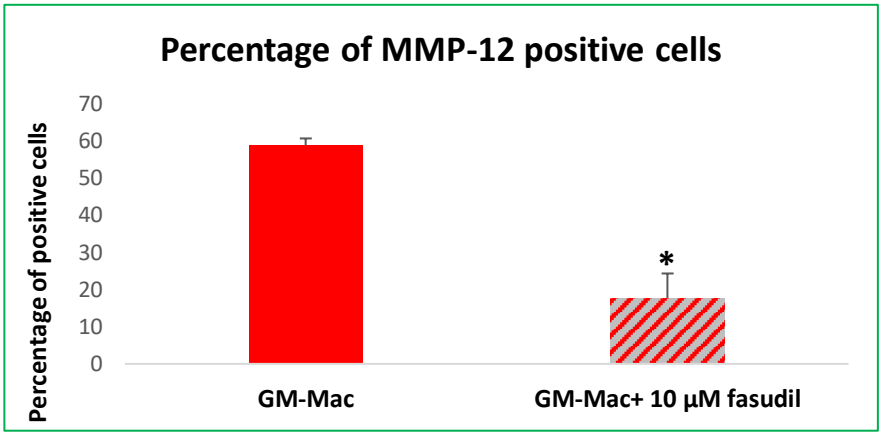

B

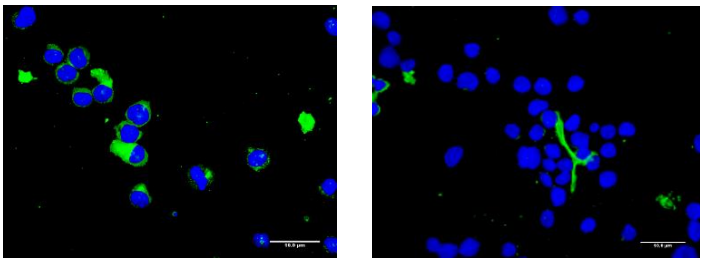

Figure 3.19 Fasudil reduced MMP-12 protein expression in GM-Macs.

A: Quantification of cellular MMP-12 protein expression in GM-Mac subset derived from THP-1 cells after 24 hour fasudil adminstration, assessed by immunocytochemistry. Data presented as percentage of MMP-12 positive cells calculated within 10 random x 40 magnification fields. *indicates $p<0.05$; two tailed, paired t-test, n=4. N-values in macrophages differentiated from THP-1 cells represent number of replicates.

B: Representative images of immunocytochemistry for MMP-12 within GM-Macs treated with fasudil for 24 hours. Positive cells are shown as green and all nuclei are stained blue with DAPI. Scale bar represents 10 µm and applies to both panels.

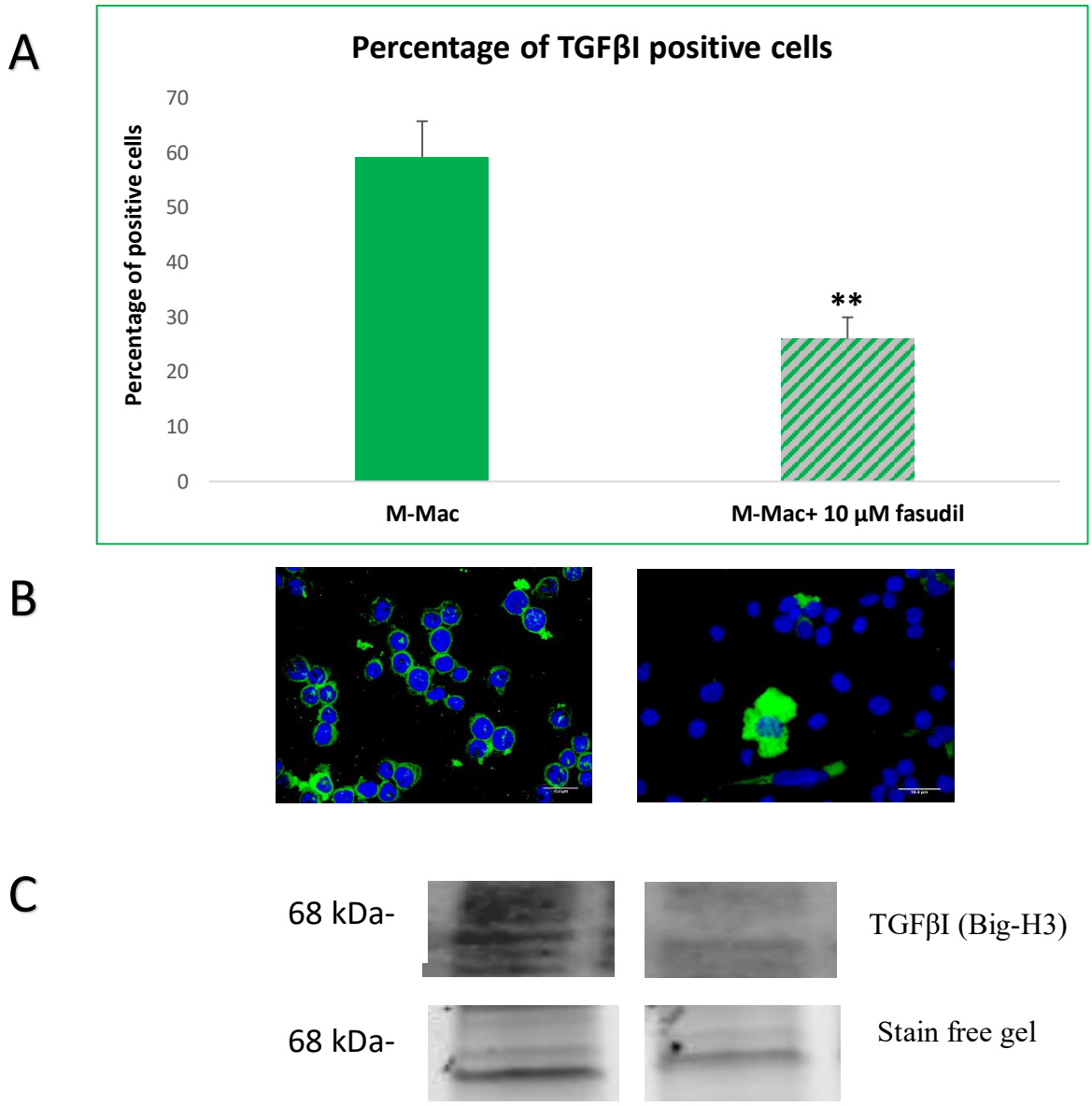

Figure 3.20 Fasudil reduced TGFβI protein expression in M-Macs.

A: Quantification of cellular TGFβI protein expression in M-Mac subset derived from THP-1 cells after 24 hour fasudil adminstration, assessed by immunocytochemistry. Data presented as percentage of TGFβI positive cells calculated within 10 random x 40 magnification fields. *indicates $p<0.05$; two tailed, paired t-test, n=4. N-values in macrophages differentiated from THP-1 cells represent number of replicates.

B: Representative images of immunocytochemistry for TGFβI within M-Macs treated with fasudil for 24 hours. Positive cells are shown as green and all nuclei are stained blue with DAPI. Scale bar represents 10 µm and applies to both panels.

C: Representative Western blot for TGFβI. Stain free gel is shown as a loading control. Approximate molecular weights are indicated on the left in kDa.

3.2.11.1 *Addition of recombinant TGFβ fails to rescue the inhibitory effect of fasudil on pSMAD3*

Considering the effects of F-actin modulation through fasudil administration is associated with changes in expression of TGFβ-induced (TGFβI), which as its name suggests is induced by TGFβ signalling, it is plausible that differences in F-actin content between macrophage subsets regulates TGFβ signalling or vice versa. Accordingly, phosphorylated SMAD3 (pSMAD3) expression was assessed in M-Mac and GM-Mac subsets, as a marker of active TGFβ signalling (Feng, Zhang et al. 2017). Quantification revealed a significant reduction in the nuclear expression of pSMAD3 within the GM-Mac subset compared to M-Macs (2.4-fold, $p<0.0001$; n=9; Figure 3.21), in keeping with concomitant decreased F-actin content and TGFBI expression in GM-Macs. Relatedly, to next determine if F-actin perturbation (through ROCK inhibition) suppressed TGFβ signalling, the effect of fasudil on pSMAD3 expression was evaluated in the M-Mac subset where F-actin is abundant. Indeed, M-Mac nuclear pSMAD3 expression was significantly reduced by fasudil treatment (67%, $p<0.0001$; n=5; Figure 3.22). Interestingly, co-incubation with recombinant TGFβ was unable to rescue the inhibitory effect of fasudil on pSMAD3 expression in M-Macs (Figure 3.22). In contrast, within the GM-Mac subset where F-actin content and TGFβI expression is low pSMAD3 positivity was unaffected by fasudil treatment or co-incubation with exogenous TGFβ (Figure 3.23).

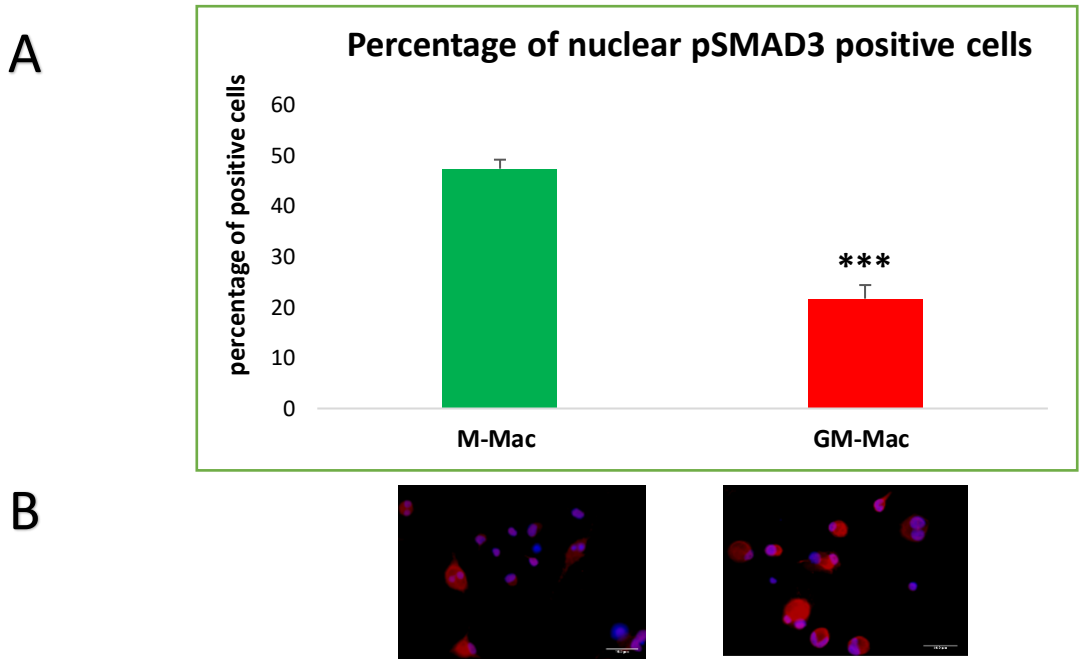

Figure 3.21 GM-Macs exhibit reduced nuclear protein expression of pSMAD3 expression compared to the M-Mac subset.

A: Quantification of nuclear pSMAD3 expression in M-Mac and GM-Mac subsets derived from THP-1 cells, assessed by immunocytochemistry. Data presented as percentage of nuclear pSMAD3 positive cells calculated within ten random x 40 magnification fields. *** indicates $p<0.001$; two tailed, paired t-test, n=9. N-values in macrophages differentiated from THP-1 cells represent number of replicates.

B: Representative images of immunocytochemistry for pSMAD3 within M-Mac and GM-subsets. Positivity of pSMAD3 is observed as red and all nuclei are stained blue with DAPI, nuclear pSMAD3 therefore appears cyan in colour. Scale bar represents 10 µm and applies to both panels.

A

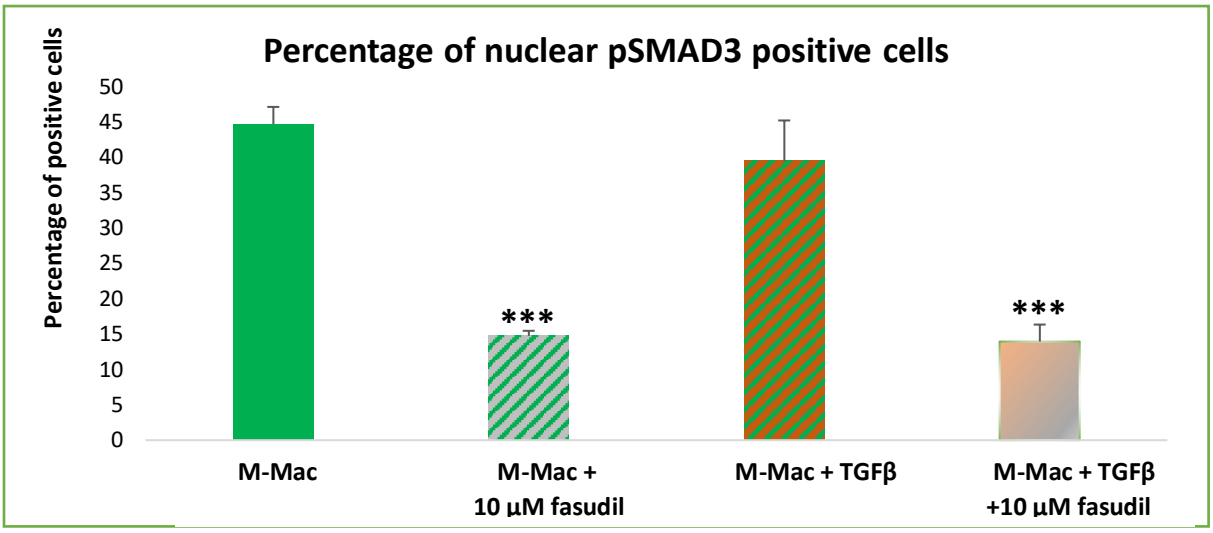

B

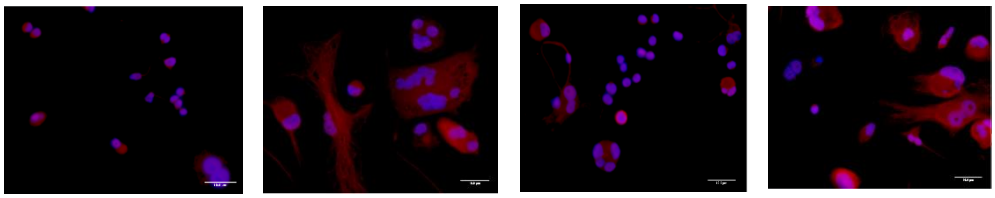

Figure 3.22 Fasudil reduces pSMAD3 expression in M-Macs, and is unaffected by exogenous TGFβ.

A: Quantification of nuclear pSMAD3 expression in M-Mac subset with and without addition of fasudil (10 µM) and/or recombinant TGFβ (0.2 ng/ml) for 24 hours, assessed by immunocytochemistry. Data presented as percentage of nuclear pSMAD3 positive cells calculated within ten random x 40 magnification fields. *** indicates $p<0.001$, ANOVA, Student-Newman-Keuls Multiple Comparisons Test, n=5. N-values in macrophages differentiated from THP-1 cells represent number of replicates.

B: Representative images of immunocytochemistry for pSMAD3 within M-Macs with and without addition of fasudil (10 µM) and/or recombinant TGFβ (0.2 ng/ml) for 24 hours. Positive cells are shown as red and all nuclei are stained blue with DAPI, nuclear pSMAD3 therefore appears cyan in colour. Scale bar represents 10 µm and applies all both panels.

A

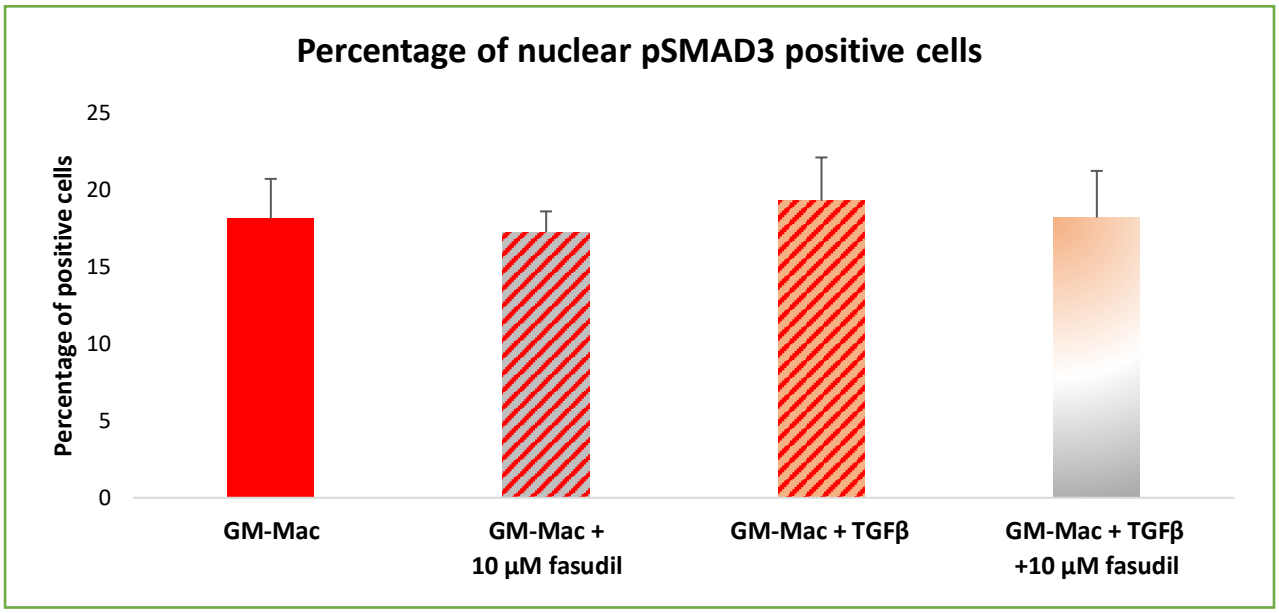

B

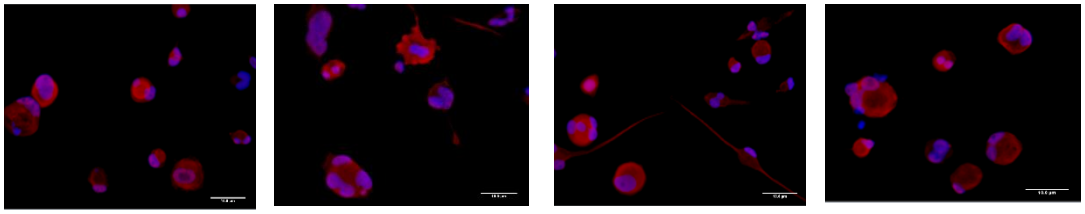

Figure 3.23 Addition of fasudil and/or recombinant TGFβ had no effect on expression of pSMAD3 in GM-Macs.

A: Quantification of nuclear pSMAD3 expression in GM-Mac subset with and without addition of fasudil (10 µM) and/or recombinant TGFβ (0.2 ng/ml) for 24 hours, assessed by immunocytochemistry. Data presented as percentage of nuclear pSMAD3 positive cells calculated within ten random x 40 magnification fields. No statitsical differences were detected by ANOVA, Student-Newman-Keuls Multiple Comparisons Test, n=5. N-values in macrophages differentiated from THP-1 cells represent number of replicates.

B: Representative images of immunocytochemistry for pSMAD3 within GM-Macs with and without addition of fasudil (10 µM) and/or recombinant TGFβ (0.2 ng/ml) for 24 hours. Positive cells are shown as red and all nuclei are stained blue with DAPI, nuclear pSMAD3 therefore appears cyan in colour. Scale bar represents 10 µm and applies all both panels.

3.2.11.2 *Addition of fasudil and/or recombinant TGFβ does not affect TGFβ receptor mRNA expression*

Considering fasudil perturbation of SMAD3 phosphorylation and associated downregulation of TGFβI protein expression in M-Macs could not be rescued through addition of recombinant TGFβ (Figure 3.22), aberrant expression of the TGFβ receptors was examined as a candidate mechanism. Quantification of qPCR revealed that mRNA expression of TGFBR1, TGFBR2, and TGFBR3 were unaffected by fasudil administration in both M-Mac and GM-Mac subsets (Figure 3.24). Furthermore, addition of recombinant TGFβ alone or in combination with fasudil also similarly did not induce any change in TGFβ receptor mRNA expression within either the M-Mac or GM-Mac subsets (Figure 3.24).

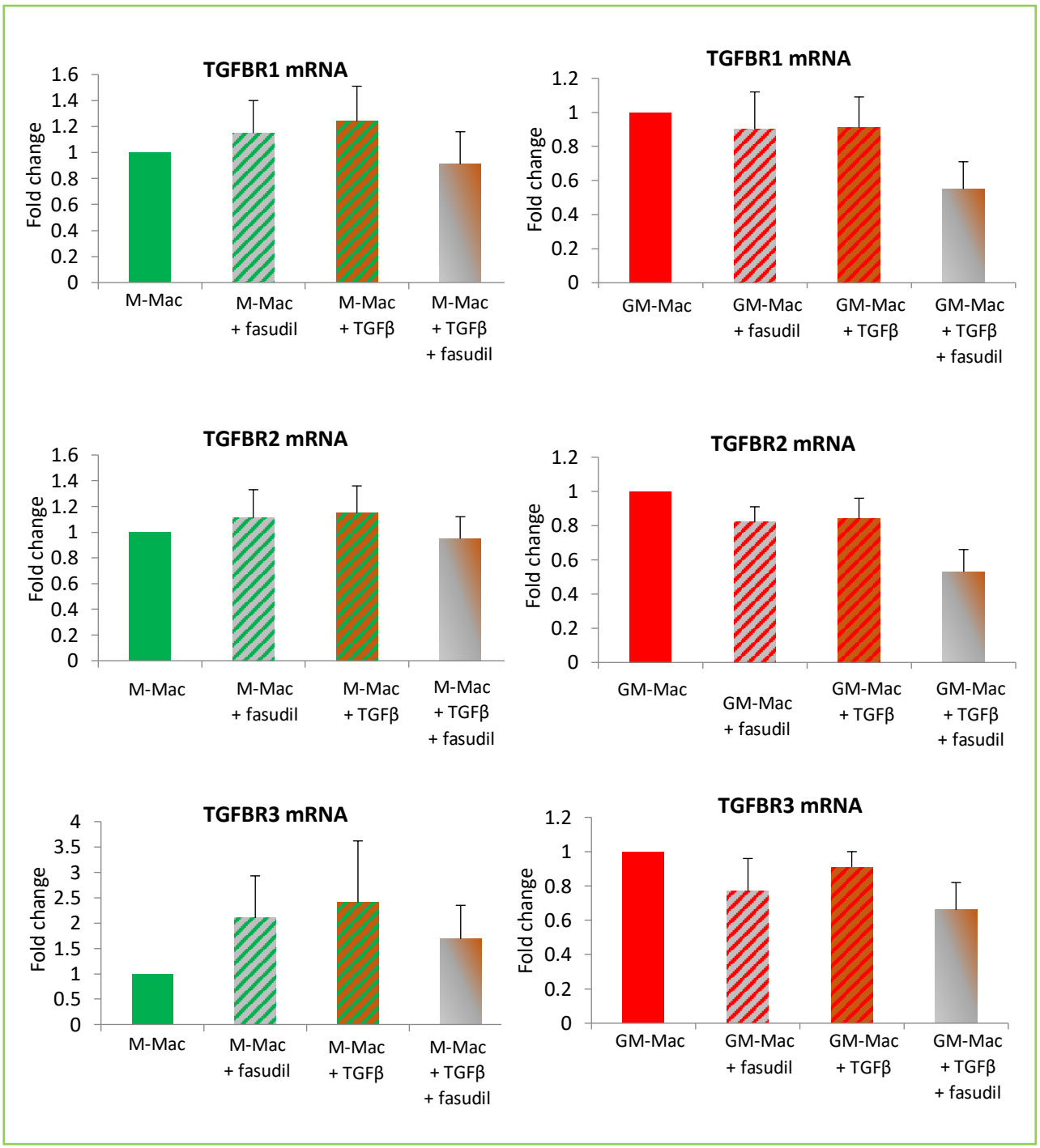

Figure 3.24 Addition of fasudil and/or recombinant TGFβ does not alter TGFβ receptor mRNA expression in M-Mac and GM-Mac subsets.

Quantification of TGFBR1, TGFBR2, and TGFBR3 mRNA expression in M-Mac and GM-Mac subsets derived from THP-1 cells, treated for 24 hours with fasudil (10 µM) and/or recombinant TGFβ (0.2 ng/ml) and assessed by RT-qPCR. Data presented as fold change against untreated M-Macs or untreated GM-Macs (mean ± SEM, ANOVA, Student-Newman-Keuls Multiple Comparisons Test, n=5). N-values represent number of replicates.

3.2.11.3 *Addition of fasudil and/or recombinant TGFβ does not affect TGFβ receptor protein expression*

To confirm that the TGFβ receptors were unaffected by fasudil treatment and/or addition of recombinant TGFβ at the protein level, western blotting was performed. Analysis confirmed TGFβR1, TGFβR2, and TGFβR3 protein expression were unchanged by fasudil administration in both M-Mac and GM-Mac subsets (Figure 3.25), or after addition of recombinant TGFβ alone or in combination with fasudil (Figure 3.25).

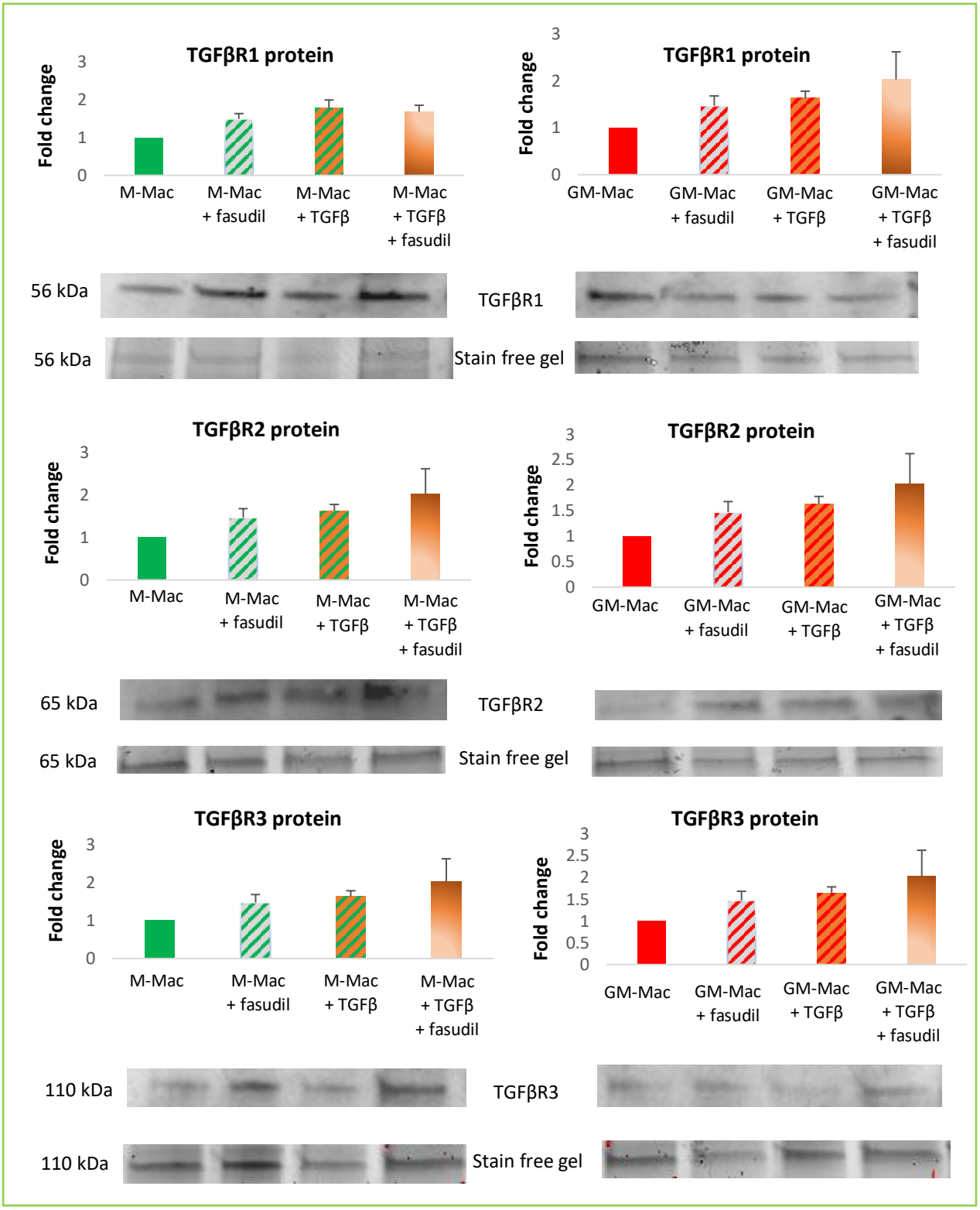

Figure 3.25 Addition of fasudil and/or recombinant TGFβ does not alter TGFβ receptor protein expression in M-Mac and GM-Mac subsets.

Quantification and representative western blots of TGFβR1, TGFβR2, and TGFβR3 protein expression in M-Mac and GM-Mac subsets derived from THP-1 cells, treated for 24 hours with fasudil (10 μM) and/or recombinant TGFβ (0.2 ng/ml). Stain free gel is shown as a loading control. Data presented as fold change against untreated M-Macs or untreated GM-Macs (mean ± SEM, ANOVA, Student-Newman-Keuls Multiple Comparisons Test, n=5). N-values represent number of replicates.

3.2.11.4 *Addition of a neutralizing TGFβ antibody blunts signalling as demonstrated by reduced pSMAD3 in M-Mac subsets but not when treated with fasudil*

The above findings confirmed fasudil administration does not affect TGFβ receptor expression and is therefore not responsible for the fasudil-mediated effects on TGFβ signalling. However, fasudil may aberrantly affect TGFβR function and subsequent down-stream signalling in M-Macs. Accordingly, a TGFβ1, 2, and 3 neutralising antibody was deployed to assess basal TGFβ signalling (through SMAD3 phosphorylation) in M-Macs alongside subsequent effects of fasudil co-incubation. Image analysis and quantification showed that addition of a TGFβ neutralising antibody (1 ng/ml) reduced the number of M-Macs with nuclear SMAD3 phosphorylation (56%; $p<0.001$; n=4; Figure 3.26), indicating TGFβ signalling is activated in the M-Mac subset under basal conditions. Moreover, the reduction in SMAD3 phosphorylation achieved with TGFβ inhibition was comparable to that observed with fasudil (Figure 3.26), implying a shared mechanism. Indeed, co-incubation with fasudil and the TGFβ neutralising antibody failed to exert a synergistic effect on pSMAD3 inhibition in M-Macs (Figure 3.26), further supporting the involvement of a common regulatory process affecting down-stream TGFβ signalling. As expected, considering the GM-Mac subset already exhibit blunted TGFβ signalling as evidenced by reduced pSMAD3 (Figure 3.21), addition of a TGFβ neutralising antibody exerted no additional effect on the number of GM-Macs expressing nuclear pSMAD3 (Figure 3.27).

A

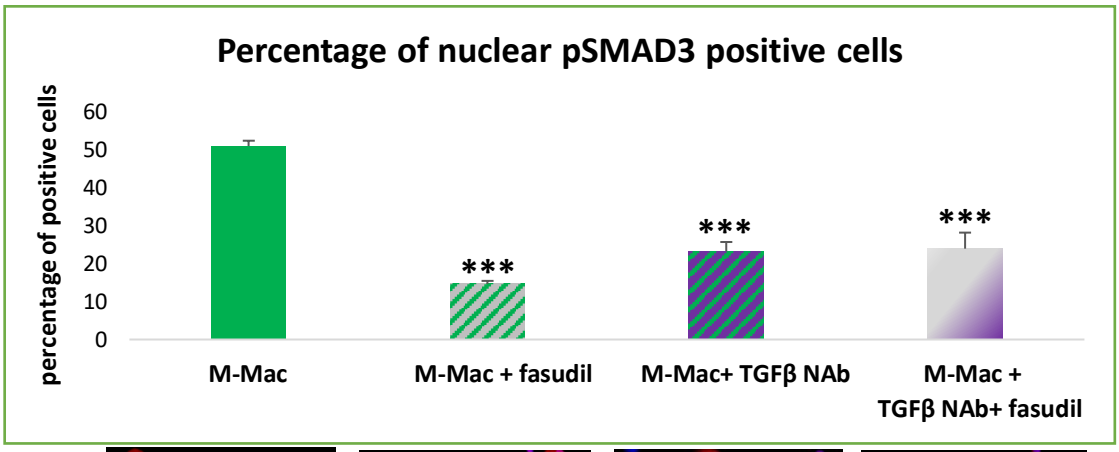

B

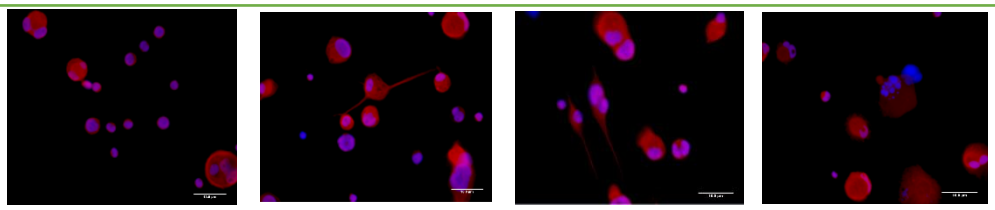

Figure 3.26 TGFβ inhibition reduces pSMAD3 expression in M-Macs to comparable levels as fasudil. Quantification of nuclear pSMAD3 expression in M-Mac subset with and without addition of fasudil (10 µM) and/or a TGFβ neutralising antibody (1 ng/ml) for 24 hours, assessed by immunocytochemistry. Data presented as percentage of nuclear pSMAD3 positive cells calculated within ten random x 40 magnification fields. *** indicates $p<0.001$, ANOVA, Student-Newman-Keuls Multiple Comparisons Test, n=4. N-values in macrophages differentiated from THP-1 cells represent number of replicates.

B: Representative images of immunocytochemistry for pSMAD3 within M-Macs with and without addition of fasudil (10 µM) and/or a TGFβ neutralising antibody (1 ng/ml) for 24 hours. Positive cells are shown as red and all nuclei are stained blue with DAPI, nuclear pSMAD3 therefore appears cyan in colour. Scale bar represents 10 µm and applies all both panels.

A

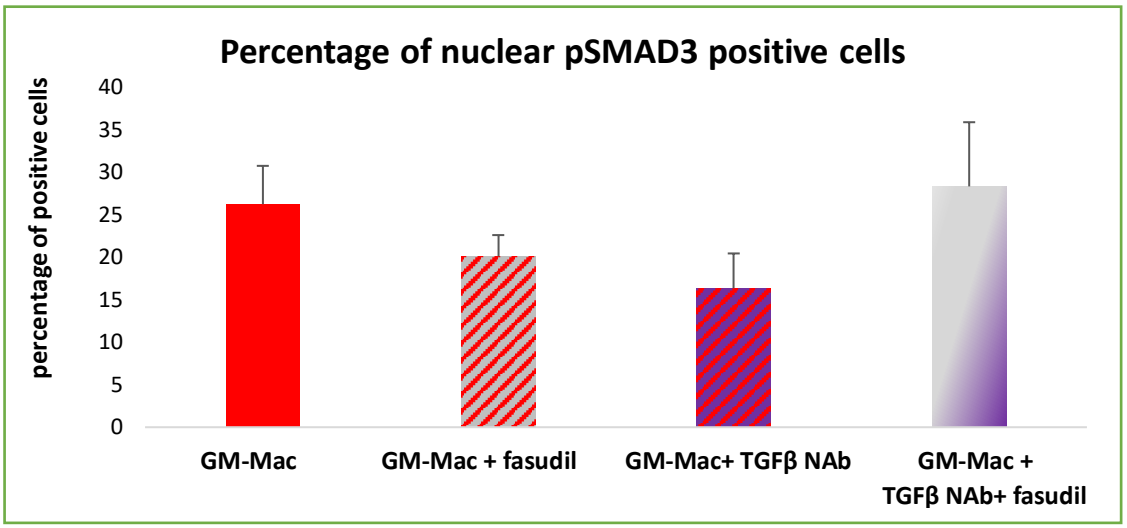

B

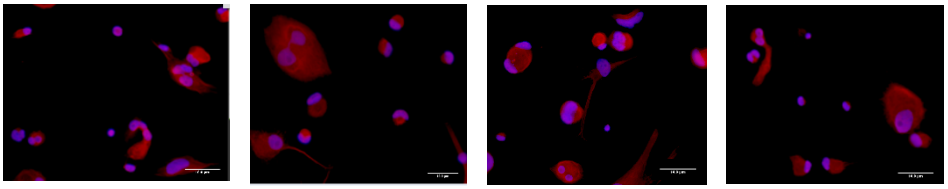

Figure 3.27 TGFβ inhibition does not affect pSMAD3 expression in GM-Macs, with and without fasudil.

Quantification of nuclear pSMAD3 expression in GM-Mac subset with and without addition of fasudil (10 µM) and/or a TGFβ neutralising antibody (1 ng/ml) for 24 hours, assessed by immunocytochemistry. Data presented as percentage of nuclear pSMAD3 positive cells calculated within ten random x 40 magnification fields. *** indicates $p<0.001$, ANOVA, Student-Newman-Keuls Multiple Comparisons Test, n=4. N-values in macrophages differentiated from THP-1 cells represent number of replicates.

B: Representative images of immunocytochemistry for pSMAD3 within GM-Macs with and without addition of fasudil (10 µM) and/or a TGFβ neutralising antibody (1 ng/ml) for 24 hours. Positive cells are shown as red and all nuclei are stained blue with DAPI, nuclear pSMAD3 therefore appears cyan in colour. Scale bar represents 10 µm and applies all both panels.

3.2.11.5 *TGFβ inhibition does not alter TGFB receptor mRNA expression in M-Mac or GM-Mac subsets*

To assess whether endogenous TGFβ regulates macrophage subset TGFB receptor expression, q-PCR was performed on both macrophage subsets treated with 10 µM of fasudil and/or 1 ng/ml of a TGFβ neutralising antibody for 24 hours. Quantification demonstrated that TGFβ inhibition does not alter the mRNA expression of TGFBR1, TGFBR2, or TGFBR3 in either the M-Mac or GM-Mac subset (Figure 3.28).

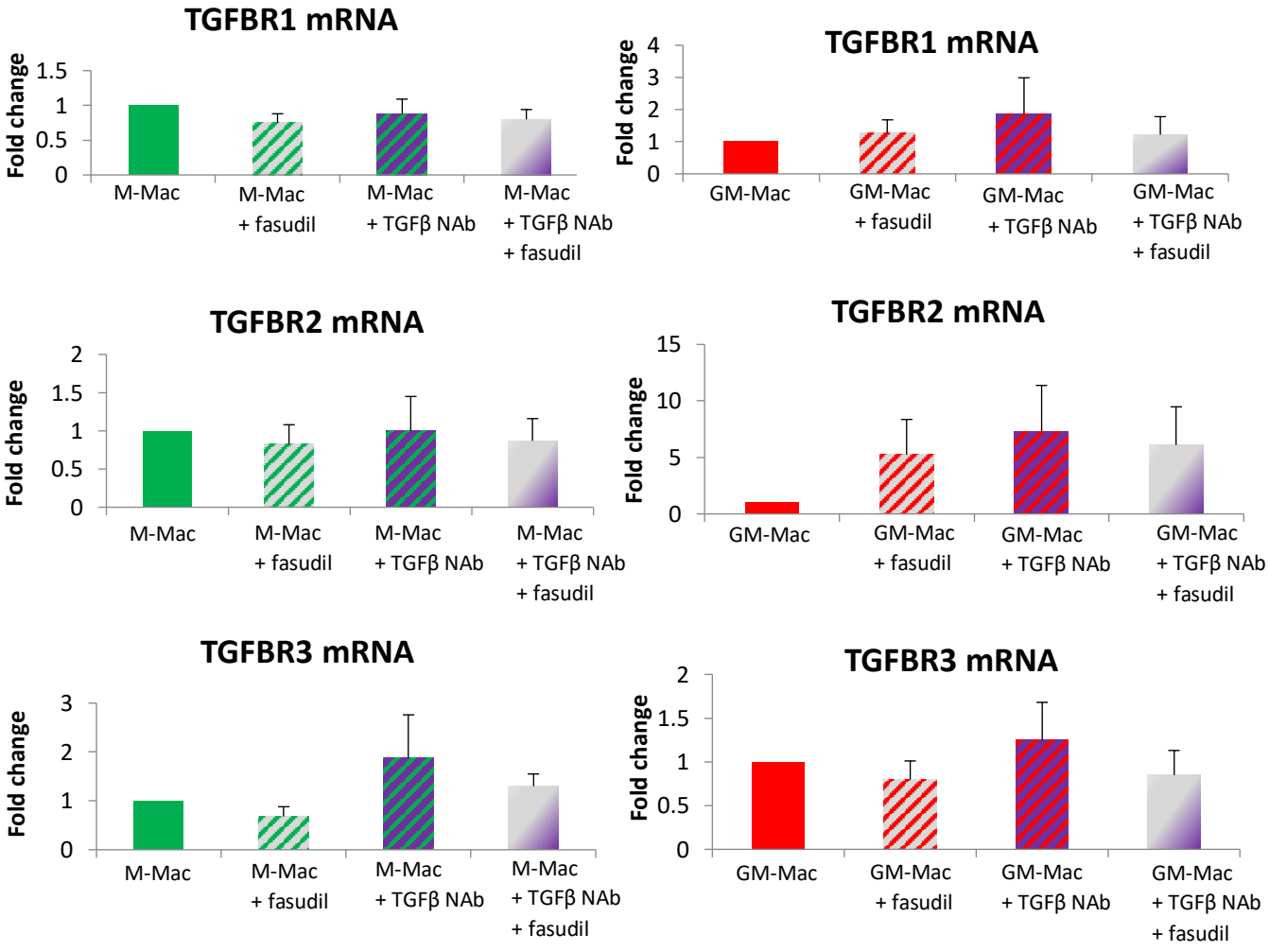

Figure 3.28 Addition of a TGFβ neutralising antibody did not affect TGFB receptor mRNA expression in either M-Mac or GM-Mac subsets.

Quantification of TGFBR1, TGFBR2, and TGFBR3 mRNA expression in M-Mac and GM-Mac subsets derived from THP-1 cells, treated for 24 hours with fasudil (10 µM) and/or a TGFβ neutralising antibody (1 ng/ml) and assessed by RT-qPCR. Data presented as fold change against untreated M-Macs or untreated GM-Macs (mean ± SEM, ANOVA, Student-Newman-Keuls Multiple Comparisons Test, n=5). N-values in macrophages differentiated from THP-1 cells represent number of replicates.

3.3 Discussion

THP-1 cells have been universally used as a model to study macrophage function and behaviour (Chanput, Mes et al. 2014), due to their accessibility, easily maintained in tissue culture, and safe due to no evidence of any viruses or toxins within the cells. The first aim within this chapter was to assess the ability of macrophages differentiated from THP-1 cells to polarise towards distinct macrophage subsets in a comparable manner to human PBMC-derived macrophages. Accordingly, due to the ease of access and use, THP-1 derived macrophages could supplement human primary macrophages during assessments of macrophage subsets. As such, in order to characterise and validate the THP-1 macrophages, alterations in specific morphological, functional, and molecular characteristics observed between primary human macrophage subsets were assessed.

The actin cytoskeleton has an essential role in modulating morphological, functional, and molecular activities in macrophages, including migration, phagocytosis and foam cell formation (Lee and Dominguez 2010). Accordingly, the second aim within this chapter was to assess the effect of two actin perturbing drugs (fasudil and pravastatin) on the behaviour of different macrophage subsets differentiated from THP-1 cells, alongside examining their effect on different cell markers at both mRNA and protein levels, and their effect on genes regulating actin cytoskeleton arrangement. It is proposed that altered actin cytoskeleton arrangement in macrophage subsets may differentially alter their behaviour and subsequently effect the progression of atherosclerosis.

3.3.1 The morphology of macrophages differentiated from THP-1 cells in response to different colony stimulating factors

Macrophages within atherosclerotic plaques exist as a heterogeneous population (Stout and Suttles 2004). Different CSFs, growth factors, and cytokines have been reported to regulate the differentiation of macrophages towards pro- and anti-inflammatory phenotypes (Waldo, Li et al. 2008, Wolfs, Donners et al. 2011). Morphological differences have been demonstrated between different macrophage subsets. Human monocyte-derived macrophages differentiated in the presence of GM-CSF for 7 days display a rounded morphology, while M-CSF directed maturation generates macrophages with an elongated shape (Waldo, Li et al. 2008). Reassuringly, macrophages differentiated from THP-1 cells also exhibited a round-shape when matured with GM-CSF, and an elongated morphology with M-CSF differentiation, suggestive of differences in their actin cytoskeleton.

Actin exists in two forms, a monomeric globular form (G-actin) and a polymeric filamentous form (F-actin). F-actin imparts a central role in the formation of the dynamic cytoskeleton of the cell, and therefore provides shape and motility to the cell (Rivero, Köppel et al. 1996). Pertinent to

macrophages, the F-actin cytoskeleton also contributes to multiple cellular functions including lamellipodia extrusion, cell locomotion, cytokinesis, and phagocytosis (Miller, Worrall et al. 2003, Rougerie, Miskolci et al. 2013). Considering the observed differences in cell morphology alongside the associated actions of the actin cytoskeleton, F-actin accumulation within macrophage subsets was examined. F-actin accumulation within anti-inflammatory M-CSF polarised macrophages was markedly greater compared to pro-inflammatory GM-CSF directed macrophages, indicating that actin filament rearrangements are different between divergent macrophage subsets. This finding and avenue of investigation is supported by the observation that disruption of F-actin filaments using the actin perturbing drug chondramide A in tumour-associated macrophages, altered cell shape and reduced the viability of anti-inflammatory macrophages while promoting pro-inflammatory macrophages properties (Pergola, Schubert et al. 2017). Taken together, the above findings confirm that the actin cytoskeleton behaves differently in distinct macrophage subsets, potentially affecting their behaviour and function.

Macrophage maturation is not considered terminal under the exposure of a single CSF. Studies have shown competition between different CSFs in macrophage differentiation and polarisation, for example, GM-CSF stimulation of M-CSF polarised macrophages can promote switching towards a pro-inflammatory phenotype (Di Gregoli and Johnson 2012). This proposition has been extended through the findings within this chapter which demonstrate MMP-12 as a robust marker for pro-inflammatory GM-CSF polarised macrophages derived from THP-1 cells (as is observed in human primary macrophages (Waldo, Li et al. 2008) which is upregulated in GM-CSF stimulated M-Macs. These effects mirror those of reduced F-actin accumulation within GM-CSF stimulated M-Macs. A possible mechanism for GM-CSF reversing the effects of M-CSF polarisation can be garnered from a previous study which showed that during inflammation GM-CSF levels are increased while macrophage expression of the M-CSF receptor (CSF1R) is compromised, favouring a GM-CSF response, due in part to the macrophages reduced ability to react to M-CSF (Becker, Liu et al. 2012). Similarly, a M-CSF resistant model has been proposed where under physiological conditions abundant M-CSF dictates that macrophages are polarised towards an anti-inflammatory phenotype, but can be converted to pro-inflammatory macrophages during inflammation due to increased levels of GM-CSF (Hamilton 2008). Subsequently, during the resolution phase of inflammation when the levels of GM-CSF are lowered, macrophages can revert to an anti-inflammatory phenotype when M-CSF concentrations are dominant (Hamilton 2008). Collectively, the results within this chapter alongside the published findings suggest that while M-CSF permits canonical macrophage polarisation, their exposure to GM-CSF promotes transition to a pro-inflammatory phenotype that is resistant to successive M-CSF stimulation. However, it is plausible that GM-Macs (differentiated from THP-1 cells) require higher

concentrations of M-CSF and/or longer incubation periods to revert back to an anti-inflammatory phenotype.

3.3.2 Validation of macrophage subsets differentiated from THP-1 cells

A primary feature associated with the polarisation of macrophages towards distinct phenotypes is their expression of specific markers at mRNA and protein levels. Evidence provided within this chapter revealed M-Macs differentiated from THP-1 cells display increased mRNA and protein expression of TGFBI, compared to pro-inflammatory GM-Macs. TGFBI is involved in tissue repair and modulation of immune responses (Singh and Ramji 2006), and studies on primary human macrophages showed that anti-inflammatory macrophages increase their production of TGFBI after their uptake of apoptotic cells (Nacu, Luzina et al. 2008). Additionally, macrophages differentiated from THP-1 cells showed increased protein expression of TGFBI after engulfment of apoptotic Jurkat T cells (Nacu, Luzina et al. 2008). A further study demonstrated that human PBMC-derived anti-inflammatory macrophages express high levels of TGFBI compared to pro-inflammatory macrophages (Gratchev, Guillot et al. 2001). Taken together, these findings demonstrate the applicability of deploying TGFBI as a marker for anti-inflammatory macrophages (such as M-Mac), both PBMC-derived and those generated from THP-1 cells.

Conversely, pro-inflammatory GM-Macs differentiated from THP-1 cells under the direction of GM-CSF displayed an upregulation of MMP-12 mRNA and protein expression when compared to M-CSF polarised anti-inflammatory M-Macs. MMP-12 is involved in the degradation of ECM proteins, especially elastin, and subsequent remodelling of the arterial wall (Harris, Smith et al. 2010, Myasoedova, Chistiakov et al. 2018). Furthermore, MMP-12 has been shown to play a major contributory role to the development and progression of atherosclerosis in mouse models and humans (Johnson, George et al. 2005, Johnson Jason, Devel et al. 2011, Scholtes, Johnson et al. 2012) In line with the findings reported here, two previous studies reported increased expression of MMP-12 in GM-CSF polarised human PBMC-derived macrophages compared to their M-CSF directed counterparts (Waldo, Li et al. 2008, Aristorena, Gallardo-Vara et al. 2019, Di Gregoli, Somerville et al. 2020). In addition, MMP-12 levels can be significantly upregulated in M-CSF polarised macrophages with pro-inflammatory mediators such as LPS, IFNγ, TNFα, and IL-1β (Huang, Sala-Newby et al. 2012) Collectively, the above support the use of MMP-12 as a marker of pro-inflammatory macrophages of both PBMC and THP-1 cell origin.

Comparable to MMP-12, the mRNA and protein expression of SPARC (also known as osteonectin) was higher in pro-inflammatory GM-Macs differentiated from THP-1 cells with GM-CSF, relative to levels

within M-CSF polarised anti-inflammatory M-Macs. Elevated SPARC expression has been associated with calcification, neovascularisation, inflammation, and increased MMP expression within aortic stenosis, which have similar characteristics within advanced atherosclerotic plaques (Charest, Pépin et al. 2006), Relatedly, it has been previously reported that SPARC promotes pro-inflammatory (M1) macrophage polarisation of human PBMC-derived macrophages (Toba, de Castro Brás et al. 2015) , and enhances their release of MMP-1 and MMP-9 (Shankavaram, DeWitt et al. 1997). Finally, transcriptomic analysis of GM-CSF polarised, and M-CSF directed human PBMC-derived macrophages demonstrated SPARC expression was markedly increased in GM-CSF macrophages (Waldo, Li et al. 2008). Therefore, SPARC can be considered a marker of pro-inflammatory GM-Macs, derived from PBMCs and THP-1 cells

Finally, and in agreement with a previous study (Waldo, Li et al. 2008), TIMP3 mRNA expression is increased in pro-inflammatory GM-Macs compared to anti-inflammatory M-Macs, of both PBMC and THP-1 origin. However, while a further study also demonstrated GM-CSF polarisation increased TIMP-3 mRNA levels, protein expression was significantly decreased through a novel post-transcriptional mechanism regulated by microRNA-181b (Di Gregoli, Mohamad Anuar Nur et al. 2017) . Comparing M1 and M2 human macrophages, elevated TIMP-3 expression was associated with the anti-inflammatory M2 macrophage subset (Huang, Sala-Newby et al. 2012) . Furthermore, macrophage TIMP-3 protein expression within atherosclerotic plaques is restricted to anti-inflammatory macrophages (Johnson, Jenkins et al. 2014) , while loss of TIMP-3 expression promotes atherosclerosis in mice and TIMP-3 restoration in macrophages prevents plaque progression (Di Gregoli, Mohamad Anuar Nur et al. 2017). As such, while decreased TIMP-3 mRNA expression may delineate macrophage subsets from both PBMC and THP-1 origin, at the protein level increased TIMP-3 expression is observed in anti-inflammatory macrophages.

Gene array studies showed specific transcriptome differences between M-CSF and GM-CSF polarised macrophages with variations in the expression of genes associated with inflammation and cholesterol homeostasis (Waldo, Li et al. 2008). Previous studies reported that expression of anti-inflammatory molecules such as IL-10 are upregulated in anti-inflammatory macrophages compared to their pro-inflammatory counterparts (Di Gregoli and Johnson 2012). Reassuringly, this response is mirrored in M-Macs differentiated from THP-1 cells.

Foam cell formation due to the uptake of ox-LDL is an essential process for the progression of atherosclerotic plaques. Modified lipids are taken-up through scavenger receptors expressed by macrophages (Ley, Miller et al. 2011). Although both M-Mac and GM-Mac subsets uptake lipid and form foam cells, it has been reported that macrophage subsets differently express genes related to

the haemostasis of lipids and expression of scavenger receptors (Waldo, Li et al. 2008). M-Macs differentiated from THP-1 cells showed increased expression of CD36, MRC1 and MSR1 while GM-Macs displayed heightened levels of LOX-1 (OLR1) at the mRNA level. Likewise, human M-CSF polarised PBMC-derived macrophages had increased expression of CD36, MSR1 and MRC1 and decreased expression of LOX-1 compared to GM-CSF directed macrophages (Di Gregoli and Johnson 2012). Supporting the use of differential scavenger receptor expression for delineating macrophage subsets, a further study demonstrated that MRC1 can be used as an M2 or anti-inflammatory macrophage marker in both mice and humans (Rőszer 2015). In conclusion, macrophages differentiated from THP-1 cells display similar expression patterns of genes that regulates their activity and behaviour to that observed in human PBMC-derived macrophages and can be utilised to identify changes in their phenotype.

3.3.3 F-actin content in macrophage subsets in response to fasudil or pravastatin

The assembly of F-actin filaments is in part directed by the Rho family of small GTP-ases and their related kinases ROCK1 and ROCK2. Accordingly, fasudil (ROCK inhibitor) and pravastatin (inhibits isoprenylation of Rho family of small GTP-ases) have been proposed to directly regulate the actin cytoskeleton of cells. Previous studies reported that fasudil caused disruption and decreased polymerisation of F-actin filaments and bundles in fibroblasts (Li, Wu et al. 2018). Another study demonstrated that fasudil inhibited F-actin filament formation while increasing G-actin content in astrocytes (Lau, O'Shea et al. 2011).These findings are in agreement with the observations in this chapter which demonstrated fasudil administration to macrophage subsets differentiated from THP-1 cells decreased their F-actin accumulation. This comparable response further supports the use of THP-1 derived macrophages for the assessment of changes in the F-actin cytoskeleton between macrophage subsets. Likewise, macrophage subsets differentiated from THP-1 cells showed decreased F-actin filament content when treated with pravastatin. In agreement, it has been demonstrated that the F-actin cytoskeleton of macrophages became disorganised after treatment with a statin (Kamal, Chakrabarty et al. 2018). Another study showed that the administration of fluvastatin caused disruption of F-actin filaments and loss of stress fibre formation in VSMCs (Kato, Hashikabe et al. 2004).

As mentioned above, fasudil and pravastatin significantly induced morphological changes in different macrophage subsets associated with F-actin rearrangement within the macrophage subsets examined. Changes in the morphology of macrophages might have consequence for cellular behaviour, including polarisation. Both M-Macs and GM-Macs treated with pravastatin showed increased expression of

TGFBI at mRNA and protein levels. This suggests that pravastatin shifts the polarisation of macrophages towards an anti-inflammatory phenotype. In support of this proposition, a previous study reported that simvastatin and atorvastatin therapy for 6 weeks reduced the number of M1 (pro-inflammatory) macrophages within human atherosclerotic aortic aneurysms while increasing the quantity of M2 (anti-inflammatory) macrophages, apportioned to shifting intra-aneurysm M1 macrophages towards an M2 phenotype (van der Meij, Koning et al. 2013). The heightened expression of TGFBI with statin treatment is in line with reports linking TGFβ levels and statins, with increased synthesis of TGFβ observed in monocytes/macrophages upon inhibition of HMG-CoA reductase levels through statin addition (Porreca, Di Febbo et al. 2002). Furthermore, studies showed that statins promote the activation of the TGFβ-induced Smad pathway, alongside enhanced expression of TGFβ receptor type II, and heightened synthesis of TGFβ in VSMCs (Rodríguez-Vita, Sánchez-Galán et al. 2008).

As previously stated, MMP-12 is a robust marker of the GM-Mac subset in human PBMC-derived macrophages (Waldo, Li et al. 2008, Aristorena, Gallardo-Vara et al. 2019, Di Gregoli, Somerville et al. 2020) and as demonstrated within this chapter, similarly for GM-CSF directed THP-1 macrophages. Supporting the proposed anti-inflammatory properties of statins, the results within this chapter show that pravastatin decreased MMP-12 protein levels of THP-1 derived GM-Macs. It has been reported previously that statins inhibit macrophage and VSMC production of MMPs (Luan, Chase Alex et al. 2003) (Hohensinner, Baumgartner et al. 2018). Specifically, simvastatin reduced fibroblast MMP-12 mRNA expression (Kamio, Liu et al. 2010). Interestingly, while the increased MMP-12 expression in GM-CSF polarised macrophages occurs at the mRNA and protein level, the inhibitory action of pravastatin administration was only observed at the protein level, suggesting statins may regulate pro-inflammatory MMP-12 protein levels through a post-transcriptional mechanism, such as microRNA regulation. Indeed, a previous study demonstrated that GM-Mac MMP-14 protein expression is repressed by a microRNA, miR-24 (Di Gregoli, Jenkins et al. 2014) .

As such, the concomitant increased expression of the anti-inflammatory marker TGFBI and decreased levels of the pro-inflammatory marker MMP-12 in macrophages after treatment with pravastatin, suggests that pravastatin shifts macrophages towards an anti-inflammatory phenotype. Considering the changes pravastatin also exerted on macrophage F-actin accumulation, a potential mechanism linked to the shifting in the polarisation of macrophages may be due to changes in gene expression of actin filament modulators. Indeed, findings within this chapter demonstrated the mRNA expression of cytoskeletal proteins which facilitate F-actin binding to the cell membrane (fascin, radixin, and vinculin) were generally increased in both M-Mac and GM-Mac macrophage subsets after treatment with pravastatin. In fact, it has been reported that simvastatin, pitavastatin, and cerivastatin

significantly enhanced the expression of genes related to the organisation of the actin cytoskeleton (Gbelcová, Rimpelová et al. 2017). Related, it was demonstrated that statins prevent activation and relocation of RhoA to the cell membrane, therefore preventing ROCK activation at the cell membrane and perturbing actin stress fibre formation (Brandes Ralf 2005, Dong, Yan et al. 2010) We can therefore speculate that the deactivation of ROCK through blunted translocation of RhoA to the cell membrane, might be due to the regulation of actin binding genes that are regulated by the administration of statins. This would suggest that statins regulate the actin cytoskeleton of macrophages and subsequently regulate their behaviour and polarisation towards, in part underlying their anti-inflammatory response during chronic inflammation, such as is seen during atherosclerotic plaque progression. However, given that TGFβ is a growth factor that can modulate intracellular signalling mechanisms and MMP expression, while MMP-12 can cleave multiple substrates which may influence cell function and TGFβ signalling (Di Gregoli, Somerville et al. 2020), these markers of M-Mac and GM-Mac subsets respectively, may exert direct effects on the actin cytoskeleton which are modulated by statins.

With regard to THP-1 derived GM-Mac expression of MMP-12, fasudil exerted a similar effect to that observed with pravastatin administration chiefly suppressed expression of MMP-12 at the protein level with no significant change in mRNA expression. Again, such findings suggest the involvement of a novel post-transcriptional mechanism, which requires further investigation to evaluate if a microRNA or another epigenetic regulatory pathway directs fasudil modulation of MMP-12 protein expression in GM-Macs. Although previous studies have reported that fasudil decreases the expression of MMPs (MMP-2 and MMP-9) in retinal microglial cells, markedly perturbing their migratory capacity (Xu, Xu et al. 2016), effects on MMP-12 levels have not been previously investigated. Nonetheless, the findings within this chapter suggests that fasudil (similar to pravastatin) shifts the polarisation of pro-inflammatory GM-Macs towards an anti-inflammatory macrophage phenotype, evidenced by decreased expression of MMP-12 (at the protein level). Supporting an anti-inflammatory action of fasudil, a previous study reported that administration of fasudil to pro-inflammatory M1 macrophages (polarised with IFNγ) shiftes their phenotype towards a M2-like macrophage, attributed through decreased expression of the M1 marker iNOS alongside upregulated expression of the M2 marker CD206 (Liu, Li et al. 2013).

It should be noted that although TGFBI mRNA expression was increased in THP-1 derived M-Macs, protein expression was decreased, suggesting that fasudil shifts the polarisation of anti-inflammatory macrophages towards a pro-inflammatory phenotype, an observation that warrants further investigation. In agreement with this observation, it has been reported that administration of fasudil (pan ROCK isoform inhibitor) or selective inhibition of ROCK2 pushed anti-inflammatory M2

macrophages towards a pro-inflammatory phenotype by decreasing the expression of anti-inflammatory macrophage markers (such as CD206) alongside the decreased secretion of anti-inflammatory molecules such as IL-10 (Zandi, Nakao et al. 2015).

3.3.4 TGFβ signalling in response to fasudil in anti-inflammatory macrophages

As mentioned earlier, TGFβ has an essential role in modulation of immune reactions and tissue repair (Singh and Ramji 2006). Moreover, TGFβ is a growth factor that can direct multiple functions involved in cell differentiation, proliferation, and survival (Gong, Shi et al. 2012). Previous studies reported that TGFβ signalling has an essential role in regulating the expression of genes characteristic of M2 (anti-inflammatory) macrophages. While loss of TGFβ type II receptor expression blunted the polarisation of macrophages towards an anti-inflammatory phenotype (Gong, Shi et al. 2012). Within this chapter, it is demonstrated that fasudil administration reduced TGFBI protein expression in anti-inflammatory M-Macs, implying a shift in polarisation towards a pro-inflammatory phenotype. ROCK (the target of fasudil) is considered as a main downstream signalling molecule within the TGFβ pathway, with a previous mouse diabetic retinopathy study demonstrating that blocking TGFβ signalling suppressed cellular responses associated with ROCK activity, such as elevated expression of α-smooth muscle actin (α-SMA) and phosphorylation of myosin light chain (MLC) (Kita, Hata et al. 2008). TGFβ biological activity depends on activation of the Smad pathway (Samarakoon, Overstreet et al. 2013), with activation of TGFβ signalling significantly augmenting phosphorylation of SMAD3 (Feng, Zhang et al. 2017). Accordingly, SMAD3 phosphorylation (pSMAD3) was deployed as a marker for the activation of TGFβ signalling in this chapter, with GM-Macs displaying reduced pSMAD3 compared to anti-inflammatory M-Macs, suggesting that TGFβ signalling is blunted in pro-inflammatory macrophages, in line with the differences in TGFBI expression. In agreement, it has been reported that the release of TGFβI as a result of the activation of TGFβ signalling, is higher in IL-4 polarised anti-inflammatory M2 macrophages compared to IFNγ-directed pro-inflammatory M1 macrophages (Gratchev et al. 2001).

Interestingly, although fasudil adminstration to M-Macs blunted TGFβ signalling (as evidenced by reduced pSMAD3 and TGFBI expression), this could not be rescued through the addition of recombinant TGFβ, suggesting the inhibitory action of fasudil is upon the pathway and not TGFβ itself. Exploring the pathway further in this chapter, fasudil did not alter the mRNA or protein expression of any TGFβ receptors in M-Macs, or their responsiveness to TGFβ, as shown through assessment of pSMAD3 after deployment of a TGFβ neutralising antibody. Therefore, it can be proposed that the inhibitory effect of fasudil on the TGFβ signalling pathway within M-Macs is between TGFβ receptor activation and phosphorylation of SMAD3, or upon another pathway/mechanism that modulates SMAD3 levels and/or phosphorylation and subsequnet down-stream signalling. In support of the latter,

administration of a ROCK inhibitor (Y-27632) to occular fibroblasts blocked TGFβ-mediated pSMAD3 levels, which was attributed to a decreased SMAD mRNA expression (Feng, Zhang et al. 2017). Accordingly, this suggests that in anti-inflammatory M-Macs TGFβ-mediated signalling through SMAD3 phosphorylation is facilitated by Rho/ROCK regulation of SMAD3 levels. This hypothesis warrants further investigation as it may explain the relationship between F-actin cytoskeleton alteration during differential macrophage polarisation and associated anti- and pro-inflammaotry actions, such as TGFβ-mediated signalling.

In conclusion, both M-Macs and GM-Macs treated with pravastatin showed increased expression of the anti-inflammatory marker TGFBI and decreased levels of the pro-inflammatory marker MMP-12. Fasudil exerted similar effect to that observed with pravastatin co-incubation. GM-Macs treated with fasudil showed increased expression of TGFBI and suppressed expression of MMP-12 suggesting that pravastatin and fasudil shift macrophages toward an anti-inflammatory phenotype. Since foam cell formation due to the uptake of ox-LDL via scavenger receptors expressed by macrophages is an essential process for the progression of atherosclerotic plaques, it is important to assess the effect of actin perturbing drugs (fasudil and pravastatin) on anti-and pro-inflammatory foam cell macrophages

4 EFFECT OF ACTIN-PERTURBING DRUGS ON FOAM CELL FORMATION IN DIVERGENT MACROPHAGE SUBSETS

4.1 Introduction

Monocytes and macrophages and have an essential role in the development of atherosclerotic plaques, especially through their uptake of oxLDL via scavenger receptors and their subsequent transformation into foam cells within developing intimal lesions (Glass and Witztum 2001). The formation of foam cells also plays a central role in the progression of atherosclerosis. As an innate immune mechanism concerning self-protection, macrophages uptake and eliminate modified lipids via reverse cholesterol transport which involves cholesterol efflux pathways and the regulation of specific transporters such as ABCA1 and ABCG1 (Schmitz, Langmann et al. 2001). However, when the engulfment of modified lipids exceeds efflux capacity in macrophages, cytoplasmic stored droplets of altered lipids accumulate and results in foam cell formation (Zhou, Mei et al. 2012). It has been reported that ROCK has a pivotal role in the development of cardiovascular diseases such as atherosclerosis. Studies have shown that deficiency of ROCK1 in macrophages inhibited their transformation into foam cells and delayed the development of atherosclerotic plaques, thought to be due to decreased uptake of modified lipoproteins (Wang, Liu et al. 2008), although it must be noted increased cholesterol efflux was not assessed as a potential contributing factor. Similarly, another study showed that oxLDL accumulation within macrophages increased ROCK2 activity, and deficiency of ROCK2 in bone marrow cells (predominantly monocyte/macrophages) significantly decreased atherosclerotic plaque formation within the aorta and aortic sinus (Zhou, Mei et al. 2012). Furthermore, ROCK2-deficiency resulted in decreased macrophage foam cell formation due to heightened cholesterol through a PPARγ/LXR/ABCA1 pathway, effects which could be replicated in wild-type macrophages through fasudil administration (Zhou, Mei et al. 2012). Accordingly, we can conclude that ROCK signalling within macrophages participates in atherogenesis and therefore ROCK inhibition in macrophages might be a therapeutic target for suppressing the development of atherosclerosis.

Treatment of symptomatic CVD patients with statins has been shown to associate with the regression of coronary atherosclerotic plaques, and subsequent diminished rates of mortality and morbidity related to CVD (Hofnagel, Luechtenborg et al. 2007). In addition to their cholesterol-lowering properties, the pleiotropic effect of statin therapy has many clinical implications to atherosclerosis including the ability of statins to ameliorate oxidative stress (Tsiara, Elisaf et al. 2003), and therefore retard the generation of oxLDL. Relatedly, studies have shown that statins reduce both lipid accumulation and foam cell formation within atherosclerotic plaques (Crisby, Nordin-Fredriksson et al. 2001). One of the mechanisms for the anti-oxidative pleiotropic ability of statins is the inhibition of

isoprenylation. Activation of the anti-oxidative enzyme catalase inhibits the translocation of Rac1 from the cytosol to the cell membrane, resulting in downregulation of NADPH oxidase activity and subsequent reduced ROS production (Wassmann, Laufs et al. 2002). It has also been reported that statins regulate the expression of scavenger receptors, through the reduced isoprenylation of small family GTP-ases such as Ras and Rho. Studies have described that inactivation of Ras and Rho results in the downregulation of the expression of multiple macrophage scavenger receptors including LOX-1 and SR-A (Umetani, Kanayama et al. 1996). Therefore, statin modulation of macrophage scavenger receptors through perturbation of Rho/ROCK signalling would be expected to reduce foam cell formation, and therefore inhibit lipid core formation/expansion, and subsequently stabilise advanced atherosclerotic plaques.

4.1.1 Aim of this chapter

In this chapter, I attempt to evaluate the effect of actin perturbing drugs (fasudil and pravastatin) on the ability of divergent macrophage subsets to accumulate modified lipids and transform into foam cells, alongside assessing the effect of fasudil and pravastatin on the ability of different macrophage subsets to uptake apoptotic cells by efferocytosis.

4.2 Results

4.2.1 Monocytes exhibit lipid accumulation and early foam cell formation, which is blunted by co-incubation with fasudil

Within the previous chapter it was confirmed that THP-1-derived macrophages display similar polarisation towards M-Mac and GM-Mac phenotypes as human blood monocyte-derived macrophages, supporting the use of THP-1-derived macrophages for in vitro studies. A further benefit of THP-1 cells is their ability to be grown and studied in vitro while remaining monocytic, a function not possible with human blood-derived monocytes. This beneficial capacity of THP-1 cells was exploited to assess whether monocytes can form foam cells, THP-1 cells without PMA-induced differentiation to ensure they remain monocytic, were incubated with either M-CSF or GM-CSF for either 24 hours or 72 hours alongside 10 µg/ml of Dil-oxLDL. Afterwards, cells were subjected to Oil red O staining to visualize oxLDL accumulation (foam cell formation). Images revealed that 24-hour M-CSF or GM-CSF stimulated monocytes were able to accumulate lipid and form foam cells to a comparable level (Figure 4.1). However, monocytes that were incubated for 72 hours with GM-CSF displayed significantly increased foam cell formation compared to monocytes incubated for 72 hours with M-CSF (62%; $p<0.05$; n=5; Figure 4.2). Comparing monocyte-derived foam cell formation between the 24-hour and 72-hour time-points revealed M-CSF stimulated monocytes displayed a significant reduction in oxLDL accumulation at the later time-point compared to their 24-hour counterparts (73%; $p<0.05$; n=5; Figure 4.1 and 4.2). However, no statistical difference was observed between 24-hour and 72-hour GM-CSF-incubated monocytes (Figure 4.1 and 4.2), suggesting M-CSF monocytes enhance their cholesterol efflux capacity overtime compared to GM-CSF stimulated monocytes.

A

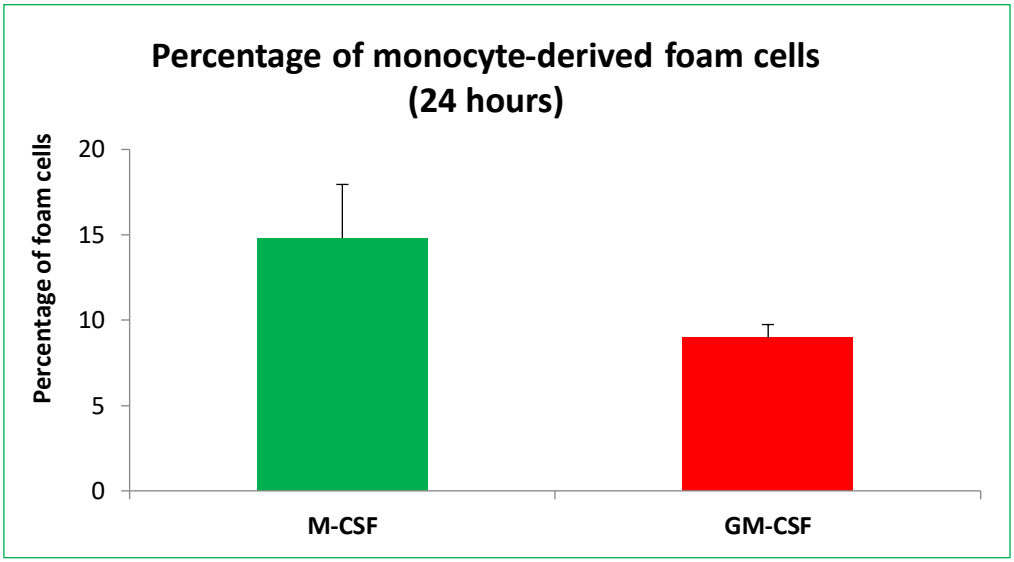

B

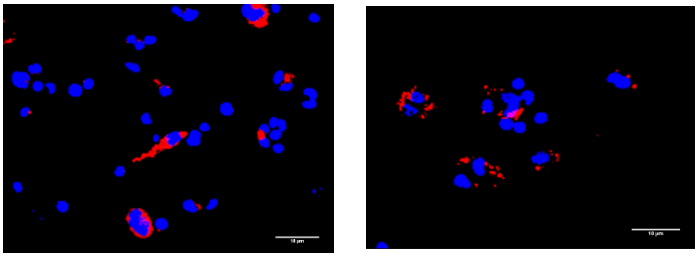

Figure 4.1 Monocytes incubated for 24 hours with M-CSF or GM-CSF were able to accumulate oxLDL and form foam cells.

A: Quantification of monocyte-derived foam cell formation after 24-hour incubation with M-CSF or GM-CSF, plus Dil-oxLDL (10 µg/ml). Monocytes were stained with Oil Red O to visualise accumulation of oxLDL. Cells were counted within 10 random x 40 magnification field. *indicates $p<0.05$, two tailed, paired t-test n=5. N-values in macrophages differentiated from THP-1 cells represent number of replicates.

B: Representative images of monocyte-derived foam cells showing lipid accumulation. Monocytes were stained with Oil Red O to visualise accumulation of oxLDL (red) and cells counterstained with DAPI (blue) to depict nuclei. Scale bar represents 10 µm and applies to both panels.

A

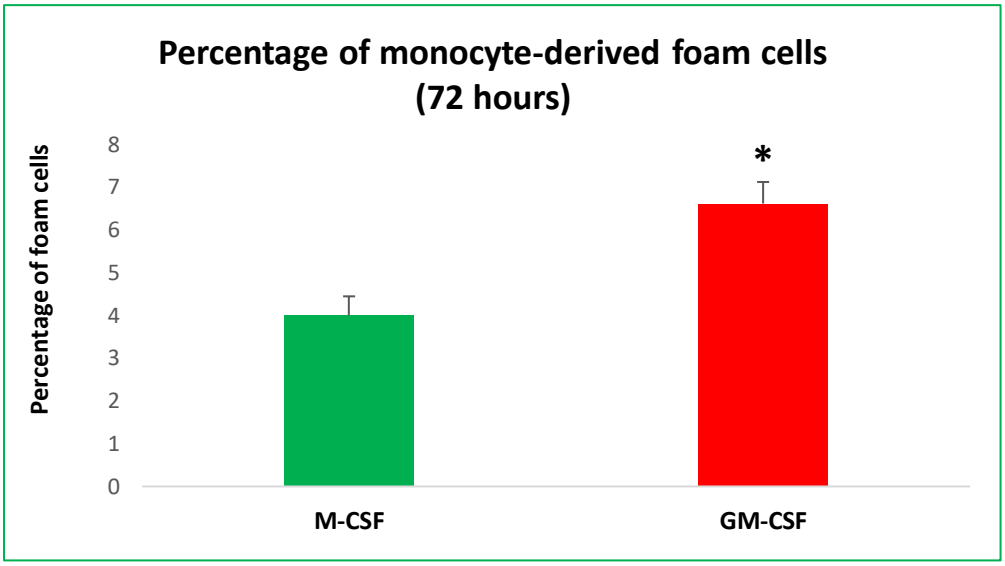

B

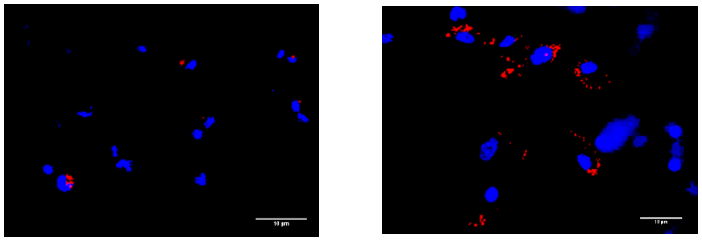

Figure 4.2 Monocytes incubated for 72 hours with M-CSF or GM-CSF differentially accumulate oxLDL and form foam cells.

A: Quantification of monocyte-derived foam cells after 72-hour incubation with M-CSF or GM-CSF, plus Dil-oxLDL (10 µg/ml). Monocytes were stained with Oil Red O to visualise accumulation of oxLDL. Cells were counted within 10 random x 40 magnification field. *indicates $p<0.05$, two tailed, paired t-test n=5. N-values in macrophages differentiated from THP-1 cells represent number of replicates.

B: Representative images of monocyte-derived foam cells showing lipid accumulation. Monocytes were stained with Oil Red O to visualise accumulation of oxLDL (red) and cells counterstained with DAPI (blue) to depict nuclei. Scale bar represents 10 µm and applies to both panels.

To assess the effect of fasudil on monocyte lipid accumulation, monocytes were incubated for 72 hours with M-CSF or GM-CSF, plus 10 µg/ml of Dil-oxLDL with and without 10 µM of fasudil. Afterwards, cells were subjected to Oil Red O staining to visualize oxLDL accumulation (foam cell formation). Image analysis demonstrated that fasudil significantly reduced the ability of monocytes incubated with GM-SCF to form foam cells (36%; $p<0.05$; n=5; Figure 4.3), whereas fasudil did not change the ability of M-CSF stimulated monocytes to form foam cells (Figure 4.3).

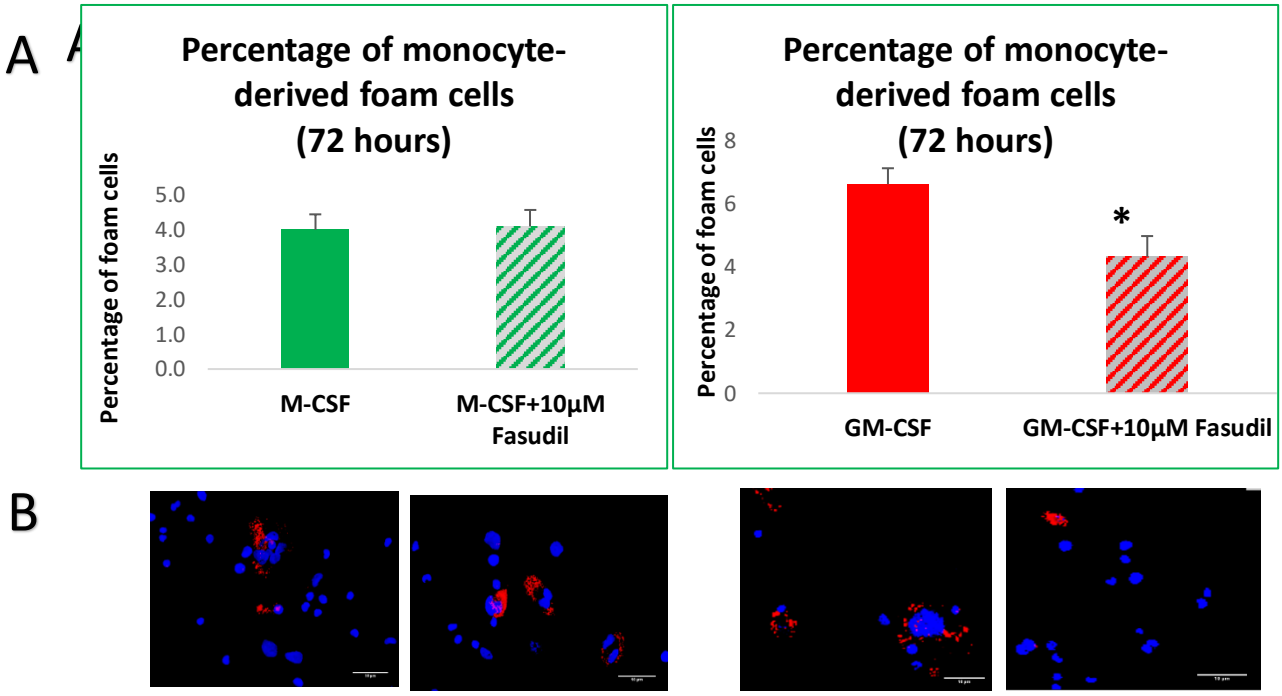

Figure 4.3 Fasudil reduced the ability of GM-CSF stimulated monocytes to accumulate oxLDL and form foam cells but not with M-CSF stimulated monocytes.

A: Quantification of monocyte-derived foam cells after 72-hour incubation with M-CSF or GM-CSF, Dil-oxLDL (10 µg/ml), plus or minus fasudil (10 µM). Monocytes were stained with Oil Red O to visualise accumulation of oxLDL. Cells were counted within 10 random x 40 magnification fields. *indicates $p<0.05$, two tailed, paired t-test n=5. N-values in macrophages differentiated from THP-1 cells represent number of replicates.

B: Representative images of monocyte-derived foam cells showing lipid accumulation. Monocytes were stained with Oil Red O to visualise accumulation of oxLDL (red) and cells counterstained with DAPI (blue) to depict nuclei. Scale bar represents 10 µm and applies to both panels.

4.2.2 Intermediate and mature GM-CSF polarised macrophages accumulate more lipid compared to M-CSF macrophages, which is blunted by the administration of fasudil or pravastatin

To assess the difference in the ability of macrophage subsets to form foam cells, macrophages obtained from THP-1 cells were divided into two groups according to the period of time that the cells were incubated with colony stimulating factors. The first group were termed intermediate macrophages which were treated with M-CSF or GM-CSF for 3 days. The second group were classified as mature macrophages and were treated with M-CSF or GM-CSF for 6 days. Subsequently, intermediate and mature macrophages were exposed to 10 μg/ml of DiI-oxLDL for 24 hours. Afterwards, cells were subjected to Oil Red O staining to visualize oxLDL accumulation (foam cell formation). Image analysis showed that macrophages in both groups were able to accumulate lipid and form foam cells (Figure 4.4). However, both intermediate and mature GM-Macs displayed significantly increased foam cell formation compared to their M-Mac counterparts (83%; $p<0.05$, and 95%; $p<0.01$ respectively; n=5; Figure 4.4).

A

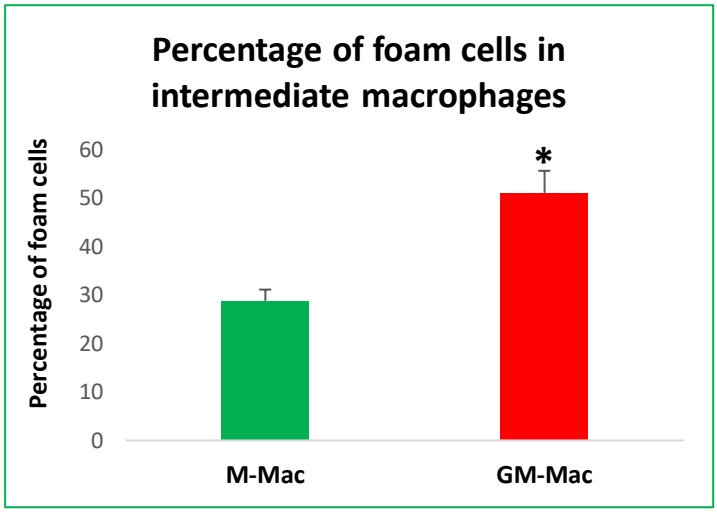

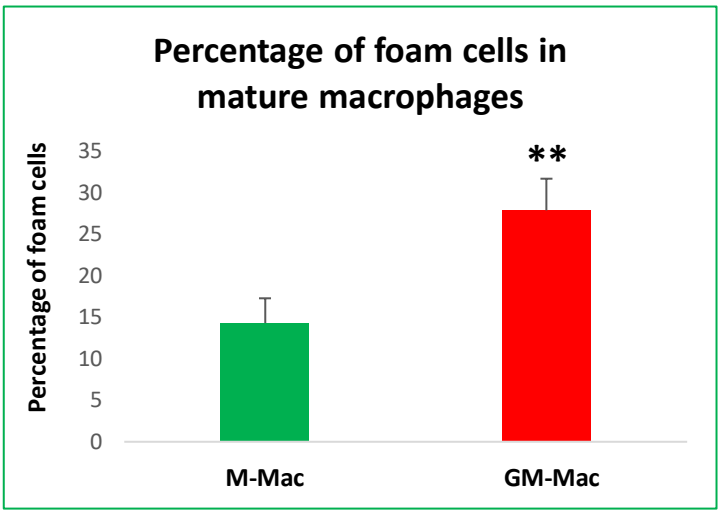

B

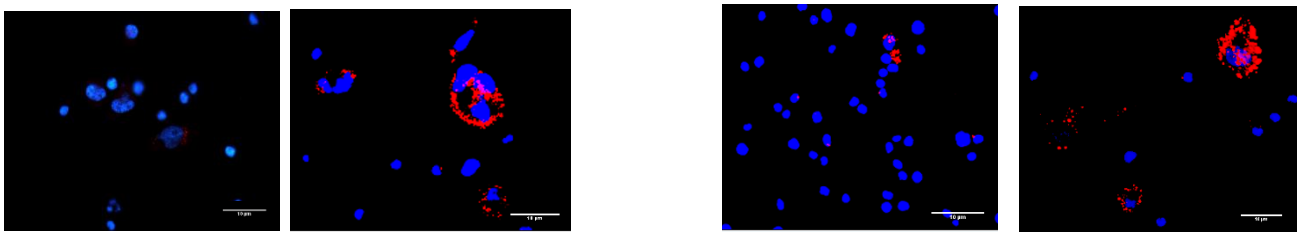

Figure 4.4 GM-Macs derived from THP-1 cells in both intermediate and mature groups displayed increased foam cell formation compared to M-Macs derived from THP-1 cells.

A: Quantification of foam cell formation in intermediate and mature M-Mac and GM-Mac after 24-hour incubation with Dil-oxLDL (10 µg/ml). Macrophages were stained with Oil Red O to visualise accumulation of oxLDL. Cells were counted within 10 random x 40 magnification fields. *indicates $p<0.05$, ** indicates $p<0.01$ compared to M-Mac, two tailed, paired t-test n=5. N-values in macrophages differentiated from THP-1 cells represent number of replicates.

B: Representative images of foam cells showing lipid accumulation within intermediate and mature M-Mac and GM-Mac. Macrophages were stained with Oil Red O to visualise accumulation of oxLDL (red) and cells counterstained with DAPI (blue) to depict nuclei. Scale bar represents 10 µm and applies to all panels.

To assess the effect of fasudil or pravastatin on the ability of intermediate and mature M-Macs to form foam cells, M-Macs in both groups were incubated with 10 µg/ml of Dil-oxLDL alongside either 10 µM of fasudil or 5 µM of pravastatin for 24 hours. Image analysis of Oil Red O-stained cells demonstrated that neither fasudil or pravastatin affected foam cell formation in intermediate (Figure 4.5) or mature M-Macs (Figure 4.6).

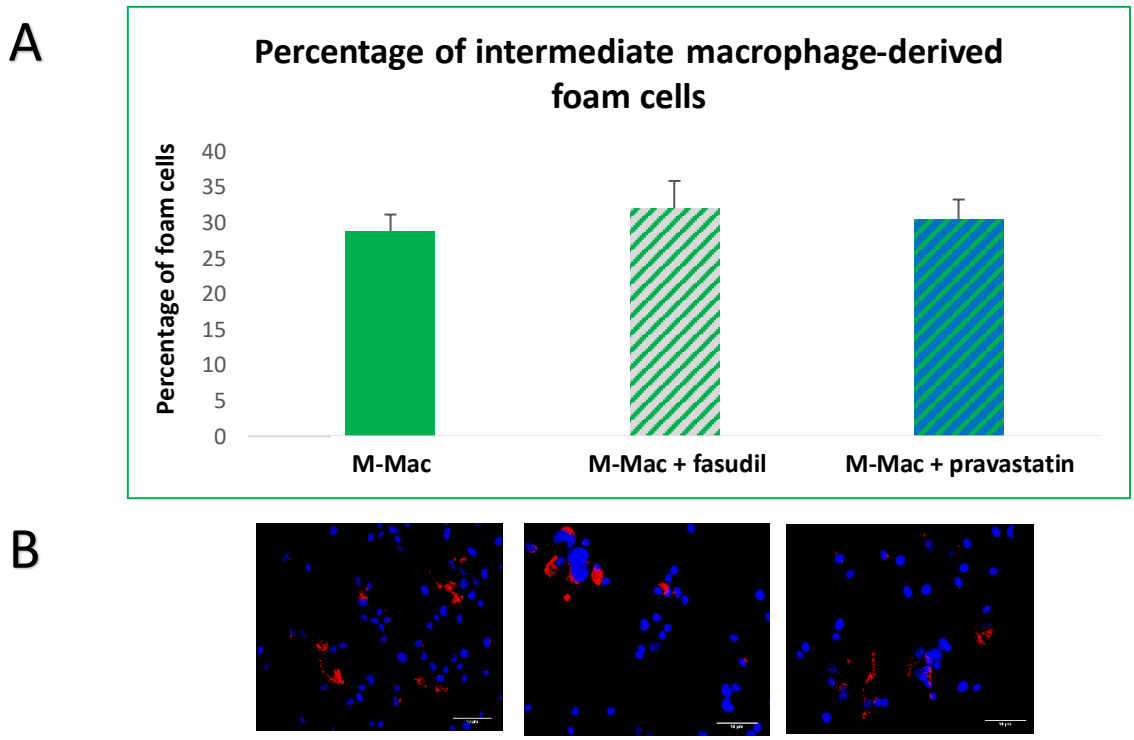

Figure 4.5 Fasudil or pravastatin did not change the ability of intermediate M-Macs derived from THP-1 cells to accumulate oxLDL and form foam cells.

A: Quantification of foam cell formation in intermediate M-Mac after 24-hour incubation with Dil-oxLDL (10 µg/ml), plus or minus fasudil (10 µM) or pravastatin (5 µM). Macrophages were stained with Oil Red O to visualise accumulation of oxLDL. Cells were counted within 10 random x 40 magnification fields. ANOVA, Student-Newman-Keuls Multiple Comparisons Test n=5. N-values in macrophages differentiated from THP-1 cells represent number of replicates.

B: Representative images of foam cells showing lipid accumulation within intermediate macrophages. Macrophages were stained with Oil Red O to visualise accumulation of oxLDL (red) and cells counterstained with DAPI (blue) to depict nuclei. Scale bar represents 10 µm and applies to all panels.

A

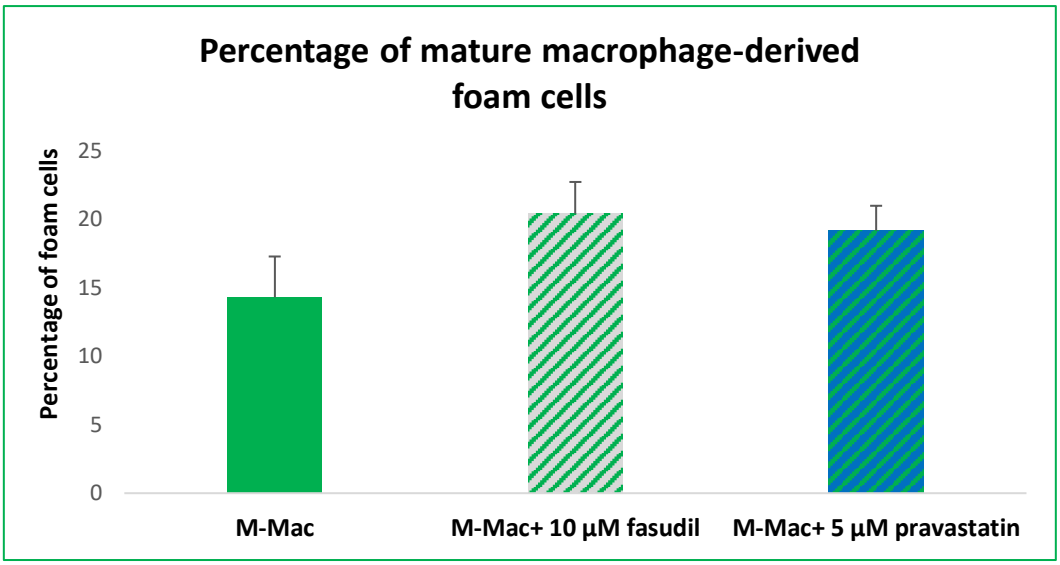

B

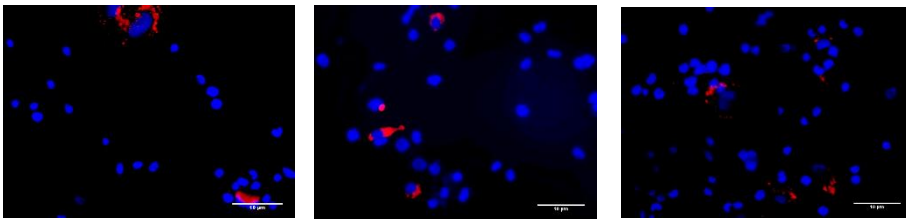

Figure 4.6 Fasudil or pravastatin did not change the ability of mature M-Macs derived from THP-1 cells to accumulate oxLDL and form foam cells.

A: Quantification of foam cell formation in mature M-Mac after 24-hour incubation with Dil-oxLDL (10 µg/ml), plus or minus fasudil (10 µM) or pravastatin (5 µM). Macrophages were stained with Oil Red O to visualise accumulation of oxLDL. Cells were counted within 10 random x 40 magnification fields. ANOVA, Student-Newman-Keuls Multiple Comparisons Test n=5. N-values in macrophages differentiated from THP-1 cells represent number of replicates.

B: Representative images of foam cells showing lipid accumulation within mature macrophages. Macrophages were stained with Oil Red O to visualise accumulation of oxLDL (red) and cells counterstained with DAPI (blue) to depict nuclei. Scale bar represents 10 µm and applies to all panels.

To assess the effect of fasudil or pravastatin on the ability of intermediate and mature GM-Macs to form foam cells, GM-Macs in both groups were incubated with 10 µg/ml of Dil-oxLDL alongside either 10 µM of fasudil or 5 µM of pravastatin for 24 hours. Quantification of Oil Red-stained cells demonstrated that in intermediate GM-Macs, fasudil and pravastatin induced a significant reduction in foam cell formation (28%; $p<0.05$, and 73%; $p<0.001$ respectively; n=5; Figure 4.7), although the inhibitory effect was markedly greater with pravastatin treatment. Similar effects were observed in mature GM-Macs with fasudil or pravastatin treatment (29%; $p<0.05$, and 72%; $p<0.01$; n=5; Figure 4.8).

A

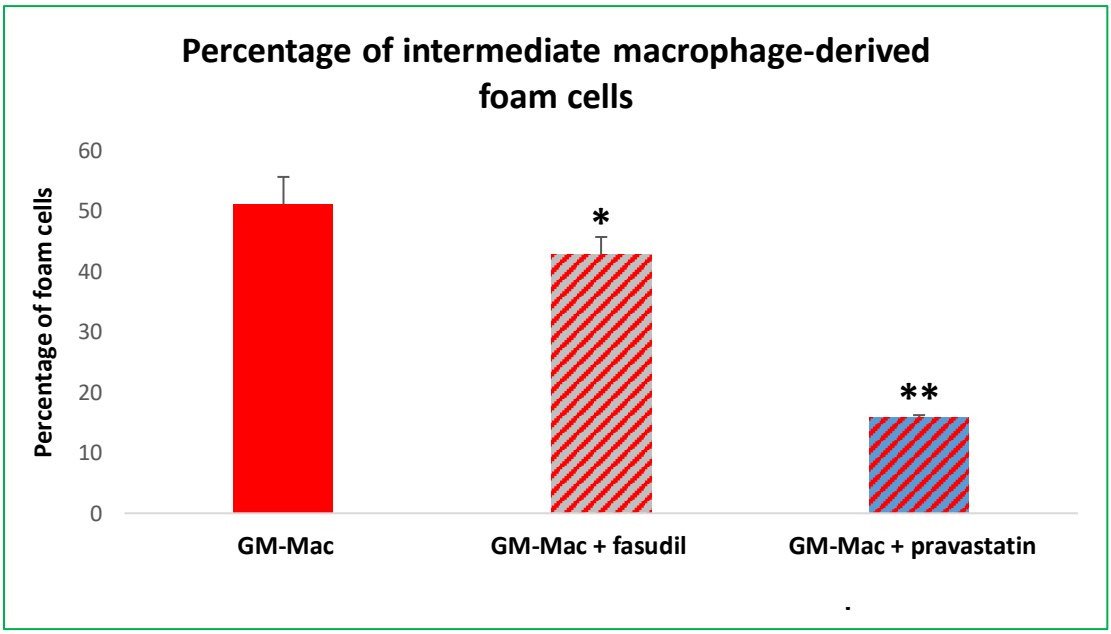

B

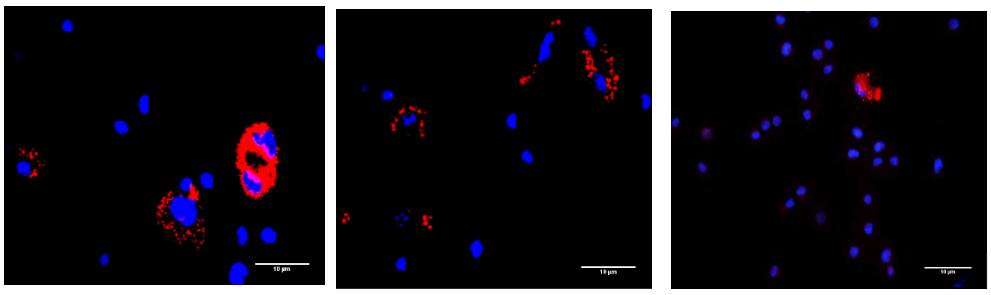

Figure 4.7 Fasudil or pravastatin reduced the ability of intermediate GM-Macs derived from THP-1 cells to accumulate oxLDL and form foam cells.

A: Quantification of foam cell formation in intermediate GM-Mac after 24-hour incubation with Dil-oxLDL (10 µg/ml), plus or minus fasudil (10 µM) or pravastatin (5 µM). Macrophages were stained with Oil Red O to visualise accumulation of oxLDL. Cells were counted within 10 random x 40 magnification fields. *indicates $p<0.05$, ** indicates $p<0.01$, ANOVA, Student-Newman-Keuls Multiple Comparisons Test n=5. N-values in macrophages differentiated from THP-1 cells represent number of replicates.

B: Representative images of foam cells showing lipid accumulation within the intermediate macrophages. Macrophages were stained with Oil Red O to visualise accumulation of oxLDL (red) and cells counterstained with DAPI (blue) to depict nuclei. Scale bar represents 10 µm and applies to all panels.

A

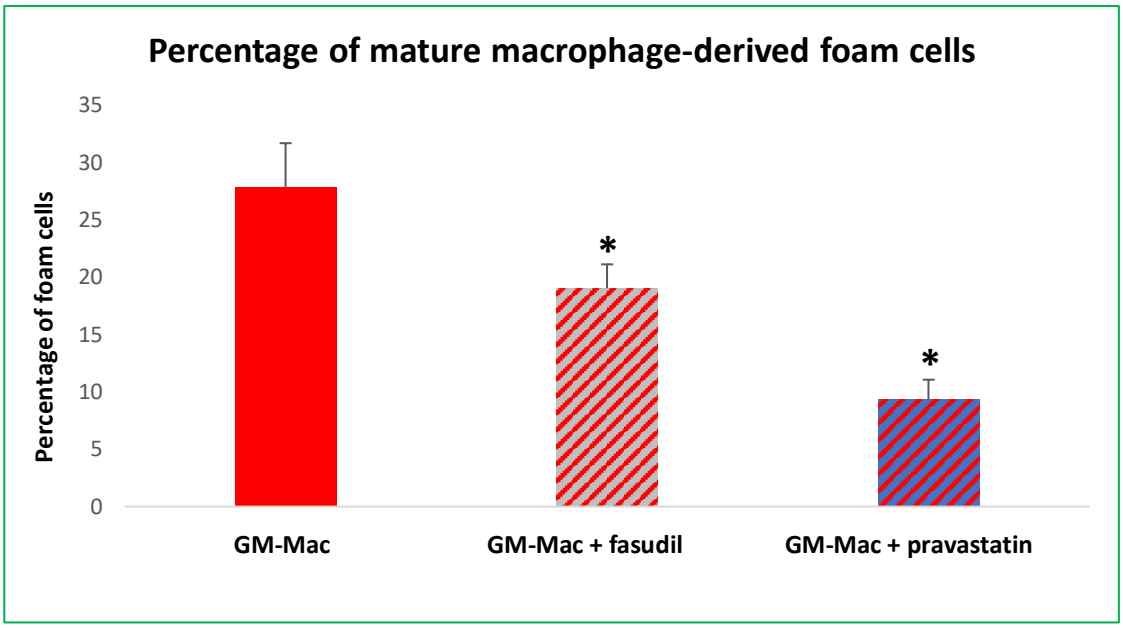

B

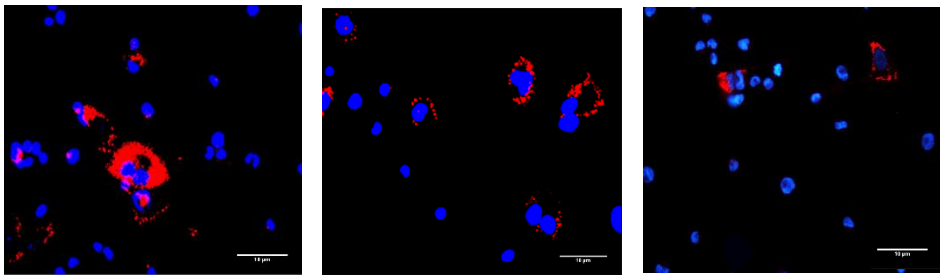

Figure 4.8 Fasudil or pravastatin reduced the ability of mature GM-Macs derived from THP-1 cells to accumulate oxLDL and form foam cells.

A: Quantification of foam cell formation in mature GM-Mac after 24-hour incubation with Dil-oxLDL (10 µg/ml), plus or minus fasudil (10 µM) or pravastatin (5 µM). Macrophages were stained with Oil Red O to visualise accumulation of oxLDL. Cells were counted within 10 random x 40 magnification fields. *indicates $p<0.05$, ANOVA, Student-Newman-Keuls Multiple Comparisons Test n=5. N-values in macrophages differentiated from THP-1 cells represent number of replicates.

B: Representative images of foam cells showing lipid accumulation within mature macrophages. Macrophages were stained with Oil Red O to visualise accumulation of oxLDL (red) and cells counterstained with DAPI (blue) to depict nuclei. Scale bar represents 10 µm and applies to all panels.

4.2.3 GM-Macs derived from human blood monocytes accumulate more lipid compared to M-Macs and this is reduced by the administration of fasudil or pravastatin

To validate the results observed in THP-1 cells, human blood-derived monocytes were polarised towards an M-Mac or GM-Mac phenotype for seven days then exposed to 10 µg/ml of Dil-oxLDL for 24 hours. As observed in THP-1-derived macrophages, primary GM-Macs displayed significantly increased foam cell formation (labelled oxLDL accumulation) compared to their M-Mac counterparts (3-fold; $p<0.05$; n=5; Figure 4.9). Also mirroring the effects observed in THP-1 cells, fasudil (10 µM) or pravastatin (5 µM) administration significantly reduced foam cell formation in primary human GM-Macs (85%; $p<0.01$, and 92%; $p<0.01$ respectively; n=5; Figure 4.10).

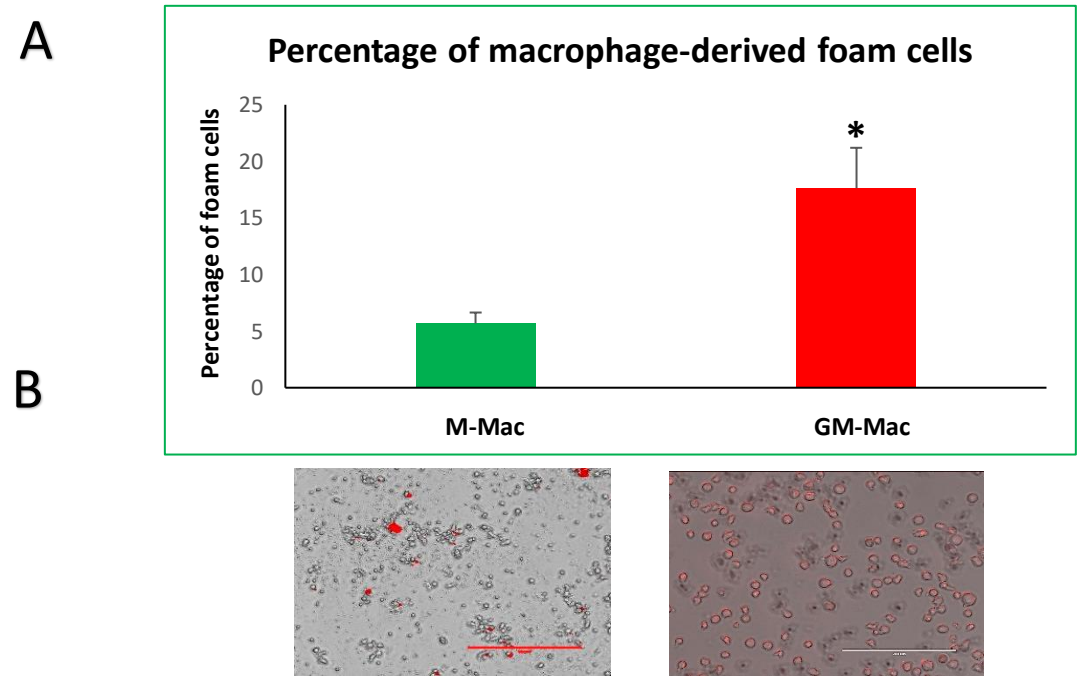

Figure 4.9 GM-Macs derived from human blood-derived monocytes displayed increased foam cell formation compared to M-Macs.

Quantification and representative phase contrast images showing the percentage of foam cells formed in human primary macrophages. Macrophages were incubated with Dil-oxLDL (10 µg/ml) for 24 hours then stained with Oil Red O to visualise oxLDL accumulation. Cells were counted within 10 random x 20 magnification fields. *indicates $p<0.05$, two tailed, paired t-test, n=5. Scale bar represents 200 µm and applies to both panels. N-values in macrophages derived from PBMCs represent the number of healthy donors.

A

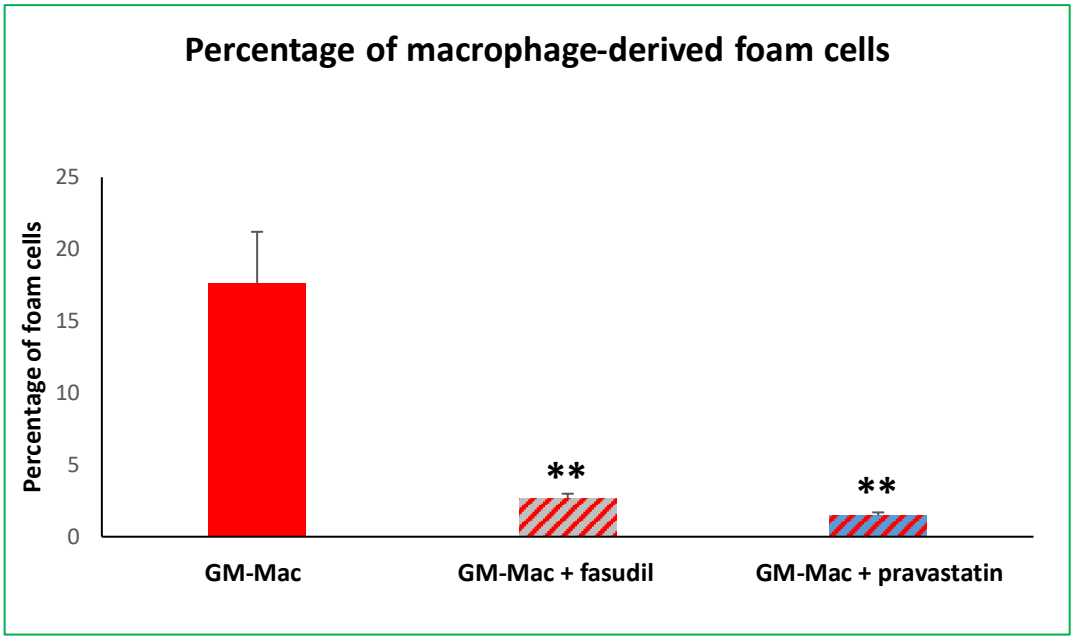

B

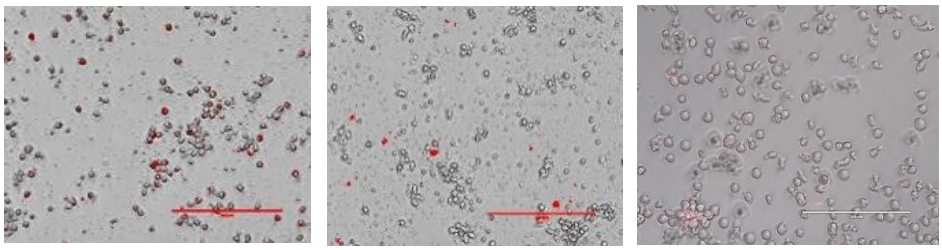

Figure 4.10 Fasudil or pravastatin reduced the ability of GM-Macs derived from human blood-derived monocytes to accumulate oxLDL and form foam cells.

Quantification and representative phase contrast images showing the percentage of foam cells formed in human primary macrophages. Macrophages were incubated with Dil-oxLDL (10 µg/ml) with and without either fasudil (10 µM) or pravastatin (5 µM) for 24 hours, after which cells were stained with Oil Red O to visualise oxLDL accumulation. Cells were counted within 10 random x 20 magnification fields. ** indicates $p<0.01$, ANOVA, Student-Newman-Keuls Multiple Comparisons Test n=5. Scale bar represents 200 µm and applies to all panels. N-values in macrophages derived from PBMCs represent the number of healthy donors.

4.2.4 Fasudil or pravastatin regulate the mRNA expression of select scavenger receptors and lipid transporters that modulate lipid homeostasis in primary human macrophages

Given the marked effect of fasudil and pravastatin on GM-Mac foam cell formation, the expression of key scavenger receptors and lipid transporters that regulate macrophage cholesterol homeostasis were examined to gain insight into potential mechanisms underlying the affect of cytoskeleton-modifying drugs on GM-Mac oxLDL accumulation. In brief, human blood-derived monocytes were polarised towards a GM-Mac phenotype for differing time periods to generate early (1 day GM-CSF), intermediate (3-day GM-CSF), and mature GM-Macs (7-day GM-CSF), which were then treated with 10 µg/ml of Dil-oxLDL with and without either 10 µM of fasudil or 5 µM of pravastatin for 24 hours. Subsequent RT-qPCR analysis was performed on RNA extracted from cells for gene expression of key lipoprotein-related scavenger receptors (MSR1, OLR1, CD36, and MRC1) and cholesterol efflux genes (ABCG1, PPARA, and NCOR1). All genes were comparable across the early, intermediate, and mature in untreated GM-Mac groups, with the exception of OLR1 which was decreased in intermediate and mature GM-Macs, and PPARA which was significantly increased in mature GM-Macs (Table 4.1). Focussing on early GM-Macs, oxLDL exposure increased MRC1 mRNA expression which could be blunted with pravastatin co-incubation, but not with fasudil (Table 4.2). ABCG1 levels were also elevated by oxLDL exposure, which was not altered by either fasudil or pravastatin co-incubation (Table 4.2). Within intermediate GM-Macs, MSR1 and OLR1 mRNA expression was decreased by oxLDL exposure and were unaffected by fasudil or pravastatin treatment (Table 4.3). Within intermediate GM-Macs, CD36 levels were similarly decreased with oxLDL addition, which was reversed with fasudil co-incubation, but not with pravastatin (Table 4.3). Interestingly, pravastatin administration alongside oxLDL exposure significantly decreased expression of MRC1 and ABCG1 in intermediated GM-Macs (Table 4.3). Finally, in mature GM-Macs mRNA expression of OLR1 was significantly decreased while PPARA was increased by oxLDL exposure compared to untreated GM-Macs, with both effects unaltered by fasudil or pravastatin treatment (Table 4.4). MSR1, ABCG1, and NCOR1 levels were also increased in mature GM-Macs exposed to oxLDL, which could be prevented with pravastatin co-incubation, but not with fasudil (Table 4.4).

GM-Mac	Early	Intermediate	Mature
Treatment	unstimulated	unstimulated	unstimulated
CD36	1	1.05 ± 0.2	2.7 ± 1.96
MSR1	1	0.81 ± 0.58	2.3 ± 1.5
MRC1	1	1.10 ± 0.83	1.79 ± 1.3
OLR1	1	0.08 ± 0.07	0.08 ± 0.06
ABCG1	1	1.49 ± 1.39	2.59 ± 1.4
PPARA	1	1.27 ± 0.18	2.99 ± 0.58
NCOR1	1	2.48 ± 1.35	2.16 ± 1.24

Table 4.1: Table summarising mRNA expression changes between human monocyte-derived early, intermediate, and mature GM-Macs.

Quantification of key lipoprotein-related scavenger receptors (MSR1, OLR1, CD36, and MRC1) and cholesterol efflux genes (ABCG1, PPARA, and NCOR1) in early, intermediate, and mature GM-Mac assessed by RT-qPCR. Data presented as fold change compared to unstimulated early GM-Mac (mean ± SEM; green filled-box indicates significantly decreased compared to unstimulated early macrophages ($p<0.05$); red filled-box indicates significantly increased compared to unstimulated early macrophages ($p<0.05$); two tailed, paired t-test, n=5). N-values in macrophages derived from PBMCs represent the number of healthy donors.

Mac	Early GM-Mac			
Treatment	unstimulated	+ oxLDL	+ oxLDL + fasudil	+ oxLDL + statin
CD36	1	1.39 ± 0.29	0.78 ± 0.19	1.05 ± 0.2
MSR1	1	2.69 ± 1.26	1.39 ± 0.32	2.23 ± 0.76
MRC1	1	2.07 ± 0.33	1.78 ± 0.58	0.82 ± 0.50
OLR1	1	1.93 ± 0.65	2.06 ± 1.86	2.5 ± 1.64
ABCG1	1	3.61 ± 0.85	2.21 ± 0.88	3.14 ± 1.31
PPARA	1	1.05 ± 0.06	1.05 ± 0.05	1.05 ± 0.05
NCOR1	1	1.7 ± 0.26	1.05 ± 0.26	1.99 ± 0.61

Table 4.2: Table summarising mRNA expression changes between human monocyte-derived early GM-Macs exposed to oxLDL, with and without fasudil or pravastatin treatment.

Quantification of key lipoprotein-related scavenger receptors (MSR1, OLR1, CD36, and MRC1) and cholesterol efflux genes (ABCG1, PPARA, and NCOR1) in early GM-Mac treated for 24 hours with 10 µg/ml of Dil-oxLDL, and with or without fasudil (10 µM) or pravastatin (5 µM) and assessed by RT-qPCR. Data presented as fold change compared to unstimulated early GM-Mac (mean ± SEM; red filled-box indicates significantly increased compared to unstimulated ($p<0.05$); two tailed, paired t-test, n=5). N-values in macrophages derived from PBMCs represent the number of healthy donors.

Mac	Intermediate GM-Mac			
Treatment	unstimulated	+ oxLDL	+ oxLDL + fasudil	+ oxLDL + statin
CD36	1	0.39 ± 0.34	1.09 ± 0.97	0.15 ± 0.14
MSR1	1	0.36 ± 0.22	0.57 ± 0.37	0.5 ± 0.26
MRC1	1	0.41 ± 0.27	0.83 ± 0.64	0.07 ± 0.06
OLR1	1	0.04 ± 0.01	0.07 ± 0.05	0.03 ± 0.02
ABCG1	1	0.66 ± 0.49	1.73 ± 1.3	0.29 ± 0.22
PPARA	1	1.27 ± 0.16	1.24 ± 0.13	1.24 ± 0.16
NCOR1	1	2.23 ± 1.25	4.49 ± 2.03	1.19 ± 0.48

Table 4.3: Table summarising mRNA expression changes between human monocyte-derived intermediate GM-Macs exposed to oxLDL, with and without fasudil or pravastatin treatment.

Quantification of key lipoprotein-related scavenger receptors (MSR1, OLR1, CD36, and MRC1) and cholesterol efflux genes (ABCG1, PPARA, and NCOR1) in intermediate GM-Mac treated for 24 hours with 10 µg/ml of Dil-oxLDL, and with or without fasudil (10 µM) or pravastatin (5 µM) and assessed by RT-qPCR. Data presented as fold change compared to unstimulated intermediate GM-Mac (mean ± SEM; green filled-box indicates significantly decreased compared to unstimulated ($p<0.05$); two tailed, paired t-test, n=5). N-values in macrophages derived from PBMCs represent the number of healthy donors.

Mac	Mature GM-Mac			
Treatment	unstimulated	+ oxLDL	+ oxLDL + fasudil	+ oxLDL + statin
CD36	1	3.59 ± 2.98	1.79 ± 1.11	2.51 ± 1.9
MSR1	1	5.43 ± 1.95	5.73 ± 2.35	2.24 ± 0.71
MRC1	1	3.27 ± 2.55	1.24 ± 0.71	1.78 ± 1.31
OLR1	1	0.06 ± 0.04	0.01 ± 0.01	0.03 ± 0.02
ABCG1	1	6.44 ± 2.9	11.12 ± 5.65	10.71 ± 5.78
PPARA	1	2.79 ± 0.42	3.05 ± 0.42	2.7 ± 0.27
NCOR1	1	6.05 ± 2.58	5.08 ± 1.53	7.33 ± 2.9

Table 4.4: Table summarising mRNA expression changes between human monocyte-derived mature GM-Macs exposed to oxLDL, with and without fasudil or pravastatin treatment.

Quantification of key lipoprotein-related scavenger receptors (MSR1, OLR1, CD36, and MRC1) and cholesterol efflux genes (ABCG1, PPARA, and NCOR1) in mature GM-Mac treated for 24 hours with 10 µg/ml of Dil-oxLDL, and with or without fasudil (10 µM) or pravastatin (5 µM) and assessed by RT-qPCR. Data presented as fold change compared to unstimulated mature GM-Mac (mean ± SEM; red filled-box indicates significantly increased compared to unstimulated ($p<0.05$); green filled-box indicates significantly decreased compared to unstimulated ($p<0.05$); two tailed, paired t-test, n=5). N-values in macrophages derived from PBMCs represent the number of healthy donors.

4.2.5 Fasudil or pravastatin regulate the protein expression of select scavenger receptors and lipid transporters in primary human macrophages polarised with GM-CSF

To further examine the results observed at the mRNA level for select scavenger recptors and cholesterol efflux regulators in GM-Macs, protein expression for the scavenger receptor OLR1, and CD36 alongside the cholesterol efflux regulatory molecules NCOR1, NCOR2, and PPARα were assesses in mature GM-Macs. Quantification of western blotting revealed that GM-Mac exposure to oxLDL for 24 hours significantly increased the protein expression of OLR1 (2.3-fold; $p<0.05$; n=5; Figure 4.11), while co-incubation with fasudil or pravastatin significantly suppressed the oxLDL-induced increased OLR1 levels (61% and 54%, $p<0.05$ respectively; n=5; Figure 4.11). Although CD36 protein expression was not significantly increased in GM-Macs exposed to oxLDL, similar to OLR1, western blotting revealed that treatment with fasudil or pravastatin significantly reduced CD36 levels compared to oxLDL stimulated GM-Macs (70% and 64%; $p<0.05$ respectively; n=5; Figure 4.12). Due to difficulties sourcing reliable antibodies for the detection of NCOR1, NCOR2, and PPARα by western blotting, immunocytochemistry was deployed to assess cell positivity for these markers. OxLDL stimulation did not alter the percentage of GM-Macs positive for NCOR-1, NCOR-2, or PPARα when compared to unstimulated GM-Macs (Figures 4.13 – 4.14). However, relative to oxLDL treated GM-Macs, fasudil co-incubation significantly increased the percentage of NCOR1, NCOR2, and PPARα positive GM-Macs (1.4-fold: $p<0.05$, 2.0-fold: $p<0.01$, and 1.2–fold, respectively; $p<0.05$; n=5; Figure 4.13 - 4.15). Similarly, pravastatin co-administration significantly increased the percentage of GM-Macs positive for NCOR1, NCOR2, and PPARα compared to oxLDL stimulated GM-Macs(1.8-fold: $p<0.001$, 1.8-fold: $p<0.01$, and 1.3-fold; $p<0.01$ respectively; n=5; Figure 4.13 - 4.15).

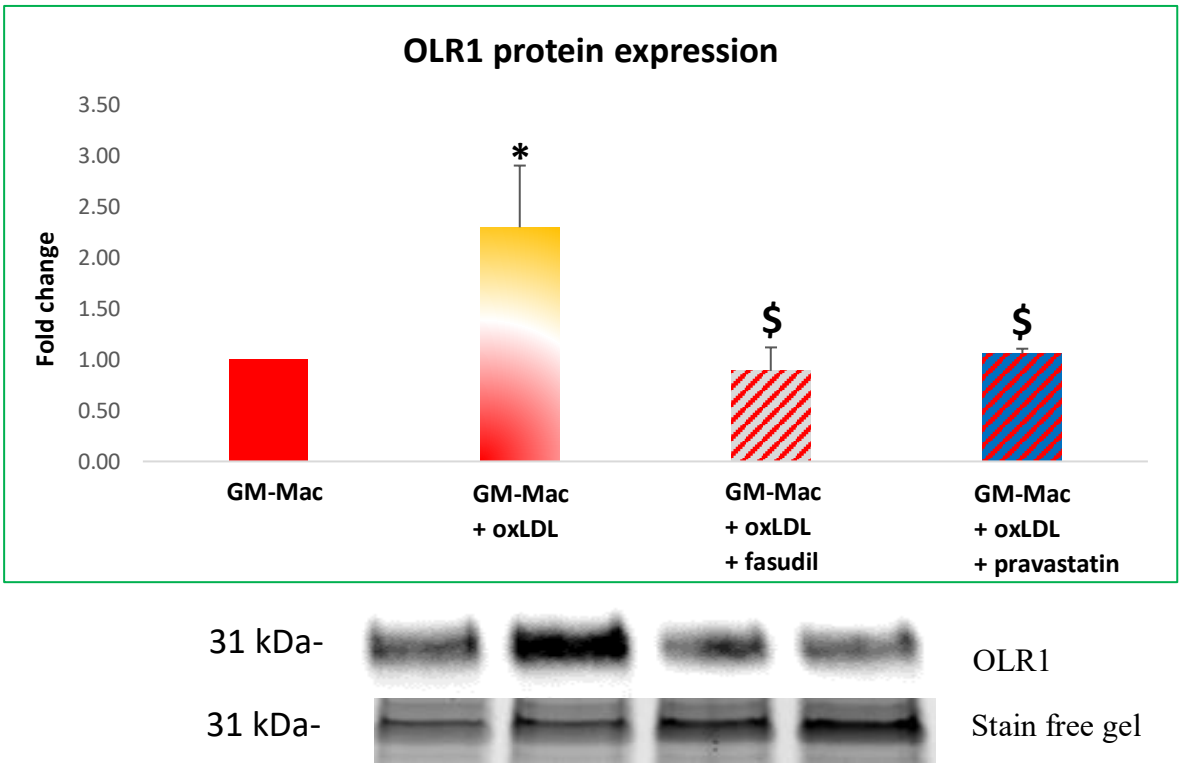

Figure 4.11 Fasudil or pravastatin co-incubation reduced OLR1 protein expression in GM-Macs derived from human blood-derived monocytes treated with oxLDL.

Quantification and representative western blot for OLR1 expression in GM-Macs treated with oxLDL (10 µg/ml) and with or without fasudil (10 µM) or pravastatin (5 µM). Stain free gel is shown as a loading control. Data presented as fold change (mean ± SEM, * indicates P< 0.05 vs GM-Mac, $ indicates P<0.05 vs GM-Mac + oxLDL. ANOVA, Student-Newman-Keuls Multiple Comparisons, n=5). N-values in macrophages derived from PBMCs represent the number of healthy donors.

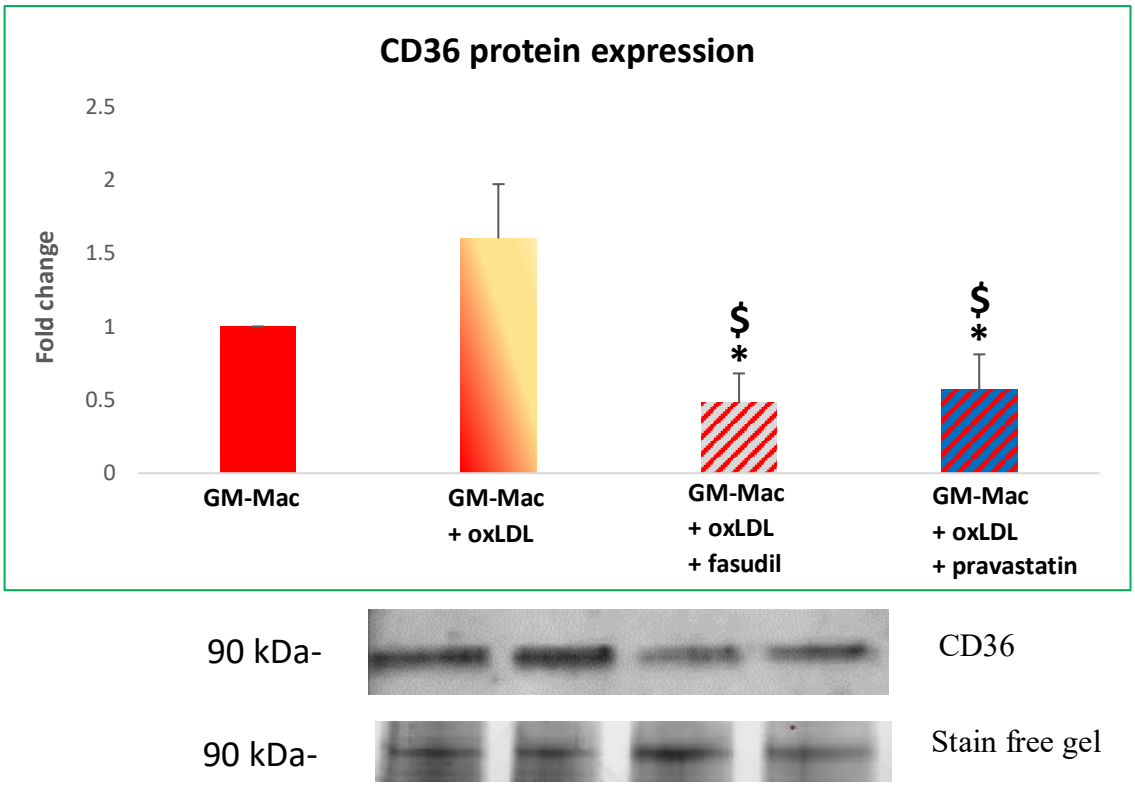

Figure4.12 Fasudil or pravastatin co-incubation reduced CD36 protein expression in GM-Macs derived from human blood-derived monocytes treated with oxLDL.

Quantification and representative western blot for CD36 expression in GM-Macs treated with oxLDL (10 µg/ml) and with or without fasudil (10 µM) or pravastatin (5 µM). Stain free gel is shown as a loading control. Data presented as fold changed (mean ± SEM, * indicates P< 0.05. ANOVA, $ indicates P<0.05 vs GM-Mac + oxLDL. ANOVA, Student-Newman-Keuls Multiple Comparisons, n=5). N-values in macrophages derived from PBMCs represent the number of healthy donors.

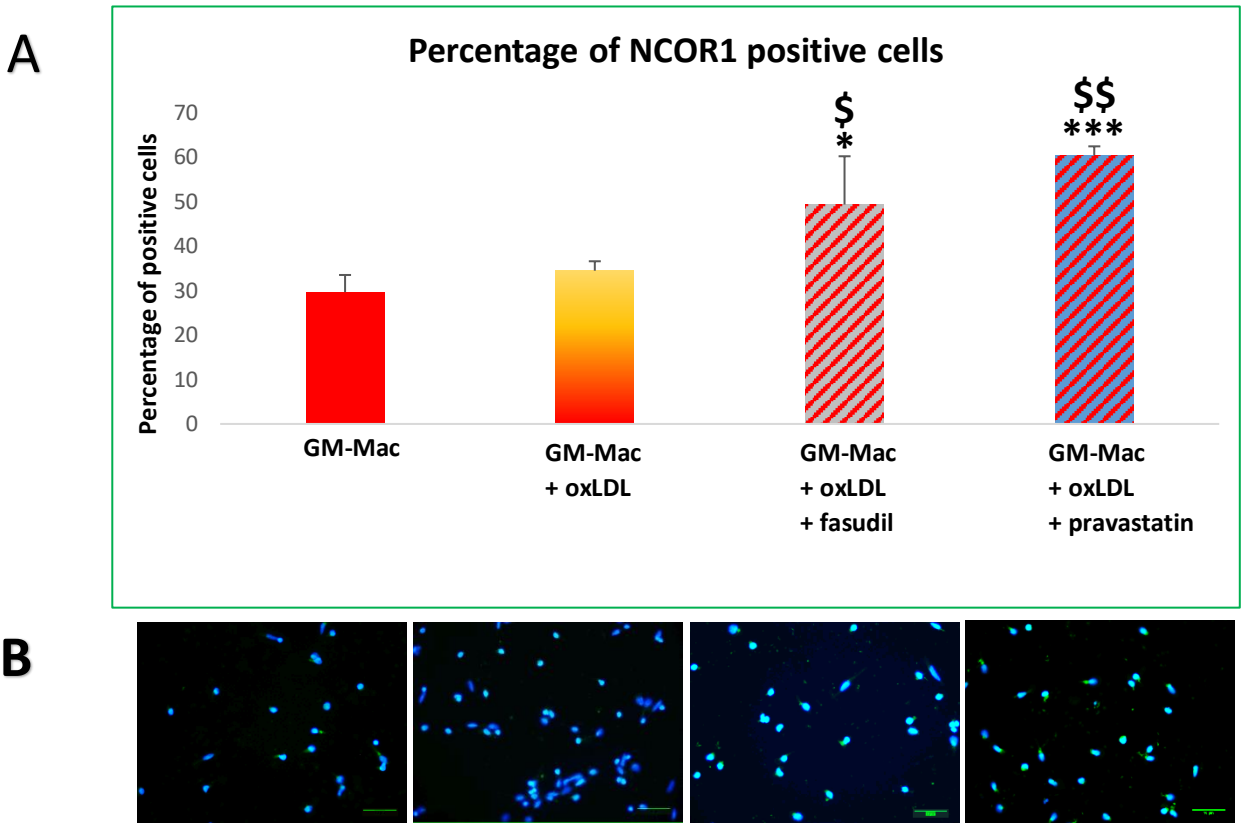

Figure 4.13 Fasudil and pravastatin co-incubation increased the percentage of NCOR1 positive GM-Macs derived from human blood-derived monocytes.

A: Quantification of cellular NCOR1 protein expression in GM-Macs exposed to oxLDL (10 µg/ml), and with or without fasudil (10 µM) or pravastatin (5 µM). Data presented as percentage of NCOR1 positive cells calculated within 10 random x 40 magnification fields. *indicates $p<0.05$, *** indicates $p<0.001$, $ indicates $P<0.05$ vs GM-Mac + oxLDL, $$ indicates $P<0.01$ vs GM-Mac + oxLDL. ANOVA, Student-Newman-Keuls Multiple Comparisons Test, n=5

B: Representative images of immunocytochemistry for NCOR1 within GM-Macs exposed to oxLDL (10 µg/ml), and with or without fasudil (10 µM) or pravastatin (5 µM). Positive cells are shown as green and all nuclei are stained blue with DAPI. Scale bar represents 10 µm and applies to all panels. N-values in macrophages derived from PBMCs represent the number of healthy donors.

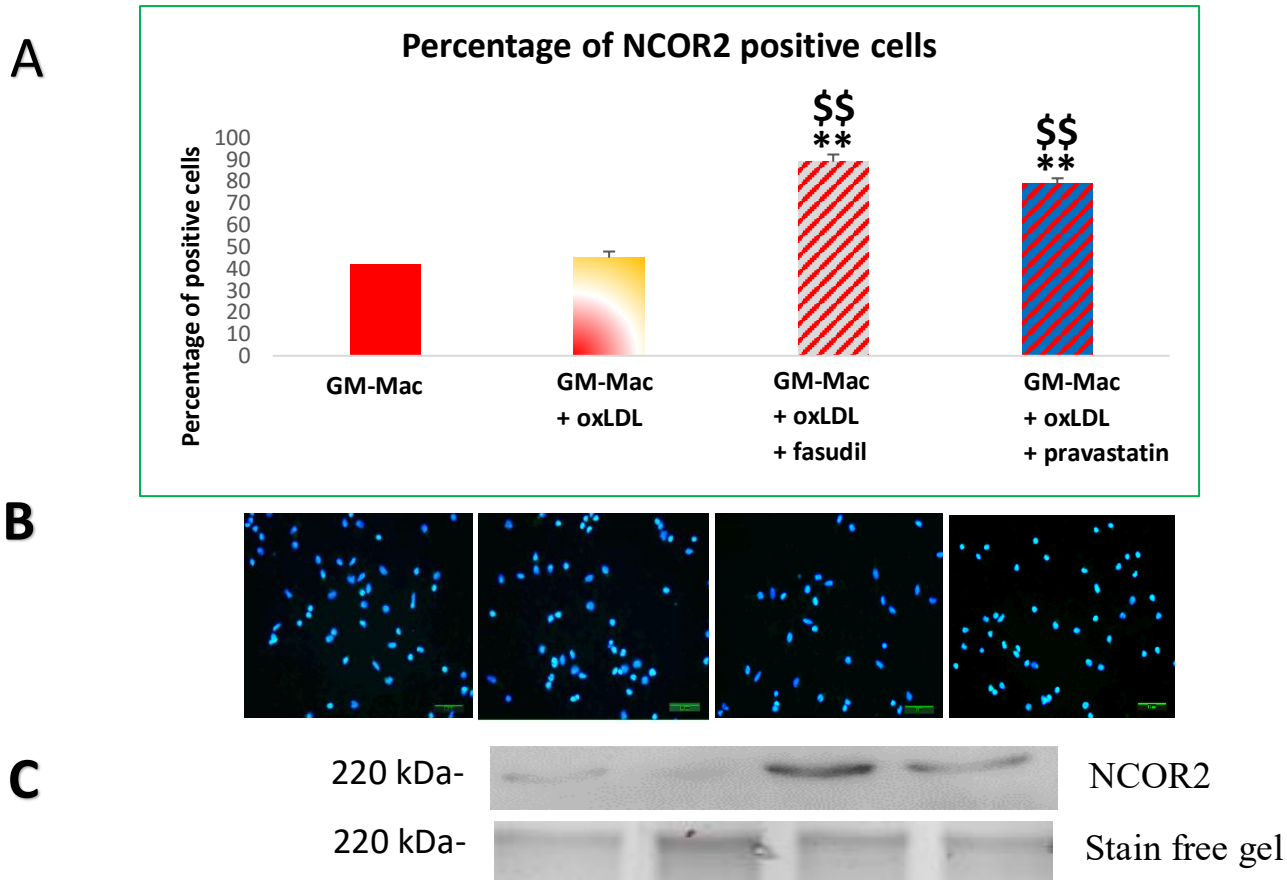

Figure 4.14 Fasudil and pravastatin co-incubation increased the percentage of NCOR2 positive GM-Macs derived from human blood-derived monocytes.

A: Quantification of cellular NCOR2 protein expression in GM-Macs exposed to oxLDL (10 µg/ml), and with or without fasudil (10 µM) or pravastatin (5 µM). Data presented as percentage of NCOR2 positive cells calculated within 10 random x 40 magnification fields. ** indicates $p<0.01$, $$ indicates $P<0.01$ vs GM-Mac + oxLDL. ANOVA, Student-Newman-Keuls Multiple Comparisons Test, n=5. N-values in macrophages derived from PBMCs represent the number of healthy donors.

B: Representative images of immunocytochemistry for NCOR2 within GM-Macs exposed to oxLDL (10 µg/ml), and with or without fasudil (10 µM) or pravastatin (5 µM). Positive cells are shown as green and all nuclei are stained blue with DAPI. Scale bar represents 10 µm and applies to all panels.

C: Representative Western blot for NCOR2. Stain free gel is shown as a loading control. Approximate molecular weights are indicated on the left in kDa.

A

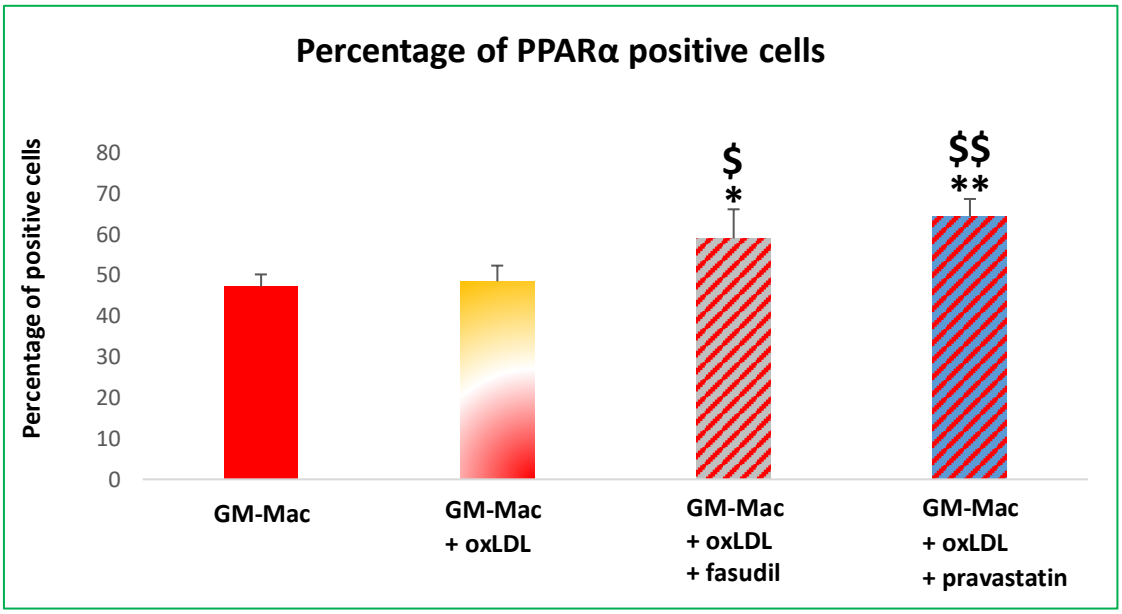

B

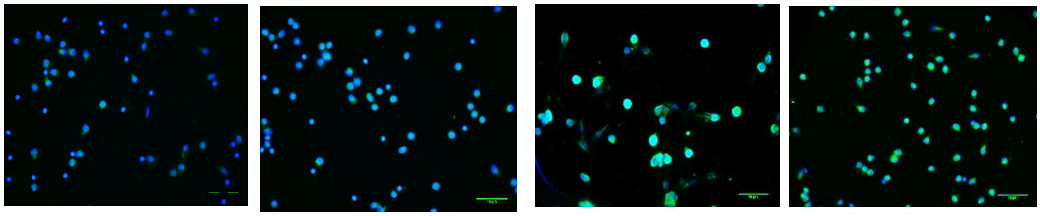

Figure 4.15 Fasudil and pravastatin co-incubation increased the percentage of PPARα positive GM-Macs derived from human blood-derived monocytes.

A: Quantification of cellular PPARα protein expression in GM-Macs exposed to oxLDL (10 µg/ml), and with or without fasudil (10 µM) or pravastatin (5 µM). Data presented as percentage of PPARα positive cells calculated within 10 random x 40 magnification fields. *indicates $p<0.05$, ** indicates $p<0.01$, $ indicates $P<0.05$ vs GM-Mac + oxLDL, $$ indicates $P<0.01$ vs GM-Mac + oxLDL. ANOVA, Student-Newman-Keuls Multiple Comparisons Test, n=5. N-values in macrophages derived from PBMCs represent the number of healthy donors.

B: Representative images of immunocytochemistry for PPARα within GM-Macs subsets exposed to oxLDL (10 µg/ml), and with or without fasudil (10 µM) or pravastatin (5 µM). Positive cells are shown as green and all nuclei are stained blue with DAPI. Scale bar represents 10 µm and applies to all panels.

4.2.6 Efferocytosis capacity is diminished in GM-CSF polarised macrophages but can be restored by fasudil and pravastatin addition

Alongside the uptake of modified lipoproteins including oxLDL, macrophages can also engulf cells undergoing apoptosis through a process termed efferocytosis. To assess the efferocytosis capacity of M-CSF and GM-CSF polarised macrophage subsets, THP-1 cells were driven towards the two opposing macrophage subsets and then subjected to an efferocytosis assay which involves the addition of pre-labelled (green fluorescent protein) apoptotic macrophages. Their subsequent engulfment is quantified by merging fluorescence and polarised light microscopy images. Image analysis and associated quantification demonstrated that GM-Macs exhibited significantly reduced efferocytosis compared to M-Macs (3-fold; $p< 0.01$; n=5; Figure 4.16). However, when GM-Macs were co-incubated with 5 µM of pravastatin their efferocytosis capacity was restored (3-fold; $p<0.01$; n=5; Figure 4.17), Moreover, co-incubation with 10 µM of fasudil was able to increase the efferocytosis capacity of GM-CSF polarised macrophages (2-fold; $p<0.05$; n=5; Figure 4.17).

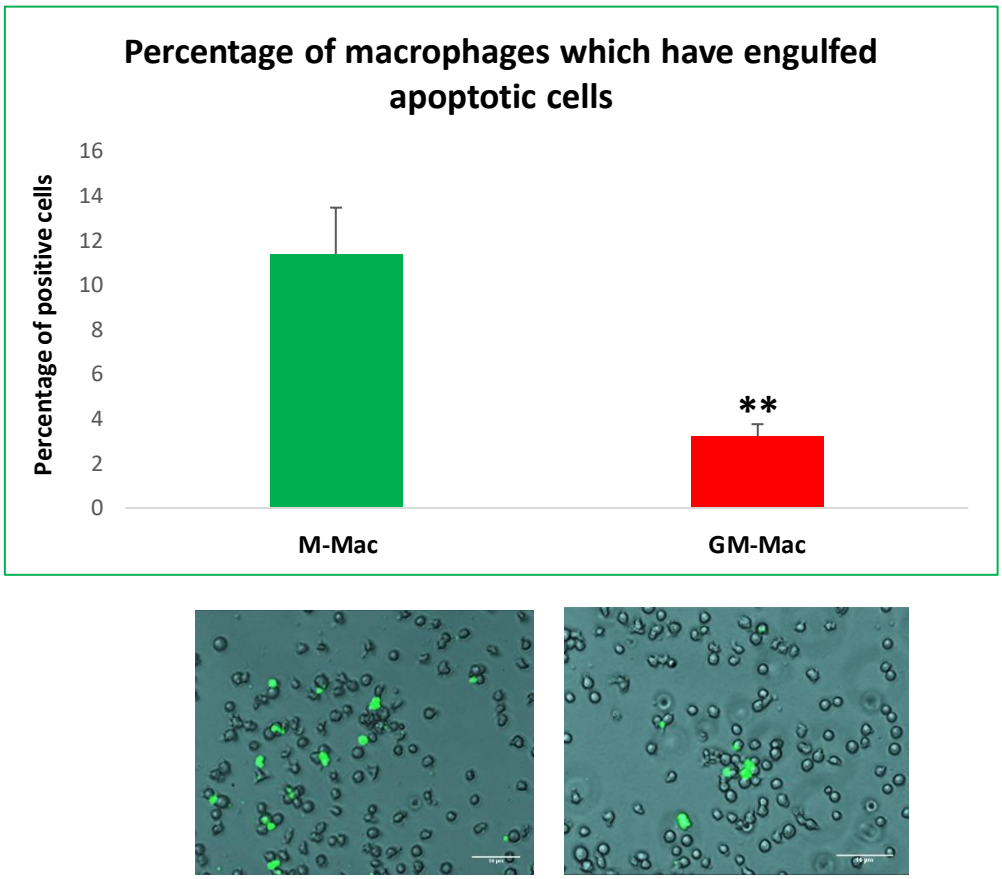

Figure 4.16 GM-Macs derived from human blood-derived monocytes display decreased efferocytosis capacity compared to M-Macs.

Quantification and representative images showing the percentage of M-Mac and GM-Mac undergoing efferocytosis as determined by the positivity for the uptake of exogenously added apototic macrophages (green). Cells were counted within 10 random x 40 magnification fields. ** indicates $p<0.01$, two tailed, paired t-test n=5. Scale bar represents 10 µm and applies to both panels. N-values in macrophages derived from PBMCs represent the number of healthy donors.

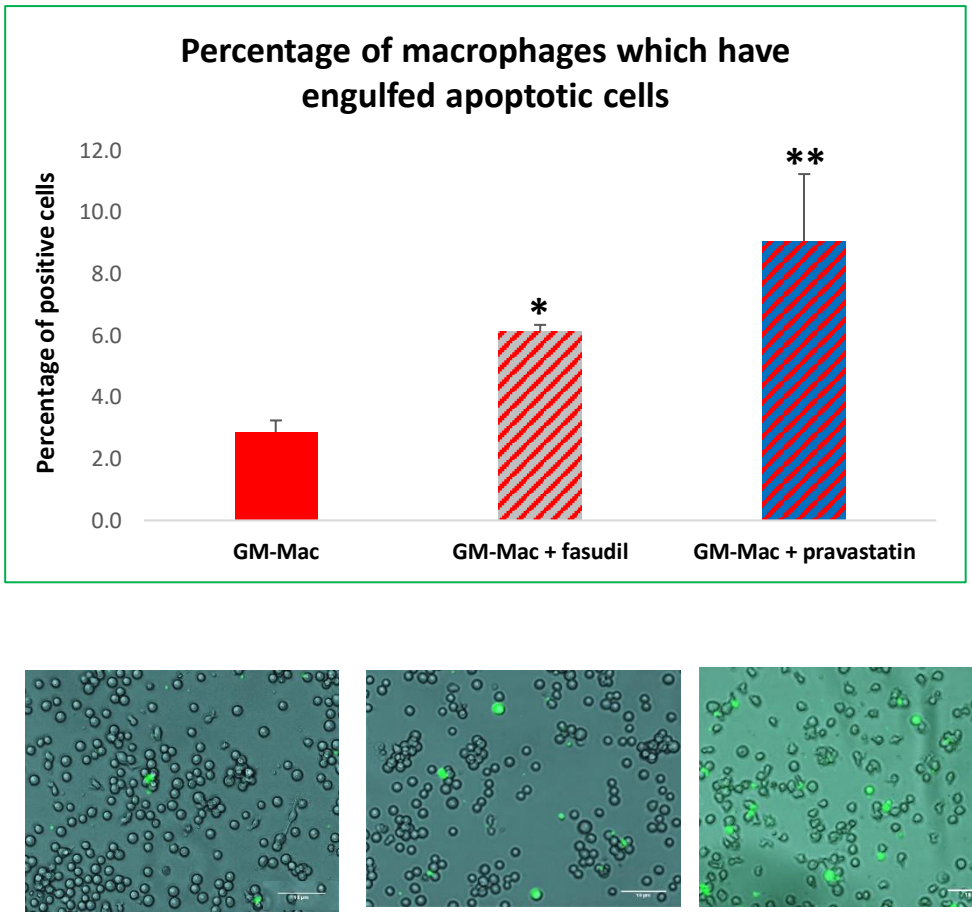

Figure 4.17 Fasudil and pravastatin increased the efferocytosis capacity of GM-Macs derived from human blood-derived monocytes.

Quantification and representative images showing the percentage of GM-Macs positive for the uptake of apototic macrophages (green) with and without co-incubation with 10 µM of fasudil or 5 µM of pravastatin. Cells were counted within 10 random x 40 magnification fields. ** indicates $p<0.01$ compared to GM-Mac, ANOVA, Student-Newman-Keuls Multiple Comparisons Test n=5. Scale bar represents 10 µm and applies to all panels. N-values in macrophages derived from PBMCs represent the number of healthy donors.

4.3 Discussion

Recent studies have shown that macrophage foam cell formation has a crucial role in both atherogenesis and the progression of atherosclerosis (Yu, Fu et al. 2013). Mechanistically, scavenger receptors including CD36 and MSR1 function as principal receptors to recognise and facilitate the uptake of modified lipoprotein, chiefly oxLDL. Once ingested, macrophages can efficiently process oxLDL-derived cholesterol to facilitate its export as HDL, with genes involved in reverse cholesterol transport and efflux, such as ABCA1 and ABCG1, capable of preventing macrophage foam cell formation (Li and Glass 2002). Consequently, in order to limit the accumulation of macrophage-derived foam cells and subsequently the development and progression of atherosclerosis, a balance is needed between the uptake of lipids and their efflux from macrophages (Yu, Fu et al. 2013). As such, the main goal of this chapter is to investigate the ability of two divergent macrophage subsets (M-CSF and GM-CSF polarised macrophages) to accumulate lipid and form foam cells, alongside examining the effect of different actin perturbing drugs (fasudil and pravastatin) on macrophage foam cell formation.

4.3.1 Lipid accumulation in monocytes and their response to fasudil treatment

During the development and progression of atherosclerotic plaques, macrophage foam cell formation is an important characteristic, and their accrual is associated with adverse atherosclerosis-related clinical events. Macrophage foam cell formation is largely dictated by the dysregulated accumulation of cholesterol-rich modified lipoproteins (such as oxLDL) by phagocytosis, a process dependent on the deformation and invagination of the plasma membrane that is mediated by remodelling of the actin cytoskeleton (Aderem and Underhill 1999, Schrijvers, De Meyer et al. 2007). Monocytes are recruited to developing atherosclerotic plaques and mature into macrophages in order to facilitate their ability to phagocytose modified lipids, but recent evidence has suggested that monocytes, to a lesser extent, can themselves accumulate lipids (Mosig, Rennert et al. 2008, Mosig, Rennert et al. 2009). Our studies (using a monocytic cell line – THP-1) showed that monocytes can indeed accumulate lipids when co-incubated with M-CSF or GM-CSF for both 24 and 72 hours. However, monocyte accumulation of oxLDL is markedly increased within GM-CSF-stimulated monocytes compared to M-CSF treated monocytes. These findings are in line with those from Mosig and colleagues who demonstrated differential oxLDL accumulation between divergent monocyte subsets retrieved from patients with familial hypercholesterolaemia, which appeared to be CD36-dependent (Mosig, Rennert et al. 2009). Moreover, monocyte accumulation of modified lipoproteins heightens their capacity to localise and transmigrate towards early atherosclerotic lesions, through augmented expression of select

chemokine receptors and adhesion molecules, such as CX3CR1 and β2-integrin (Mosig, Rennert et al. 2009). Furthermore, proof-of-principle studies in hypercholesterolaemic Apoe-deficient mice also demonstrated monocyte accumulation of modified lipoproteins with associated altered function and phenotype of monocytes, and contributed to accelerated atherosclerotic plaque formation (Xu, Dai Perrard et al. 2015). Similarly, in hypercholesterolaemic Ldlr-deficient mice the accumulation of modified lipoproteins within circulating monocytes has been described, subsequently impairing their chemotaxis (Jackson, Weinrich et al. 2016). Mechanistically, monocyte engulfment of modified lipoproteins directly altered the dynamics of their actin cytoskeleton, through changes in the activity of RhoA (Jackson, Weinrich et al. 2016). Collectively, these findings suggest that modulating the actin cytoskeleton of monocytes, through perturbation of Rho signalling for instance, may prevent their uptake of modified lipoproteins and associated adverse contribution to atherosclerotic plaque development.

4.3.2 Lipid accumulation in GM-Macs and modulation through fasudil or pravastatin treatment

The findings presented reveal that in comparison to M-CSF, GM-CSF treatment of human monocytes or GM-CSF directed polarisation of either THP-1 cells or PBMC-derived macrophages, increased cytoplasmic lipid accumulation and subsequent foam cell formation. Published supporting findings have suggested that M-CSF and GM-CSF may have divergent effects on macrophage foam cell formation by differently expressing genes related to the homeostatsis of cholesterol (Waldo, Li et al. 2008). Within the previous chapter, it was demonstrated that the actin cytoskeleton of macrophages is differentially affected by M-CSF or GM-CSF polarisation, which may be associated with the similar divergent regulation of foam cell formation between the two macrophage subsets. Indeed, in line with the proposition that the actin cytoskeleton may regulate lipid accumulation, foam cell formation was suppressed in GM-Macs (either THP-1 or PBMC-derived) through the addition of fasudil or pravastatin. This data suggest that statins are pleiotropic, and some of their beneficial effects on atherosclerosis are through anti-inflammatory mechanisms. Indeed, we can speculate from our findings that, through its pleiotropic effects, statin treatment suppresses macrophage foam cell formation through modulation of the actin cytoskeleton in pro-inflammatory, pro-atherosclerotic macrophages (GM-Macs).It has been demonstrated that statin treatment is effective at reducing adverse coronary events (atherosclerosis-dependent MI) in patients with elevated CRP levels but low LDL-cholesterol levels (Ridker, Rifai et al. 2001). It has been reported in the Pravastatin Inflammation/CRP Evaluation (PRINCE); a multicentre, community-based trial, demonstrated that pravastatin (40 mg/day) reduced average CRP levels by 17% in coronary disease patients, mainly independent of lipid lowering (Albert, Danielson et al. 2001). Similar effects have been reported for other statin family members, it has been

demonstrated that simvastatin (20 mg/day), pravastatin (40 mg/day), and atorvastatin (10 mg/day) significantly decreased high-sensitive CRP levels in patients suffering from hyperlipidaemia, which supports the anti-inflammatory effect of these drugs (Jialal, Stein et al. 2001). Another study showed that cerivastatin therapy for 8 weeks significantly reduced CRP levels by 13.3% among 785 patients suffering from primary hypercholesterolemia mainly in a lipid-independent manner (Ridker Paul, Rifai et al. 2001).

As scavenger receptors are fundamental for the uptake of modified lipoproteins such as oxLDL, associated assessment of the key molecules demonstrated that several scavenger receptors, such as CD36 at mRNA level, is not changed by the co-incubation with fasudil or pravastatin, while the protein expression of CD36 is significantly reduced. Similarly, the mRNA expression of OLR1 is significantly reduced with the addition of oxLDL which is unaffected by the co-incubation with fasudil or pravastatin. On the other hand, the protein expression of OLR1 was significantly increased with the addition of oxLDL and it was significantly reduced with the co-incubation of fasudil or pravastatin. This suggests the involvement of a post-transcriptional mechanism that needs further investigation. Alongside the uptake of modified lipoproteins, efficient reverse cholesterol transport including cholesterol efflux from macrophages ensures that modified lipoproteins do not adversely accumulate within cells. Considering the increased foam cell formation observed within GM-CSF polarised macrophages, it is plausible that cholesterol efflux-associated genes/proteins are dysregulated in addition to increased scavenger receptor expression, and that modifying the actin cytoskeleton reverses such deleterious effects. Indeed, although mRNA expression of some cholesterol efflux genes such as NCOR1 were not altered in GM-CSF polarised macrophages, According to table 4.4, oxLDL addition to GM-Macs increased the mRNA expression of ABCG1, NCOR1, and PPARA, which was unaffected by fasudil, and suppressed by statin co-incubation for ABCG1 and NCRO1. Opposingly, the protein expression for NCOR1, NCOR2, and PPARα was not changed by oxLDL addition, but significantly increased by fasudil or pravastatin co-incubation suggesting enhanced cholesterol efflux. These findings highlight that a discrepancy exists between the mRNA and protein expression of cholesterol efflux mediators in mature GM-CSF polarised macrophages upon oxLDL accumulation. Similarly, in GM-Mac-derived foam cells, the actin cytoskeleton modifying drugs fasudil and pravastatin, differentially affect NCOR1 or PPARA mRNA and protein levels. Collectively, these novel results imply the involvement of a post-transcriptional regulatory mechanism, such as the involvement of microRNAs, or protein modification pathways including ubiquitination or SUMOylation. In support of this proposition it has been reported that microRNA-generating enzyme Dicer has an essential role in macrophage activation in atherosclerotic plaque. $Apoe^{-/-}$ mice with Dicer deficient macrophages showed increased accumulation of lipid in macrophages and increased inflammatory reaction (Wei, Corbalán-Campos et

al. 2018). Another study showed miR-10b decrease the ability of peritoneal macrophages to efflux cholesterol by downregulating the expression of ABCA1, the expression of miR-10b is upregulated in advanced atherosclerotic plaques of $Apoe^{-/-}$ mice and the treatment with antagomiR-10b was able to promote reverse cholesterol transport in peritoneal macrophages by upregulating the expression of ABCA1 (Wang, Wang et al. 2018). It has been demonstrated that miR-19b enhances accumulation of cholesterol in THP-1 derived macrophages as well as mouse peritoneal macrophages and the formation of foam cells by blocking the efflux cholesterol of macrophages to apolipoprotein A-I (apoA-I), the main protein component in HDL. MiR-19b directly binds to 3'UTR of ABCA1 transporter and regulates its expression resulting in the progression of aortic atherosclerotic plaques(Lv, Tang et al. 2014). Corroborating studies have demonstrated a contributory role for PPARα in suppressing macrophage foam cell formation and subsequent atherosclerotic plaque development (Li, Binder et al. 2004, Srivastava 2011). Furthermore, statins have been shown to inhibit Rho/ROCK signalling and subsequently increase PPARα activity and suggest increased reverse cholesterol transport (Martin, Duez et al. 2001), providing additional credence to the findings within this chapter.

As discussed previously, the aim of this study was to assess the effects of modulating the actin cytoskeleton on M-CSF polarised (M-Mac) and GM-CSF directed (GM-Mac) macrophage phenotypes, with particular focus on their ability to accumulate modified lipoproteins and subsequently modulate foam cell formation. Consequently, and in light of the above findings, using strategies to modulate the macrophage actin cytoskeleton or down-stream modulated pathways may be deployed therapeutically to influence the progression of cardiovascular diseases such as atherosclerosis. It has been demonstrated that ROCK2 deficiency in macrophages decreased macrophages lipid accumulation through enhanced cholesterol efflux PPARγ/ABCA1-dependent, and in association, decreased atherosclerosis (Zhou, Mei et al. 2012).

4.3.3 Efferocytosis capacity between different macrophage subsets and modulation through fasudil or pravastatin treatment

Efferocytosis is a process in which immune cells, especially macrophages, can engulf apoptotic cell debris and remove dying cells, and is essential to prevent non-resolving inflammatory diseases such as atherosclerosis (Yurdagul, Doran et al. 2017). Accordingly, it has been demonstrated that defective efferocytosis is a crucial determinant of atherosclerosis lesion progression and the development of unstable advanced plaques (Yurdagul, Doran et al. 2017). Within this chapter I have demonstrated that GM-CSF polarised macrophages display impaired efferocytosis capacity compared to M-CSF polarised macrophages, which can be restored to M-Mac levels through the addition of pravastatin and fasudil. That is in line with a previous study which demonstrated that treatment with lovastatin

and Rho kinase inhibitor (Y-27632) significantly enhanced the efferocytosis capacity in macrophages via their ability to inactivate RhoA in both in vitro and in vivo studies (Morimoto, Janssen et al. 2006). Another study demonstrated that during lipopolysaccharide-induced neutrophil influx in the pleural cavity of mice, ROCK inhibition by fasudil, or Y-27632 was able to increase the efferocytosis capacity in macrophages (Galvão, Athayde et al. 2019). This data suggests a possible strategy to activate and accelerate the resolution process in CVD such as atherosclerosis.

5 EFFECT OF SUMOYLATION ON MACROPHAGE SUBSET BEHAVIOUR AND VALIDATIVE STUDIES IN HUMAN ATHEROSCLEROTIC PLAQUES

5.1 Introduction

SUMOylation is a posttranslational modification that involves the covalent attachment of a small ubiquitin-like modifier (SUMO) proteins to lysine residues within specific protein substrates via an enzymatic cascade (Dehnavi, Sadeghi et al. 2019). SUMOylation is an essential modification that regulates the cellular, molecular, and systemic properties and functions of proteins (Dehnavi, Sadeghi et al. 2019) SUMO proteins have a molecular weight of 10 kDa and are considered members of the ubiquitin-like family. In humans, the SUMO family consists of four isoforms (Chang and Abe 2016); SUMO1 shares 50% sequence similarity to SUMO2, while SUMO2 shares 97% sequence identity to SUMO3. SUMO1, 2, and 3 are widely expressed, while SUMO4 can only be found within the spleen, lymph nodes, and kidneys. Additionally, the expression of mature SUMO4 has been demonstrated within cells under extreme stress conditions (Le, Sandhu et al. 2017). SUMO proteins are released in an inactive form that requires activation and maturation via sentrin-specific peptidases (SENPs). Binding of SUMOs to their substrates occur in three steps. First, mature SUMOs attach to SUMO-Activating Enzyme Subunit 1 or 2 (SAE1/SAE2) that is known as E1 activating enzyme, the first step is ATP-dependent and needs ATP to be activated. Second, SUMO is passed to the E2 conjugating enzyme Ubc9. Finally, Ubc9 passes SUMO onto the E3 ligase Pc2 (polycomb protein 2), PIAS (protein inhibitor of activated STAT), and RanBP2 (Ran-binding protein 2) so that it can be attached to its target substrate. The attachment of a SUMO protein to its substrate is reversible, with deSUMOylation occuring via SENPs that leads to the release of mature SUMO from its target protein (as illustrated in figure 5.1) (Gao, Huang et al. 2014).

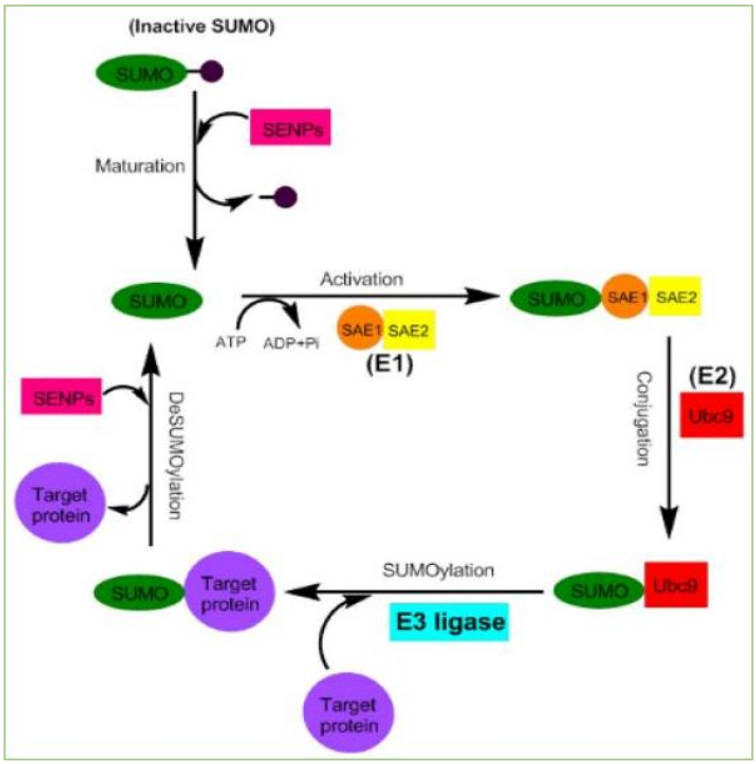

Figure 5.1 Summary of SUMOylation pathway

The precursor of small ubiquitin-like modifier (SUMO) is released in an inactive form and is matured and activated by sentrin specific proteases (SENPs). The first step which is an ATP-dependent step where mature SUMOs bind to (SAE1/SAE2) known as E1 activating enzyme. Second step, SUMO is passed to Ubc9 ,the E2 conjugating enzyme. Final step, Ubc9 passes SUMO onto the E3 ligase to be attached to target protein. SUMO protein attachment is reversible, with deSUMOylation occuring via SENPs. SENPs, sentrin specific proteases; SAE1/SAE2, SUMO-Activating Enzyme subunit 1/2; Ubc9, Ubiquitin carriere protein 9. Figure is taken from (Dehnavi, Sadeghi et al. 2019)

Sumoylation has been proposed to modulate multiple divergent and complimentary signalling pathways associated with atherosclerosis, including the pro-inflammatory NFκB pathway. NFκB is located in the cytoplasm of cells in an inactive form due to its attachment to members of the endogenous inhibitors of NFκB, such as NFκB Inhibitor Alpha (NFKBIA), also known as IkBα. Within atherosclerotic plaques, NFκB is activated due to the presence of different pro-inflammatory factors including pro-inflammatory cytokines such as TNFα, or disturbed blood flow and associated low shear stress that leads to the upregulation of IkB kinase and subsequent phosphorylation of IkBα (Brown, Gerstberger et al. 1995). Phosphorylation of IkBα leads to its inactivation and the free NFκB is able to translocate to the nucleus and mediate the upregulation of pro-inflammatory genes such as SELE (E-selectin), VCAM1, ICAM1, and MCP1 (Xiao, Liu et al. 2013). It has been reported that SUMOylation regulates the activity of NFκB. SUMOylation of IkBα via SUMO1 reduces its destruction and subsequently blocks NFκB nuclear translocation and therefore downregulates the activation of NFκB pathway. On the other hand, SUMOylation of IkBα via SUMO2/3 inactivates IkBα and subsequently upregulates NFκB pathway (Desterro, Rodriguez et al. 1998) (Le, Sandhu et al. 2017). A similar pathway which has also been linked to atherosclerosis and proposed to undergo regulation through SUMOylation is the MAP kinase pathway. It has been reported that ROS and disturbed blood flow/low shear stress increases SUMOylation of Mitogen-Activated Protein Kinase 7 (MAPK7; also known as ERK5), a transcription factor that has an essential role in the growth and differentiation of endothelial cells. SUMOylation of MAPK7 inhibits the protein expression of eNOS in endothelial cells leading to endothelial cell dysfunction and inflammation, mechanisms associated with early atherosclerotic plaque formation (Le, Corsetti et al. 2012). These studies highlight the potential for the SUMOylation pathway to modulate cellular function and processes involved in atherosclerosis, although the role of SUMOylation in macrophage behaviour is understudied.

A recent study reported that SUMOylation regulates processes related to the cellular cytoskeleton, including microtubule-associated proteins, intermediate filaments, actin polymerisation, and actin-regulatory proteins (Alonso, Greenlee et al. 2015). It has been shown that SUMO2/3 are the preferential isoforms responsible for the modification of the actin cytoskeleton. Cellular fractionation experiments demonstrated that SUMOylation of actin (monomeric G-actin) was more abundant within the nuclear fraction, resulting in the inhibition actin filament formation (polymerisation into F-actin) (Hofmann, Arduini et al. 2009). The Rho family of GTPases (such as Rac1 and RhoA) have also been shown to undergo regulation by SUMO proteins (Dehnavi, Sadeghi et al. 2019). It has been reported that SUMOylation of Rac1 by SUMO1 enhances cell migration and the formation of lamellipodia. SUMOylation is important for optimal binding of GTP to Rac1, and it has been demonstrated that SUMOylation of Rac1 occurs when in its GTP-bound active state, rather than an

inactive GDP-bound state. Relatedly, Rho GDP-dissociation inhibitors (RhoGDI) are also regulated by SUMOylation, and activation of RhoGDI via SUMOylation downregulates the activity of the Rho family of GTPases, which results in the inhibition of actin filament polymerisation (Yu, Zhang et al. 2012). Given the differences observed between M-Mac and GM-Mac morphology and associated F-actin accumulation, it is plausible that SUMOylation may differentially regulate the actin cytoskeleton in the two macrophage subsets.

Topotecan is a topoisomerase I inhibitor agent used as a chemotherapeutic drug to treat cervical cancer, ovarian cancer, and small cell lung cancer (Pommier 2006). Topotecan is water-soluble and a semi-synthetic analogue of a natural camptothecin compound that was originally isolated from a Chinese tree, *Camptotheca acuminate* (Robati, Holtz et al. 2008). Topotecan blocks the activity of topoisomerase I and enhances the separation and repair of DNA strands during division; it prevents cancer cells from differentiation and growth, and therefore induces the death of cancerous cells. Moreover, topotecan has been shown to modulate the SUMOylation status of DNA topoisomerase I (Mo, Yu et al. 2002), and therefore topotecan has subsequently been proposed as a global inhibitor of SUMOylation (Bernstock, Ye et al. 2017). One of the cytotoxic properties of topotecan is due to its interference with the cytoskeletal elements of the cell such as actin filaments and microtubules (Wang, Tanaka et al. 2016). It has been reported that topotecan can instigate degradation and changes in cytoskeletal proteins (Cohen, Geva-Zatorsky et al. 2008). An in vitro study using Hela cells showed that topotecan reduced actin polymerisation (less F-actin) which was associated with a change in cell morphology and inhibiting their motility (Wang, Tanaka et al. 2016). As such, topotecan is a suitable compound to explore modulation of SUMOylation and subsequent effects on the actin cytoskeleton in divergent macrophage populations, which display disparate morphologies.

Given the results from the previous two chapters demonstrate GM-CSF polarisation dictates the generation of a distinct macrophage phenotype compared to M-CSF polarisation, an understanding of the down-stream signalling pathways triggered by GM-CSF is of importance. The Janus Kinase/Signal Transducer and Activator of Transcription (JAK/STAT) signalling pathway is one of the most essential pathways responsible for the differentiation and maturation of monocyte/macrophages (Leonard and O'Shea 1998). The STAT family consists of seven members, STAT 1- 4, 5A, 5B, and STAT6. Binding of GM-CSF to its receptor activates the JAK tyrosine kinases, in turn, activated JAKs such as JAK2 results in activation of cytoplasmic STAT5A/B via phosphorylation, and the formation of homo- or heterodimers that are able to enter the nucleus and regulate the expression of distinct target genes (Lehtonen, Matikainen et al. 2002). Other than tyrosine phosphorylation, it has been shown that acetylation, ubiquitylation, and SUMOylation can modulate STAT signalling. SUMOylation of STAT5A/B takes place on the lysine residues that are located adjacent to the tyrosine residue where

phosphorylation of STAT5A/B occurs, suggesting that SUMOylation and phosphorylation of STAT5A/B act antagonistically to each other (Krämer and Moriggl 2012). A recently developed compound, 3-hydroxy-1, 2, 3-benzotriazin-4(3H)-one (HODHBt), a benzotriazole derivative, which is a specific STAT5-SUMO protein-protein interaction inhibitor, that blocks SUMOylation of phosphorylated STAT5. As such, HODHBt retards the inhibitory effect of SUMO2/3 on STAT5 and therefore permits phosphorylation and activation of STAT5 and its translocation to the nucleus to drive gene expression (Bosque, Nilson et al. 2017).

5.1.1 Aims of this chapter

In the previous chapter, discrepancies were observed between mRNA and protein levels of some key molecules, suggesting the involvement of a post-transcriptional regulatory mechanism, such as SUMOylation. In this chapter, the aim is to evaluate the effect of SUMOylation on pro-inflammatory macrophage (GM-Mac) behaviour by using a global SUMOylation inhibitor (topotecan), alongside a specific inhibitor of STAT5 SUMOylation (HODHBt). In addition, the potential mechanisms by which SUMOylation regulates the properties of GM-Macs are assessed alongside preliminary investigation on the expression of SUMOylation-related proteins within human atherosclerotic plaques, to support this avenue of research.

5.2 Results

5.2.1 Unstable plaques exhibit decreased SUMO1 and SUMO2/3 protein expression compared to non-diseased arteries and stable plaques

In light of the recent evidence (provided in the introduction) demonstrating SUMOylation can regulate the actin cytoskeleton of cells alongside modulating functions related to inflammation such as phagocytosis and efferocytosis, the expression of key SUMOylation proteins was examined within human coronary artery atherosclerotic plaques. Specifically, to ascertain whether SUMOylation proteins (SUMO1 and SUMO2/3), inhibitors of SUMOylation (SENP3), and a potential SUMOylation target key to GM-CSF polarisation (pSTAT5A) were differentially expressed during atherosclerotic plaque progression and related to inflammation, immunohistochemistry was performed in three groups; sections of non-diseased coronary arteries, stable plaques, and unstable plaques. Image analysis and associated quantification of regions known to be rich in macrophage accumulation, demonstrated a significantly increased number of cells expressing pSTAT5A in stable and unstable plaques compared to non-diseased arteries (1.6-fold: $p<0.01$, 1.5-fold: $p<0.05$, respectively; n=10; Figure 5.2). The majority of positive cells were within the macrophage-rich shoulder regions of the atherosclerotic plaques. The percentage of intra-plaque cells expressing SUMO1 was also increased in stable plaques compared to non-diseased arteries SUMO1 (1.5-fold; $p<0.001$; n=10; Figure 5.3). However, a significant decrease in SUMO1 positive cell percentage was observed in unstable plaques when compared to stable lesions (49%; $p<0.001$; n=10; Figure 5.3) and non-diseased arteries (22%; $p<0.05$; n=10; Figure 5.3). SUMO2/3 positive cell percentage was also increased within stable plaques compared to non-diseased arteries (2.5-fold; $p<0.001$; n=10; Figure 5.4) and unstable plaques (1.9-fold; $p<0.001$; n=10; Figure 5.4), while no statistically significant difference was detected between unstable plaques and non-diseased artery sections (Figure 5.4). Mirroring the changes seen for pSTAT5A, the percentage of intra-plaque cells positive for SENP3 was increased within stable (1.6-fold; $p<0.01$; n=10; Figure 5.5) and unstable plaques (1.3-fold; $p<0.05$; n=10; Figure 5.5), when compared to non-diseased artery sections. Taken together, these observations indicate key proteins involved in the SUMOylation pathway are differentially expressed during atherosclerotic plaque development and progression, particularly within macrophage-rich shoulder regions, and therefore warrants further investigation.

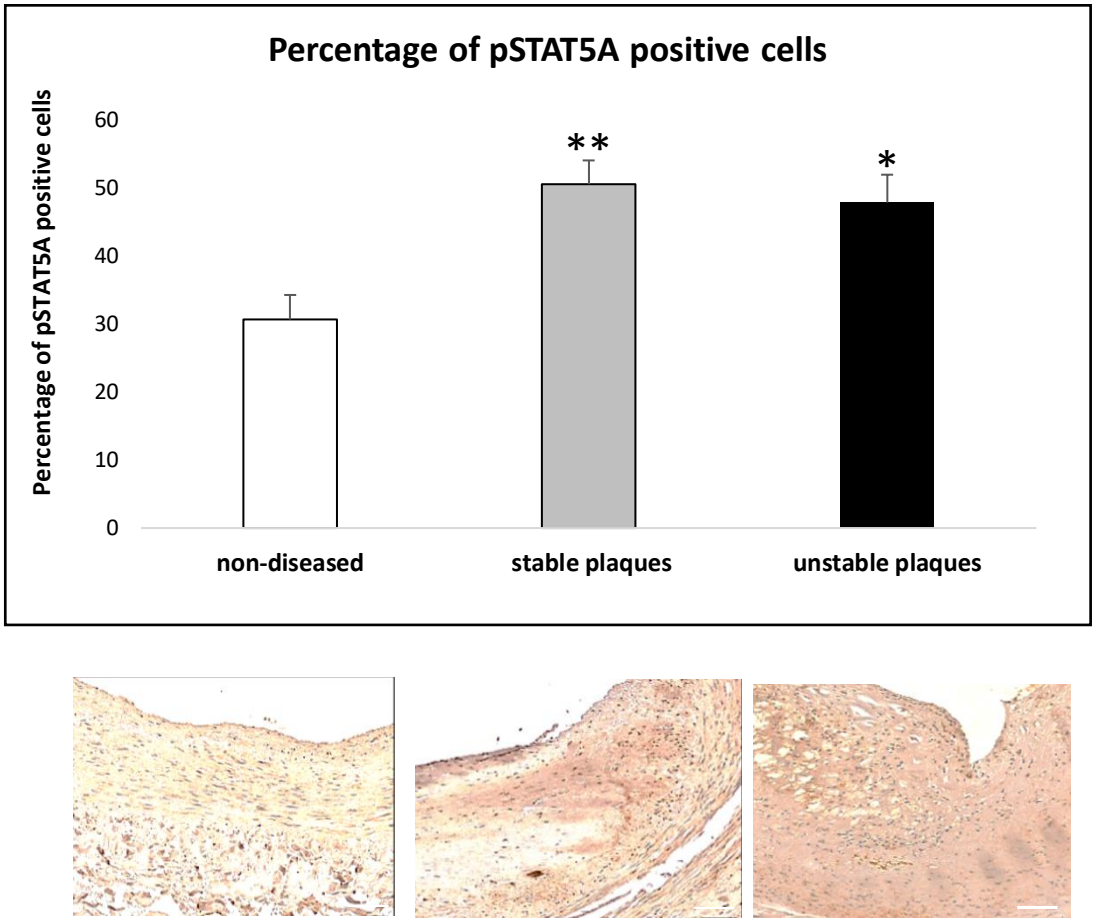

Figure 5.2 The percentage of pSTAT5A positive cells is increased in both stable and unstable human plaques.

Quantification and representative images of immunohistochemistry for pSTAT5A showing the percentage of pSTAT5A positive cells within non- diseased and atherosclerotic human coronary arteries defined as stable and unstable. Positive cells are stained brown and all nuclei are stained blue with haematoxylin. Percentage of positive cells was calculated within 10 random x 40 magnification fields. * indicates $p<0.05$, ** indicates $p<0.01$, ANOVA, Student-Newman-Keuls Multiple Comparisons Test, n=10. Scale bar represents 100 µm and applies to all panels. N-values represent number of patients with coronary arteries histologically defined as non-diseased, harbouring stable, or unstable plaques (n=10/group) were of similar age and gender ratio.

.

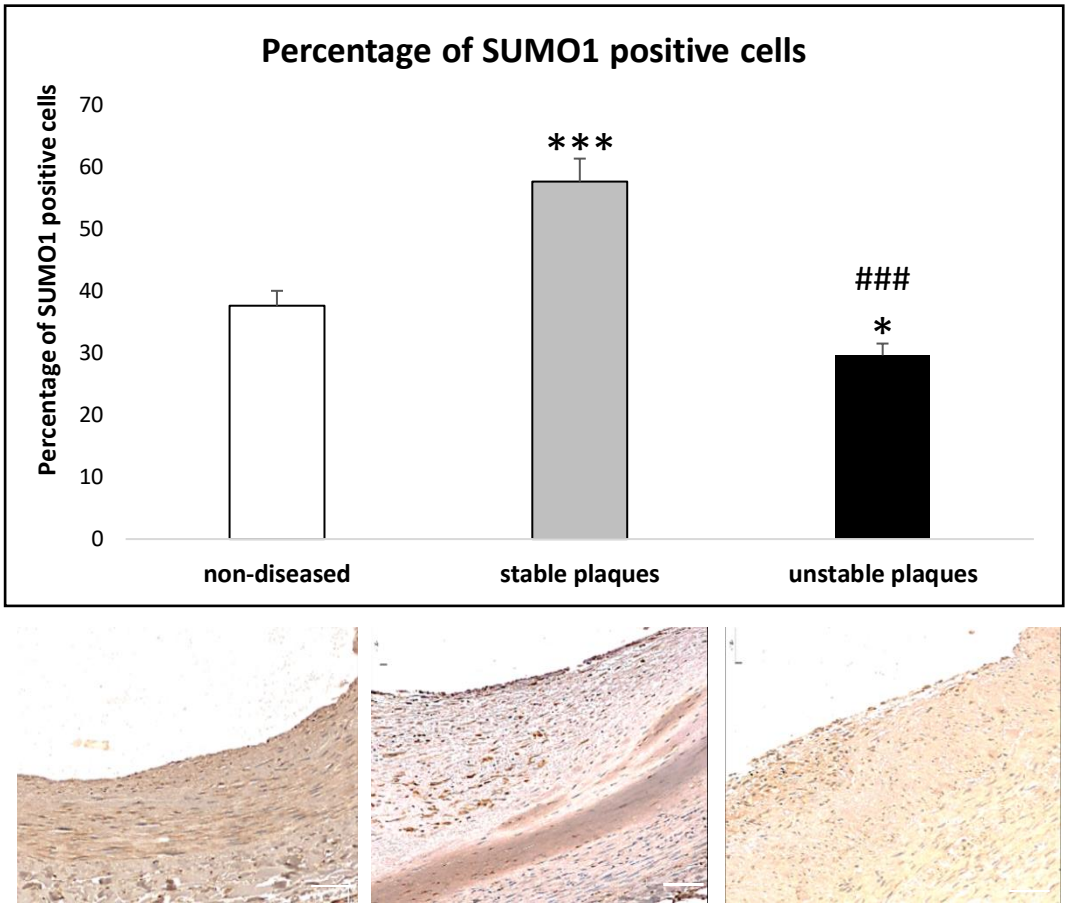

Figure 5.3 The percentage of SUMO1 positive cells is increased in stable plaques and decreased in unstable human plaques.

Quantification and representative images of immunohistochemistry for SUMO1 showing the percentage of SUMO1 positive cells within non- diseased and atherosclerotic human coronary arteries defined as stable and unstable. Positive cells are stained brown and all nuclei are stained blue with haematoxylin. Percentage of positive cells was calculated within 10 random x 40 magnification fields. * indicates $p<0.05$ and *** indicates $p<0.001$ compared to non-diseased, ### indicates $p<0.001$ compared to stable plaques, ANOVA, Student-Newman-Keuls Multiple Comparisons Test, n=10. Scale bar represents 100 µm and applies to all panels. N-values represent number of patients with coronary arteries histologically defined as non-diseased, harbouring stable, or unstable plaques (n=10/group) were of similar age and gender ratio.

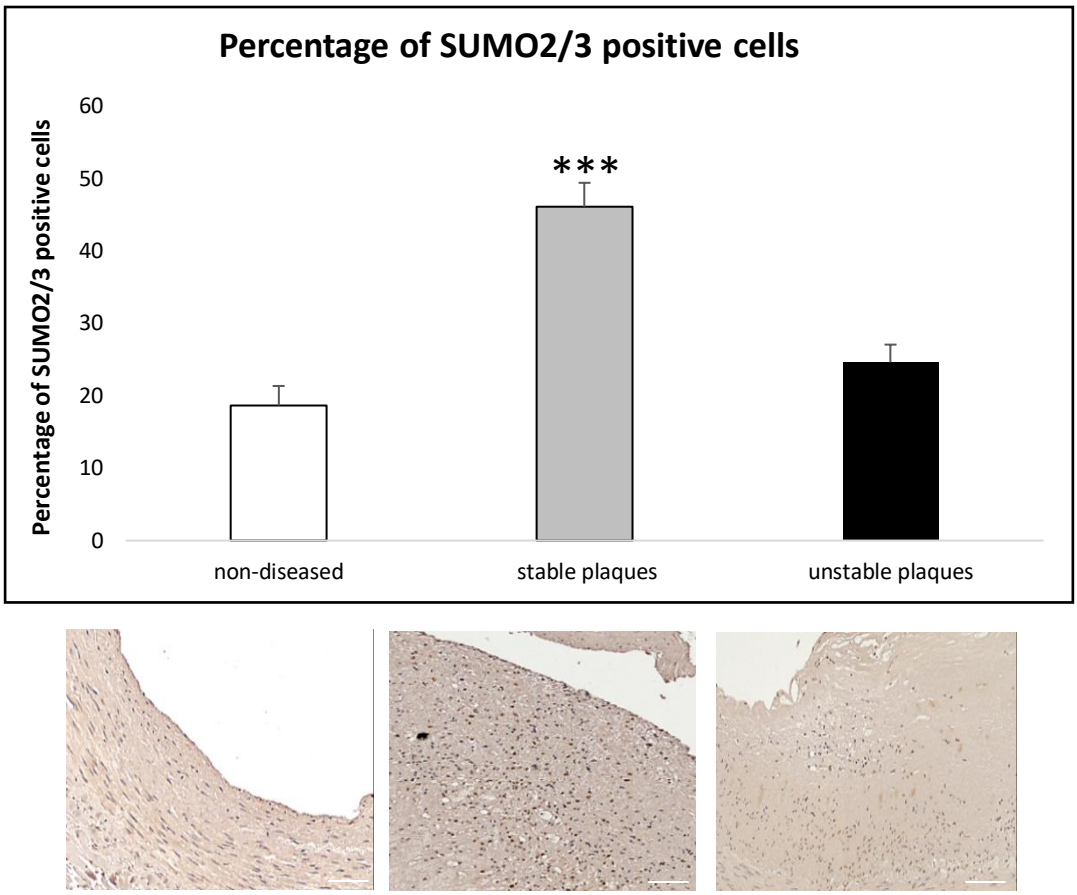

Figure 5.4 The percentage of SUMO2/3 positive cells is increased in stable human plaques.

Quantification and representative images of immunohistochemistry for SUMO2/3 showing the percentage of SUMO2/3 positive cells within non- diseased and atherosclerotic human coronary arteries defined as stable and unstable. Positive cells are stained brown and all nuclei are stained blue with haematoxylin. Percentage of positive cells was calculated within 10 random x 40 magnification fields. *** indicates $p<0.001$ compared to non-diseased and unstable plaques, ANOVA, Student-Newman-Keuls Multiple Comparisons Test, n=10. Scale bar represents 100 µm and applies to all panels. N-values represent number of patients with coronary arteries histologically defined as non-diseased, harbouring stable, or unstable plaques (n=10/group) were of similar age and gender ratio.

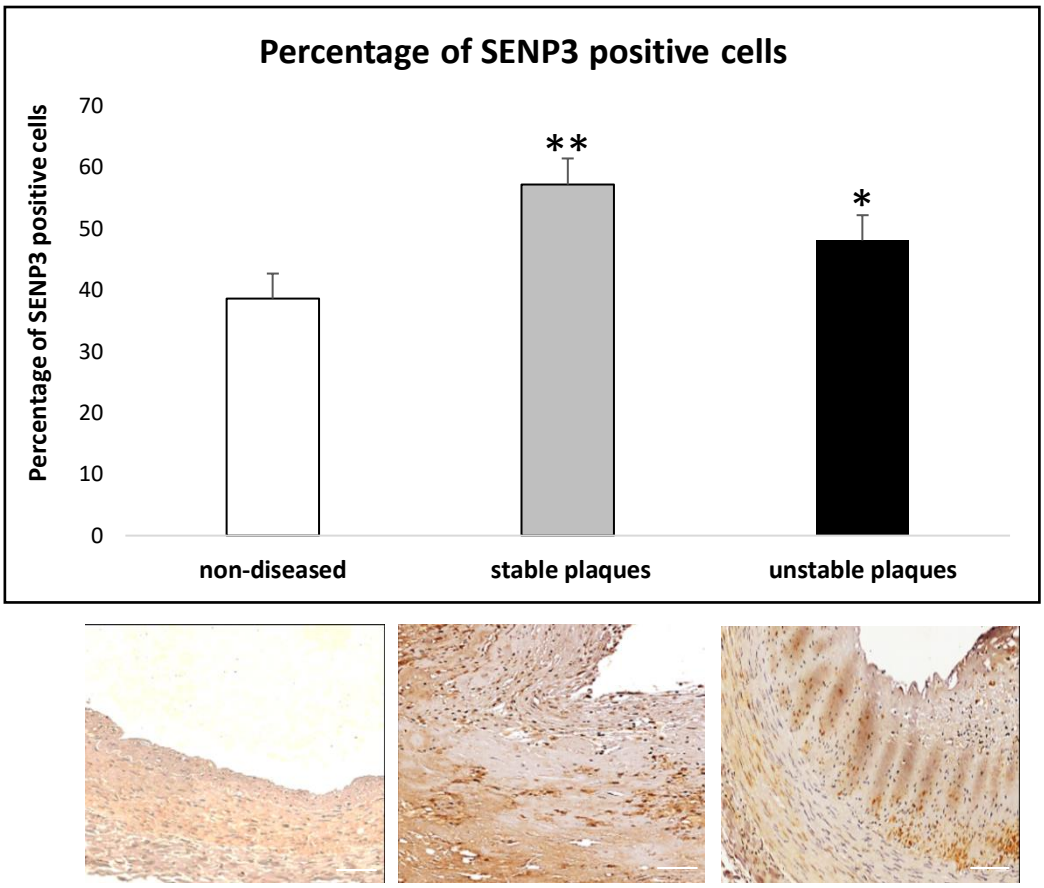

Figure 5.5 The percentage of SENP3 positive cells is increased in both stable and unstable human plaques.

Quantification and representative images of immunohistochemistry for SENP3 showing the percentage of SENP3 positive cells within non- diseased and atherosclerotic human coronary arteries defined as stable and unstable. Positive cells are stained brown and all nuclei are stained blue with haematoxylin. Percentage of positive cells was calculated within 10 random x 40 magnification fields. ** indicates $p<0.01$ and * indicates $p<0.05$ compared to non-diseased arteries, ANOVA, Student-Newman-Keuls Multiple Comparisons Test, n=10. Scale bar represents 100 µm and applies to all panels. N-values represent number of patients with coronary arteries histologically defined as non-diseased, harbouring stable, or unstable plaques (n=10/group) were of similar age and gender ratio.

5.2.2 Topotecan reduces the ability of M-Mac and GM-Mac macrophages to uptake lipid and form foam cells

Given the differential expression patterns of SUMO proteins, SENP3, and pSTAT5A (a key signalling molecule in GM-CSF macrophage polarisation), perturbation of SUMOylation in divergent macrophage subsets was explored. As discussed within the introduction, topotecan acts as a global SUMOylation inhibitor. Accordingly, to detect the effect of SUMOylation on the activity of different macrophage subsets, in the first instance a range of different doses of topotecan was administered to macrophages in order to identify the appropriate concentration of topotecan to modulate macrophage subsets without affecting cell viability (cytotoxicity).

Results with topotecan treatment showed that 5 µM and 1 µM of topotecan caused a significant increase in the percentage of dying cells (65.1%, 295% respectively) for M-Mac, and (69.8%, 33.9% respectively) for GM-Mac (Figure 5.6) and therefore considered cytotoxic. However, 0.5 µM of topotecan did not significantly increase cell death numbers in the GM-Mac subset, but marginally remained significantly cytotoxic to the M-Mac subset (22.4%; $p<0.05$; Figure 5.6). Based on these results, a concentration of 0.25 µM topotecan was used for all subsequent experiments.

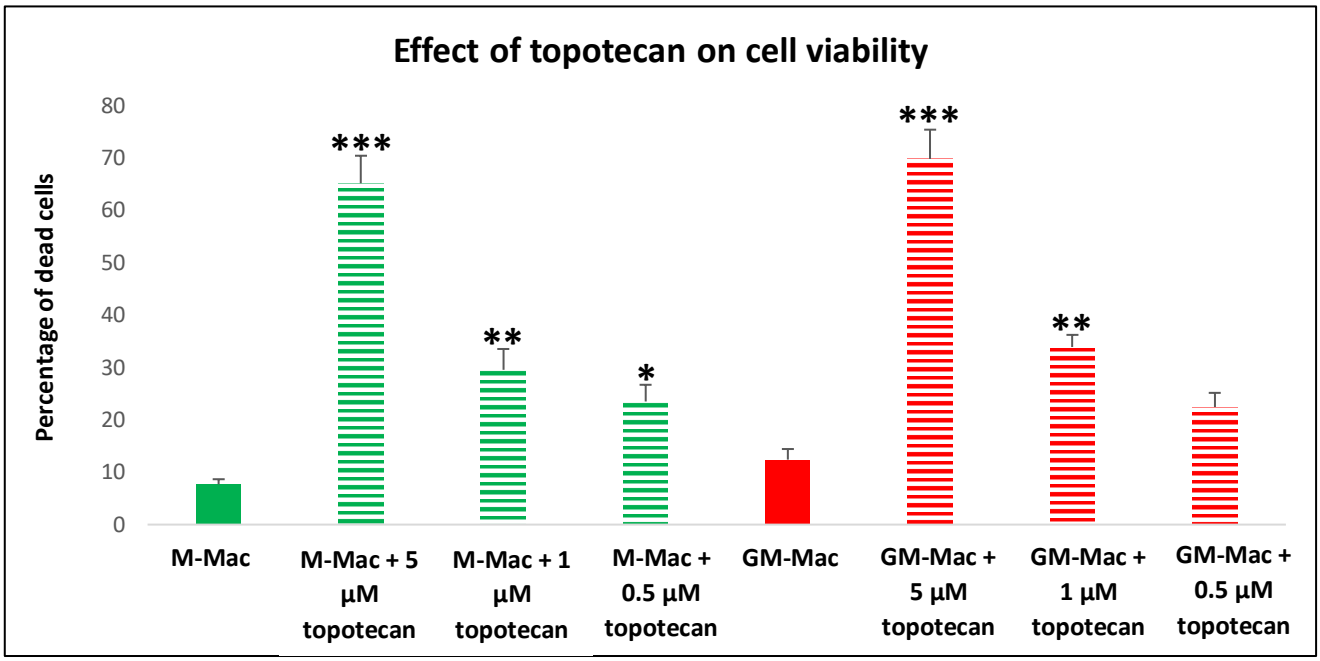

Figure 5.6 Effect of topotecan on M-Mac and GM-Mac cell viability

Quantification of cell death in M-Mac and GM-Mac subsets derived from primary human macrophages and treated for 24 hours with increasing doses of topotecan, assessed by immunocytochemistry. Data presented as percentage of dead cells calculated within six random x 20 magnification fields. *** indicates $p<0.001$, ** indicates $p<0.01$, * indicates $p<0.05$ compared to respective unstimulated M-Mac or GM-Mac control; ANOVA, Student-Newman-Keuls Multiple Comparisons Test, n=4. N-values in macrophages derived from PBMCs represent the number of healthy donors.

Next, the selected dose of topotecan was assessed and validated for its ability to alter foam cell formation in the two different macrophage subsets derived from primary human macrophages. Human blood-derived monocytes were divided into two groups according to the period of time that the cells were incubated with colony stimulating factors. The first group were termed early macrophages, which were freshly isolated monocytes treated with M-CSF or GM-CSF for one day. The second group were classified as mature macrophages, which were freshly isolated monocytes treated with M-CSF or GM-CSF for 7 days. Finally, both groups were exposed to 10 μg/ml of Dil-oxLDL with and without 0.25 μM topotecan for 24 hours. Cells were subjected to Oil Red O staining to visualize oxLDL accumulation (foam cell formation). Image analysis and subsequent quantification demonstrated that in early macrophages, 0.25 μM of topotecan induced a significant reduction in foam cell formation for both M-Mac and GM-Mac subsets (53.4%; $p<0.05$, and 48.5%; $p<0.05$ respectively; n=5; Figure 5.7). Similar effects were observed in mature macrophages with topotecan treatment of both M-Mac and GM-Mac subsets (46.9%; $p<0.05$, and 49%; $p<0.05$; n=5; Figure 5.8).

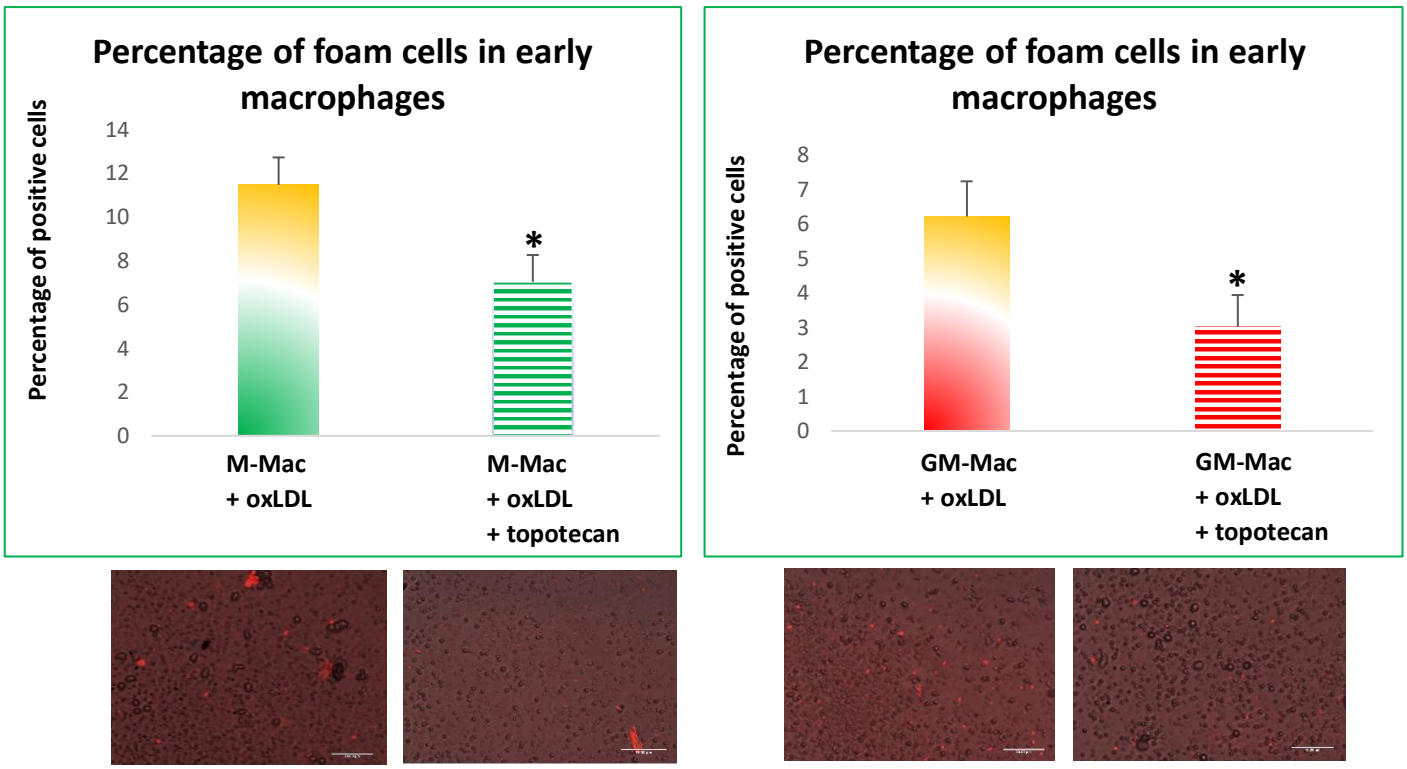

Figure 5.7 Topotecan reduced the ability of early M-Mac and GM-Mac subsets derived from human PBMCs to accumulate oxLDL and form foam cells.

Quantification and representative images showing the percentage of foam cells formed from human primary macrophages. Macrophages were incubated with Dil-oxLDL (10 µg/ml) with and without topotecan (0.25 µM) for 24 hours, after which cells were stained with Oil Red O to visualise oxLDL accumulation. Cells were counted within 10 random x 40 magnification fields. * indicates $p<0.05$, two tailed, paired t-test n=5. N-values in macrophages derived from PBMCs represent the number of healthy donors.

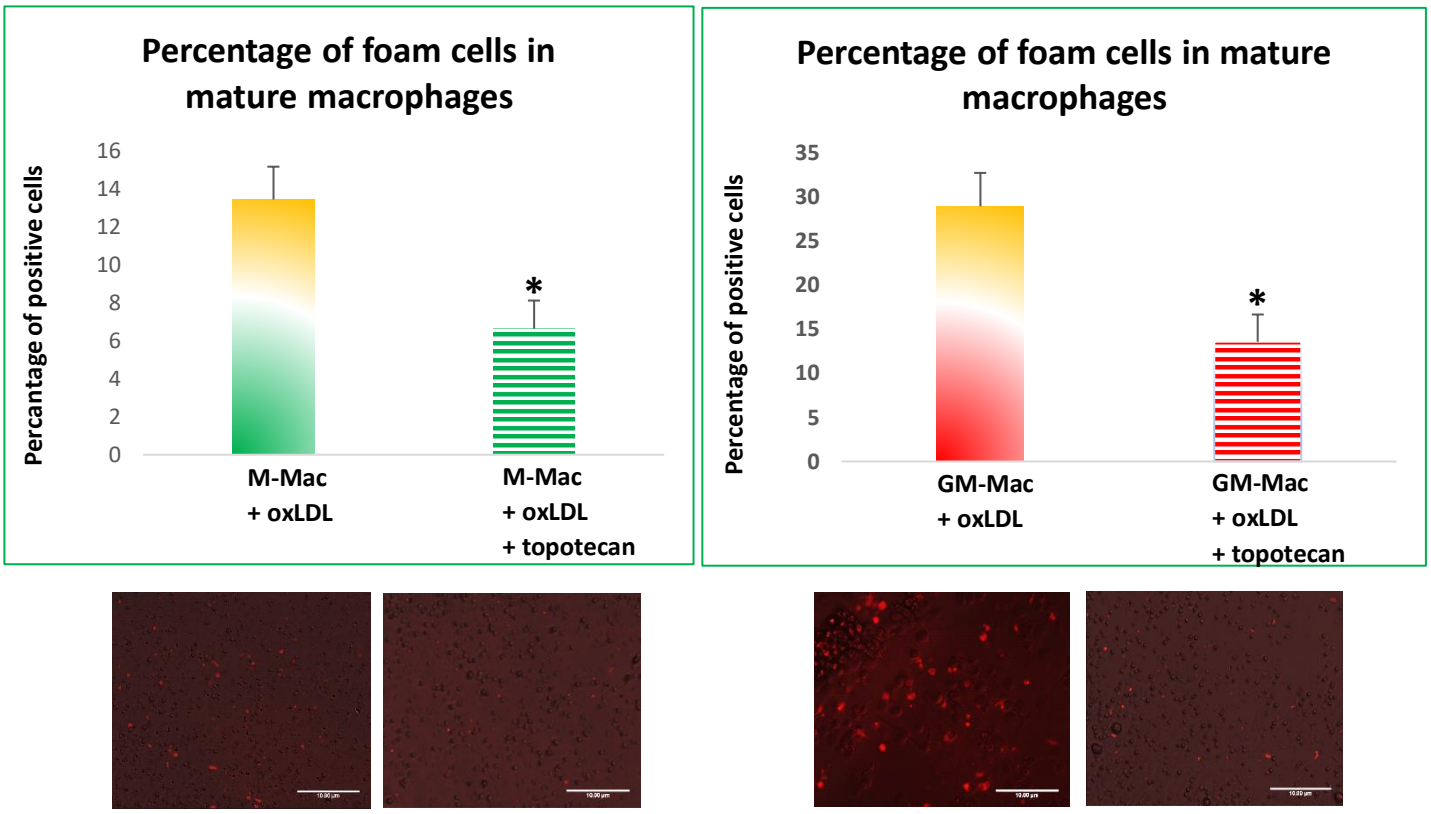

Figure 5.8 Topotecan reduced the ability of mature M-Mac and GM-Mac subsets derived from human PBMCs to accumulate oxLDL and form foam cells.

Quantification and representative images showing the percentage of foam cells formed from human primary macrophages. Macrophages were incubated with Dil-oxLDL (10 µg/ml) with and without topotecan (0.25 µM) for 24 hours, after which cells were stained with Oil Red O to visualise oxLDL accumulation. Cells were counted within 10 random x 40 magnification fields. * indicates $p<0.05$, two tailed, paired t-test n=5. N-values in macrophages derived from PBMCs represent the number of healthy donors.

5.2.3 Topotecan regulates the mRNA expression of scavenger receptors MSR1 and CD36 as well as lipid transporters ABCA1 and ABCG1 in primary human macrophage subsets

The previous results showed that topotecan (0.25 µM) was able to regulate foam cell formation in both M-Mac and GM-Mac subsets derived from primary human macrophages. As such, qPCR was performed to assess whether alterations in foam cell formation were associated with changes in the mRNA expression of key scavenger receptors and lipid tranporters that regulate cholesterol homeostasis, and to gain insight into potential mechanisms underlying the effect of topotecan on foam cell formation. Human blood-derived monocytes were polarised to M-Mac and GM-Mac over 7 days and then treated with 10 µg/ml of Dil-oxLDL with and without 0.25 µM of topotecan for 24 hours. Subsequent RT-qPCR analysis was performed on RNA extracted from cells for gene expression of key lipoprotein-related scavenger receptors (MSR1, OLR1, MRC1, and CD36), and cholesterol efflux-related genes (NCOR1, PPARA, ABCG1, and ABCA1). The data revealed that although topotecan did not significantly affect the mRNA expression of MRC1, OLR1, or PPARA in M-Macs (Figure 5.9), topotecan co-adminstration increased oxLDL-induced mRNA expression of the cholesterol efflux-related genes ABCA1, ABCG1, and NCOR1) in M-Macs (3.4-fold; $p<0.05$; 5.8-fold ; $p<0.001$; and 14.4-fold; $p<0.001$ respectively; n=5; Figure 5.9). Conversely, mRNA levels of the scavenger receptor MSR1 were downregulated by topotecan treatment of oxLDL stimulated M-Macs (2.4-fold; $p<0.05$; n=5; Figure 5.9). Whereas in GM-Macs, only the mRNA expression of the key lipoprotein-related scavenger receptor CD36 was suppressed by topotecan co-adminstration to oxLDL-exposed macrophages(1.7-fold; $p<0.05$; n=5; Figure 5.9).

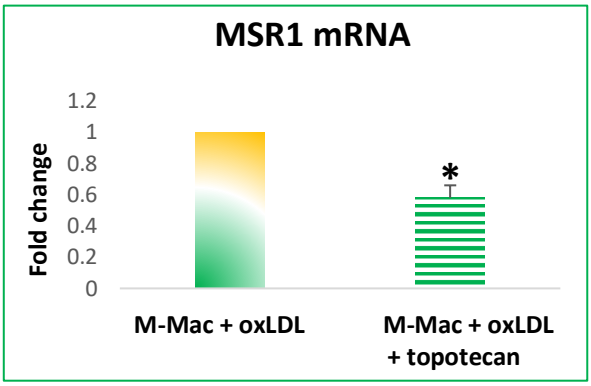
MSR1 mRNA
Fold change
1.2
1
0.8
0.6
0.4
0.2
0
*
M-Mac + oxLDL
M-Mac + oxLDL + topotecan

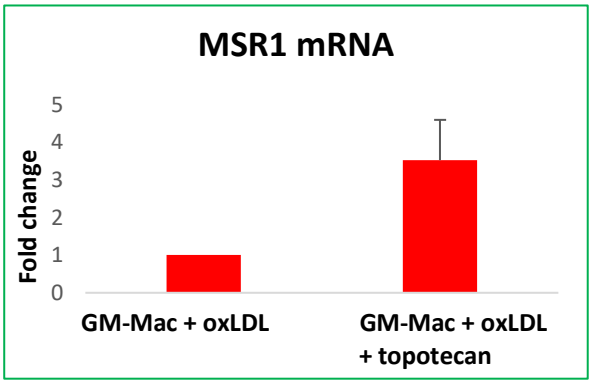
MSR1 mRNA
Fold change
5
4
3
2
1
0
GM-Mac + oxLDL
GM-Mac + oxLDL + topotecan

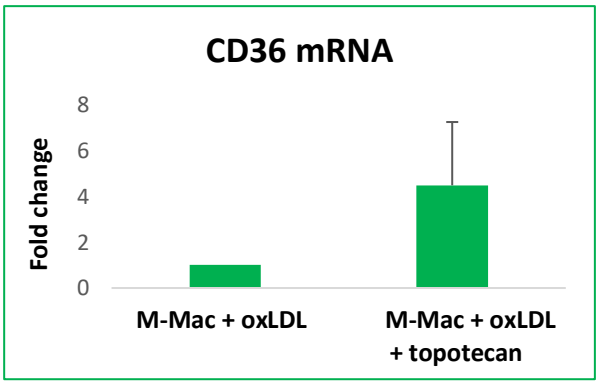
CD36 mRNA
Fold change
8
6
4
2
0
M-Mac + oxLDL
M-Mac + oxLDL + topotecan

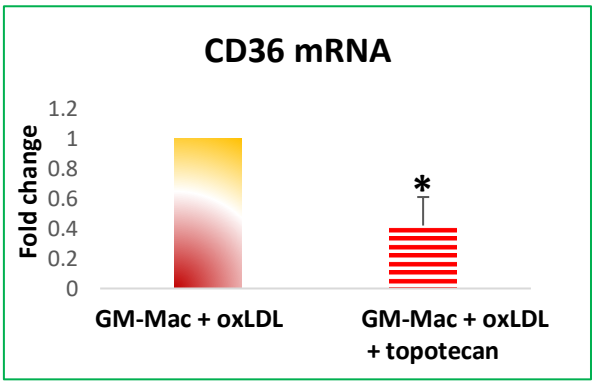
CD36 mRNA
Fold change
1.2
1
0.8
0.6
0.4
0.2
0
*
GM-Mac + oxLDL
GM-Mac + oxLDL + topotecan

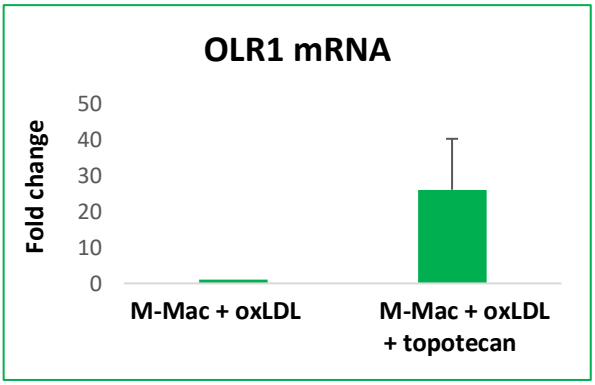
OLR1 mRNA
Fold change
50
40
30
20
10
0
M-Mac + oxLDL
M-Mac + oxLDL + topotecan

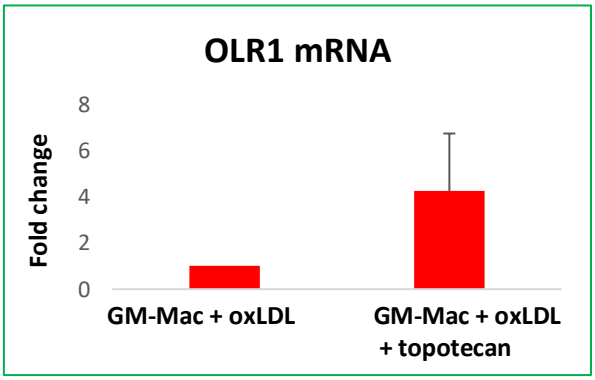
OLR1 mRNA
Fold change
8
6
4
2
0
GM-Mac + oxLDL
GM-Mac + oxLDL + topotecan

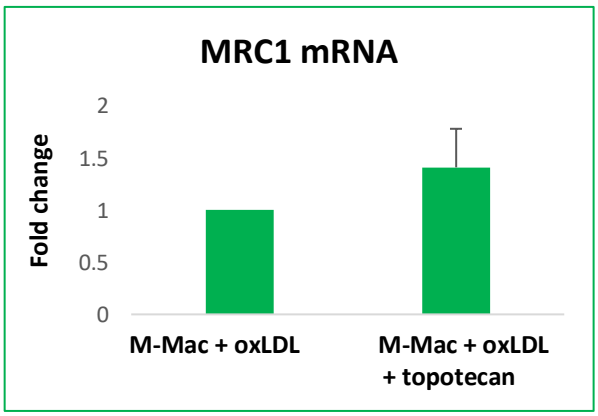
MRC1 mRNA
Fold change
2
1.5
1
0.5
0
M-Mac + oxLDL
M-Mac + oxLDL + topotecan

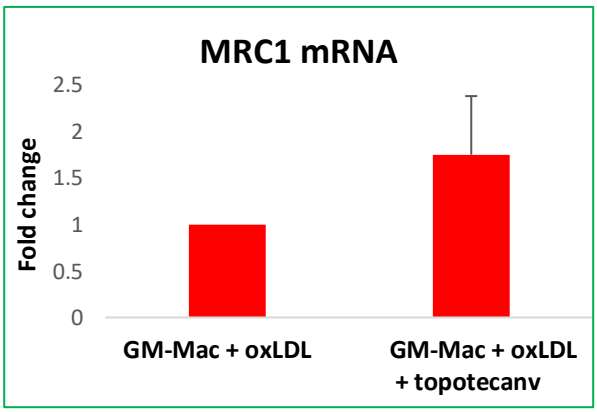
MRC1 mRNA
Fold change
2.5
2
1.5
1
0.5
0
GM-Mac + oxLDL
GM-Mac + oxLDL + topotecanv

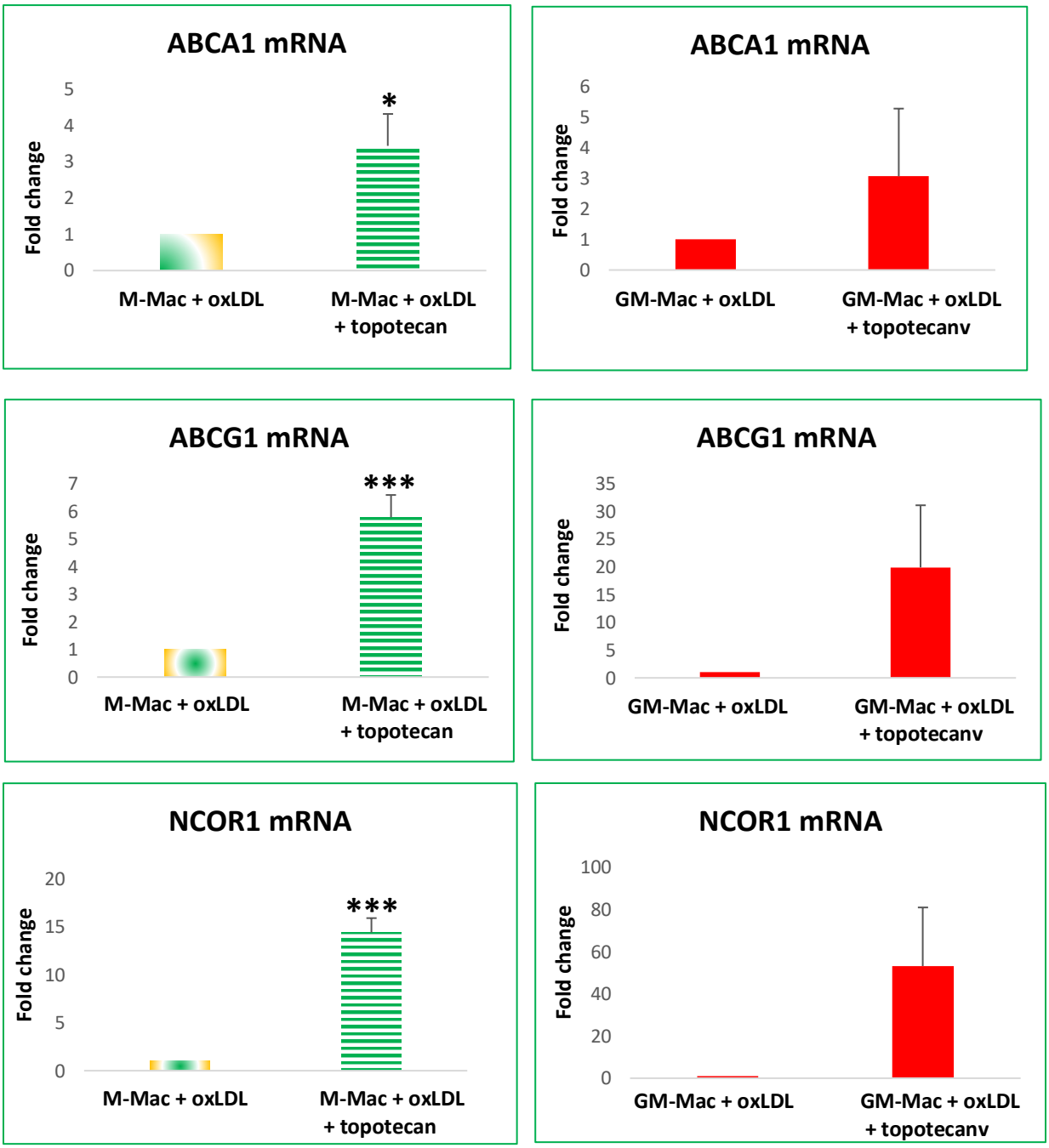

Figure 5.9 Topotecan addition alters the mRNA expression of select key lipoprotein-related scavenger receptors and lipid transporters in M-Macs and GM-Macs derived from human PBMCs. Quantification of MSR1, CD36, OLR1, MRC1, ABCA1, ABCG1, and NCOR1 mRNA expression in M-Mac and GM-Mac subsets exposed to oxLDL (10 µg/ml) with and without topotecan (0.25 µM) for 24 hours and assessed by RT-qPCR. Data presented as fold change against M-Macs or GM-Macs exposed to oxLDL alone (mean ± SEM, *indicates $p<0.05$, and *** indicates $p<0.001$, two tailed, paired t-test, n=5). N-values in macrophages derived from PBMCs represent the number of healthy donors.

5.2.4 Topotecan regulates the protein expression of scavenger receptors in primary human macrophages

Next, validative studies were perfomred to determine if the changes observed at the mRNA level translated to differential protein expression, first focussing on the scavenger receptors MSR1 and CD36 in M-Mac and GM-Mac, respectively. In agreement, western blotting demonstrated that topotecan co-administration to oxLDL-exposed early and mature M-Macs significantly decreased protein expression of MSR1 (3-fold: $p<0.001$ and 1.6-fold: $p<0.05$ respectively; n=5; Figure 5.10). Interestingly, a similar reduction in OLR1 protein levels was also detected (2-fold: $p<0.05$, and 1.7-fold; $p<0.05$ respectively; n=5; Figure 5.10), in discordance with mRNA levels which were unchanged, suggesting the involvement of a post-transcriptional mechanism. In GM-Macs, topotecan co-administration significantly decreased protein expression of CD36 in both early and mature cells (1.5-fold: $p<0.05$, and 1.4-fold; $p<0.05$ respectively; n=5; Figure 5.11), in line with the changes observed at the mRNA level.

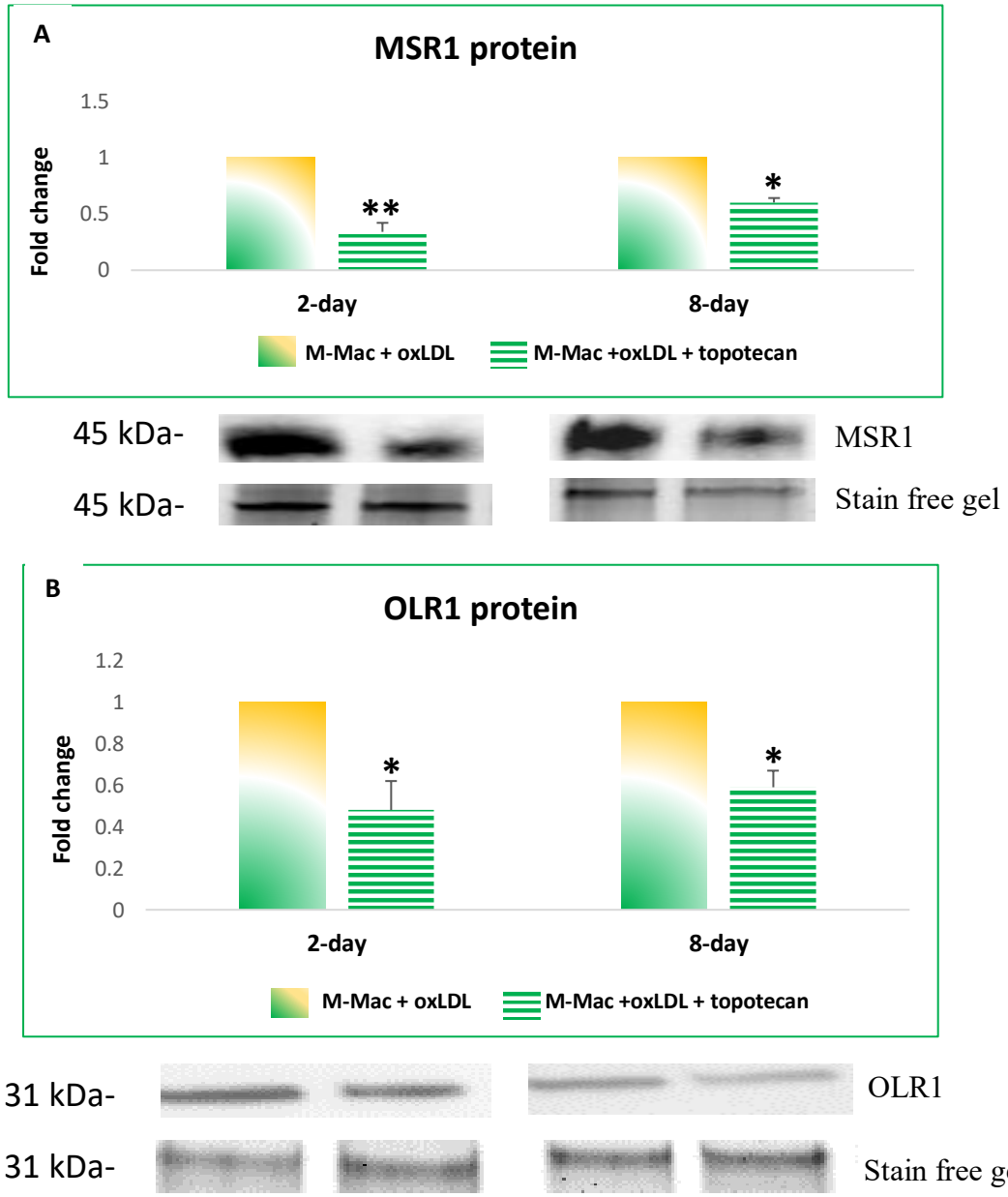

Figure 5.10 Topotecan reduced MSR1 and OLR1 protein levels in early and mature M-Macs derived from human PBMCs.

Quantification and representative western blots for (A) MSR1 and (B) OLR1 protein expression in early and mature M-Macs treated with oxLDL (10 µg/ml) and with or without topotecan (0.25 µM). Stain free gel is shown as a loading control. Data presented as fold change (mean ± SEM, *indicates $p<0.05$, two tailed, paired t-test, n=5). N-values in macrophages derived from PBMCs represent the number of healthy donors.

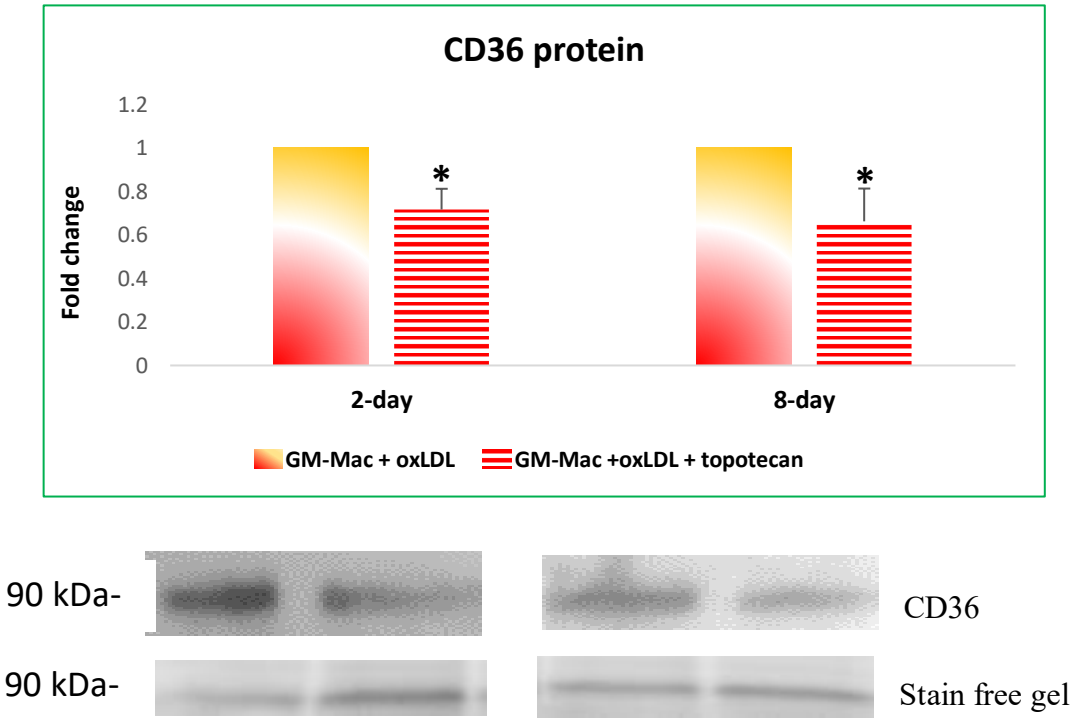

Figure 5.11 Topotecan significantly reduced the protein expression of scavenger receptors CD36 in GM-Macs derived from human blood monocytes.

Quantification and representative western blots for CD36 protein expression in early and mature GM-Macs treated with oxLDL (10 µg/ml) and with or without topotecan (0.25 µM). Stain free gel is shown as a loading control. Data presented as fold change (mean ± SEM, *indicates $p<0.05$, two tailed, paired t-test, n=5). N-values in macrophages derived from PBMCs represent the number of healthy donors.

5.2.5 Topotecan increases the efferocytosis capacity of GM-CSF polarised macrophages

As mentioned earlier, efferocytosis is a process in which macrophages can engulf dying cells to eliminate necrosis-associated inflammation. The results in Chapter 4 (Figure 4.17) demonstrated that GM-Macs display diminished efferocytosis capacity compared to their M-Mac counterparts. Given that topotecan altered macrophage expression of scavenger receptors (which can also facilitate efferocytosis), the effect of topotecan on efferocytosis of pre-labelled (green fluorescent protein) apoptotic macrophages was assessed. Image analysis and associated quantification confirmed human PBMC-derived GM-Macs have reduced capacity compared to M-CSF controls, but is restored to comparable levels with administration of 0.25 µM topotecan (1.4-fold; $p< 0.01$; n=5; Figure 5.12). However, topotecan did not alter the efferocytosis capacity of M-Macs (Figure 5.12).

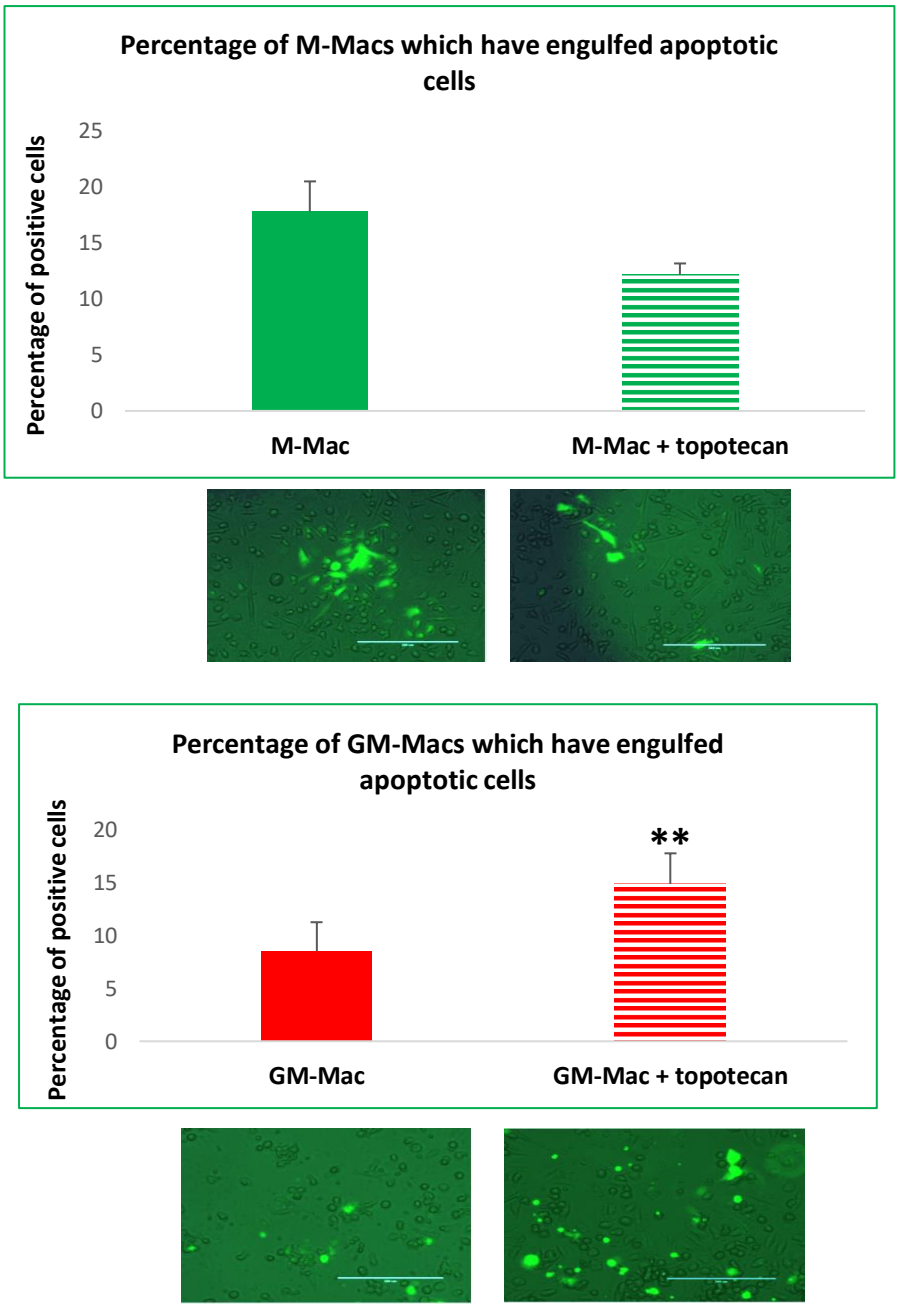

Figure 5.12 Topotecan increased the efferocytosis capacity of GM-Macs

Quantification and representative images showing the percentage of M-Mac and GM-Mac undergoing efferocytosis as determined by the positive uptake of exogenously added apototic macrophages (green), with and without co-incubation with topotecan (0.25 µM). Cells were counted within 10 random x 40 magnification fields. ** indicates $p<0.01$, two tailed, paired t-test, n =5. Scale bar represents 200 µm and applies to all panels. N-values in macrophages derived from PBMCs represent the number of healthy donors.

5.2.6 Topotecan regulates the protein expression of pSTAT5A in primary human GM-CSF polarised macrophages

Considering the global SUMOylation inhibitor topotecan exerted profound effects on GM-Mac behaviour of foam cell formation and efferocytosis capacity, and differential expression patterns of SUMO proteins and pSTAT5A are associated with human coronary atherosclerotic plaque progression, the effect of topotecan on STAT5A phosphorylation was examined in GM-Macs. Human blood-derived monocytes were polarised to GM-Macs for 7 days and subsequently treated with 10 µg/ml of DiI-oxLDL with and without 0.25 µM topotecan for 24 hours. Then, cells were assessed for differential protein expression by western blotting and fluorescent immunocytochemistry for pSTAT5A. Quantification of western blotting revealed that topotecan increased pSTAT5A protein levels in GM-Macs exposed to oxLDL (3.5-fold; $p<0.05$; n=5; Figure 5.13). Topotecan upregulation of GM-Mac pSTAT5A expression was corroborated by immunocytochemistry (3-fold: $p<0.001$; n=5; Figure 5.14).

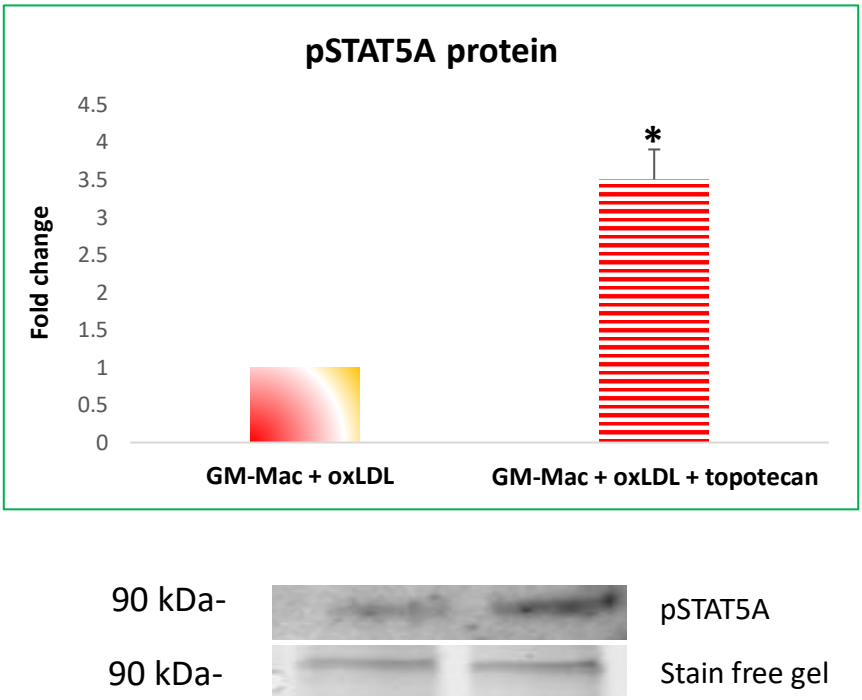

Figure 5.13 Topotecan increased pSTAT5A levels in GM-Macs co-incubated with oxLDL.

Quantification and representative western blot for pSTAT5A expression for GM-Macs treated with oxLDL (10 µg/ml) and with or without topotecan (0.25 µM). Stain free gel is shown as a loading control. Data presented as fold change (mean ± SEM, * indicates $P< 0.05$. two tailed, paired t-test, n=5). N-values in macrophages derived from PBMCs represent the number of healthy donors.

A

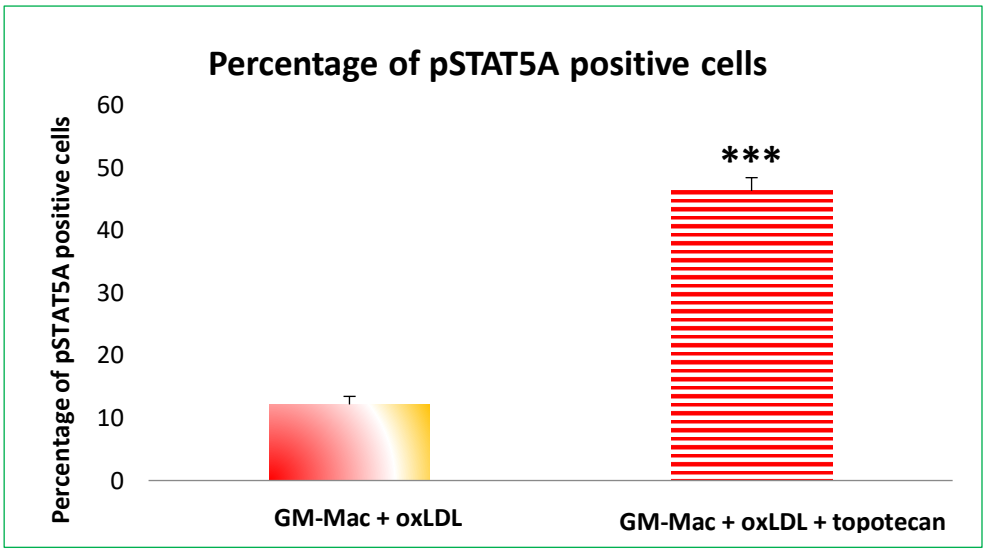

B

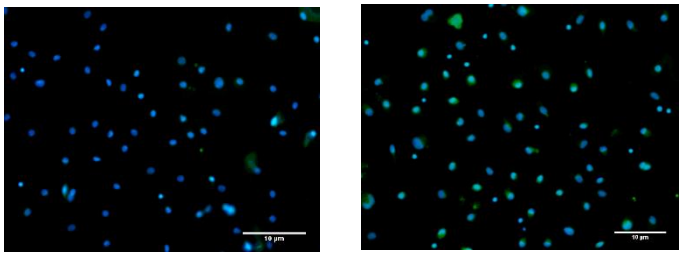

Figure 5.14 Topotecan increased pSTAT5A expression in GM-Macs co-incubated with oxLDL.

A: Quantification of cellular pSTAT5A protein expression in GM-Macs exposed to oxLDL (10 µg/ml) with and without topotecan (0.25 µM) for 24 hours, assessed by immunocytochemistry. Data presented as percentage of pSTAT5A positive cells calculated within 10 random x 40 magnification fields. ***indicates $p<0.001$; two tailed, paired t-test, n=4. N-values in macrophages derived from PBMCs represent the number of healthy donors.

B: Representative images of immunocytochemistry for pSTAT5A within GM-Macs exposed to oxLDL (10 µg/ml) with and without topotecan (0.25 µM) for 24 hours. Positive cells are shown as green and all nuclei are stained blue with DAPI. Scale bar represents 10 µm and applies to both panels.

5.2.7 HODHBt increases STAT5A phosphorylation in primary human macrophages polarised with GM-CSF

As topotecan acts as a global SUMOylation inhibitor, the observed effects on pSTAT5A levels maybe indirect. To explore if indeed STAT5 phosphorylation is directly regulated by SUMOylation, HODHBt was deployed. HODHBt is a SUMO:STAT5 interaction inhibitor, and therefore blocks STAT5-specific SUMOylation, resulting in increased STAT5 phosphorylation and associated activity. Human blood-derived monocytes were polarised to GM-Macs for 7 days and subsequently treated with 10 µg/ml of DiI-oxLDL with or without 100 µM HODHBt for 24 hours. A recent study showed that addition of 100 µM of HODHBt inhibited the SUMOylation of STAT5 (Bosque, Nilson et al. 2017). This protocol was used throughout this chapter to assess the effect of HODHBt on GM-Mac gene expression and behaviour. Then, cells were assessed for protein expression analysis by fluorescent immunocytochemistry for pSTAT5A. Image analysis and associated quantification demonstrated that HODHBt co-administration significantly increased protein expression of pSTAT5A (3.5-fold: $p<0.05$; n=5; Figure 5.15), to comparable levels as topotecan, demonstrating SUMOylation regulates STAT5A phosphorylation in human GM-Macs.

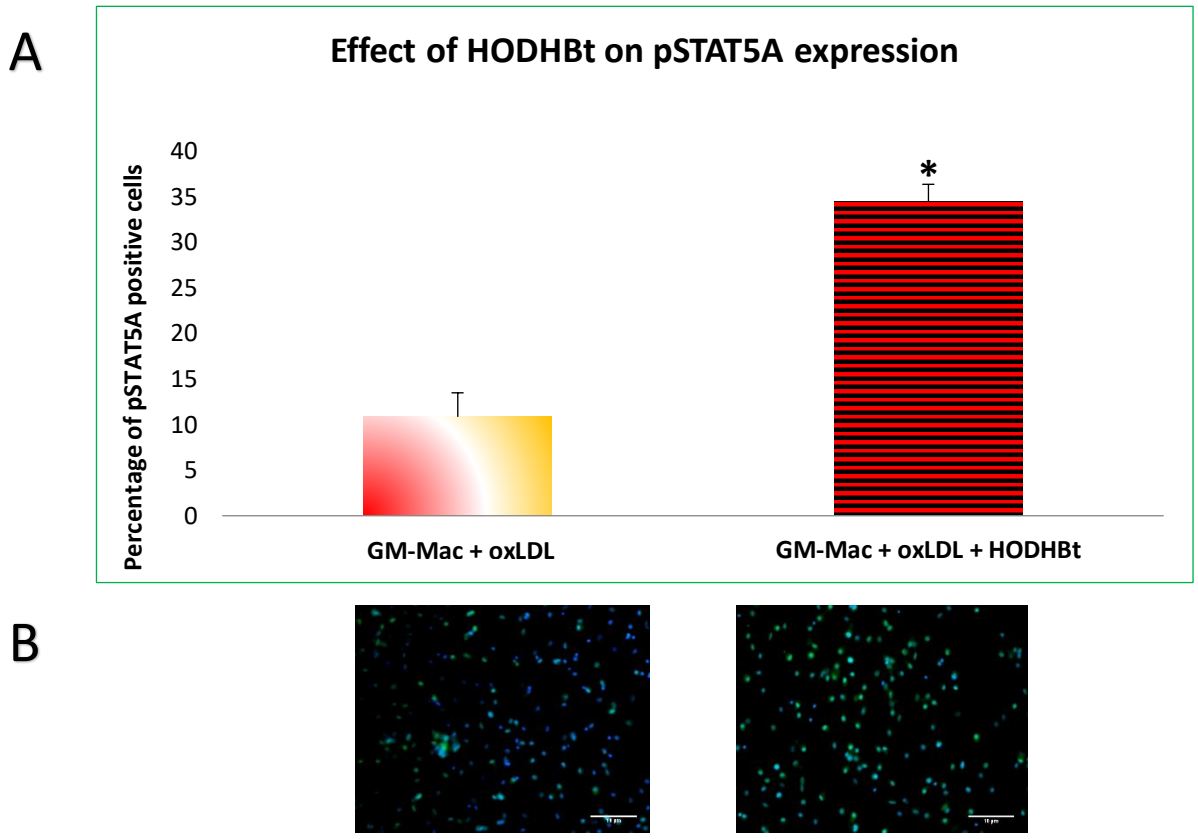

Figure 5.15 HODHBt increased pSTAT5A expression in GM-Macs co-incubated with oxLDL.

A: Quantification of cellular pSTAT5A protein expression in GM-Macs exposed to oxLDL (10 µg/ml) with and without HODHBt (100 µM) for 24 hours, assessed by immunocytochemistry. Data presented as percentage of pSTAT5A positive cells calculated within 10 random x 20 magnification fields. *indicates $p<0.05$; two tailed, paired t-test, n=4. N-values in macrophages derived from PBMCs represent the number of healthy donors.

B: Representative images of immunocytochemistry for pSTAT5A within GM-Macs exposed to oxLDL (10 µg/ml) with and without HODHBt (100 µM) for 24 hours. Positive cells are shown as green and all nuclei are stained blue with DAPI. Scale bar represents 10 µm and applies to both panels.

5.2.8 HODHBt decreases the F-actin content in GM-CSF polarised macrophage foam cells

Results from the previous chapters demonstrated that perturbation of F-actin accumulation in GM-Macs is associated with their shift towards an anti-inflammatory phenotype, as evidenced by increased expression of TGFBI and TIMP-3, alongside a concomitant decrease in MMP-12 (a STAT5 regulated gene). Accordingly, the effect of blocking STAT5:SUMO interaction (and therefore increasing STAT5 phosphorylation) on F-actin accumulation was assessed in GM-Macs exposed to oxLDL alongside HODHBt. Image analysis and quantification of AlexaFluor 594-conjugated phalloidin fluorescent images demonstrated that GM-Macs exposed to oxLDL alongside treatment with HODHBt (100 µM) showed a significant reduction in the accumulation of F-actin filaments (59%; $p<0.01$; n=5; Figure 5.16).

A

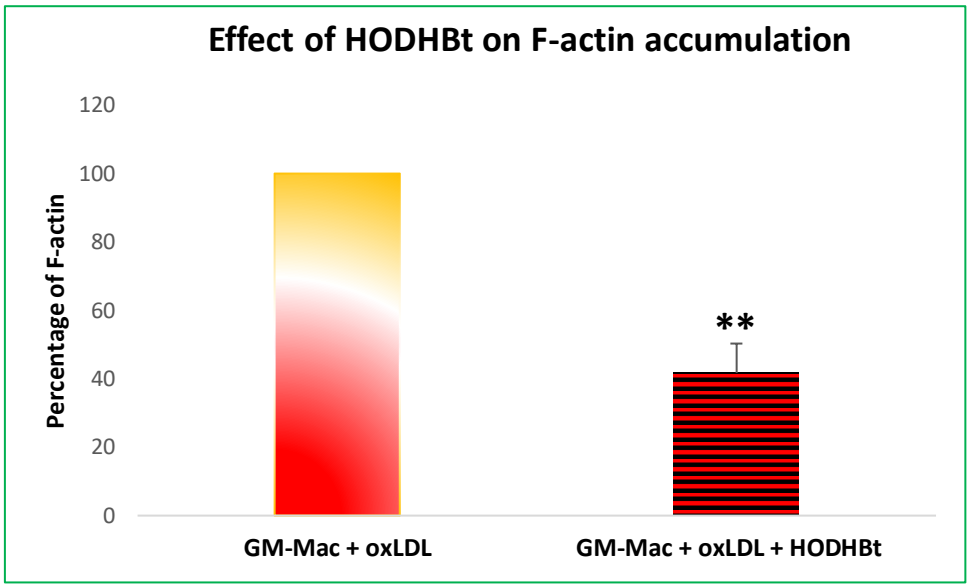

B

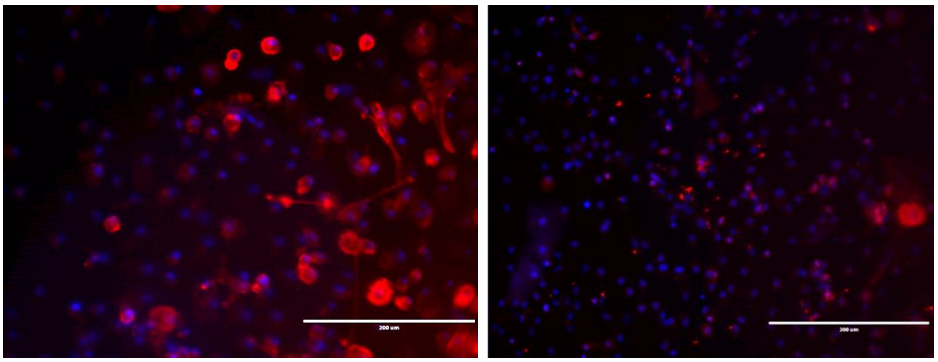

Figure 5.16 HODHBt treatment reduced GM-Mac foam cell F-actin content.

A: Quantification of F-actin content within GM-Macs exposed to oxLDL (10 µg/ml) with or without HODHBt (100 µM) for 24 hours, measured within 10 random x 20 magnification fields. ** indicates $p<0.01$; two tailed, paired t-test, n=5. N-values in macrophages derived from PBMCs represent the number of healthy donors.

B: Representative images of F-actin within GM-Macs treated with oxLDL (10 µg/ml) with or without HODHBt (100 µM) for 24 hours, stained with AlexaFluor 594-conjugated phalloidin (red) alongside a DAPI nuclear counterstain (blue). Scale bar represents 200 µm and applies to both panels.

5.2.9 HODHBt increases the ability of GM-CSF polarised macrophages derived from human blood monocytes to accumulate lipid and form foam cells

To assess if the effect of HODHBt on GM-Mac F-actin content is related to their ability to accumulate modified lipoproteins, the capacity of GM-Macs to form foam cells in the presence of HODHBt was assessed. Oil Red O staining of GM-Macs to visualise oxLDL accumulation (foam cell formation) was subjected to image analysis and quantification, which demonstrated that in GM-Macs, HODHBt induced a significant increase in foam cell formation (2.5-fold; $p<0.01$; n=5; Figure 5.17). These results indicate SUMOylation of STAT5 and resultant decreased phosphorylation/activity, blunts the capacity of GM-Macs to form foam cells.

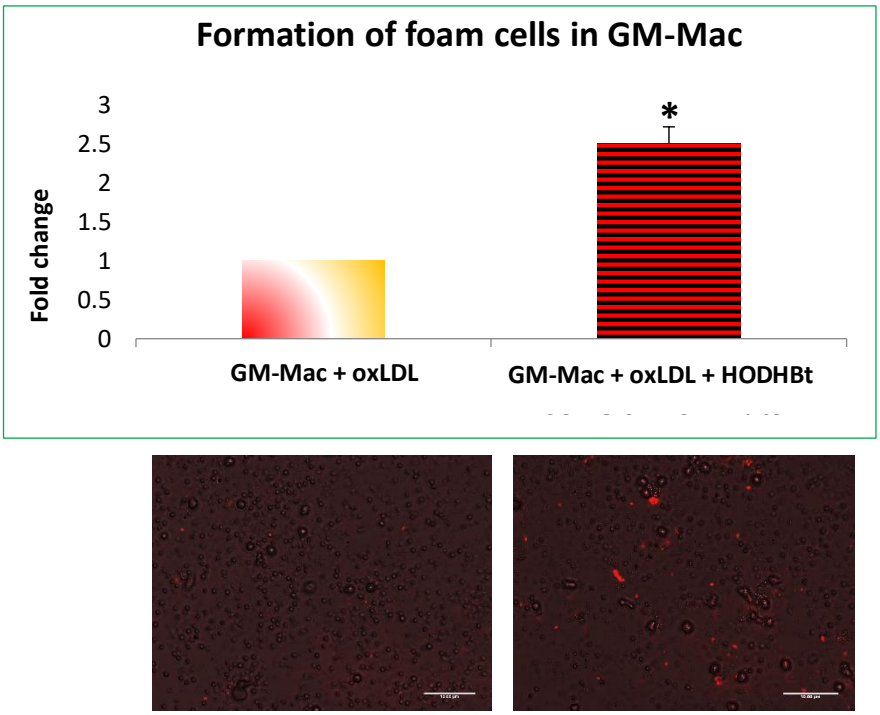

Figure 5.17 HODHBt increased the ability of GM-Macs to accumulate oxLDL and form foam cells. Quantification and representative images of foam cells formation in human GM-Macs after 24-hour incubation with oxLDL (10 µg/ml), plus or minus HODHBt (100 µM).Macrophages were stained with Oil Red O to visualise accumulation of oxLDL. Cells were counted within 10 random x 20 magnification fields. * indicates $p<0.05$, two tailed, paired t-test n=5. Scale bar represents 10 µm and applies to both panels. N-values in macrophages derived from PBMCs represent the number of healthy donors.

5.2.10 HODHBt upregulates OLR1 and MMP12 mRNA expression in GM-CSF polarised macrophages derived from human blood monocytes

Given the heightened foam cell formation afforded by HODHBt treatment of GM-Macs, the effect of HODHBt on the expression of select scavenger receptors (OLR1, MSR1, and CD36), and lipid tranporters (PPARA, and NCOR1) were assessed to elucidate the effect of inhibiting STAT5 SUMOylation on foam cell formation. In addition, the expression of the STAT5-responsive gene and cell marker of the GM-Mac susbet, MMP12, was also examined. Subsequent RT-qPCR analysis demonstrated that there was no significant change at the mRNA level of the scavenger receptors MSR1 and CD36, or the lipid transporters PPARA and NCOR1 (data not shown). However, HODHBt (100 µm) addition significantly increased the mRNA expression of OLR1 (2-fold; $p<0.05$; n=5; Figure 5.18) and MMP12 (5-fold; $p<0.01$; n=5; Figure 5.18) in GM-Macs exposed to oxLDL.

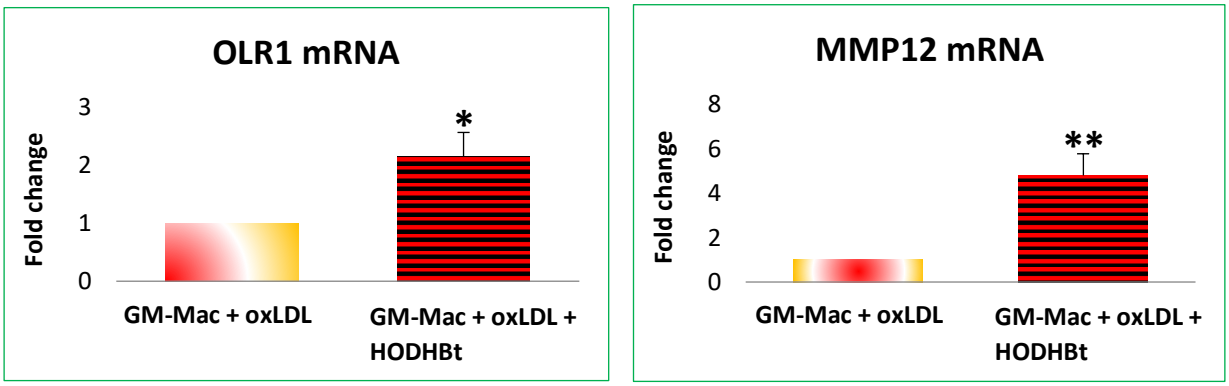

Figure 5.18 HODHBt addition upregulated the mRNA expression of OLR1 and MMP12 in GM-Mac foam cells.

Quantification of OLR1 and MMP12 mRNA expression in GM-Macs exposed to oxLDL (10 µg/ml) with and without HODHBt (100 µM) for 24 hours and assessed by RT-qPCR. Data presented as fold change against untreated GM-Macs (mean ± SEM, *indicates $p<0.05$, ** indicates $p<0.01$, two tailed, paired t-test, n=5). N-values in macrophages derived from PBMCs represent the number of healthy donors.

5.2.11 HODHBt upregulates OLR1 and MMP-12 protein expression in GM-CSF polarised macrophages derived from human blood monocytes

Data revealed that GM-Macs exposed to oxLDL and treated with HODHBt (100 µM) significantly increased the protein levels of OLR1 (1.8-fold; p<0.01; n=5; Figure 5.19). Similarly, HODHBt administration significantly increased and the percentage of MMP-12 positive GM-Macs (2-fold; p<0.01; n=5; Figure 5.20).

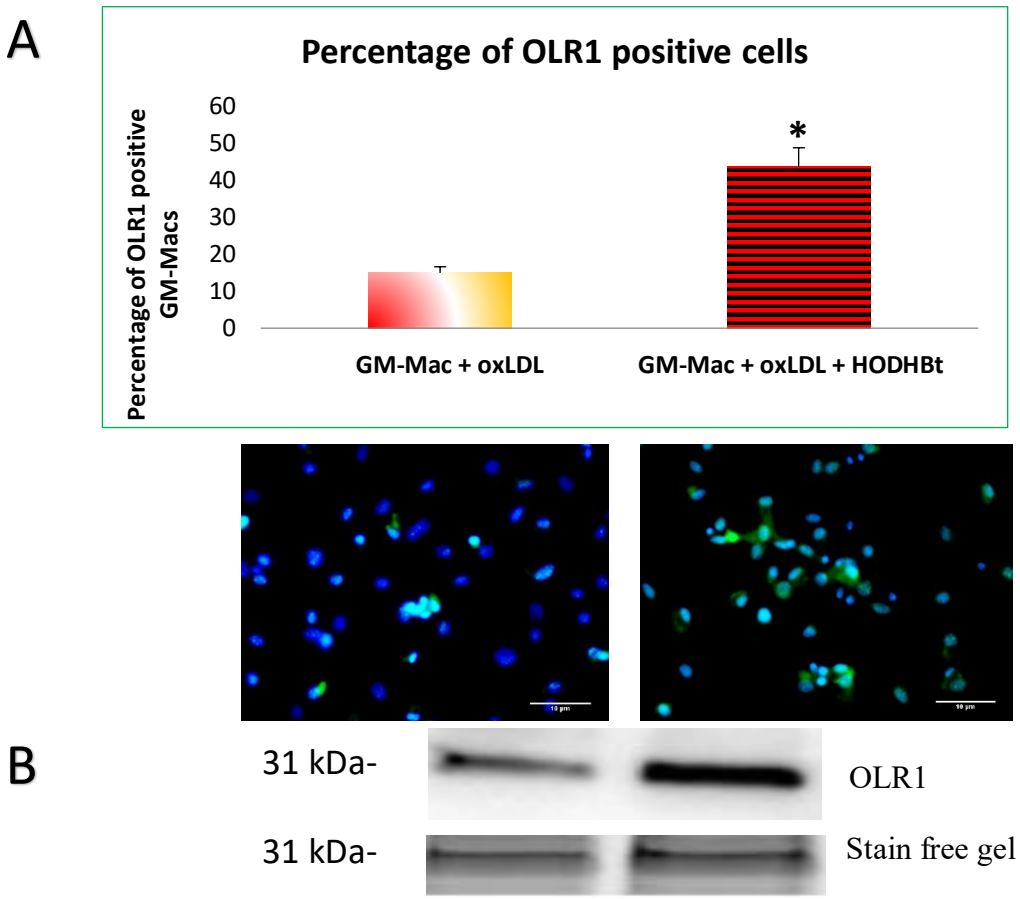

Figure 5 19 HODHBt increased GM-Mac foam cell OLR1 protein expression.

A: Quantification and representative images of OLR1 protein expression in GM-Macs exposed to oxLDL (10 µg/ml) with and without HODHBt (100 µM) for 24 hours, as assessed by immunocytochemistry. Positive cells are shown as green and all nuclei are stained blue with DAPI. Data presented as percentage of OLR1 positive cells calculated within 10 random x 20 magnification fields. **indicates p<0.01; two tailed, paired t-test, n=5. Scale bar represents 10 µm and applies to both panels. N-values in macrophages derived from PBMCs represent the number of healthy donors.

B**:** Representative western blot for OLR1 expression of GM-Macs treated exposed to oxLDL (10 µg/ml) with and without HODHBt (100 µM) for 24 hours. Stain free gel is shown as a loading control. Approximate molecular weights are indicated on the left in kDa.

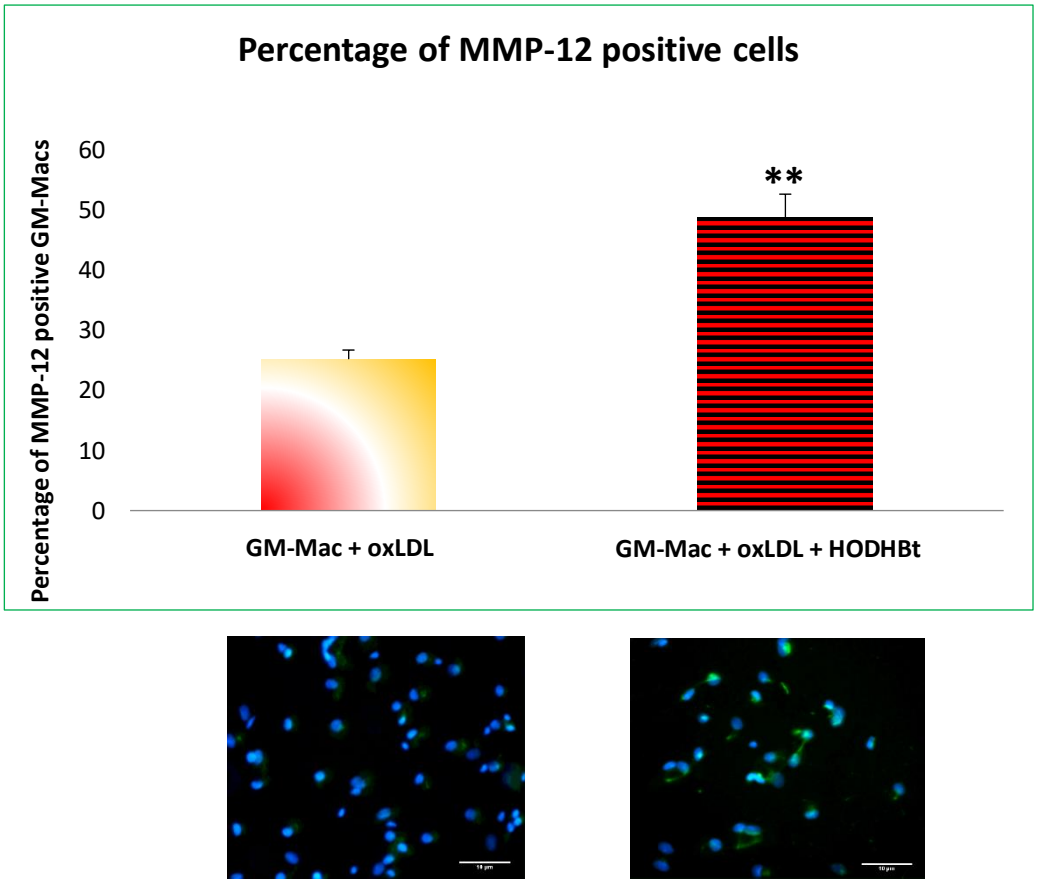

Figure 5 20 HODHBt increased GM-Mac MMP-12 protein expression.

Quantification and representative images of MMP-12 protein expression in GM-Macs exposed to oxLDL (10 µg/ml) with and without HODHBt (100 µM) for 24 hours, as assessed by immunocytochemistry. Positive cells are shown as green and all nuclei are stained blue with DAPI. Data presented as percentage of MMP-12 positive cells calculated within 10 random x 40 magnification fields. **indicates $p<0.01$; two tailed, paired t-test, n=5. Scale bar represents 10 µm and applies to both panels. N-values in macrophages derived from PBMCs represent the number of healthy donors.

5.2.12 HODHBt upregulates POU2F1 protein expression and increases its co-localisation with pSTAT5A in GM-Mac foam cells

Considering the elevated STAT5 phosphorylation afforded from HODHBt treatment in GM-Macs (through blocking SUMOylation of STAT5) resulted in increased OLR1 expression, it is surprising that there are no predicted STAT5 binding sites observed within the promoter region of the human OLR1 gene (Figure 5.21). However, a previous study has shown that after phosphorylation, STAT5 can bind to POU2F1 (also known as OCT1) within the nucleus to form a complex that is necessary for the activation of target genes such as cyclin D1, in epithelial cells (Magné, Caron et al. 2003). Subsequent analysis of the predicted transcription factor binding sites within the human OLR1 promoter region identfied 12 POU2F1 (Oct-1) binding sites (Figure 5.21), greater than sites for any other transcription factor.Consequently, it was determined whether POU2F1 and pSTAT5A do indeed co-localise within human GM-Mac foam cells, and if treatment with HODHBt increases their co-expression. Dual-fluorescence immunocytochemistry and associated quantification confirmed the nuclear co-localisation of POU2F1 and pSTAT5A in GM-Mac foam cells (Figure 5.22), and demonstrated that HODHBt treatment significantly increased the co-expression of POU2F1 and pSTAT5A (1.5-fold; $p<0.05$ respectively; n=4; Figure 5.22).

Figure 5.21 Predicted transcription factor binding sites within the promoter of human OLR1.

The thirteen predicting POU2F1 (Oct-1) binding sites within the promoter region of human OLR1 are indicated by the red arrows. Image generated using TransFac (TFBLAST (gene-regulation.com).

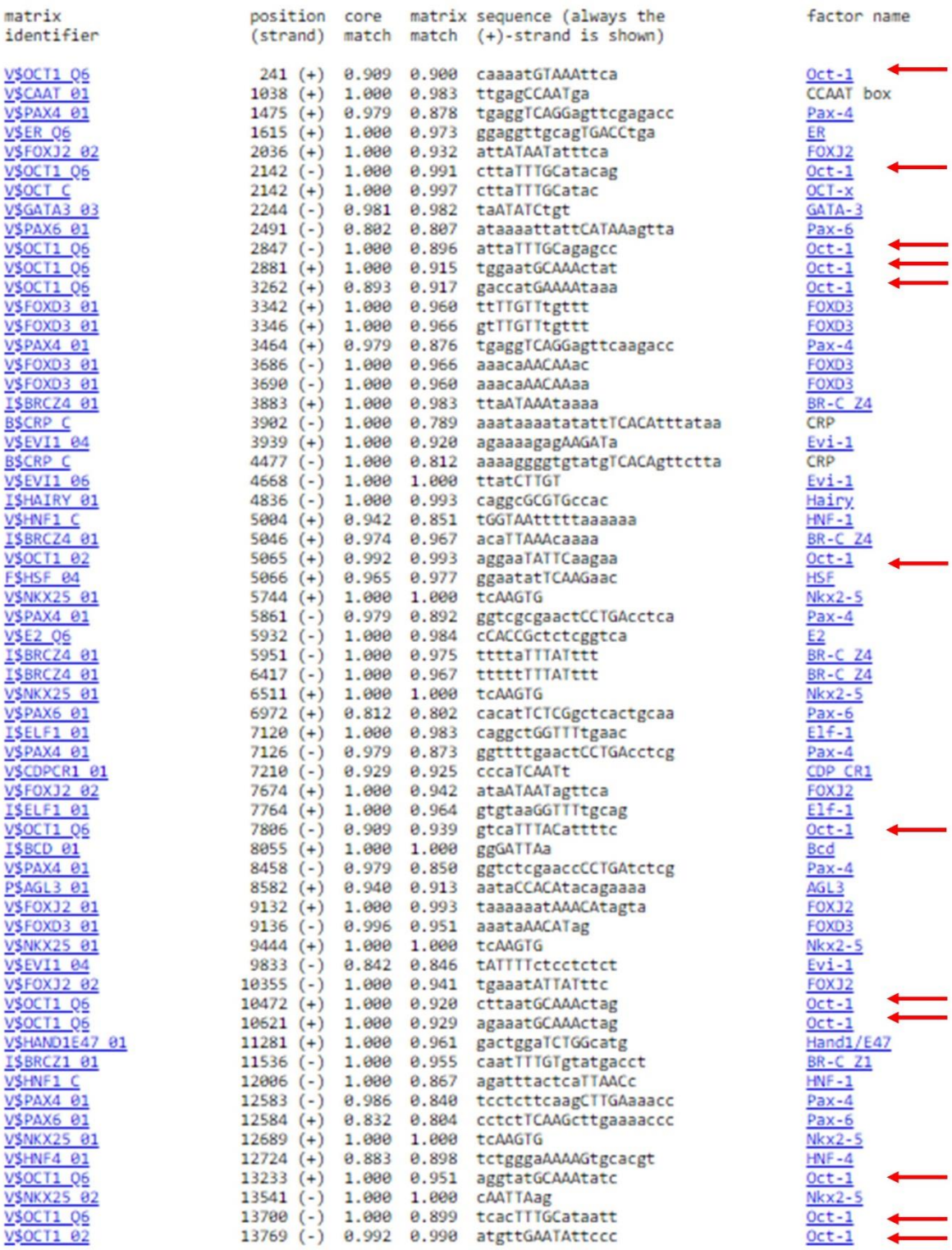

matrix identifier	position (strand)	core match	matrix match	sequence (always the (+)-strand is shown)	factor name
V$OCT1_Q6	241 (+)	0.909	0.900	caaaatGTAAAttca	Oct-1
V$CAAT_01	1038 (+)	1.000	0.983	ttgagCCAATga	CCAAT box
V$PAX4_01	1475 (+)	0.979	0.878	tgaggTCAGGagttcgagacc	Pax-4
V$ER_Q6	1615 (+)	1.000	0.973	ggaggttgcagTGACCtga	ER
V$FOXJ2_02	2036 (+)	1.000	0.932	attATAATatttca	FOXJ2
V$OCT1_Q6	2142 (-)	1.000	0.991	cttaTTTGCatacag	Oct-1
V$OCT_C	2142 (+)	1.000	0.997	cttaTTTGCatac	OCT-x
V$GATA3_03	2244 (-)	0.981	0.982	taATATCtgt	GATA-3
V$PAX6_01	2491 (-)	0.802	0.807	ataaaattattCATAAagtta	Pax-6
V$OCT1_Q6	2847 (-)	1.000	0.896	attaTTTGCagagcc	Oct-1
V$OCT1_Q6	2881 (+)	1.000	0.915	tggaatGCAAActat	Oct-1
V$OCT1_Q6	3262 (+)	0.893	0.917	gaccatGAAAAtaaa	Oct-1
V$FOXD3_01	3342 (+)	1.000	0.960	ttTTGTTtgttt	FOXD3
V$FOXD3_01	3346 (+)	1.000	0.966	gtTTGTTtgttt	FOXD3
V$PAX4_01	3464 (+)	0.979	0.876	tgaggTCAGGagttcaagacc	Pax-4
V$FOXD3_01	3686 (-)	1.000	0.966	aaacaAACAAac	FOXD3
V$FOXD3_01	3690 (-)	1.000	0.960	aaacaAACAAaa	FOXD3
I$BRCZ4_01	3883 (+)	1.000	0.983	ttaATAAAtaaaa	BR-C_Z4
B$CRP_C	3902 (-)	1.000	0.789	aaataaaatatattTCACAtttataa	CRP
V$EVI1_04	3939 (+)	1.000	0.920	agaaaagagAAGATa	Evi-1
B$CRP_C	4477 (-)	1.000	0.812	aaaaggggtgtatgTCACAgttctta	CRP
V$EVI1_06	4668 (-)	1.000	1.000	ttatCTTGT	Evi-1
I$HAIRY_01	4836 (-)	1.000	0.993	caggcGCGTGccac	Hairy
V$HNF1_C	5004 (+)	0.942	0.851	tGGTAAtttttaaaaaa	HNF-1
I$BRCZ4_01	5046 (+)	0.974	0.967	acaTTAAAcaaaa	BR-C_Z4
V$OCT1_02	5065 (+)	0.992	0.993	aggaaTATTCaagaa	Oct-1
F$HSF_04	5066 (+)	0.965	0.977	ggaatatTCAAGaac	HSF
V$NKX25_01	5744 (+)	1.000	1.000	tcAAGTG	Nkx2-5
V$PAX4_01	5861 (-)	0.979	0.892	ggtcgcgaactCCTGAcctca	Pax-4
V$E2_Q6	5932 (-)	1.000	0.984	cCACCGctctcggtca	E2
I$BRCZ4_01	5951 (-)	1.000	0.975	ttttaTTTATttt	BR-C_Z4
I$BRCZ4_01	6417 (-)	1.000	0.967	tttttTTTATttt	BR-C_Z4
V$NKX25_01	6511 (+)	1.000	1.000	tcAAGTG	Nkx2-5
V$PAX6_01	6972 (+)	0.812	0.802	cacatTCTCGgctcactgcaa	Pax-6
I$ELF1_01	7120 (+)	1.000	0.983	caggctGGTTTtgaac	Elf-1
V$PAX4_01	7126 (-)	0.979	0.873	ggttttgaactCCTGAcctcg	Pax-4
V$CDPCR1_01	7210 (-)	0.929	0.925	cccaTCAATt	CDP_CR1
V$FOXJ2_02	7674 (+)	1.000	0.942	ataATAATagttca	FOXJ2
I$ELF1_01	7764 (+)	1.000	0.964	gtgtaaGGTTTtgcag	Elf-1
V$OCT1_Q6	7806 (-)	0.909	0.939	gtcaTTTACattttc	Oct-1
I$BCD_01	8055 (+)	1.000	1.000	ggGATTAa	Bcd
V$PAX4_01	8458 (-)	0.979	0.850	ggtctcgaaccCCTGAtctcg	Pax-4
P$AGL3_01	8582 (+)	0.940	0.913	aataCCACAtacagaaaa	AGL3
V$FOXJ2_01	9132 (+)	1.000	0.993	taaaaaatAAACAtagta	FOXJ2
V$FOXD3_01	9136 (-)	0.996	0.951	aaataAACATag	FOXD3
V$NKX25_01	9444 (+)	1.000	1.000	tcAAGTG	Nkx2-5
V$EVI1_04	9833 (-)	0.842	0.846	tATTTTctcctctct	Evi-1
V$FOXJ2_02	10355 (-)	1.000	0.941	tgaaatATTATttc	FOXJ2
V$OCT1_Q6	10472 (+)	1.000	0.920	cttaatGCAAActag	Oct-1
V$OCT1_Q6	10621 (+)	1.000	0.929	agaaatGCAAActag	Oct-1
V$HAND1E47_01	11281 (+)	1.000	0.961	gactggaTCTGGcatg	Hand1/E47
I$BRCZ1_01	11536 (-)	1.000	0.955	caatTTTGTgtatgacct	BR-C_Z1
V$HNF1_C	12006 (-)	1.000	0.867	agatttactcaTTAACc	HNF-1
V$PAX4_01	12583 (-)	0.986	0.840	tcctcttcaagCTTGAaaacc	Pax-4
V$PAX6_01	12584 (+)	0.832	0.804	cctctTCAAGcttgaaaaccc	Pax-6
V$NKX25_01	12689 (+)	1.000	1.000	tcAAGTG	Nkx2-5
V$HNF4_01	12724 (+)	0.883	0.898	tctgggaAAAAGtgcacgt	HNF-4
V$OCT1_Q6	13233 (+)	1.000	0.951	aggtatGCAAAtatc	Oct-1
V$NKX25_02	13541 (-)	1.000	1.000	cAATTAag	Nkx2-5
V$OCT1_Q6	13700 (-)	1.000	0.899	tcacTTTGCataatt	Oct-1
V$OCT1_02	13769 (-)	0.992	0.990	atgttGAATAttccc	Oct-1

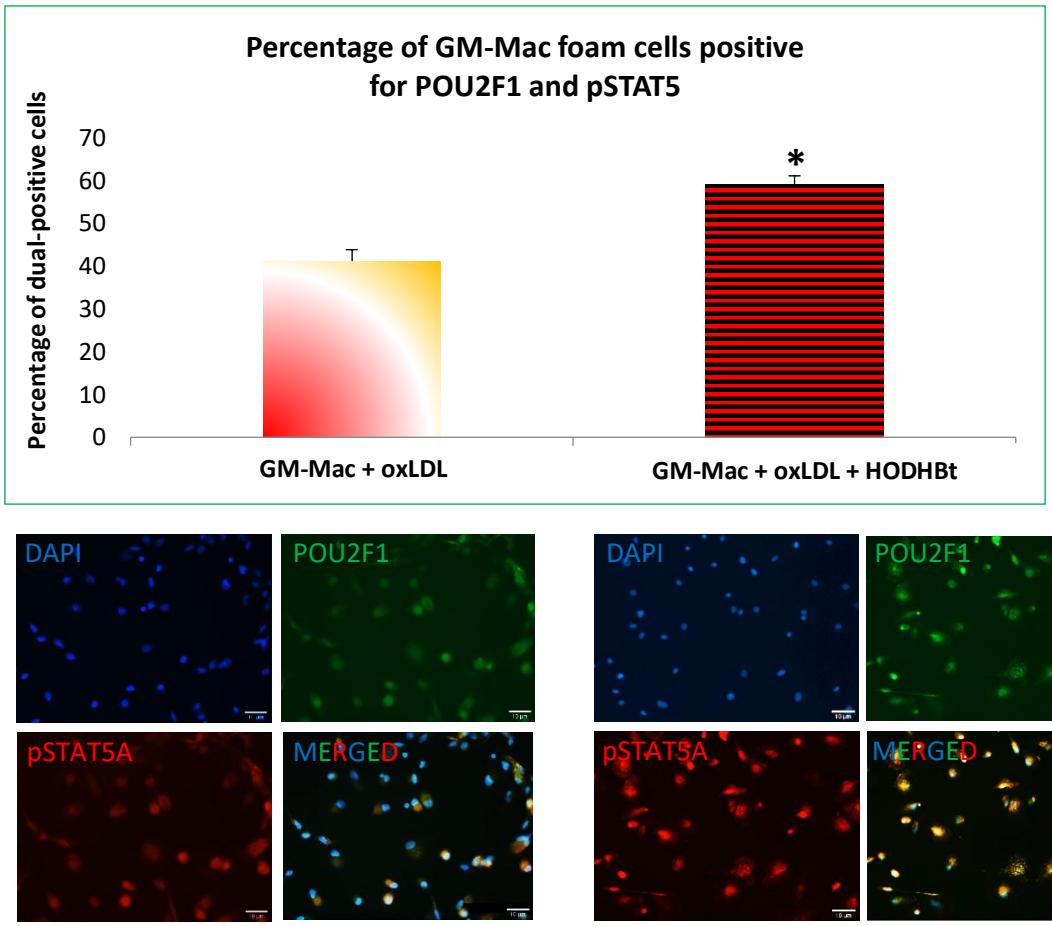

Figure 5 22 HODHBt increased GM-Mac foam cell co-expression of POU2F1 and pSTAT5A.

Quantification and representative images of POU2F1 and pSTAT5A expression in GM-Macs exposed to oxLDL (10 µg/ml) with and without HODHBt (100 µM) for 24 hours, as assessed by dual-immunocytochemistry. Cells positive for POU2F1 are shown as green, pSTAT5A positive cells are in red and all nuclei are stained blue with DAPI. Cells positive for POU2F1 and pSTAT5A appear as yellow within the merged images. Data presented as percentage of cells positive for POU2F1 and pSTAT5A calculated within 10 random x 40 magnification fields. **indicates $p<0.01$; two tailed, paired t-test, n=5. Scale bar represents 10 µm and applies to both panels. N-values in macrophages derived from PBMCs represent the number of healthy donors.

5.2.13 HODHBt heightens the efferocytosis capacity of GM-CSF polarised foam cell macrophages derived from human blood monocytes

As mentioned earlier, efferocytosis is a process in which macrophages can uptake cells undergoing apoptosis to eliminate succeeding necrosis and associated inflammation. Earlier in this Chapter, global inhibition of SUMOylation (with topotecan) was shown to increase GM-Mac efferocytosis (Figure 5.12). Therefore, to determine if SUMOylation specifically of STAT5 modulates GM-Mac efferocytosis capacity, macrophages were subjected to an efferocytosis assay in the presence of HODHBt. Image analysis and associated quantification demonstrated that the low efferocytosis capacity of GM-Macs was significantly heightened after treatment with 100 µM of HODHBt (3.6-fold; $p< 0.001$; n=5; Figure 5.23), echoing the effect observed with topotecan. Interestingly, HODHBt did not alter the efferocytosis capacity of non-foam cell GM-Macs (Figure 5.23). A plausible explanation for this discrepancy is that SUMOylation of STAT5 and subsequent heightened efferocytosis in GM-Macs is induced as a result of oxLDL uptake and foam cell formation.

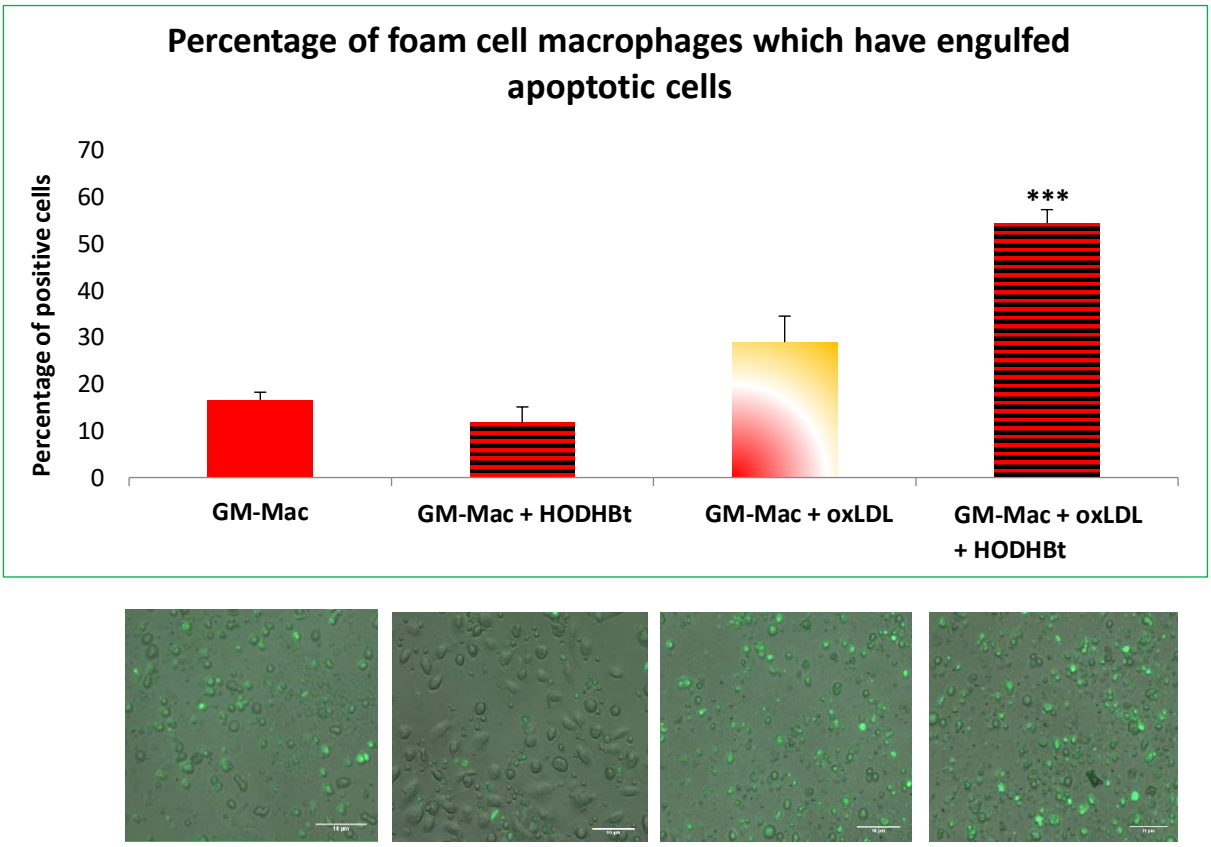

Figure 5.23 HODHBt increased the efferocytosis capacity of GM-Mac foam cells, but not non-foamy GM-Macs.

Quantification and representative images showing the percentage of GM-Mac foam cells positive for the uptake of apototic macrophages (green) with and without HODHBt (100 µM) co-incubation for 24 hours. Cells were counted within 10 random x 40 magnification fields. *** indicates $p<0.001$ compared to all groups; ANOVA, Student-Newman-Keuls Multiple Comparisons Test; n=5. Scale bar represents 10 µm and applies to all panels. N-values in macrophages derived from PBMCs represent the number of healthy donors.

5.2.14 Fasudil interferes with HODHBt-mediated efferocytosis of GM-CSF foam cell macrophages, but nifedipine is ineffective

Efficient efferocytosis can be mediated by actin cytoskeleton and Ca^{+2} signalling-mediated mechanisms (Tajbakhsh, Rezaee et al. 2018) To assess if the enhanced efferocytosis capacity of GM-Mac foam cells provided by HODHBt treatment relies on the aformentioned mechanisms, fasudil and nifedipine were deployed to prevent actin polymerisaton and stress fibre formation, alongside the modulation of Ca^{+2} signalling, respectively. Image analysis and associated quantification demonstrated that GM-Mac foam cells co-incubated with fasudil (10 µM) and HODHBt (100 µM) exhibited significantly reduced efferocytosis compared to GM-Mac foam cells treated with fasudil alone (2-fold; $p< 0.01$; n=4; Figure 5.24). However, the efferocytosis capacity of GM-Mac foam cells was unaffected by co-incubation with of nifedipine (10 nM) and HODHBt (100 µM) compared to nifedipine alone (Figure 5.25). These findings suggest that the heightened efferocytosis engendered in GM-Mac foam cells through sustained STAT5 phosphorylation (HODHBt blocking of STAT5 SUMOylation), is mediated through the actin cytoskeleton.

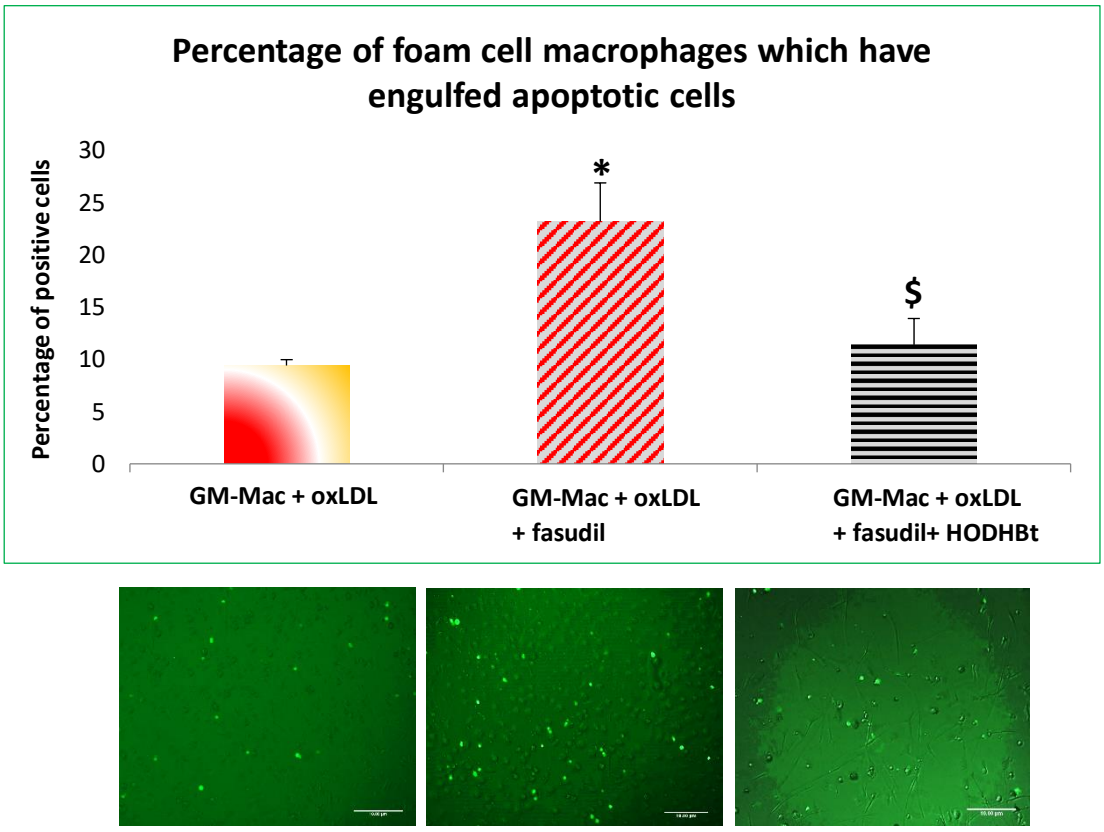

Figure 5.24 Fasudil co-incubation reduced the HODHBt-induced efferocytosis capacity of GM-Mac foam cells.

Quantification and representative images showing the percentage of GM-Mac foam cells positive for the uptake of apototic macrophages (green) with and without co-incubation of fasudil (10 µM) and HODHBt (100 µM) for 24 hours. Cells were counted within 10 random x 20 magnification fields. * indicates $p<0.05$ vs GM-Mac + oxLDL, $ indicates $p<0.05$ vs GM-Mac + oxLDL + fasudil; ANOVA, Student-Newman-Keuls Multiple Comparisons Test; n=4. Scale bar represents 10 µm and applies to all panels. N-values in macrophages derived from PBMCs represent the number of healthy donors.

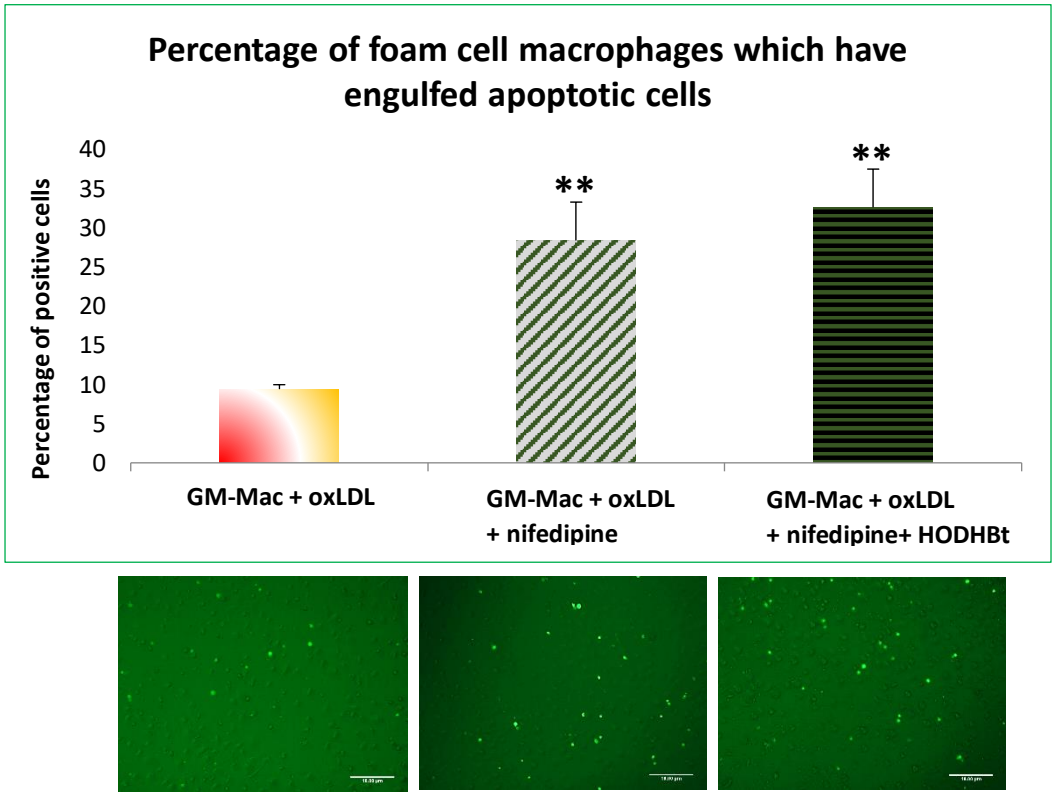

Figure 5.25 Nifedipine co-incubation did not alter the HODHBt-induced efferocytosis capacity of GM-Mac foam cells

Quantification and representative images showing the percentage of GM-Mac foam cells positive for the uptake of apototic macrophages (green) with and without co-incubation of nifedipine (10 Nm) and HODHBt (100 µM) for 24 hours. Cells were counted within 10 random x 20 magnification fields. ** indicates $p<0.01$ compared to GM-Mac + oxLDL control; ANOVA, Student-Newman-Keuls Multiple Comparisons Test; n=4. Scale bar represents 10 µm and applies to all panels. N-values in macrophages derived from PBMCs represent the number of healthy donors.

5.2.15 Fasudil alters GM-Mac foam cell membrane expression of OLR1

Previous data presented within this chapter demonstrates that the mRNA and protein levels of the scavenger receptor OLR1 are increased in GM-Macs when treated with HODHBt (100 µM), suggesting that HODHBt-amplified STAT5 activity (through blocking its SUMOylation) upregulates the expression of OLR1, and facilitates foam cell formation and efferocytosis capacity. Given that fasudil blocks the beneficial effect of HODHBt on efferocytosis in GM-Mac foam cells (Figure 5.24), while OLR1 expression is increased with HODHBt treatment (Figure 5.19), the effect of fasudil on the augmented OLR1 expression within GM-Mac foam cells induced by HODHBt, was explored. Quantification of western blotting confirmed HODHBt treatment increased GM-Mac foam cell total OLR1 levels (1.8-fold; $p<0.01$; n=4; Figure 5.26), whereas fasudil had no effect in isolation or on co-incubation with HODHBt (Figure 5.26). Considering OLR1 traffics to the cell membrane to undertake the engulfment of modified lipoproteins and apoptotic bodies, cell fractionation was performed to allow assessment of cell membrane OLR1 protein levels. Quantification of western blotting revealed that, in line with total levels, membrane-localised expression of OLR1 was increased by HODHBt treatment of GM-Mac foam cells (2.1-fold; $p<0.001$; n=4; Figure 5.27). However, co-incubation of GM-Mac foam cells with HODHBt and fasudil significantly decreased cell membrane protein expression of OLR1 (67 %; $p<0.001$; n=4; Figure 5.27), when compared to HODHBt alone. These findings indicate that while STAT5 upregulation of OLR1 is independent of F-actin cytoskeletal rearrangement, a competent actin cytoskeleton is necessary for OLR1 accumulation at the cell membrane and associated efferocytosis capacity.

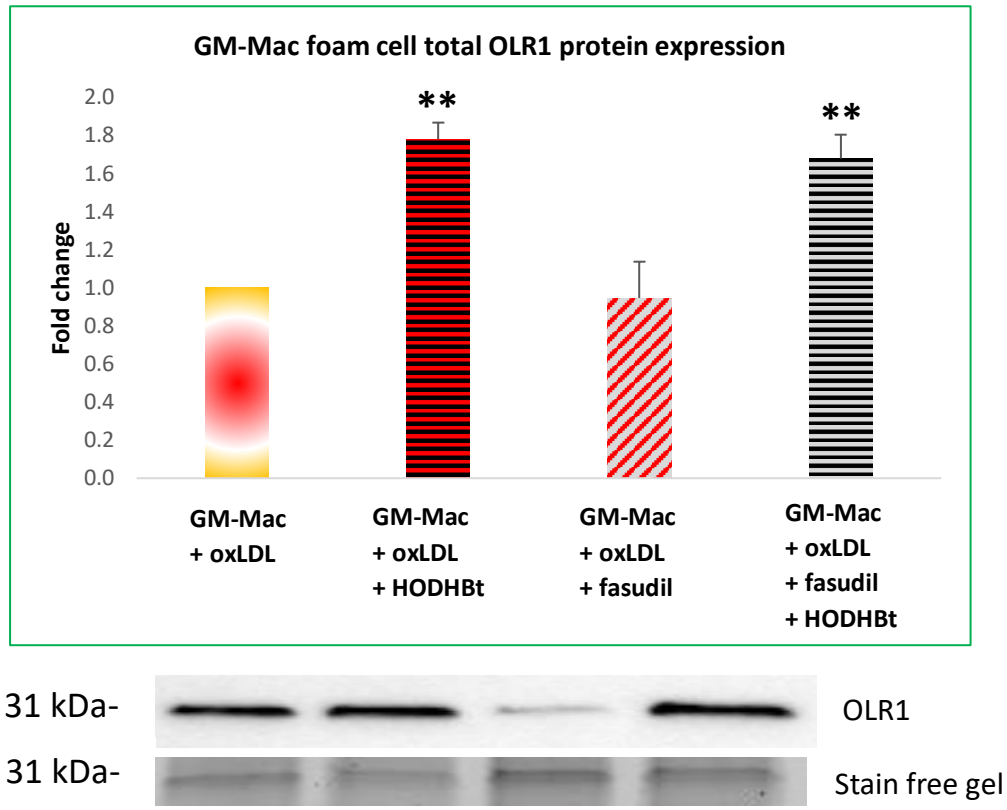

Figure 5.26 Fasudil does not regulate total OLR1 protein levels in GM-Mac foam cells.

Quantification and representative western blot for total cellular OLR1 expression in GM-Mac foam cells treated co-incubated with or without fasudil (10 µM) or HODHBt (100 µM) for 24 hours. Stain free gel is shown as a loading control. Data presented as fold change (mean ± SEM, ** indicates P< 0.01 compared to GM-Mac + oxLDL, and GM-Mac + oxLDL + fasudil; ANOVA, Student-Newman-Keuls Multiple Comparisons; n=4). N-values in macrophages derived from PBMCs represent the number of healthy donors.

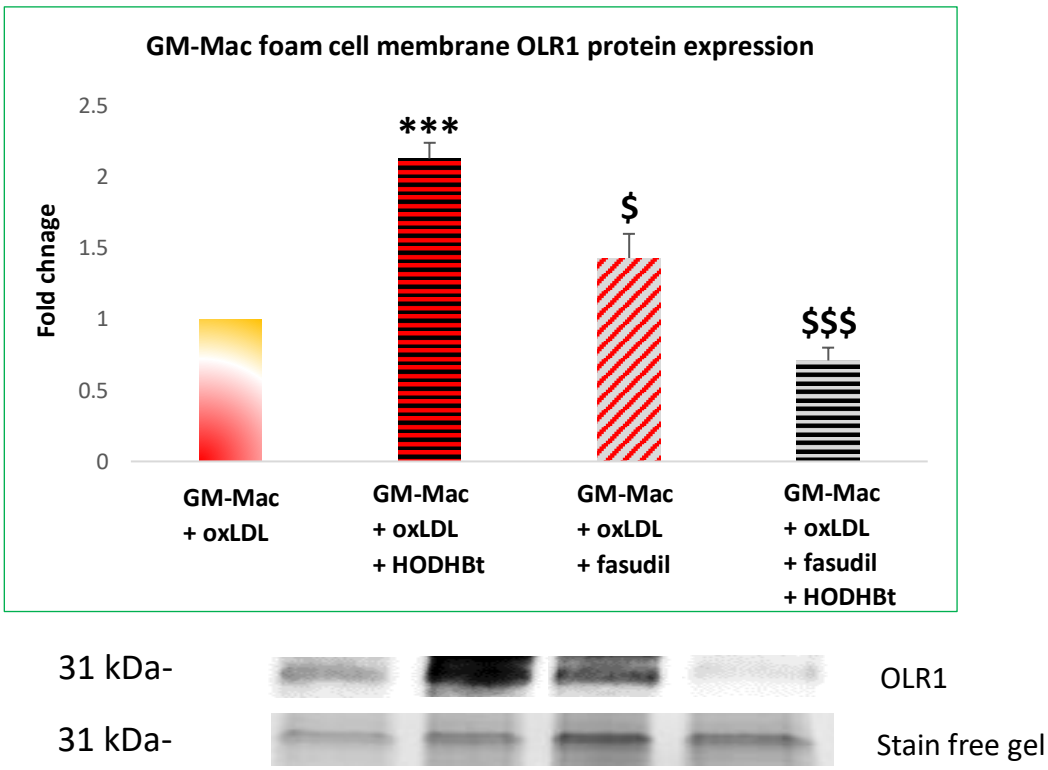

Figure 5.27 Fasudil blunts HODHBt-mediated OLR1 membrane protein levels in GM-Mac foam cells. Quantification and representative western blot for OLR1 expression in the membrane fraction of GM-Mac foam cells co-incubated with or without fasudil (10 µM) or HODHBt (100 µM) for 24 hours. Stain free gel is shown as a loading control. Data presented as fold change (mean ± SEM, *** indicates p< 0.001 compared to GM-Mac + oxLDL, $ indicates p< 0.05 vs GM-Mac + oxLDL + HODHBt, $$$ indicates p< 0.001 vs GM-Mac + oxLDL + HODHBt. ANOVA, Student-Newman-Keuls Multiple Comparisons, n=4). N-values in macrophages derived from PBMCs represent the number of healthy donors.

5.3 DISCUSSION

Previous studies have proposed that SUMOylation, a post-translational modification, may contribute an important role in the progression of atherosclerosis (Dehnavi, Sadeghi et al. 2019) . At a cellular level, SUMOylation can modulate the expression of numerous cytoskeletal proteins associated with the formation and function of actin filaments. Within macrophages, actin filaments can regulate their behaviour and function, including their migration, phagocytosis, and their transformation into foam cells, all processes associated with the development of atherosclerotic plaques. As such, the main goal of this chapter was to investigate the effect of SUMOylation on the properties of pro-inflammatory macrophages (GM-CSF polarised; GM-Mac), with particular focus on efferocytosis and foam cell formation given the results in the previous chapters. Furthermore, preliminary investigation into the signalling pathways regulated through SUMOylation were investigated, including their contribution to macrophage behaviour and relationship to the modulation of the actin cytoskeleton.

5.3.1 Expression of SUMOylation pathway proteins in human atherosclerotic plaques

Advanced human plaques with marked accumulation of foam cell macrophages are associated with heightened expression of GM-CSF levels which greatly exceeds the expression of M-CSF, favouring macrophage polarisation towards a more pro-inflammatory phenotype (Di Gregoli, Jenkins et al. 2014). Furthermore, GM-CSF–directed macrophage polarisation has been associated with the development and progression of human atherosclerotic plaques, in part through promoting the protein levels of key deleterious proteases (such as MMP-12 and MMP-14) alongside suppressing TIMP-3 protein expression (Di Gregoli, Jenkins et al. 2014, Di Gregoli, Mohamad Anuar Nur et al. 2017, Di Gregoli, Somerville et al. 2020). Relatedly, STAT5 phosphorylation is significantly induced during GM-CSF-directed macrophage polarisation of macrophage, but not through M-CSF polarisation, and is therefore considered indicative of canonical GM-CSF–directed downstream signalling (Di Gregoli, Jenkins et al. 2014). In this chapter, it is shown that a high proportion of cells within the macrophage-rich shoulder regions of human atherosclerotic plaques display STAT5 phosphorylation. This infers the accumulation of GM-polarised macrophages during plaque progression, as postulated by others (Waldo, Li et al. 2008) . Supporting modulation of the SUMOylation pathway during plaque formation, an increased percentage of cells expressing SUMO-1, -2, and -3 were detected in atherosclerotic compared to non-diseased coronary arteries. Interestingly, when assessing the foam cell macrophage-rich intra-plaque regions where STAT5 phosphorylation was abundant, the proportion of cells expressing SUMO1, 2, and 3, were decreased in advanced unstable plaques compared to stable lesions, implying SUMOylation is reduced during plaque progression. This novel finding supports

further investigation into the regulation of the SUMOylation pathway between macrophage subsets (when transformed into foam cells), especially with regard to key signalling pathways such as the GM-CSF/STAT5 pathway.

5.3.2 Effects of non-specific inhibition of SUMOylation on foam cell formation and efferocytosis in divergent macrophage subsets

Findings presented within this thesis so far reveal that GM-CSF polarised macrophages display a heightened ability to uptake modified lipoproteins (oxLDL) and form foam cells in comparison to M-CSF polarised macrophages, which is related to differences in their actin cytoskeleton. As such, it is proposed that the actin cytoskeleton may modulate endocytosis and phagocytosis of modified lipoproteins, and other related processes such as the efferocytosis of apoptotic bodies. However, the mechanisms underlying the disparities in function between GM-Mac and M-Mac subsets have yet to be fully elucidated. SUMOylation is a recently identified epigenetic/post-translational mechanism which has been suggested to regulate macrophage function during atherosclerosis (Dehnavi, Sadeghi et al. 2019). Accordingly, the effect of blocking SUMOylation on macrophage function was assessed within this chapter, utilising the broad-spectrum SUMOylation inhibitor topotecan. Topotecan was originally identified as a DNA topoisomerase inhibitor, and therefore can induce cell death and underlies it use as a chemotherapeutic agent. However, a non-cytotoxic concentration of topotecan was used in this chapter (0.25 μM) which suppressed foam cell formation in both pro- (GM-Mac) and anti-inflammatory macrophages (M-Mac) during different stages of maturation, implying a regulatory role for SUMOylation in macrophage foam cell formation. In support, a recent study demonstrated that a DNA topoisomerase II inhibitor (etoposide) was able to inhibit macrophage foam cell formation through enhancing reverse cholesterol transport via LXR-dependent upregulation of ABCA1 expression (de la Llera-Moya, Rothblat et al. 1992). Although the mechanism through which etoposide regulated LXR activity was not explored (and therefore not attributed to affecting SUMOylation, probably as SUMOylation was a poorly defined mechanism when this study was published), an ancillary study demonstrated that etoposide suppressed atherosclerotic plaque development in cholesterol-fed rabbits (de la Llera-Moya, Rothblat et al. 1992). However, another study has shown that treatment of mice with topotecan induced a significant lowering in serum HDL levels which was associated with a marked increase in cholesterol and triglyceride levels, effects expected to promote the development of atherosclerosis (Saunders, Fujii et al. 2010). Again, the regulation of SUMOylation

was not addressed in this study but highlighted that topotecan could modulate lipoprotein transport independent of chemotherapeutic mechanisms.

As macrophage expression of scavenger receptors is essential for their phagocytosis of materials including modified lipoproteins, perhaps the aforementioned effects of topotecan on lipid profiles is in part through SUMOylation-dependent regulation of macrophage cholesterol transport? Associated assessment presented within this chapter show indeed that topotecan can downregulate the expression of select scavenger receptors in GM-Mac (CD36) and M-Mac subsets (MSR1 and OLR1) in the presence of oxLDL. In support, it was previously reported that administration of the topoisomerase inhibitor teniposide to Apoe KO mice fed a high cholesterol diet, reduced intra-plaque lipid accumulation within aortic root lesions, indicating suppressed foam cell accumulation, attributable to down regulation of LDLR and scavenger receptor class B type 1 (SRB1) expression alongside upregulation of the cholesterol efflux genes (Liu, Zeng et al. 2018). Collectively, these findings suggest a regulatory role of SUMOylation on the behaviour of different macrophage subsets with relevance to atherosclerosis, such as the repressed expression of scavenger receptors and ensuing oxLDL accumulation/foam cell formation.

As mentioned previously, alongside the uptake of modified lipoproteins, efficient reverse transport including cholesterol efflux from macrophages ensures that modified lipoproteins do not adversely accumulate within cells. Considering the decreased foam cell formation observed within M-CSF or GM-CSF polarised macrophages with topotecan co-incubation, it is plausible that cholesterol efflux-associated genes/proteins are dysregulated in addition to the observed increased scavenger receptor expression, and that regulation of SUMOylation reverses the deleterious effects. Indeed, the mRNA expression for select efflux regulators such as NCOR1, ABCA1, and ABCG1, were upregulated by the addition of topotecan (0.25 μM). This observation is supported by two previous studies which reported that addition of the topoisomerase II inhibitors etoposide or teniposide upregulated macrophage expression of ABCA1 and ABCG1 (Zhang, Jiang et al. 2013, Liu, Zeng et al. 2018). Accordingly, in the context of atherosclerosis SUMOylation would appear a detrimental process as addition of the global SUMOylation inhibitor topotecan to M-CSF polarised (M-Mac) or GM-CSF directed (GM-Mac) macrophage subsets, suppressed foam cell formation. These findings would support further studies to evaluate the potential athero-protective effects of topotecan However, the SUMOylation of individual proteins may impart beneficial effects on macrophages and other intra-plaque cells (such as endothelial cells or VSMCs), as suggested previously (Dehnavi, Sadeghi et al. 2019) , which would caution the therapeutic use of broad spectrum SUMOylation inhibitors for the treatment of atherosclerosis.

Similar to the mechanism of oxLDL uptake, efferocytosis is a process in which immune cells, such as macrophages, can engulf apoptotic cell debris and remove dying cells, and is essential to prevent non-resolving inflammatory diseases, such as atherosclerosis (Yurdagul, Doran et al. 2017). The findings in this chapter demonstrated that although GM-CSF polarised macrophages have impaired efferocytosis capacity compared to M-CSF polarised macrophages, blocking SUMOylation with topotecan restored their efferocytosis potential to comparable levels as that detected by M-CSF polarised macrophages. A previous study reported that similar to topotecan, the topoisomerase inhibitor teniposide imparted anti-inflammatory effects during cancer immunotherapy, which were associated with increased clearance of apoptotic cancer cells (efferocytosis) (Wang, Chen et al. 2019). Restoration of efferocytosis has been shown to prevent the progression of atherosclerotic plaques in mouse models, as it limits ensuing inflammation and prevents expansion of the necrotic/lipid-rich core (Schrijvers Dorien, De Meyer Guido et al. 2005). As such, the above findings provide further evidence that inhibition of SUMOylation could be a possible strategy to resolve atherosclerosis, limiting both macrophage foam cell formation while also promoting the clearance of apoptotic cells.

However, the preliminary investigation of human coronary plaques within this thesis demonstrated a decreased proportion of cells positive for SUMO proteins within the foam cell macrophage-rich regions of histologically characterised unstable plaques compared to stable lesions. This would infer that SUMOylation is suppressed within advanced clinically-relevant plaques and argue against blocking SUMOylation to prevent plaque progression. Given that foam cell macrophages in unstable plaques display characteristics associated with the GM-Mac subset alongside an abundance of GM-CSF and STAT5 phosphorylation, it is possible SUMOylation of STAT5 plays a role in atherosclerosis. Interestingly, our findings revealed that although STAT5 phosphorylation was detected in GM-CSF polarised foam cell macrophages, treatment with topotecan markedly increased pSTAT5 levels and its nuclear localisation. This novel observation suggests a prominent role of SUMOylation in the regulation of STAT5 signalling down-stream of GM-CSF induced polarisation of macrophages. Accordingly, a selective STAT5-SUMO protein-protein interaction inhibitor which blocks SUMOylation of phosphorylated STAT5 was deployed, named HODHBt. Specifically, HODHBt inhibits the binding of SUMO2/3 to STAT5 and subsequently maintains the phosphorylation and activation of STAT5, and its retention within the nucleus and subsequent interaction with STAT5 transcription factor binding sites within target genes (Bosque, Nilson et al. 2017).

5.3.3 Specific inhibition of STAT5 SUMOylation on foam cell formation and efferocytosis GM-CSF polarised macrophages

In this study, and in line with proposed action of HODHBt, an increased number of GM-CSF polarised foam cell macrophages displayed STAT5 phosphorylation with heightened nuclear localisation after treatment with HODHBt, confirming SUMOylation of STAT5 occurs in GM-Macs. Pertinent to atherosclerosis and supporting the propositions suggested from the human coronary plaque investigations detailed within this chapter, suppressing STAT5 SUMOylation with HODHBt augmented foam cell formation in GM-Macs. Therefore, in opposition to broad-spectrum inhibition of SUMOylation, specifically retarding the SUMOylation of STAT5 (consequently sustaining STAT5 phosphorylation and associated STAT5-dependent gene upregulation) would potentially accelerate atherosclerosis. Although the role of STAT5 signalling has not been directly assessed during atherosclerotic plaque formation and progression, some indirect evidence exists. For example, inhibition of JAK2 activity, a critical node between GM-CSF/STAT5 signalling, suppressed aortic atherosclerosis in Apoe KO mice, which was associated with reduced STAT5 phosphorylation in monocytes/macrophages (Tang, Liu et al. 2020). A previous study reported the relation between overproduction of GM-CSF and persistence of STAT5 phosphorylation (Litherland, Grebe et al. 2005), an association highlighted earlier in human advanced coronary atherosclerotic plaques. It has also been demonstrated that the presence of persistent levels of phosphorylated STAT5 is linked to other chronic inflammatory responses such as in thyroid autoimmune diseases (Litherland, Xie et al. 2005). Interestingly, it was shown that the effect of persistent STAT5 phosphorylation eventually becomes independent to GM-CSF levels (Litherland, Xie et al. 2005), perhaps through loss of STAT5 SUMOylation. Accordingly, application of HODHBt to GM-Mac foam cells results in persistent STAT5 phosphorylation, which may replicate the effect of GM-CSF overproduction.

As shown earlier in this thesis, GM-CSF induces the polarisation of macrophages towards a pro-inflammatory phenotype, and that GM-Mac are more able to accumulate lipid and form foam cells. As previously mentioned, GM-CSF polarised macrophages have reduced F-actin content, and the findings in this chapter showed that HODHBt administration further diminished the F-actin content in GM-CSF polarised foam cell macrophages, indicating that the cells additionally increase their GM-Mac properties, potentially as a result of sustained STAT5 phosphorylation. This proposition is supported by the increased expression of MMP-12 detected in GM-CSF polarised macrophages with HODHBt treatment. One of the potential mechanisms underlying the effect of heightened STAT5 phosphorylation afforded by HODHBt on GM-Mac foam cell formation is modulation of OLR1 expression, which was significantly increased at both the mRNA and protein level with HODHBt

treatment. Previous studies have confirmed OLR1 as a major scavenger receptor highly expressed in GM-Mac compared to its counterpart M-Mac (Di Gregoli and Johnson 2012).

However, assessment of the transcription factor binding sites within the human OLR promoter revealed no STAT5 DNA-binding sites. Interestingly a previous study reported that upon phosphorylation and translocation to the nucleus, STAT5 can bind to POU2F1 (also known as OCT1) to form a stable complex and upregulate gene expression of cyclin D1 (Magné, Caron et al. 2003). Further assessment of the human OLR1 promoter revealed multiple POU2F1 DNA-binding sites, the most for any transcription factor, suggesting STAT5/POU2F1 complexes drive the upregulation of OLR1 in GM-CSF-polarised foam cell macrophages. In agreement, data within this chapter demonstrated that co-expression of nuclear pSTAT5 and POU2F1 are significantly increased in GM-CSF polarised macrophages with HODHBt treatment. This original finding indicates that STAT5-mediated transcription of OLR1 and subsequent foam cell formation in GM-Macs is in part dependent on POU2F1, although further investigations are needed to confirm this interaction.

Previous data in this chapter demonstrated that global inhibition of SUMOylation with topotecan heightened the efferocytosis capacity of GM-Macs. However, suppression of STAT5 specific SUMOylation with HODHBt did not affect efferocytosis capacity in GM-Macs, but efferocytosis was augmented in GM-CSF-polarised foam cells. The disparate effect of HODHBt treatment on efferocytosis between macrophages and foam cell macrophages suggest oxLDL uptake and foam cell formation may regulate SUMOylation of STAT5 and subsequent heightened efferocytosis in GM-Macs. Accordingly, to understand the mechanism underlying the increased efferocytosis observed in GM-Mac foam cells afforded through HODHBt-dependent augmented STAT5 activity, two potential mechanisms were proposed; regulation reliant on Ca^{+2} signalling, or actin cytoskeleton rearrangement (Tajbakhsh, Rezaee et al. 2018). Nifedipine and fasudil were deployed respectively to interrogate the involvement of these processes. Previous study reported that calcium channel blocker (diltiazem) significantly inhibits the expression and activity of LOX-1 and results in decreasing the apoptosis of VSMCs with high glucose levels (Rudijanto 2010). Results revealed that fasudil attenuated the efferocytosis capacity of HODHBt treated GM-CSF polarised foam cell macrophages, whereas nifedipine was ineffective. These findings suggest that upregulated efferocytosis in GM-CSF polarised foam cell macrophages afforded through sustained STAT5 activity with HODHBt, is dependent on modulation of the actin cytoskeleton. These observations are similar to those seen for oxLDL accumulation and foam cell formation in GM-Macs, which are considered to be OLR1-mediated due to the aligned changes in expression of this scavenger receptor. Intriguingly, OLR1 has been shown to harbour the ability to bind negatively charged phospholipids such as phosphatidylserine (PS)

(Moriwaki, Kume et al. 1998), and consequently OLR1 can promote efferocytosis through recognition of PS-presenting apoptotic bodies (Chen, Masaki et al. 2002, Murphy, Tacon et al. 2005). Considering fasudil blocked HODHBt-mediated efferocytosis in GM-Mac foam cells, while OLR1 expression was increased with HODHBt treatment (Figure 5.18), effects on the actin cytoskeleton may alter OLR1 expression within GM-Mac foam cells with sustained STAT5 activity. Indeed, fasudil administration significantly downregulated GM-Mac foam cell membrane expression of OLR1, without affecting total cellular levels. Collectively, these findings suggest that inhibition of STAT5 SUMOylation and subsequent STAT5-mediated upregulation of OLR1 is independent of F-actin cytoskeletal rearrangement. However, a competent actin cytoskeleton is required for OLR1 accumulation at the cell membrane and associated efferocytosis capacity, and perhaps oxLDL engulfment.

In conclusion, HODHBt, which blocks SUMOylation of phosphorylated STAT5 and subsequently maintains the phosphorylation and activation of STAT5, augmented foam cell formation in GM-Macs, diminished the F-actin content with the cells, and heightened the efferocytosis capacity in GM-CSF polarised foam cells. However, fasudil co-incubation attenuated the efferocytosis capacity of HODHBt treated GM-CSF polarised foam cell macrophages and significantly downregulated cell membrane expression of OLR1, suggesting the requirement of actin cytoskeleton for the accumulation of OLR1 at the cell membrane in order to regulate efferocytosis and perhaps foam cell formation.

6 GENERAL DISCUSSION

Atherosclerosis is a chronic inflammatory disease affecting medium- and large-sized arteries, and is characterised by the presence of heterogenous populations of macrophages (Stout and Suttles 2004). Different growth factors and cytokines have been proposed as key effectors of macrophage polarisation towards pro- and anti-inflammatory subsets, with the caveat that most studies are performed in vitro. However, M-CSF and GM-CSF have been shown to promote distinct macrophage subsets which are not only characterised by differential expression of specific genes, but also display discrete morphologies (Waldo, Li et al. 2008). Moreover, multiple studies have inferred that GM-CSF polarised macrophages, also termed GM-Mac, preferentially populate advanced atherosclerotic plaques and associate with their progression, through the deployment of protein markers specific for the GM-Mac subset (Waldo, Li et al. 2008, Di Gregoli, Jenkins et al. 2014, Di Gregoli, Mohamad Anuar Nur et al. 2017, Di Gregoli, Somerville et al. 2020). Considering the contrasting morphologies between the M-Mac and GM-Mac subsets, it is salient to reflect that the actin cytoskeleton is central to modulating the shape of cells (Karp 2010). Accordingly, in this thesis changes in the actin cytoskeleton between different macrophage phenotypes were explored, alongside examining the effects of actin perturbing drugs (such as fasudil and pravastatin) on macrophage subset gene expression and associated behaviour. With the aim that actin perturbing drugs could be deployed therapeutically to modulate macrophage subset function and hence suppress the progression of atherosclerosis.

ROCK exists as two isoforms (ROCK1 and ROCK2) and is the first down-stream kinase activated by RhoA, a member of the Rho family of small GTPases. ROCK1/2 and RhoA are well-characterised regulators of the actin cytoskeleton and have also been ascribed a role in atherogenesis. In support of this proposition, administration of a ROCK1/2 inhibitor (Y-27632) to Ldlr-deficient mice inhibited the formation of atherosclerotic plaques within the aortic sinus and thoracic aorta, which was associated with reduced ROCK1/2 activity (Mallat, Gojova et al. 2003). Similarly, ROCK1/2 inhibition in Apoe-deficient mice through delivery of fasudil suppressed atherosclerotic plaque formation within the brachiocephalic and common carotid arteries (Wu, Xu et al. 2009). Furthermore, the same study demonstrated that delayed administration of fasudil could retard progression of established plaques, which was associated with limiting intra-plaque macrophage accumulation (Wu, Xu et al. 2009). Taken together, these studies strongly suggest that modulation of the actin cytoskeleton in macrophages through inhibition of ROCK1/2 maybe exploited for targeting atherosclerosis therapeutically. However, fasudil administration to Apoe-deficient mice co-infused with Ang II (to induce vascular inflammation and aortic aneurysm formation), had no effect on carotid artery and aortic arch atherosclerotic lesion area (Wang, Martin-McNulty et al. 2005).

Considering it is now well accepted that macrophages display marked heterogeneity with divergent effects proposed on atherosclerosis, ROCK-mediated actin cytoskeleton changes may differ between

macrophage subsets. Accordingly, both fasudil and pravastatin were deployed in this thesis as ROCK1/2 inhibitors, albeit acting through different mechanisms, to assess the effects of actin cytoskeleton modulation on the behaviour of different macrophage subsets. The results show that both fasudil and pravastatin alter the morphology of M-CSF or GM-CSF polarised macrophages (M-Mac and GM-Mac, respectively) which was associated with reduced F-actin accumulation. Consequently, changes in cell shape are usually associated with alterations in cell behaviour, which may also include macrophage polarisation. Indeed, pravastatin or fasudil administration to GM-Macs decreased the expression of MMP-12 (a robust marker of the GM-Mac subset), while the levels of TGFβ (an anti-inflammatory marker) was increased, suggesting that pravastatin (and by inference actin depolymerisation) favours macrophage polarisation towards an anti-inflammatory phenotype. In support, a previous study reported that macrophages within atherosclerotic aortic aneurysms of patients receiving atorvastatin or simvastatin therapy shifted towards an anti-inflammatory phenotype, compared to lesions from placebo-treated individuals (van der Meij, Koning et al. 2013). This suggests that modulation of the actin cytoskeleton (via fasudil or pravastatin) influences macrophage phenotype, and may also exert direct or indirect effects on their behaviour.

Macrophages within atherosclerotic plaques are able to uptake oxLDL via scavenger receptors and thereupon transform into macrophage foam cells, a process which is considered central to the development and progression of atherosclerosis (Glass and Witztum 2001). As mentioned previously, administration of ROCK1/2 inhibitors to atherosclerotic mice influences disease development and progression, an effect attributed to diminished macrophage foam cell formation (Mallat, Gojova et al. 2003, Wu, Xu et al. 2009). In agreement, bone marrow-restricted deficiency of ROCK1 blunted macrophage phagocytic capacity and associated foam cell formation, translating in vivo to reduced development of aortic atherosclerosis (Wang, Liu et al. 2008). Likewise, loss of ROCK2 in bone marrow-derived macrophages resulted in decreased foam cell formation and suppressed atherosclerotic plaque generation in Ldlr-knockout mice, ascribed to increased cholesterol efflux through upregulation of the PPARɣ/LXR/ABCA1 pathway (Zhou, Mei et al. 2012). Accordingly, the ROCK1/2 signalling pathway, which is a central regulator of the actin cytoskeleton, promotes macrophage foam cell formation and atherosclerosis. However, if such effects are observed in all macrophages, such as disparate phenotypes, has not been discerned.

As with previous observations, monocytes (THP-1 human monocytic cell line) and macrophages readily accumulated oxLDL and transformed into foam cells, and in agreement with recent evidence, demonstrated that monocytes are able to accumulate modified lipoproteins (Mosig, Rennert et al. 2008, Mosig, Rennert et al. 2009). However, disparities were observed between M-CSF and GM-CSF-directed monocyte/macrophages, as GM-CSF-stimulated monocytes more readily transformed into

foam cells after prolonged exposure to oxLDL, compared to M-CSF treated monocytes. This novel observation is aligned with those from Mosig and colleagues, who demonstrated differential oxLDL accumulation between divergent monocyte subsets, retrieved from patients with familial hypercholesterolaemia (Mosig, Rennert et al. 2009). Monocyte uptake of modified lipoproteins require the modulation of their actin cytoskeleton via the regulation of RhoA activity (Jackson, Weinrich et al. 2016). In agreement our study showed that the administration of fasudil reduced the GM-CSF-treated monocyte oxLDL accumulation. Similarly, GM-CSF polarised macrophages accumulated more oxLDL compared to M-CSF polarised macrophages derived from either THP-1 cells or human PBMCs, which was reduced with the administration of fasudil or pravastatin, mirroring the effects observed in monocytes. It is possible that the prolonged exposure of GM-CSF-stimulated monocytes to oxLDL induces their adhesion and accelerates their subsequent maturation into macrophages, which would require actin cytoskeleton rearrangement, and consequently promote oxLDL uptake – in part explaining the observed effects of fasudil co-administration. Indeed, previous evidence suggests select monocyte subsets mature into macrophages in response to oxLDL, which is then rapidly taken up by the cell (Mosig, Rennert et al. 2009).

Fasudil or pravastatin suppressed oxLDL accumulation and foam cell formation in GM-CSF polarised macrophages which accompanied with altered expression of key scavenger receptors and genes/proteins associated with cholesterol efflux. Our findings showed that the protein expression of two key scavenger receptors, OLR1 and CD36, were decreased in GM-CSF polarised macrophages with co-incubation of fasudil or pravastatin, implying a role for the modulation of the actin cytoskeleton during macrophage foam cell formation. Conversely, while ABCG1, NCOR1, and PPARα protein levels were not changed by exposure to oxLDL, they were significantly increased by co-incubation with fasudil or pravastatin, indeed suggesting enhanced cholesterol efflux ability. Congruent findings reported PPARα protects macrophages from foam cell formation (Li, Binder et al. 2004, Srivastava 2011). A study on isolated peritoneal macrophages from type 2 diabetic mice showed that downregulation of the expression of ABCG1 resulted in 2-fold increase in the accumulation of esterified cholesterol and subsequently increased foam cell formation in macrophages (Mauldin, Srinivasan et al. 2006). Another study on myeloid cell-specific NCOR1 knockout mice showed that deficiency of the expression of NCOR1 in macrophages increased the ability of macrophages to uptake oxLDL and form foam cells due to the upregulation in the expression of CD36 which was associated with the progression of atherosclerosis (Oppi, Stein et al. 2019). Collectively, the above findings suggest that perturbation of actin cytoskeleton reorganisation blunts GM-CSF-polarised macrophage foam cell formation, through suppressed oxLDL uptake and augmented cholesterol efflux.

Comparable to phagocytosis and uptake of modified lipoproteins, efficient efferocytosis is associated with alterations of the cell membrane through rearrangement of cells actin cytoskeleton. Defective efferocytosis is related to atherosclerotic plaque progression through necrotic/lipid core expansion and perpetuating a pro-inflammatory environment (Thorp and Tabas 2009). In line with attributing a deleterious role to GM-CSF polarised macrophages during plaque advancement and instability, GM-Macs displayed decreased efferocytosis capacity compared to M-Macs. However, impaired efferocytosis by GM-CSF polarised macrophages was restored to M-Mac levels through co-incubation with either fasudil or pravastatin. Although these novel observations are the first to demonstrate divergent efferocytosis capacities between macrophage subsets which can be modulated by actin-perturbing drugs, there is supporting evidence for the RhoA/ROCK pathway regulating macrophage efferocytosis. For example, lovastatin increased the efferocytosis capacity of macrophages in both in vitro and in vivo studies by inactivating the RhoA signalling pathway (Morimoto, Janssen et al. 2006). Relatedly, administration of a ROCK inhibitor (Y-27632) to a macrophage cell line increased their engulfment of apoptotic bodies (Tosello-Trampont, Nakada-Tsukui et al. 2004). Moreover, directly suppressing RhoA activity with a dominant negative approach also promoted macrophage clearance of apoptotic cells (Nakaya, Tanaka et al. 2006).

In advanced human plaques, with marked localised accumulation of foam cell macrophages, the expression of GM-CSF is heightened, favouring the polarisation of macrophages towards a pro-inflammatory phenotype (Di Gregoli, Jenkins et al. 2014). In line with this proposition, we demonstrated that STAT5 phosphorylation (an indicator of GM-CSF-induced signalling) was abundant within the foam cell macrophage-rich shoulder regions of human advanced atherosclerotic plaques. Recent evidence has suggested that SUMOylation and phosphorylation of STAT5 act antagonistically to each other (Krämer and Moriggl 2012), and that blocking SUMOylation of STAT5 potentiates its phosphorylation and translocation to the nucleus to drive gene expression (Bosque, Nilson et al. 2017). Interestingly, SUMOylation can also regulate actin polymerisation and other key processes related to the organisation and remodelling of the cytoskeleton (Alonso, Greenlee et al. 2015). As such, SUMOylation may represent a novel mechanism of GM-Mac responses related to their actin cytoskeleton and accumulation of modified lipoproteins. Supporting this proposition, further analysis of human plaques revealed increased expression of SUMO-1, -2, and -3 compared to non-diseased coronary arteries inferring the SUMOylation pathway is modulated during plaque formation. Importantly however, the percentage of SUMO-1, -2, and -3 positive cells within foam cell macrophage-rich regions of advanced unstable plaques, was decreased compared to stable lesions, suggesting that SUMOylation is reduced in foam cell macrophages during the progression of atherosclerotic plaques. Accordingly, preservation or restoration of SUMOylation within foam cell

macrophages would be expected to suppress atherosclerotic plaque progression, while conversely, inhibition of the SUMOylation could accelerate atherosclerosis.

The studies within this thesis using human PBMC-derived macrophages suggested that in the context of atherosclerosis, the SUMOylation pathway is deleterious as pan-SUMOylation inhibition (with topotecan) blunted foam cell formation in both M-CSF (M-Mac) or GM-CSF directed (GM-Mac) macrophage subsets. The blocking of SUMOylation was associated with decreased expression of important scavenger receptors that mediate oxLDL uptake, including CD36, MSR1, and OLR1. Conversely, levels of the key cholesterol efflux genes/proteins ABCA1, ABCG1, and NCOR1 were elevated by inhibition of SUMOylation. These dual effects would be expected to perturb macrophage foam cell formation, in keeping with the effect observed when blocking SUMOylation. These findings would support further studies to evaluate the potential athero-protective effects of topotecan-induced pan-SUMOylation inhibition. However, the SUMOylation of individual proteins may also impart beneficial effects on macrophages and other intra-plaque cells (such as endothelial cells or VSMCs), as suggested previously (Dehnavi, Sadeghi et al. 2019), while the mechanism-of-action of topotecan as a topoisomerase I inhibitor also induces apoptosis of proliferating cells. These considerations would caution the therapeutic use of broad spectrum SUMOylation inhibitors for the treatment of atherosclerosis. To circumvent these potential caveats, focussing on key proteins or pathways dominant in GM-CSF-polarised macrophages may reveal specific SUMOylation targets that give rise to athero-protective effects.

Relatedly and surprisingly, phosphorylation levels of STAT5 were increased within GM-Macs after topotecan administration, suggesting that SUMOylation dampens the activity of STAT5 and down-stream target gene expression. To confirm this proposition, HODHBt, a selective STAT5-SUMO protein-protein interaction inhibitor which blocks SUMOylation of phosphorylated STAT5 resulting in sustained pSTAT5 transcriptional activity was deployed. As expected, specifically blocking SUMOylation of STAT5 in GM-Macs resulted in heightened levels of STAT5 phosphorylation alongside retaining its accumulation within the nucleus, which translated to increased expression of MMP-12. However, in opposition to the effects observed with suppressing global-SUMOylation, this observation would imply that SUMOylation of STAT5 is a protective mechanism, as evidenced by the elevation in MMP-12 levels when SUMOylation of STAT5 is suppressed. Supporting a beneficial role for SUMOylation of STAT5 in GM-Macs, oxLDL-induced foam cell formation was increased in GM-Macs through suppression of STAT5 SUMOylation with HODHBt. Therefore, these findings suggest that loss of STAT5-targetted SUMOylation results in sustained STAT5 activation and signalling, subsequently augmenting the pro-inflammatory and pro-atherosclerotic phenotype of GM-Macs through heightened foam cell formation and MMP-12 production.

The enhanced foam cell formation afforded from perturbing STAT5 SUMOylation was associated with increased expression (both mRNA and protein level) of OLR1, providing a potential mechanism for augmented oxLDL accumulation within HODHBt-treated GM-Macs. However, no STAT5 DNA-binding sites could be identified within the OLR1 promoter region, arguing against STAT5 directly regulating OLR1 expression. The most prevalent predicted binding sites were for POU2F1 (also known as OCT1), a transcription factor shown to upregulate macrophage OLR1 expression and therefore promote subsequent foam cell formation (Hu, Hui et al. 2020). Moreover, activated STAT5 can bind to POU2F1 to transactivate target gene expression (Magné, Caron et al. 2003), raising the intriguing possibility that STAT5/POU2F1 complexes drive the upregulation of OLR1 in GM-CSF-polarised foam cell macrophages. In support, augmented pSTAT5 and POU2F1 co-localisation was detected within the nuclei of GM-CSF polarised macrophages after suppression of STAT5 SUMOylation. This novel finding implies that STAT5-mediated transcription of OLR1 and subsequent enhanced efferocytosis and foam cell formation in GM-Macs, is in part dependent on POU2F1, and moderated by the sustained STAT5 activity afforded from blocking its SUMOylation. However, these original observations require further investigation and validation to confirm this interaction, including assessing the effects of GM-CSF polarisation and early foam cell formation on the expression levels of POU2F1.

It has also been previously shown that OLR1 is able to bind phosphatidylserine (PS), and can therefore recognise PS-presenting apoptotic cells and promote efferocytosis (Moriwaki, Kume et al. 1998). Although, blocking SUMOylation of STAT5 in GM-Macs did not affect their efferocytosis capacity, it was significantly increased in GM-Mac foam cells. This observation suggests that the uptake of oxLDL and the formation of foam cells in GM-Macs may regulate the expression of SUMO proteins (or their inhibitors) and associated SUMOylation of STAT5, and therefore increase their efferocytosis capacity through upregulation of OLR1. Indeed, in Chapter 4 it was reported that OLR1 expression was increased in GM-Macs during foam cell formation, an effect which was interestingly suppressed by the actin-perturbing drugs fasudil or pravastatin. Connectedly, the inhibition of STAT5 SUMOylation decreased the F-actin content within GM-Macs, implying depolymerisation of F-actin and re-organisation of the cytoskeleton are STAT5-dependent. Moreover, as fasudil was able to attenuate the increased efferocytosis observed in HODHBt-treated GM-Macs, this indicates that the enhanced efferocytosis capacity in GM-CSF polarised macrophage foam cells is dependent on the modulation of the actin cytoskeleton. It must be noted however, that efferocytosis is commonly considered an athero-protective process due to its function of clearing apoptotic cells and limiting ensuing pro-inflammatory secondary necrosis. Conversely, enhanced efferocytosis may also impart detrimental effects, particularly in advanced plaques where foam cell macrophages are abundant. Indeed, it has recently been shown that macrophage, and importantly, foam cell macrophage efferocytosis

perpetuates foam cell formation due to the breakdown and release of neutral lipids from the cell membrane of apoptotic cells, particularly within pro-inflammatory macrophage subsets (Ford, Zeboudj et al. 2019). This evidence would align with a detrimental role for GM-CSF polarised macrophages during atherosclerotic plaque progression.

Accordingly, oxLDL uptake and foam cell formation may suppress SUMOylation of STAT5 and subsequently augment efferocytosis in GM-Macs, through a mechanism dependent upon actin cytoskeleton remodelling and the expression of OLR1. Interestingly, blunting remodelling of the actin cytoskeleton with fasudil had no effect on total OLR1 protein levels in GM-Mac foam cells treated with HODHBt but did markedly reduce membrane expression. Therefore, suggesting that actin cytoskeleton remodelling is necessary for translocation of OLR1 to the cell membrane and the associated heightened efferocytosis capacity detected in GM-Mac foam cells that display SUMOylation-dependent sustained STAT5 activity. Accordingly, these connected novel regulatory mechanisms (as summarised in Figure 6.1) support and underpin the proposed deleterious role of GM-CSF polarised macrophages in atherosclerotic plaque progression and instability. It can be proposed that; 1) increased GM-CSF within advanced atherosclerotic plaques favours macrophage polarisation towards a pro-inflammatory phenotype with associated increased expression of scavenger receptors; 2) subsequent increased uptake of oxLDL and early foam cell formation suppresses the SUMOylation pathway, specifically of STAT5 (the main transcription factor in GM-CSF signalling), enhancing STAT5 activation and target gene upregulation; 3) increased expression of OLR1 and its translocation to the membrane facilitates enhanced oxLDL uptake and efferocytosis of neighbouring apoptotic macrophages, perpetuating foam cell size and propensity to die; 4) STAT5 directly or indirectly regulates remodelling of the actin cytoskeleton to facilitate OLR1 membrane translocation alongside phagocytosis and efferocytosis mechanisms.

In conclusion, modulation of the actin cytoskeleton (via fasudil or pravastatin) influences macrophage phenotype and may also exert direct or indirect effects on their behaviour such as polaristion. Furthermore, perturbation of actin cytoskeleton reorganisation blunts GM-Macs foam cell formation through suppressed oxLDL uptake and augmented cholesterol efflux. Moreover, foam cell macrophage-rich intra-plaque regions in advanced unstable plaques shows increased STAT5 phosphorylation and decreased SUMO1, 2, 3 expression implying SUMOylation is reduced. Accordingly, regulation of SUMOylation pathway especially with regard to GM-CSF/STAT5 pathway (via HODHBt or perhaps due to the uptake of oxLDL and foam cell formation) suppresses SUMOylation of STAT5 and activates STAT5 via phosphorylation. Phosphorylated STAT5 with POU2F1 forms a stable complex and upregulates target genes such as MMP-12 and OLR1. Increased expression of OLR1 and its translocation to the membrane via rearrangements of the actin cytoskeleton (regulated directly or

indirectly by STAT5) facilitates efferocytosis and enhanced oxLDL uptake (Figure 6.1). However, perturbation of actin cytoskeleton reorganisation (via fasudil) blunts the translocation of OLR1 to the membrane. Taken together, actin cytoskeleton regulates the inflammatory phenotype of macrophages, including the novel regulation by STAT5 SUMOylation, suggesting that targeting actin cytoskeleton remodelling in GM-CSF polarised macrophages, may have therapeutic potential for reducing plaque progression and improving stability.

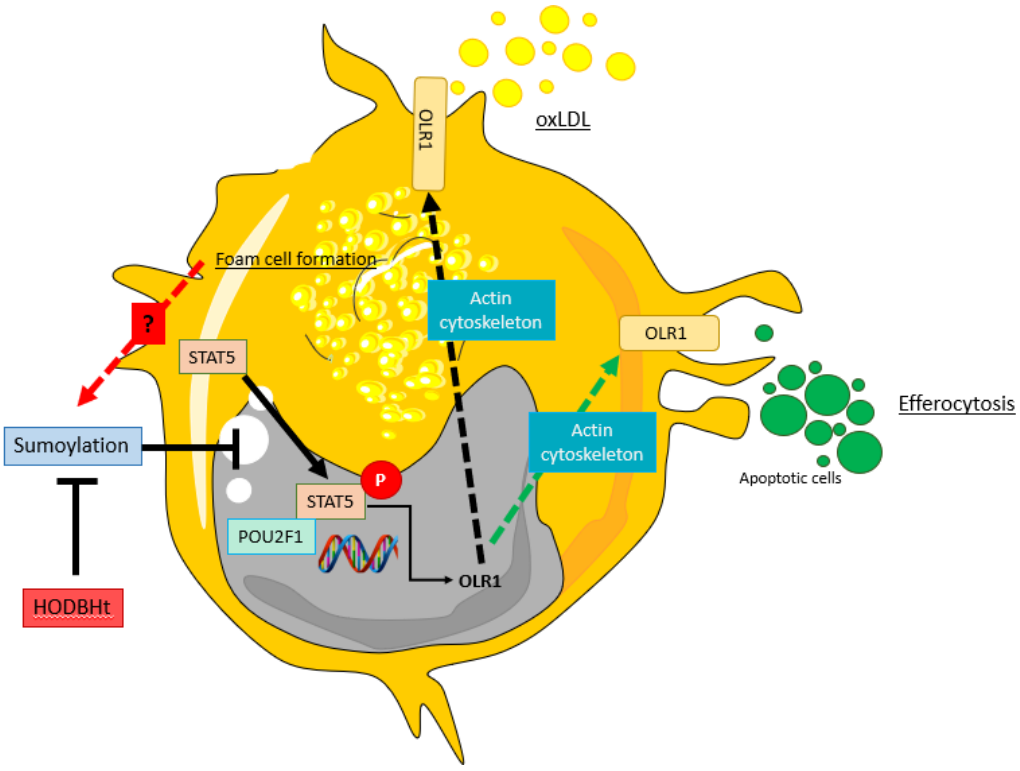

Figure 6.1 Schematic representation of our finding in GM-CSF polarised macrophages.

STAT5 signalling pathway is activated in pro-inflammatory macrophages (GM-Macs). Activation of STAT5 occurs via phosphorylation. Phosphorylated STAT5 enters the nucleus and binds to POU2F1 to form a stable complex that can activate target genes including MMP12 and OLR1. OLR1 requires the rearrangements of actin cytoskeleton (regulated directly or indirectly by STAT5) for its translocation and accumulation at the cell membrane, which is associated with efferocytosis capacity, and perhaps oxLDL engulfment. SUMOylation and phosphorylation of STAT5 act antagonistically. Accordingly, inhibition of SUMOylation of STAT5 (via HODHBt or perhaps due to the uptake of oxLDL and foam cell formation) retain the activation and phosphorylation of STAT5.

6.1 Limitations

There are several limitations associated with the findings presented in this thesis that are addressed throughout. However, some salient caveats are discussed here. For example, fasudil and pravastatin were used to modulate the actin cytoskeleton within different macrophage subsets. Although both fasudil and pravastatin can serve as actin perturbing drugs due to their capacity to modulate Rho/ROCK activity, they also affect other related and unrelated (in the case of pravastatin) signalling pathways. As such, in future experiments it would be sensible to deploy more direct F-actin filament disrupting reagents, such as cytochalasin D and latrunculin B, alongside adoption of an F-actin filament-stabilising reagent such as, jasplakinolide to validate the findings made in this study.

Although the bulk of studies within Chapter 5 were performed in human PBMC-derived monocyte/macrophages, some of the initial findings in Chapters 3 and 4 were only undertaken in macrophages differentiated from THP-1 cells, a human monocytic cell line. Therefore, these studies would benefit from validation in human PBMC- derived macrophages.

Throughout this thesis, F-actin content and associated quantification was performed using fluorescently-conjugated phalloidin labelling, but the expression of monomeric G-actin was not assessed. The formation of the actin cytoskeleton and its remodelling is regulated by the polymerisation and depolymerisation of F-actin and is best interrogated through the assessment of both F-actin and G-actin content within cells. Therefore, future experiments would ideally also examine G-actin content and quantify the G-actin/F-actin ratio between the different macrophage subsets.

In Chapter 3, it is suggested that in comparison to GM-Macs, the anti-inflammatory M-Macs display enhanced TGFβ-mediated signalling through increased SMAD3 phosphorylation, which is dependent upon Rho/ROCK activity, and by inference, remodelling of the actin cytoskeleton. This proposition warrants further investigation as it may explain the relationship between F-actin cytoskeleton alteration during differential macrophage polarisation and associated anti- and pro-inflammaotry actions, such as TGFβ-mediated signalling.

In this thesis, the majority of the studies were conducted in vitro, which while facilitating extensive experimentation, is far removed from the in vivo pathophysiological relevant setting. The investigation of the key findings in an animal model of atherosclerosis (such as the high fat-fed Apoe-deficient mouse) would be pertinent in order to validate the results reported here within.

6.2 Future work

Due to restrictions in time and available funding, the work proposed below could not be performed during this PhD but would form salient future work.

Chapter 3. In chapter 3 we demonstrated that co-incubation of GM-CSF polarised macrophages with fasudil (10 μM) and pravastatin (5 μM) did not change the mRNA expression of MMP12. On the other hand, the protein expression of MMP-12 was significantly decreased, suggesting the involvement of posttranscriptional modification. This finding would benefit from further investigation to evaluate the posttranscriptional mechanisms underlying this discrepancy, such as identification and assessment of microRNA-regulation of MMP-12 in GM-CSF polarised macrophages.

In this study we demonstarted that fasudil adminstration to M-Macs blunted TGFβ signalling (as evidenced by reduced pSMAD3 and TGFBI expression), which could not be rescued through the addition of recombinant TGFβ. Fasudil did not alter the mRNA or protein expression of any TGFβ receptors in M-Macs, or their responsiveness to TGFβ, as shown through assessment of pSMAD3 after deployment of a TGFβ neutralising antibody. Therefore, it can be proposed that the inhibitory effect of fasudil on the TGFβ signalling pathway within M-Macs is in between TGFβ receptor activation and phosphorylation of SMAD3, or upon another pathway/mechanism that modulates SMAD3 levels and/or phosphorylation and subsequnet down-stream signalling. These aspects would benefit from further investigation.

Chapter 4. In Chapter 4 we demonstrated that addition of oxLDL to GM-CSF polarised macrophages significantly increased the expression of efflux genes ABCG1, NCOR1, and PPARA at mRNA level, an effect which was unaffected by co-incubation with fasudil, but suppressed with the addition of pravastatin for ABCG1 and NCOR1 levels. Discrepant observations were observed at the protein level, with oxLDL exerting no change in the expression of ABCG1, NCOR1, and PPARα, while co-incubation with fasudil or pravastatin significantly increased their protein expression. Suggesting that fasudil and pravastatin enhance cholesterol efflux proteins (and therefore mechanism) in GM-CSF polarised macrophages through a post-transcriptional mechanism that needs further investigation.

Some similar discrepancies were observed between the mRNA and protein levels of CD36 and OLR1, similarly suggesting the involvement of a posttranscriptional mechanism which warrants additional examination.

Chapter 5. In Chapter 5 we demonstrated that co-incubation of GM-CSF polarised macrophages with HODHBt significantly increased the nuclear co-localisation of POU2F1 and pSTAT5, suggesting the

cooperation of POU2F1 in STAT5 in transactivation of OLR1 gene expression. However, further investigation and experimentation is needed to confirm and validate these findings. This could include CHIP assays alongside determination if POU2F1 silencing/knockdown reduces STAT5 associated upregulation of OLR1, confirming whether STAT5 transcription of OLR1 is indeed dependent on POU2F1.

7 REFERENCES

Acton, S., A. Rigotti, K. T. Landschulz, S. Xu, H. H. Hobbs and M. Krieger (1996). "Identification of scavenger receptor SR-BI as a high density lipoprotein receptor." Science **271**(5248): 518-520.
Aderem, A. and D. M. Underhill (1999). "MECHANISMS OF PHAGOCYTOSIS IN MACROPHAGES." Annual Review of Immunology **17**(1): 593-623.
Aderem, A. and D. M. Underhill (1999). "Mechanisms of phagocytosis in macrophages." Annu Rev Immunol **17**: 593-623.
Albert, M. A., E. Danielson, N. Rifai and P. M. Ridker (2001). "Effect of statin therapy on C-reactive protein levels: the pravastatin inflammation/CRP evaluation (PRINCE): a randomized trial and cohort study." Jama **286**(1): 64-70.
Allahverdian, S., A. C. Chehroudi, B. M. McManus, T. Abraham and G. A. Francis (2014). "Contribution of intimal smooth muscle cells to cholesterol accumulation and macrophage-like cells in human atherosclerosis." Circulation **129**(15): 1551-1559.
Allahverdian, S., C. Chehroudi Ali, M. McManus Bruce, T. Abraham and A. Francis Gordon (2014). "Contribution of Intimal Smooth Muscle Cells to Cholesterol Accumulation and Macrophage-Like Cells in Human Atherosclerosis." Circulation **129**(15): 1551-1559.
Allen, L. A. and A. Aderem (1996). "Mechanisms of phagocytosis." Curr Opin Immunol **8**(1): 36-40.
Alonso, A., M. Greenlee, J. Matts, J. Kline, K. J. Davis and R. K. Miller (2015). "Emerging roles of sumoylation in the regulation of actin, microtubules, intermediate filaments, and septins." Cytoskeleton (Hoboken) **72**(7): 305-339.
Aoyama, T., T. Sawamura, Y. Furutani, R. Matsuoka, M. C. Yoshida, H. Fujiwara and T. Masaki (1999). "Structure and chromosomal assignment of the human lectin-like oxidized low-density-lipoprotein receptor-1 (LOX-1) gene." Biochem J **339 (Pt 1)**(Pt 1): 177-184.
Arandjelovic, S. and K. S. Ravichandran (2015). "Phagocytosis of apoptotic cells in homeostasis." Nat Immunol **16**(9): 907-917.
Aristorena, M., E. Gallardo-Vara, M. Vicen, M. de Las Casas-Engel, L. Ojeda-Fernandez, C. Nieto, F. J. Blanco, A. C. Valbuena-Diez, L. M. Botella, P. Nachtigal, A. L. Corbi, M. Colmenares and C. Bernabeu (2019). "MMP-12, Secreted by Pro-Inflammatory Macrophages, Targets Endoglin in Human Macrophages and Endothelial Cells." International Journal of Molecular Sciences **20**(12).
Audoy-Rémus, J., J. F. Richard, D. Soulet, H. Zhou, P. Kubes and L. Vallières (2008). "Rod-Shaped monocytes patrol the brain vasculature and give rise to perivascular macrophages under the influence of proinflammatory cytokines and angiopoietin-2." J Neurosci **28**(41): 10187-10199.
Auffray, C., M. H. Sieweke and F. Geissmann (2009). "Blood monocytes: development, heterogeneity, and relationship with dendritic cells." Annu Rev Immunol **27**: 669-692.
Babaev, V. R., M. B. Patel, C. F. Semenkovich, S. Fazio and M. F. Linton (2000). "Macrophage lipoprotein lipase promotes foam cell formation and atherosclerosis in low density lipoprotein receptor-deficient mice." J Biol Chem **275**(34): 26293-26299.
Badimon, L. and G. Vilahur (2014). "Thrombosis formation on atherosclerotic lesions and plaque rupture." J Intern Med **276**(6): 618-632.
Barrett Tessa, J. (2020). "Macrophages in Atherosclerosis Regression." Arteriosclerosis, Thrombosis, and Vascular Biology **40**(1): 20-33.
Bauriedel, G., R. Hutter, U. Welsch, R. Bach, H. Sievert and B. Lüderitz (1999). "Role of smooth muscle cell death in advanced coronary primary lesions: implications for plaque instability." Cardiovascular Research **41**(2): 480-488.
Bea, F., E. Blessing, B. Bennett, M. Levitz, P. Wallace Elizabeth and E. Rosenfeld Michael (2002). "Simvastatin Promotes Atherosclerotic Plaque Stability in ApoE-Deficient Mice Independently of Lipid Lowering." Arteriosclerosis, Thrombosis, and Vascular Biology **22**(11): 1832-1837.
Becker, L., S. A. Gharib, A. D. Irwin, E. Wijsman, T. Vaisar, J. F. Oram and J. W. Heinecke (2010). "A macrophage sterol-responsive network linked to atherogenesis." Cell Metab **11**(2): 125-135.
Becker, L., N. C. Liu, M. M. Averill, W. Yuan, N. Pamir, Y. Peng, A. D. Irwin, X. Fu, K. E. Bornfeldt and J. W. Heinecke (2012). "Unique proteomic signatures distinguish macrophages and dendritic cells." PLoS One **7**(3): e33297.

Bekkering, S., B. A. Blok, L. A. B. Joosten, N. P. Riksen, R. van Crevel and M. G. Netea (2016). "In Vitro Experimental Model of Trained Innate Immunity in Human Primary Monocytes." Clinical and vaccine immunology : CVI **23**(12): 926-933.
Bentzon, J. F., F. Otsuka, R. Virmani and E. Falk (2014). "Mechanisms of plaque formation and rupture." Circ Res **114**(12): 1852-1866.
Berg Katarina, E., I. Ljungcrantz, L. Andersson, C. Bryngelsson, B. Hedblad, N. Fredrikson Gunilla, J. Nilsson and H. Björkbacka (2012). "Elevated CD14++CD16− Monocytes Predict Cardiovascular Events." Circulation: Cardiovascular Genetics **5**(1): 122-131.
Bernstock, J. D., D. Ye, F. A. Gessler, Y.-J. Lee, L. Peruzzotti-Jametti, P. Baumgarten, K. R. Johnson, D. Maric, W. Yang, D. Kögel, S. Pluchino and J. M. Hallenbeck (2017). "Topotecan is a potent inhibitor of SUMOylation in glioblastoma multiforme and alters both cellular replication and metabolic programming." Scientific reports **7**(1): 7425-7425.
Bhatnagar, P., K. Wickramasinghe, E. Wilkins and N. Townsend (2016). "Trends in the epidemiology of cardiovascular disease in the UK." Heart **102**(24): 1945.
Bochem, A. E., D. F. van Wijk, A. G. Holleboom, R. Duivenvoorden, M. M. Motazacker, G. M. Dallinga-Thie, E. de Groot, J. J. Kastelein, A. J. Nederveen, G. K. Hovingh and E. S. Stroes (2013). "ABCA1 mutation carriers with low high-density lipoprotein cholesterol are characterized by a larger atherosclerotic burden." Eur Heart J **34**(4): 286-291.
Boring, L., J. Gosling, M. Cleary and I. F. Charo (1998). "Decreased lesion formation in CCR2-/- mice reveals a role for chemokines in the initiation of atherosclerosis." Nature **394**(6696): 894-897.
Borm, B., R. P. Requardt, V. Herzog and G. Kirfel (2005). "Membrane ruffles in cell migration: indicators of inefficient lamellipodia adhesion and compartments of actin filament reorganization." Exp Cell Res **302**(1): 83-95.
Bosque, A., K. A. Nilson, A. B. Macedo, A. M. Spivak, N. M. Archin, R. M. Van Wagoner, L. J. Martins, C. L. Novis, M. A. Szaniawski, C. M. Ireland, D. M. Margolis, D. H. Price and V. Planelles (2017). "Benzotriazoles Reactivate Latent HIV-1 through Inactivation of STAT5 SUMOylation." Cell Reports **18**(5): 1324-1334.
Brandes Ralf, P. (2005). "Statin-Mediated Inhibition of Rho." Circulation Research **96**(9): 927-929.
Brown, E. J. (1991). "Complement receptors and phagocytosis." Curr Opin Immunol **3**(1): 76-82.
Brown, K., S. Gerstberger, L. Carlson, G. Franzoso and U. Siebenlist (1995). "Control of I kappa B-alpha proteolysis by site-specific, signal-induced phosphorylation." Science **267**(5203): 1485-1488.
Brown, S., I. Heinisch, E. Ross, K. Shaw, C. D. Buckley and J. Savill (2002). "Apoptosis disables CD31-mediated cell detachment from phagocytes promoting binding and engulfment." Nature **418**(6894): 200-203.
Burgstaller, G. and M. Gimona (2005). "Podosome-mediated matrix resorption and cell motility in vascular smooth muscle cells." Am J Physiol Heart Circ Physiol **288**(6): H3001-3005.
Bursill, C. A., M. L. Castro, D. T. Beattie, S. Nakhla, E. van der Vorst, A. K. Heather, P. J. Barter and K. A. Rye (2010). "High-density lipoproteins suppress chemokines and chemokine receptors in vitro and in vivo." Arterioscler Thromb Vasc Biol **30**(9): 1773-1778.
Byrne, P., J. Cullinan, A. Smith and S. M. Smith (2019). "Statins for the primary prevention of cardiovascular disease: an overview of systematic reviews." BMJ Open **9**(4): e023085.
Calle, Y., H. C. Chou, A. J. Thrasher and G. E. Jones (2004). "Wiskott-Aldrich syndrome protein and the cytoskeletal dynamics of dendritic cells." J Pathol **204**(4): 460-469.
Caron, E. and A. Hall (1998). "Identification of two distinct mechanisms of phagocytosis controlled by different Rho GTPases." Science **282**(5394): 1717-1721.
Cermelli, S., Y. Guo, S. P. Gross and M. A. Welte (2006). "The lipid-droplet proteome reveals that droplets are a protein-storage depot." Curr Biol **16**(18): 1783-1795.
Chang, E. and J.-I. Abe (2016). "Kinase-SUMO networks in diabetes-mediated cardiovascular disease." Metabolism: clinical and experimental **65**(5): 623-633.
Chanput, W., J. J. Mes and H. J. Wichers (2014). "THP-1 cell line: An in vitro cell model for immune modulation approach." International Immunopharmacology **23**(1): 37-45.

Chappell, J., J. L. Harman, V. M. Narasimhan, H. Yu, K. Foote, B. D. Simons, M. R. Bennett and H. F. Jørgensen (2016). "Extensive Proliferation of a Subset of Differentiated, yet Plastic, Medial Vascular Smooth Muscle Cells Contributes to Neointimal Formation in Mouse Injury and Atherosclerosis Models." Circ Res **119**(12): 1313-1323.
Charest, A., A. Pépin, R. Shetty, C. Côté, P. Voisine, F. Dagenais, P. Pibarot and P. Mathieu (2006). "Distribution of SPARC during neovascularisation of degenerative aortic stenosis." Heart (British Cardiac Society) **92**(12): 1844-1849.
Chen, M., T. Masaki and T. Sawamura (2002). "LOX-1, the receptor for oxidized low-density lipoprotein identified from endothelial cells: implications in endothelial dysfunction and atherosclerosis." Pharmacology & Therapeutics **95**(1): 89-100.
Chhabra, E. S. and H. N. Higgs (2007). "The many faces of actin: matching assembly factors with cellular structures." Nat Cell Biol **9**(10): 1110-1121.
Chiu, J. J. and S. Chien (2011). "Effects of disturbed flow on vascular endothelium: pathophysiological basis and clinical perspectives." Physiol Rev **91**(1): 327-387.
Choi, S. H., R. Harkewicz, J. H. Lee, A. Boullier, F. Almazan, A. C. Li, J. L. Witztum, Y. S. Bae and Y. I. Miller (2009). "Lipoprotein accumulation in macrophages via toll-like receptor-4-dependent fluid phase uptake." Circ Res **104**(12): 1355-1363.
Clarke, M. C., S. Talib, N. L. Figg and M. R. Bennett (2010). "Vascular smooth muscle cell apoptosis induces interleukin-1-directed inflammation: effects of hyperlipidemia-mediated inhibition of phagocytosis." Circ Res **106**(2): 363-372.
Cohen, A. A., N. Geva-Zatorsky, E. Eden, M. Frenkel-Morgenstern, I. Issaeva, A. Sigal, R. Milo, C. Cohen-Saidon, Y. Liron, Z. Kam, L. Cohen, T. Danon, N. Perzov and U. Alon (2008). "Dynamic Proteomics of Individual Cancer Cells in Response to a Drug." Science **322**(5907): 1511.
Cole, J. E., E. Georgiou and C. Monaco (2010). "The expression and functions of toll-like receptors in atherosclerosis." Mediators Inflamm **2010**: 393946.
Collins, R. G., R. Velji, N. V. Guevara, M. J. Hicks, L. Chan and A. L. Beaudet (2000). "P-Selectin or intercellular adhesion molecule (ICAM)-1 deficiency substantially protects against atherosclerosis in apolipoprotein E-deficient mice." J Exp Med **191**(1): 189-194.
Collot-Teixeira, S., J. Martin, C. McDermott-Roe, R. Poston and J. L. McGregor (2007). "CD36 and macrophages in atherosclerosis." Cardiovasc Res **75**(3): 468-477.
Cooke, J. P. and P. S. Tsao (1994). "Is NO an endogenous antiatherogenic molecule?" Arterioscler Thromb **14**(5): 653-655.
Cox, D., P. Chang, Q. Zhang, P. G. Reddy, G. M. Bokoch and S. Greenberg (1997). "Requirements for Both Rac1 and Cdc42 in Membrane Ruffling and Phagocytosis in Leukocytes." Journal of Experimental Medicine **186**(9): 1487-1494.
Crisby, M., G. Nordin-Fredriksson, P. K. Shah, J. Yano, J. Zhu and J. Nilsson (2001). "Pravastatin treatment increases collagen content and decreases lipid content, inflammation, metalloproteinases, and cell death in human carotid plaques: implications for plaque stabilization." Circulation **103**(7): 926-933.
Crowley, M. T., P. S. Costello, C. J. Fitzer-Attas, M. Turner, F. Meng, C. Lowell, V. L. Tybulewicz and A. L. DeFranco (1997). "A critical role for Syk in signal transduction and phagocytosis mediated by Fcgamma receptors on macrophages." J Exp Med **186**(7): 1027-1039.
Cybulsky, M. I. and M. A. Gimbrone, Jr. (1991). "Endothelial expression of a mononuclear leukocyte adhesion molecule during atherogenesis." Science **251**(4995): 788-791.
Davies, M. J., P. D. Richardson, N. Woolf, D. R. Katz and J. Mann (1993). "Risk of thrombosis in human atherosclerotic plaques: role of extracellular lipid, macrophage, and smooth muscle cell content." Br Heart J **69**(5): 377-381.
de la Llera-Moya, M., G. H. Rothblat, J. M. Glick and J. M. England (1992). "Etoposide treatment suppresses atherosclerotic plaque development in cholesterol-fed rabbits." Arteriosclerosis and Thrombosis: A Journal of Vascular Biology **12**(11): 1363-1370.

Dehnavi, S., M. Sadeghi, P. E. Penson, M. Banach, T. Jamialahmadi and A. Sahebkar (2019). "The Role of Protein SUMOylation in the Pathogenesis of Atherosclerosis." Journal of clinical medicine **8**(11): 1856.
Dehnavi, S., M. Sadeghi, P. E. Penson, M. Banach, T. Jamialahmadi and A. Sahebkar (2019). "The Role of Protein SUMOylation in the Pathogenesis of Atherosclerosis." Journal of Clinical Medicine **8**(11).
Desterro, J. M., M. S. Rodriguez and R. T. Hay (1998). "SUMO-1 modification of IkappaBalpha inhibits NF-kappaB activation." Mol Cell **2**(2): 233-239.
Di Gregoli, K., N. Jenkins, R. Salter, S. White, C. Newby Andrew and L. Johnson Jason (2014). "MicroRNA-24 Regulates Macrophage Behavior and Retards Atherosclerosis." Arteriosclerosis, Thrombosis, and Vascular Biology **34**(9): 1990-2000.
Di Gregoli, K. and J. L. Johnson (2012). "Role of colony-stimulating factors in atherosclerosis." Current Opinion in Lipidology **23**(5).
Di Gregoli, K. and J. L. Johnson (2012). "Role of colony-stimulating factors in atherosclerosis." Curr Opin Lipidol **23**(5): 412-421.
Di Gregoli, K., N. Mohamad Anuar Nur, R. Bianco, J. White Stephen, C. Newby Andrew, J. George Sarah and L. Johnson Jason (2017). "MicroRNA-181b Controls Atherosclerosis and Aneurysms Through Regulation of TIMP-3 and Elastin." Circulation Research **120**(1): 49-65.
Di Gregoli, K., M. Somerville, R. Bianco, C. Thomas Anita, A. Frankow, C. Newby Andrew, J. George Sarah, L. Jackson Christopher and L. Johnson Jason (2020). "Galectin-3 Identifies a Subset of Macrophages With a Potential Beneficial Role in Atherosclerosis." Arteriosclerosis, Thrombosis, and Vascular Biology **40**(6): 1491-1509.
Dichtl, W., J. Dulak, M. Frick, H. F. Alber, S. P. Schwarzacher, M. P. Ares, J. Nilsson, O. Pachinger and F. Weidinger (2003). "HMG-CoA reductase inhibitors regulate inflammatory transcription factors in human endothelial and vascular smooth muscle cells." Arterioscler Thromb Vasc Biol **23**(1): 58-63.
Dickhout, J. G., S. Basseri and R. C. Austin (2008). "Macrophage Function and Its Impact on Atherosclerotic Lesion Composition, Progression, and Stability." Arteriosclerosis, Thrombosis, and Vascular Biology **28**(8): 1413-1415.
Doll, R., R. Peto, J. Boreham and I. Sutherland (2005). "Mortality from cancer in relation to smoking: 50 years observations on British doctors." Br J Cancer **92**(3): 426-429.
Dominguez, L. (2014). "Regulation of Actin Cytoskeleton Dynamics in Cells."
Dong, M., B. P. Yan, J. K. Liao, Y.-Y. Lam, G. W. K. Yip and C.-M. Yu (2010). "Rho-kinase inhibition: a novel therapeutic target for the treatment of cardiovascular diseases." Drug discovery today **15**(15-16): 622-629.
Dong, Z. M., S. M. Chapman, A. A. Brown, P. S. Frenette, R. O. Hynes and D. D. Wagner (1998). "The combined role of P- and E-selectins in atherosclerosis." The Journal of clinical investigation **102**(1): 145-152.
Elliott, M. R., F. B. Chekeni, P. C. Trampont, E. R. Lazarowski, A. Kadl, S. F. Walk, D. Park, R. I. Woodson, M. Ostankovich, P. Sharma, J. J. Lysiak, T. K. Harden, N. Leitinger and K. S. Ravichandran (2009). "Nucleotides released by apoptotic cells act as a find-me signal to promote phagocytic clearance." Nature **461**(7261): 282-286.
Ensan, S., A. Li, R. Besla, N. Degousee, J. Cosme, M. Roufaiel, E. A. Shikatani, M. El-Maklizi, J. W. Williams, L. Robins, C. Li, B. Lewis, T. J. Yun, J. S. Lee, P. Wieghofer, R. Khattar, K. Farrokhi, J. Byrne, M. Ouzounian, C. C. Zavitz, G. A. Levy, C. M. Bauer, P. Libby, M. Husain, F. K. Swirski, C. Cheong, M. Prinz, I. Hilgendorf, G. J. Randolph, S. Epelman, A. O. Gramolini, M. I. Cybulsky, B. B. Rubin and C. S. Robbins (2016). "Self-renewing resident arterial macrophages arise from embryonic CX3CR1(+) precursors and circulating monocytes immediately after birth." Nat Immunol **17**(2): 159-168.
Essig, M., G. Nguyen, D. Prié, B. Escoubet, J.-D. Sraer and G. Friedlander (1998). "3-Hydroxy-3-Methylglutaryl Coenzyme A Reductase Inhibitors Increase Fibrinolytic Activity in Rat Aortic Endothelial Cells." Circulation Research **83**(7): 683-690.
Fadok, V. A., D. L. Bratton, A. Konowal, P. W. Freed, J. Y. Westcott and P. M. Henson (1998). "Macrophages that have ingested apoptotic cells in vitro inhibit proinflammatory cytokine

production through autocrine/paracrine mechanisms involving TGF-beta, PGE2, and PAF." The Journal of Clinical Investigation **101**(4): 890-898.
Falk, E. (2006). "Pathogenesis of atherosclerosis." J Am Coll Cardiol **47**(8 Suppl): C7-12.
Falk, E., M. Nakano, J. F. Bentzon, A. V. Finn and R. Virmani (2013). "Update on acute coronary syndromes: the pathologists' view." European Heart Journal **34**(10): 719-728.
Felton, C. V., D. Crook, M. J. Davies and M. F. Oliver (1997). "Relation of plaque lipid composition and morphology to the stability of human aortic plaques." Arterioscler Thromb Vasc Biol **17**(7): 1337-1345.
Feng, J., J. Han, S. F. Pearce, R. L. Silverstein, A. M. Gotto, Jr., D. P. Hajjar and A. C. Nicholson (2000). "Induction of CD36 expression by oxidized LDL and IL-4 by a common signaling pathway dependent on protein kinase C and PPAR-gamma." J Lipid Res **41**(5): 688-696.
Feng, Y., Z. R. Cai, Y. Tang, G. Hu, J. Lu, D. He and S. Wang (2014). "TLR4/NF-κB signaling pathway-mediated and oxLDL-induced up-regulation of LOX-1, MCP-1, and VCAM-1 expressions in human umbilical vein endothelial cells." Genet Mol Res **13**(1): 680-695.
Feng, Z.-H., X.-H. Zhang, J.-Q. Zhao and J.-Z. Ma (2017). "Involvement of Rho-associated coiled-coil kinase signaling inhibition in TGF-β1/Smad2, 3 signal transduction in vitro." International journal of ophthalmology **10**(12): 1805-1811.
Fielding, C. J. and P. E. Fielding (1995). "Molecular physiology of reverse cholesterol transport." J Lipid Res **36**(2): 211-228.
Ford, H. Z., L. Zeboudj, G. S. D. Purvis, A. Ten Bokum, A. E. Zarebski, J. A. Bull, H. M. Byrne, M. R. Myerscough and D. R. Greaves (2019). "Efferocytosis perpetuates substance accumulation inside macrophage populations." Proc Biol Sci **286**(1904): 20190730.
Fraser, I., D. Hughes and S. Gordon (1993). "Divalent cation-independent macrophage adhesion inhibited by monoclonal antibody to murine scavenger receptor." Nature **364**(6435): 343-346.
Fukata, M., M. Nakagawa and K. Kaibuchi (2003). "Roles of Rho-family GTPases in cell polarisation and directional migration." Curr Opin Cell Biol **15**(5): 590-597.
Galvão, I., R. M. Athayde, D. A. Perez, A. C. Reis, L. Rezende, V. L. S. de Oliveira, B. M. Rezende, W. A. Gonçalves, L. P. Sousa, M. M. Teixeira and V. Pinho (2019). "ROCK Inhibition Drives Resolution of Acute Inflammation by Enhancing Neutrophil Apoptosis." Cells **8**(9).
Gao, C., W. Huang, K. Kanasaki and Y. Xu (2014). "The role of ubiquitination and sumoylation in diabetic nephropathy." BioMed research international **2014**: 160692-160692.
Gbelcová, H., S. Rimpelová, T. Ruml, M. Fenclová, V. Kosek, J. Hajšlová, H. Strnad, M. Kolář and L. Vítek (2017). "Variability in statin-induced changes in gene expression profiles of pancreatic cancer." Scientific reports **7**: 44219-44219.
Geissmann, F., C. Auffray, R. Palframan, C. Wirrig, A. Ciocca, L. Campisi, E. Narni-Mancinelli and G. Lauvau (2008). "Blood monocytes: distinct subsets, how they relate to dendritic cells, and their possible roles in the regulation of T-cell responses." Immunol Cell Biol **86**(5): 398-408.
Gentry, R., L. Ye and Y. Nemerson (1995). "Surface-mediated enzymatic reactions: simulations of tissue factor activation of factor X on a lipid surface." Biophys J **69**(2): 362-371.
Ghazizadeh, S., J. B. Bolen and H. B. Fleit (1995). "Tyrosine phosphorylation and association of Syk with Fc gamma RII in monocytic THP-1 cells." The Biochemical journal **305 (Pt 2)**(Pt 2): 669-674.
Glass, C. K. and J. L. Witztum (2001). "Atherosclerosis. the road ahead." Cell **104**(4): 503-516.
Gong, D., W. Shi, S. J. Yi, H. Chen, J. Groffen and N. Heisterkamp (2012). "TGFβ signaling plays a critical role in promoting alternative macrophage activation." BMC Immunol **13**: 31.
Gratchev, A., P. Guillot, N. Hakiy, O. Politz, C. E. Orfanos, K. Schledzewski and S. Goerdt (2001). "Alternatively Activated Macrophages Differentially Express Fibronectin and Its Splice Variants and the Extracellular Matrix Protein βIG-H3." Scandinavian Journal of Immunology **53**(4): 386-392.
Greenberg, S. (1995). "Signal transduction of phagocytosis." Trends Cell Biol **5**(3): 93-99.
Griffin, E. E., J. C. Ullery, B. E. Cox and W. G. Jerome (2005). "Aggregated LDL and lipid dispersions induce lysosomal cholesteryl ester accumulation in macrophage foam cells." J Lipid Res **46**(10): 2052-2060.

Grosheva, I., A. S. Haka, C. Qin, L. M. Pierini and F. R. Maxfield (2009). "Aggregated LDL in contact with macrophages induces local increases in free cholesterol levels that regulate local actin polymerization." Arteriosclerosis, thrombosis, and vascular biology **29**(10): 1615-1621.
Guilbert, J. J. (2003). "The world health report 2002 - reducing risks, promoting healthy life." Educ Health (Abingdon) **16**(2): 230.
Hackam, D. J., O. D. Rotstein, A. Schreiber, W. j. Zhang and S. Grinstein (1997). "Rho is required for the initiation of calcium signaling and phagocytosis by Fcgamma receptors in macrophages." The Journal of experimental medicine **186**(6): 955-966.
Hall (1994). "small GTP-Binding Proteins and the regulation of the actin cytoskeleton."
Hamilton, J. A. (2008). "Colony-stimulating factors in inflammation and autoimmunity." Nat Rev Immunol **8**(7): 533-544.
Hansson, G. K., A. K. Robertson and C. Söderberg-Nauclér (2006). "Inflammation and atherosclerosis." Annu Rev Pathol **1**: 297-329.
Harris, L. K., S. D. Smith, R. J. Keogh, R. L. Jones, P. N. Baker, M. Knöfler, J. E. Cartwright, G. S. J. Whitley and J. D. Aplin (2010). "Trophoblast- and Vascular Smooth Muscle Cell-Derived MMP-12 Mediates Elastolysis during Uterine Spiral Artery Remodeling." The American Journal of Pathology **177**(4): 2103-2115.
Henney, A. M., P. R. Wakeley, M. J. Davies, K. Foster, R. Hembry, G. Murphy and S. Humphries (1991). "Localization of stromelysin gene expression in atherosclerotic plaques by *in situ* hybridization." Proc Natl Acad Sci **88**: 8154-8158.
Hochreiter-Hufford, A. and K. S. Ravichandran (2013). "Clearing the dead: apoptotic cell sensing, recognition, engulfment, and digestion." Cold Spring Harb Perspect Biol **5**(1): a008748.
Hoffmann , P. R., A. M. deCathelineau , C. A. Ogden , Y. Leverrier , D. L. Bratton , D. L. Daleke , A. J. Ridley , V. A. Fadok and P. M. Henson (2001). "Phosphatidylserine (PS) induces PS receptor–mediated macropinocytosis and promotes clearance of apoptotic cells." Journal of Cell Biology **155**(4): 649-660.
Hofmann, W. A., A. Arduini, S. M. Nicol, C. J. Camacho, J. L. Lessard, F. V. Fuller-Pace and P. de Lanerolle (2009). "SUMOylation of nuclear actin." Journal of Cell Biology **186**(2): 193-200.
Hofnagel, O., B. Luechtenborg, G. Weissen-Plenz and H. Robenek (2007). "Statins and foam cell formation: impact on LDL oxidation and uptake of oxidized lipoproteins via scavenger receptors." Biochim Biophys Acta **1771**(9): 1117-1124.
Hohensinner, P. J., J. Baumgartner, B. Ebenbauer, B. Thaler, M. B. Fischer, K. Huber, W. S. Speidl and J. Wojta (2018). "Statin treatment reduces matrix degradation capacity of proinflammatory polarized macrophages." Vascular Pharmacology **110**: 49-54.
Hood, J. D. and D. A. Cheresh (2002). "Role of integrins in cell invasion and migration." Nat Rev Cancer **2**(2): 91-100.
Hu, Z., B. Hui, X. Hou, R. Liu, S. Sukhanov and X. Liu (2020) "APE1 inhibits foam cell formation from macrophages via LOX1 suppression." American journal of translational research **12**, 6559-6568.
Huang, W.-C., G. B. Sala-Newby, A. Susana, J. L. Johnson and A. C. Newby (2012). "Classical Macrophage Activation Up-Regulates Several Matrix Metalloproteinases through Mitogen Activated Protein Kinases and Nuclear Factor-κB." PLOS ONE **7**(8): e42507.
Iijima, M., Y. E. Huang and P. Devreotes (2002). "Temporal and spatial regulation of chemotaxis." Dev Cell **3**(4): 469-478.
Indik, Z., J. Park, X. Pan and A. Schreiber (1995). "Induction of phagocytosis by a protein tyrosine kinase." Blood **85**(5): 1175-1180.
Insull, W., Jr. (2009). "The pathology of atherosclerosis: plaque development and plaque responses to medical treatment." Am J Med **122**(1 Suppl): S3-s14.
Irvine, K. M., M. R. Andrews, M. A. Fernandez-Rojo, K. Schroder, C. J. Burns, S. Su, A. F. Wilks, R. G. Parton, D. A. Hume and M. J. Sweet (2009). "Colony-stimulating factor-1 (CSF-1) delivers a proatherogenic signal to human macrophages." J Leukoc Biol **85**(2): 278-288.

Jackson, W. D., T. W. Weinrich and K. J. Woollard (2016). "Very-low and low-density lipoproteins induce neutral lipid accumulation and impair migration in monocyte subsets." Scientific reports **6**: 20038-20038.
Jerome, W. G. (2006). "Advanced atherosclerotic foam cell formation has features of an acquired lysosomal storage disorder." Rejuvenation Res **9**(2): 245-255.
Jerome, W. G., L. K. Minor, J. M. Glick, G. H. Rothblat and J. C. Lewis (1991). "Lysosomal lipid accumulation in vascular smooth muscle cells." Exp Mol Pathol **54**(2): 144-158.
Jialal, I., D. Stein, D. Balis, S. M. Grundy, B. Adams-Huet and S. Devaraj (2001). "Effect of Hydroxymethyl Glutaryl Coenzyme A Reductase Inhibitor Therapy on High Sensitive C-Reactive Protein Levels." Circulation **103**(15): 1933-1935.
Johnson, J., K. Carson, H. Williams, S. Karanam, A. Newby, G. Angelini, S. George and C. Jackson (2005). "Plaque Rupture After Short Periods of Fat Feeding in the Apolipoprotein E–Knockout Mouse." Circulation **111**(11): 1422-1430.
Johnson Jason, L., L. Devel, B. Czarny, J. George Sarah, L. Jackson Christopher, V. Rogakos, F. Beau, A. Yiotakis, C. Newby Andrew and V. Dive (2011). "A Selective Matrix Metalloproteinase-12 Inhibitor Retards Atherosclerotic Plaque Development in Apolipoprotein E–Knockout Mice." Arteriosclerosis, Thrombosis, and Vascular Biology **31**(3): 528-535.
Johnson, J. L., S. J. George, A. C. Newby and C. L. Jackson (2005). "Divergent effects of matrix metalloproteinases 3, 7, 9, and 12 on atherosclerotic plaque stability in mouse brachiocephalic arteries." Proceedings of the National Academy of Sciences **102**(43): 15575.
Johnson, J. L., N. P. Jenkins, W.-C. Huang, K. Di Gregoli, G. B. Sala-Newby, V. P. W. Scholtes, F. L. Moll, G. Pasterkamp and A. C. Newby (2014). "Relationship of MMP-14 and TIMP-3 Expression with Macrophage Activation and Human Atherosclerotic Plaque Vulnerability." Mediators of Inflammation **2014**: 276457.
Johnson, J. L. and A. C. Newby (2009). "Macrophage heterogeneity in atherosclerotic plaques." Curr Opin Lipidol **20**(5): 370-378.
Jones, G. E. (2000). "Cellular signaling in macrophage migration and chemotaxis." J Leukoc Biol **68**(5): 593-602.
Julian, L. and M. F. Olson (2014). "Rho-associated coiled-coil containing kinases (ROCK): structure, regulation, and functions." Small GTPases **5**: e29846.
Jun, H. J., M. H. Hoang, S. K. Yeo, Y. Jia and S. J. Lee (2013). "Induction of ABCA1 and ABCG1 expression by the liver X receptor modulator cineole in macrophages." Bioorg Med Chem Lett **23**(2): 579-583.
Kadl, A., P. R. Sharma, W. Chen, R. Agrawal, A. K. Meher, S. Rudraiah, N. Grubbs, R. Sharma and N. Leitinger (2011). "Oxidized phospholipid-induced inflammation is mediated by Toll-like receptor 2." Free Radic Biol Med **51**(10): 1903-1909.
Kamal, A. H. M., J. K. Chakrabarty, S. M. N. Udden, M. H. Zaki and S. M. Chowdhury (2018). "Inflammatory Proteomic Network Analysis of Statin-treated and Lipopolysaccharide-activated Macrophages." Scientific reports **8**(1): 164-164.
Kamio, K., X. D. Liu, H. Sugiura, S. Togo, S. Kawasaki, X. Wang, Y. Ahn, C. Hogaboam and S. I. Rennard (2010). "Statins inhibit matrix metalloproteinase release from human lung fibroblasts." Eur Respir J **35**(3): 637-646.
Kapellos, T. S., L. Bonaguro, I. Gemünd, N. Reusch, A. Saglam, E. R. Hinkley and J. L. Schultze (2019). "Human Monocyte Subsets and Phenotypes in Major Chronic Inflammatory Diseases." Frontiers in Immunology **10**(2035).
Kaplan, G. (1977). "Differences in the mode of phagocytosis with Fc and C3 receptors in macrophages." Scand J Immunol **6**(8): 797-807.
Karp, G. (2010). Cell and Molecular Biology: Concepts and Experiments 6th Edition Binder Ready Version with Binder Ready Survey Flyer Set, John Wiley & Sons, Incorporated.
Karper, J. C., M. M. Ewing, K. L. Habets, M. R. de Vries, E. A. Peters, A. M. van Oeveren-Rietdijk, H. C. de Boer, J. F. Hamming, J. Kuiper, E. R. Kandimalla, N. La Monica, J. W. Jukema and P. H. Quax (2012).

"Blocking toll-like receptors 7 and 9 reduces postinterventional remodeling via reduced macrophage activation, foam cell formation, and migration." Arterioscler Thromb Vasc Biol **32**(8): e72-80.
Kato, T., H. Hashikabe, C. Iwata, K. Akimoto and Y. Hattori (2004). "RETRACTED: Statin blocks Rho/Rho-kinase signalling and disrupts the actin cytoskeleton: relationship to enhancement of LPS-mediated nitric oxide synthesis in vascular smooth muscle cells." Biochimica et Biophysica Acta (BBA) - Molecular Basis of Disease **1689**(3): 267-272.
Kattoor, A. J., A. Goel and J. L. Mehta (2019). "LOX-1: Regulation, Signaling and Its Role in Atherosclerosis." Antioxidants **8**(7).
Kattoor, A. J., A. Goel and J. L. Mehta (2019). "LOX-1: Regulation, Signaling and Its Role in Atherosclerosis." Antioxidants (Basel, Switzerland) **8**(7): 218.
Kidani, Y. and S. J. Bensinger (2012). "Liver X receptor and peroxisome proliferator-activated receptor as integrators of lipid homeostasis and immunity." Immunological Reviews **249**(1): 72-83.
Kim, K., D. Shim, J. S. Lee, K. Zaitsev, J. W. Williams, K. W. Kim, M. Y. Jang, H. Seok Jang, T. J. Yun, S. H. Lee, W. K. Yoon, A. Prat, N. G. Seidah, J. Choi, S. P. Lee, S. H. Yoon, J. W. Nam, J. K. Seong, G. T. Oh, G. J. Randolph, M. N. Artyomov, C. Cheong and J. H. Choi (2018). "Transcriptome Analysis Reveals Nonfoamy Rather Than Foamy Plaque Macrophages Are Proinflammatory in Atherosclerotic Murine Models." Circ Res **123**(10): 1127-1142.
Kim, Y. R. and K. H. Han (2013). "Familial hypercholesterolemia and the atherosclerotic disease." Korean Circ J **43**(6): 363-367.
Kita, T., Y. Hata, R. Arita, S. Kawahara, M. Miura, S. Nakao, Y. Mochizuki, H. Enaida, Y. Goto, H. Shimokawa, A. Hafezi-Moghadam and T. Ishibashi (2008). "Role of TGF-beta in proliferative vitreoretinal diseases and ROCK as a therapeutic target." Proceedings of the National Academy of Sciences of the United States of America **105**(45): 17504-17509.
Kojima, Y., K. Downing, R. Kundu, C. Miller, F. Dewey, H. Lancero, U. Raaz, L. Perisic, U. Hedin, E. Schadt, L. Maegdefessel, T. Quertermous and N. J. Leeper (2019). "Cyclin-dependent kinase inhibitor 2B regulates efferocytosis and atherosclerosis." The Journal of Clinical Investigation **124**(3): 1083-1097.
Kojima, Y., J. P. Volkmer, K. McKenna, M. Civelek, A. J. Lusis, C. L. Miller, D. Direnzo, V. Nanda, J. Ye, A. J. Connolly, E. E. Schadt, T. Quertermous, P. Betancur, L. Maegdefessel, L. P. Matic, U. Hedin, I. L. Weissman and N. J. Leeper (2016). "CD47-blocking antibodies restore phagocytosis and prevent atherosclerosis." Nature **536**(7614): 86-90.
Kojima, Y., I. L. Weissman and N. J. Leeper (2017). "The Role of Efferocytosis in Atherosclerosis." Circulation **135**(5): 476-489.
Kolodgie Frank, D., P. Burke Allen, G. Nakazawa and R. Virmani (2007). "Is Pathologic Intimal Thickening the Key to Understanding Early Plaque Progression in Human Atherosclerotic Disease?" Arteriosclerosis, Thrombosis, and Vascular Biology **27**(5): 986-989.
Krämer, O. and R. Moriggl (2012). "Acetylation and sumoylation control STAT5 activation antagonistically." JAK-STAT **1**: 203-207.
Kratofil Rachel, M., P. Kubes and F. Deniset Justin (2017). "Monocyte Conversion During Inflammation and Injury." Arteriosclerosis, Thrombosis, and Vascular Biology **37**(1): 35-42.
Ku, C. S., Y. Park, S. L. Coleman and J. Lee (2012). "Unsaturated fatty acids repress expression of ATP binding cassette transporter A1 and G1 in RAW 264.7 macrophages." J Nutr Biochem **23**(10): 1271-1276.
Kunjathoor, V. V., M. Febbraio, E. A. Podrez, K. J. Moore, L. Andersson, S. Koehn, J. S. Rhee, R. Silverstein, H. F. Hoff and M. W. Freeman (2002). "Scavenger receptors class A-I/II and CD36 are the principal receptors responsible for the uptake of modified low density lipoprotein leading to lipid loading in macrophages." J Biol Chem **277**(51): 49982-49988.
Lau, C. L., R. D. O'Shea, B. V. Broberg, L. Bischof and P. M. Beart (2011). "The Rho kinase inhibitor Fasudil up-regulates astrocytic glutamate transport subsequent to actin remodelling in murine cultured astrocytes." British journal of pharmacology **163**(3): 533-545.

Lauffenburger, D. A. and A. F. Horwitz (1996). "Cell migration: a physically integrated molecular process." Cell **84**(3): 359-369.
Laufs, U., V. La Fata, J. Plutzky and K. Liao James (1998). "Upregulation of Endothelial Nitric Oxide Synthase by HMG CoA Reductase Inhibitors." Circulation **97**(12): 1129-1135.
Le, N.-T., J. P. Corsetti, J. L. Dehoff-Sparks, C. E. Sparks, K. Fujiwara and J.-I. Abe (2012). "Reactive Oxygen Species, SUMOylation, and Endothelial Inflammation." International journal of inflammation **2012**: 678190-678190.
Le, N.-T., U. G. Sandhu, R. A. Quintana-Quezada, N. M. Hoang, K. Fujiwara and J.-I. Abe (2017). "Flow signaling and atherosclerosis." Cellular and molecular life sciences : CMLS **74**(10): 1835-1858.
Le, N. T., U. G. Sandhu, R. A. Quintana-Quezada, N. M. Hoang, K. Fujiwara and J. I. Abe (2017). "Flow signaling and atherosclerosis." Cell Mol Life Sci **74**(10): 1835-1858.
Lee, S. H. and R. Dominguez (2010). "Regulation of actin cytoskeleton dynamics in cells." Molecules and cells **29**(4): 311-325.
Lee, S. M., J. Moon, Y. Cho, J. H. Chung and M. J. Shin (2013). "Quercetin up-regulates expressions of peroxisome proliferator-activated receptor gamma, liver X receptor alpha, and ATP binding cassette transporter A1 genes and increases cholesterol efflux in human macrophage cell line." Nutr Res **33**(2): 136-143.
Leeper, N. J., A. Raiesdana, Y. Kojima, R. K. Kundu, H. Cheng, L. Maegdefessel, R. Toh, G. O. Ahn, Z. A. Ali, D. R. Anderson, C. L. Miller, S. C. Roberts, J. M. Spin, P. E. de Almeida, J. C. Wu, B. Xu, K. Cheng, M. Quertermous, S. Kundu, K. E. Kortekaas, E. Berzin, K. P. Downing, R. L. Dalman, P. S. Tsao, E. E. Schadt, G. K. Owens and T. Quertermous (2013). "Loss of CDKN2B promotes p53-dependent smooth muscle cell apoptosis and aneurysm formation." Arterioscler Thromb Vasc Biol **33**(1): e1-e10.
Lehtonen, A., S. Matikainen, M. Miettinen and I. Julkunen (2002). "Granulocyte-macrophage colony-stimulating factor (GM-CSF)-induced STAT5 activation and target-gene expression during human monocyte/macrophage differentiation." J Leukoc Biol **71**(3): 511-519.
Leonard, W. J. and J. J. O'Shea (1998). "Jaks and STATs: biological implications." Annu Rev Immunol **16**: 293-322.
Letterio, J. J. and A. B. Roberts (1998). "Regulation of immune responses by TGF-beta." Annu Rev Immunol **16**: 137-161.
Lewis, G. F. and D. J. Rader (2005). "New insights into the regulation of HDL metabolism and reverse cholesterol transport." Circ Res **96**(12): 1221-1232.
Ley, K., Y. I. Miller and C. C. Hedrick (2011). "Monocyte and macrophage dynamics during atherogenesis." Arteriosclerosis, thrombosis, and vascular biology **31**(7): 1506-1516.
Li, A. C., C. J. Binder, A. Gutierrez, K. K. Brown, C. R. Plotkin, J. W. Pattison, A. F. Valledor, R. A. Davis, T. M. Willson, J. L. Witztum, W. Palinski and C. K. Glass (2004). "Differential inhibition of macrophage foam-cell formation and atherosclerosis in mice by PPARalpha, beta/delta, and gamma." J Clin Invest **114**(11): 1564-1576.
Li, A. C. and C. K. Glass (2002). "The macrophage foam cell as a target for therapeutic intervention." Nature Medicine **8**(11): 1235-1242.
Li, X.-D., Y.-P. Wu, S.-H. Chen, Y.-C. Liang, T.-T. Lin, T. Lin, Y. Wei, X.-Y. Xue, Q.-S. Zheng and N. Xu (2018). "Fasudil inhibits actin polymerization and collagen synthesis and induces apoptosis in human urethral scar fibroblasts via the Rho/ROCK pathway." Drug design, development and therapy **12**: 2707-2713.
Li, Y.-S. J., J. H. Haga and S. Chien (2005). "Molecular basis of the effects of shear stress on vascular endothelial cells." Journal of Biomechanics **38**(10): 1949-1971.
Libby, P., P. M. Ridker and A. Maseri (2002). "Inflammation and atherosclerosis." Circulation **105**(9): 1135-1143.
Linder, S. and M. Aepfelbacher (2003). "Podosomes: adhesion hot-spots of invasive cells." Trends Cell Biol **13**(7): 376-385.

Linton, M. F., P. G. Yancey, S. S. Davies, W. G. Jerome, E. F. Linton, W. L. Song, A. C. Doran and K. C. Vickers (2000). The Role of Lipids and Lipoproteins in Atherosclerosis. Endotext. K. R. Feingold, B. Anawalt, A. Boyce et al. South Dartmouth (MA), MDText.com, Inc.

Litherland, S., K. Grebe, N. Belkin, E. Paek, J. Elf, M. Atkinson, L. Morel, M. Clare-Salzler and M. McDuffie (2005). "Nonobese Diabetic Mouse Congenic Analysis Reveals Chromosome 11 Locus Contributing to Diabetes Susceptibility, Macrophage STAT5 Dysfunction, and Granulocyte-Macrophage Colony-Stimulating Factor Overproduction." Journal of immunology (Baltimore, Md. : 1950) **175**: 4561-4565.
Litherland, S. A., T. X. Xie, K. M. Grebe, A. Davoodi-Semiromi, J. Elf, N. S. Belkin, L. L. Moldawer and M. J. Clare-Salzler (2005). "Signal transduction activator of transcription 5 (STAT5) dysfunction in autoimmune monocytes and macrophages." J Autoimmun **24**(4): 297-310.
Liu, C., Y. Li, J. Yu, L. Feng, S. Hou, Y. Liu, M. Guo, Y. Xie, J. Meng, H. Zhang, B. Xiao and C. Ma (2013). "Targeting the shift from M1 to M2 macrophages in experimental autoimmune encephalomyelitis mice treated with fasudil." PLoS One **8**(2): e54841.
Liu, L., P. Zeng, X. Yang, Y. Duan, W. Zhang, C. Ma, X. Zhang, S. Yang, X. Li, J. Yang, Y. Liang, H. Han, Y. Zhu, J. Han and Y. Chen (2018). "Inhibition of Vascular Calcification." Arterioscler Thromb Vasc Biol **38**(10): 2382-2395.
Liu, X. Y., Q. Lu, X. P. Ouyang, S. L. Tang, G. J. Zhao, Y. C. Lv, P. P. He, H. J. Kuang, Y. Y. Tang, Y. Fu, D. W. Zhang and C. K. Tang (2013). "Apelin-13 increases expression of ATP-binding cassette transporter A1 via activating protein kinase C alpha signaling in THP-1 macrophage-derived foam cells." Atherosclerosis **226**(2): 398-407.
Lodish, H. F., A. Berk, C. Kaiser, M. Krieger, M. P. Scott, A. Bretscher, H. L. Ploegh and P. T. Matsudaira (2008). Molecular cell biology. New York, W.H. Freeman.
Luan, Z., J. Chase Alex and C. Newby Andrew (2003). "Statins Inhibit Secretion of Metalloproteinases-1, -2, -3, and -9 From Vascular Smooth Muscle Cells and Macrophages." Arteriosclerosis, Thrombosis, and Vascular Biology **23**(5): 769-775.
Lv, Y. C., Y. Y. Tang, J. Peng, G. J. Zhao, J. Yang, F. Yao, X. P. Ouyang, P. P. He, W. Xie, Y. L. Tan, M. Zhang, D. Liu, D. P. Tang, F. S. Cayabyab, X. L. Zheng, D. W. Zhang, G. P. Tian and C. K. Tang (2014). "MicroRNA-19b promotes macrophage cholesterol accumulation and aortic atherosclerosis by targeting ATP-binding cassette transporter A1." Atherosclerosis **236**(1): 215-226.
Magné, S., S. Caron, M. Charon, M.-C. Rouyez and I. Dusanter-Fourt (2003). "STAT5 and Oct-1 Form a Stable Complex That Modulates Cyclin D1 Expression." Molecular and Cellular Biology **23**(24): 8934.
Magné, S., S. Caron, M. Charon, M. C. Rouyez and I. Dusanter-Fourt (2003). "STAT5 and Oct-1 form a stable complex that modulates cyclin D1 expression." Mol Cell Biol **23**(24): 8934-8945.
Maguire, E. M., S. W. A. Pearce and Q. Xiao (2019). "Foam cell formation: A new target for fighting atherosclerosis and cardiovascular disease." Vascular Pharmacology **112**: 54-71.
Mallat, Z., S. Besnard, M. Duriez, V. Deleuze, F. Emmanuel, F. Bureau Michel, F. Soubrier, B. Esposito, H. Duez, C. Fievet, B. Staels, N. Duverger, D. Scherman and A. Tedgui (1999). "Protective Role of Interleukin-10 in Atherosclerosis." Circulation Research **85**(8): e17-e24.
Mallat, Z., A. Gojova, V. Sauzeau, V. Brun, J. S. Silvestre, B. Esposito, R. Merval, H. Groux, G. Loirand and A. Tedgui (2003). "Rho-associated protein kinase contributes to early atherosclerotic lesion formation in mice." Circ Res **93**(9): 884-888.
Mallat, Z., B. Hugel, J. Ohan, G. Lesèche, J. M. Freyssinet and A. Tedgui (1999). "Shed membrane microparticles with procoagulant potential in human atherosclerotic plaques: a role for apoptosis in plaque thrombogenicity." Circulation **99**(3): 348-353.
Mangan, D. F. and S. M. Wahl (1991). "Differential regulation of human monocyte programmed cell death (apoptosis) by chemotactic factors and pro-inflammatory cytokines." The Journal of Immunology **147**(10): 3408.

Mantovani, A., A. Sica, S. Sozzani, P. Allavena, A. Vecchi and M. Locati (2004). "The chemokine system in diverse forms of macrophage activation and polarization." Trends Immunol **25**(12): 677-686.
Martin, G., H. Duez, C. Blanquart, V. Berezowski, P. Poulain, J. C. Fruchart, J. Najib-Fruchart, C. Glineur and B. Staels (2001). "Statin-induced inhibition of the Rho-signaling pathway activates PPARalpha and induces HDL apoA-I." The Journal of clinical investigation **107**(11): 1423-1432.
Martin, S. and R. G. Parton (2006). "Lipid droplets: a unified view of a dynamic organelle." Nat Rev Mol Cell Biol **7**(5): 373-378.
Martinet, W., D. M. Schrijvers and G. R. De Meyer (2011). "Necrotic cell death in atherosclerosis." Basic Res Cardiol **106**(5): 749-760.
Martinez, F. O., S. Gordon, M. Locati and A. Mantovani (2006). "Transcriptional Profiling of the Human Monocyte-to-Macrophage Differentiation and Polarization: New Molecules and Patterns of Gene Expression." The Journal of Immunology **177**(10): 7303.
Martinez, J., R. K. S. Malireddi, Q. Lu, L. D. Cunha, S. Pelletier, S. Gingras, R. Orchard, J.-L. Guan, H. Tan, J. Peng, T.-D. Kanneganti, H. W. Virgin and D. R. Green (2015). "Molecular characterization of LC3-associated phagocytosis reveals distinct roles for Rubicon, NOX2 and autophagy proteins." Nature Cell Biology **17**(7): 893-906.
Mauldin, J. P., S. Srinivasan, A. Mulya, A. Gebre, J. S. Parks, A. Daugherty and C. C. Hedrick (2006). "Reduction in ABCG1 in Type 2 Diabetic Mice Increases Macrophage Foam Cell Formation*." Journal of Biological Chemistry **281**(30): 21216-21224.
Mignatti, P. and D. B. Rifkin (1993). "Biology and biochemistry of proteinases in tumor invasion." Physiol Rev **73**(1): 161-195.
Miki, H., T. Sasaki, Y. Takai and T. Takenawa (1998). "Induction of filopodium formation by a WASP-related actin-depolymerizing protein N-WASP." Nature **391**(6662): 93-96.
Miller, Y. I., D. S. Worrall, C. D. Funk, J. R. Feramisco and J. L. Witztum (2003). "Actin Polymerization in Macrophages in Response to Oxidized LDL and Apoptotic Cells: Role of 12/15-Lipoxygenase and Phosphoinositide 3-Kinase." Molecular Biology of the Cell **14**(10): 4196-4206.
Mo, Y. Y., Y. Yu, Z. Shen and W. T. Beck (2002). "Nucleolar delocalization of human topoisomerase I in response to topotecan correlates with sumoylation of the protein." J Biol Chem **277**(4): 2958-2964.
Moore, K. J., V. V. Kunjathoor, S. L. Koehn, J. J. Manning, A. A. Tseng, J. M. Silver, M. McKee and M. W. Freeman (2005). "Loss of receptor-mediated lipid uptake via scavenger receptor A or CD36 pathways does not ameliorate atherosclerosis in hyperlipidemic mice." J Clin Invest **115**(8): 2192-2201.
Morimoto, K., W. J. Janssen, M. B. Fessler, Y. Q. Xiao, K. A. McPhillips, V. M. Borges, J. A. Kench, P. M. Henson and R. W. Vandivier (2006). "Statins enhance clearance of apoptotic cells through modulation of Rho-GTPases." Proc Am Thorac Soc **3**(6): 516-517.
Moriwaki, H., N. Kume, T. Sawamura, T. Aoyama, H. Hoshikawa, H. Ochi, E. Nishi, T. Masaki and T. Kita (1998). "Ligand Specificity of LOX-1, a Novel Endothelial Receptor for Oxidized Low Density Lipoprotein." Arteriosclerosis, Thrombosis, and Vascular Biology **18**(10): 1541-1547.
Mosig, S., K. Rennert, P. Büttner, S. Krause, D. Lütjohann, M. Soufi, R. Heller and H. Funke (2008) "Monocytes of patients with familial hypercholesterolemia show alterations in cholesterol metabolism." BMC medical genomics **1**, 60 DOI: 10.1186/1755-8794-1-60.
Mosig, S., K. Rennert, S. Krause, J. Kzhyshkowska, K. Neunübel, R. Heller and H. Funke (2009). "Different functions of monocyte subsets in familial hypercholesterolemia: potential function of CD14+ CD16+ monocytes in detoxification of oxidized LDL." Faseb j **23**(3): 866-874.
Mosig, S., K. Rennert, S. Krause, J. Kzhyshkowska, K. Neunübel, R. Heller and H. Funke (2009). "Different functions of monocyte subsets in familial hypercholesterolemia: potential function of CD14+CD16+ monocytes in detoxification of oxidized LDL." The FASEB Journal **23**(3): 866-874.
Mouchemore, K. A. and F. J. Pixley (2012). "CSF-1 signaling in macrophages: pleiotrophy through phosphotyrosine-based signaling pathways." Crit Rev Clin Lab Sci **49**(2): 49-61.

Munteanu, A., M. Taddei, I. Tamburini, E. Bergamini, A. Azzi and J. M. Zingg (2006). "Antagonistic effects of oxidized low density lipoprotein and alpha-tocopherol on CD36 scavenger receptor expression in monocytes: involvement of protein kinase B and peroxisome proliferator-activated receptor-gamma." J Biol Chem **281**(10): 6489-6497.
Murphy, A. J., M. Akhtari, S. Tolani, T. Pagler, N. Bijl, C. L. Kuo, M. Wang, M. Sanson, S. Abramowicz, C. Welch, A. E. Bochem, J. A. Kuivenhoven, L. Yvan-Charvet and A. R. Tall (2011). "ApoE regulates hematopoietic stem cell proliferation, monocytosis, and monocyte accumulation in atherosclerotic lesions in mice." J Clin Invest **121**(10): 4138-4149.
Murphy, A. J., K. J. Woollard, A. Hoang, N. Mukhamedova, R. A. Stirzaker, S. P. McCormick, A. T. Remaley, D. Sviridov and J. Chin-Dusting (2008). "High-density lipoprotein reduces the human monocyte inflammatory response." Arterioscler Thromb Vasc Biol **28**(11): 2071-2077.
Murphy, Jane E., D. Tacon, Philip R. Tedbury, Jonathan M. Hadden, S. Knowling, T. Sawamura, M. Peckham, Simon E. V. Phillips, John H. Walker and S. Ponnambalam (2005). "LOX-1 scavenger receptor mediates calcium-dependent recognition of phosphatidylserine and apoptotic cells." Biochemical Journal **393**(1): 107-115.
Myasoedova, V. A., D. A. Chistiakov, A. V. Grechko and A. N. Orekhov (2018). "Matrix metalloproteinases in pro-atherosclerotic arterial remodeling." Journal of Molecular and Cellular Cardiology **123**: 159-167.
Nacu, N., I. G. Luzina, K. Highsmith, V. Lockatell, K. Pochetuhen, Z. A. Cooper, M. P. Gillmeister, N. W. Todd and S. P. Atamas (2008). "Macrophages produce TGF-beta-induced (beta-ig-h3) following ingestion of apoptotic cells and regulate MMP14 levels and collagen turnover in fibroblasts." Journal of immunology (Baltimore, Md. : 1950) **180**(7): 5036-5044.
Nagenborg, J., P. Goossens, E. A. L. Biessen and M. M. P. C. Donners (2017). "Heterogeneity of atherosclerotic plaque macrophage origin, phenotype and functions: Implications for treatment." European Journal of Pharmacology **816**: 14-24.
Nakagawa, K. and Y. Nakashima (2018). "Pathologic intimal thickening in human atherosclerosis is formed by extracellular accumulation of plasma-derived lipids and dispersion of intimal smooth muscle cells." Atherosclerosis **274**: 235-242.
Nakashima, Y., H. Fujii, S. Sumiyoshi, N. Wight Thomas and K. Sueishi (2007). "Early Human Atherosclerosis." Arteriosclerosis, Thrombosis, and Vascular Biology **27**(5): 1159-1165.
Nakaya, M., M. Kitano, M. Matsuda and S. Nagata (2008). "Spatiotemporal activation of Rac1 for engulfment of apoptotic cells." Proceedings of the National Academy of Sciences **105**(27): 9198-9203.
Nakaya, M., M. Tanaka, Y. Okabe, R. Hanayama and S. Nagata (2006). "Opposite effects of rho family GTPases on engulfment of apoptotic cells by macrophages." J Biol Chem **281**(13): 8836-8842.
Navab, M., J. A. Berliner, A. D. Watson, S. Y. Hama, M. C. Territo, A. J. Lusis, D. M. Shih, B. J. Van Lenten, J. S. Frank, L. L. Demer, P. A. Edwards and A. M. Fogelman (1996). "The Yin and Yang of oxidation in the development of the fatty streak. A review based on the 1994 George Lyman Duff Memorial Lecture." Arterioscler Thromb Vasc Biol **16**(7): 831-842.
Nichols, B. A., D. F. Bainton and M. G. Farquhar (1971). "Differentiation of monocytes. Origin, nature, and fate of their azurophil granules." The Journal of cell biology **50**(2): 498-515.
Nikiforov, N. G., R. Wetzker, M. V. Kubekina, A. V. Petukhova, T. V. Kirichenko and A. N. Orekhov (2019). "Trained Circulating Monocytes in Atherosclerosis: Ex Vivo Model Approach." Frontiers in Pharmacology **10**(725).
Nissen, S. E., T. Tsunoda, E. M. Tuzcu, P. Schoenhagen, C. J. Cooper, M. Yasin, G. M. Eaton, M. A. Lauer, W. S. Sheldon, C. L. Grines, S. Halpern, T. Crowe, J. C. Blankenship and R. Kerensky (2003). "Effect of recombinant ApoA-I Milano on coronary atherosclerosis in patients with acute coronary syndromes: a randomized controlled trial." Jama **290**(17): 2292-2300.
Nofer, J.-R., B. Kehrel, M. Fobker, B. Levkau, G. Assmann and A. v. Eckardstein (2002). "HDL and arteriosclerosis: beyond reverse cholesterol transport." Atherosclerosis **161**(1): 1-16.

Oesterle, A., U. Laufs and J. K. Liao (2017). "Pleiotropic Effects of Statins on the Cardiovascular System." Circ Res **120**(1): 229-243.
Oppi, S., S. Stein, V. Marzolla, E. Osto, Z. Rancic, T. F. Luscher, M. Oosterveer and S. Stein (2019). "P1941The nuclear receptor corepressor 1 blocks CD36-mediated foam cell formation in atherogenesis." European Heart Journal **40**(Supplement_1).
Out, R., M. Hoekstra, R. B. Hildebrand, J. K. Kruit, I. Meurs, Z. Li, F. Kuipers, T. J. Van Berkel and M. Van Eck (2006). "Macrophage ABCG1 deletion disrupts lipid homeostasis in alveolar macrophages and moderately influences atherosclerotic lesion development in LDL receptor-deficient mice." Arterioscler Thromb Vasc Biol **26**(10): 2295-2300.
Palecek, S. P., J. C. Loftus, M. H. Ginsberg, D. A. Lauffenburger and A. F. Horwitz (1997). "Integrin-ligand binding properties govern cell migration speed through cell-substratum adhesiveness." Nature **385**(6616): 537-540.
Park, S.-H., J. H. Y. Park, J.-S. Kang and Y.-H. Kang (2003). "Involvement of transcription factors in plasma HDL protection against TNF-alpha-induced vascular cell adhesion molecule-1 expression." The international journal of biochemistry & cell biology **35**(2): 168-182.
Pergola, C., K. Schubert, S. Pace, J. Ziereisen, F. Nikels, O. Scherer, S. Hüttel, S. Zahler, A. M. Vollmar, C. Weinigel, S. Rummler, R. Müller, M. Raasch, A. Mosig, A. Koeberle and O. Werz (2017). "Modulation of actin dynamics as potential macrophage subtype-targeting anti-tumour strategy." Scientific Reports **7**(1): 41434.
Perk, J., G. De Backer, H. Gohlke, I. Graham, Z. Reiner, M. Verschuren, C. Albus, P. Benlian, G. Boysen, R. Cifkova, C. Deaton, S. Ebrahim, M. Fisher, G. Germano, R. Hobbs, A. Hoes, S. Karadeniz, A. Mezzani, E. Prescott, L. Ryden, M. Scherer, M. Syvänne, W. J. Scholte op Reimer, C. Vrints, D. Wood, J. L. Zamorano and F. Zannad (2012). "European Guidelines on cardiovascular disease prevention in clinical practice (version 2012). The Fifth Joint Task Force of the European Society of Cardiology and Other Societies on Cardiovascular Disease Prevention in Clinical Practice (constituted by representatives of nine societies and by invited experts)." Eur Heart J **33**(13): 1635-1701.
Petrie, R. J., A. D. Doyle and K. M. Yamada (2009). "Random versus directionally persistent cell migration." Nat Rev Mol Cell Biol **10**(8): 538-549.
Pixley, F. J. (2012). "Macrophage Migration and Its Regulation by CSF-1." Int J Cell Biol **2012**: 501962.
Pixley, F. J. and E. R. Stanley (2004). "CSF-1 regulation of the wandering macrophage: complexity in action." Trends Cell Biol **14**(11): 628-638.
Pommier, Y. (2006). "Topoisomerase I inhibitors: camptothecins and beyond." Nat Rev Cancer **6**(10): 789-802.
Porreca, E., C. Di Febbo, G. Baccante, M. Di Nisio and F. Cuccurullo (2002). "Increased transforming growth factor-beta₁circulating levels and production in human monocytes after 3-hydroxy-3-methyl-glutaryl-coenzyme a reductase inhibition with pravastatin." Journal of the American College of Cardiology **39**(11): 1752.
Potteaux, S., B. Esposito, O. van Oostrom, V. Brun, P. Ardouin, H. Groux, A. Tedgui and Z. Mallat (2004). "Leukocyte-derived interleukin 10 is required for protection against atherosclerosis in low-density lipoprotein receptor knockout mice." Arterioscler Thromb Vasc Biol **24**(8): 1474-1478.
Qin, Z. (2012). "The use of THP-1 cells as a model for mimicking the function and regulation of monocytes and macrophages in the vasculature." Atherosclerosis **221**(1): 2-11.
Qualmann, B. and H. Mellor (2003). "Regulation of endocytic traffic by Rho GTPases." The Biochemical journal **371**(Pt 2): 233-241.
Rao, J., Z. Ye, H. Tang, C. Wang, H. Peng, W. Lai, Y. Li, W. Huang and T. Lou (2017). "The RhoA/ROCK Pathway Ameliorates Adhesion and Inflammatory Infiltration Induced by AGEs in Glomerular Endothelial Cells." Sci Rep **7**: 39727.
Rauch, U., J. I. Osende, V. Fuster, J. J. Badimon, Z. Fayad and J. H. Chesebro (2001). "Thrombus Formation on Atherosclerotic Plaques: Pathogenesis and Clinical Consequences." Annals of Internal Medicine **134**(3): 224-238.
Ravetch, J. V. (1997). "Fc receptors." Curr Opin Immunol **9**(1): 121-125.

Ravichandran, K. S. (2010). "Find-me and eat-me signals in apoptotic cell clearance: progress and conundrums." J Exp Med **207**(9): 1807-1817.
Ravichandran, K. S. and U. Lorenz (2007). "Engulfment of apoptotic cells: signals for a good meal." Nat Rev Immunol **7**(12): 964-974.
Ridker Paul, M., N. Rifai and P. Lowenthal Susan (2001). "Rapid Reduction in C-Reactive Protein With Cerivastatin Among 785 Patients With Primary Hypercholesterolemia." Circulation **103**(9): 1191-1193.
Ridker, P. M., N. Rifai, M. Clearfield, J. R. Downs, S. E. Weis, J. S. Miles and A. M. Gotto, Jr. (2001). "Measurement of C-reactive protein for the targeting of statin therapy in the primary prevention of acute coronary events." N Engl J Med **344**(26): 1959-1965.
Ridley, A. J. (2011). "Life at the leading edge." Cell **145**(7): 1012-1022.
Ridley, A. J. and A. Hall (1992). "The small GTP-binding protein rho regulates the assembly of focal adhesions and actin stress fibers in response to growth factors." Cell **70**(3): 389-399.
Rivero, F., B. Köppel, B. Peracino, S. Bozzaro, F. Siegert, C. J. Weijer, M. Schleicher, R. Albrecht and A. A. Noegel (1996). "The role of the cortical cytoskeleton: F-actin crosslinking proteins protect against osmotic stress, ensure cell size, cell shape and motility, and contribute to phagocytosis and development." J Cell Sci **109 (Pt 11)**: 2679-2691.
Robati, M., D. Holtz and C. J. Dunton (2008). "A review of topotecan in combination chemotherapy for advanced cervical cancer." Ther Clin Risk Manag **4**(1): 213-218.
Robbins, C. S., I. Hilgendorf, G. F. Weber, I. Theurl, Y. Iwamoto, J. L. Figueiredo, R. Gorbatov, G. K. Sukhova, L. M. Gerhardt, D. Smyth, C. C. Zavitz, E. A. Shikatani, M. Parsons, N. van Rooijen, H. Y. Lin, M. Husain, P. Libby, M. Nahrendorf, R. Weissleder and F. K. Swirski (2013). "Local proliferation dominates lesional macrophage accumulation in atherosclerosis." Nat Med **19**(9): 1166-1172.
Robenek, H., O. Hofnagel, I. Buers, M. J. Robenek, D. Troyer and N. J. Severs (2006). "Adipophilin-enriched domains in the ER membrane are sites of lipid droplet biogenesis." J Cell Sci **119**(Pt 20): 4215-4224.
Robertson, A.-K. L., M. Rudling, X. Zhou, L. Gorelik, R. A. Flavell and G. K. Hansson (2003). "Disruption of TGF-beta signaling in T cells accelerates atherosclerosis." The Journal of clinical investigation **112**(9): 1342-1350.
Rodríguez-Vita, J., E. Sánchez-Galán, B. Santamaría, E. Sánchez-López, R. Rodrigues-Díez, L. M. Blanco-Colio, J. Egido, A. Ortiz and M. Ruiz-Ortega (2008). "Essential role of TGF-beta/Smad pathway on statin dependent vascular smooth muscle cell regulation." PloS one **3**(12): e3959-e3959.
Rogers, P. D., J. Thornton, K. S. Barker, D. O. McDaniel, G. S. Sacks, E. Swiatlo and L. S. McDaniel (2003). "Pneumolysin-Dependent and -Independent Gene Expression Identified by cDNA Microarray Analysis of THP-1 Human Mononuclear Cells Stimulated by Streptococcus pneumoniae." Infection and Immunity **71**(4): 2087.
Ross, R. (1999). "Atherosclerosis — An Inflammatory Disease." New England Journal of Medicine **340**(2): 115-126.
Rőszer, T. (2015). "Understanding the Mysterious M2 Macrophage through Activation Markers and Effector Mechanisms." Mediators of Inflammation **2015**: 816460.
Rougerie, P., V. Miskolci and D. Cox (2013). "Generation of membrane structures during phagocytosis and chemotaxis of macrophages: role and regulation of the actin cytoskeleton." Immunological Reviews **256**(1): 222-239.
Rudijanto, A. (2010). "Calcium channel blocker (diltiazem) inhibits apoptosis of vascular smooth muscle cell exposed to high glucose concentration through lectin-like oxidized low density lipoprotein receptor-1 (LOX-1) pathway." Acta medica Indonesiana **42**: 59-65.
Samarakoon, R., J. M. Overstreet and P. J. Higgins (2013). "TGF-β signaling in tissue fibrosis: redox controls, target genes and therapeutic opportunities." Cell Signal **25**(1): 264-268.
Sasaki, Y., K. Ohsawa, H. Kanazawa, S. Kohsaka and Y. Imai (2001). "Iba1 is an actin-cross-linking protein in macrophages/microglia." Biochem Biophys Res Commun **286**(2): 292-297.

Saunders, R. A., K. Fujii, L. Alabanza, R. Ravatn, T. Kita, K. Kudoh, M. Oka and K.-V. Chin (2010). "Altered phospholipid transfer protein gene expression and serum lipid profile by topotecan." Biochemical pharmacology **80**(3): 362-369.
Sawada, N. and J. K. Liao (2013). "Rho/Rho-Associated Coiled-Coil Forming Kinase Pathway as Therapeutic Targets for Statins in Atherosclerosis." Antioxidants & Redox Signaling **20**(8): 1251-1267.
Sawamura, T., N. Kume, T. Aoyama, H. Moriwaki, H. Hoshikawa, Y. Aiba, T. Tanaka, S. Miwa, Y. Katsura, T. Kita and T. Masaki (1997). "An endothelial receptor for oxidized low-density lipoprotein." Nature **386**(6620): 73-77.
Schlitt, A., G. H. Heine, S. Blankenberg, C. Espinola-Klein, J. F. Dopheide, C. Bickel, K. J. Lackner, M. Iz, J. Meyer, H. Darius and H. J. Rupprecht (2004). "CD14+CD16+ monocytes in coronary artery disease and their relationship to serum TNF-alpha levels." Thromb Haemost **92**(2): 419-424.
Schmitz, G., T. Langmann and S. Heimerl (2001). "Role of ABCG1 and other ABCG family members in lipid metabolism." J Lipid Res **42**(10): 1513-1520.
Scholtes, V. P. W., J. L. Johnson, N. Jenkins, G. B. Sala-Newby, J.-P. P. M. de Vries, G. J. de Borst, D. P. V. de Kleijn, F. L. Moll, G. Pasterkamp and A. C. Newby (2012). "Carotid atherosclerotic plaque matrix metalloproteinase-12-positive macrophage subpopulation predicts adverse outcome after endarterectomy." Journal of the American Heart Association **1**(6): e001040-e001040.
Schrijvers, D. M., G. R. De Meyer, A. G. Herman and W. Martinet (2007). "Phagocytosis in atherosclerosis: Molecular mechanisms and implications for plaque progression and stability." Cardiovasc Res **73**(3): 470-480.
Schrijvers, D. M., G. R. De Meyer, M. M. Kockx, A. G. Herman and W. Martinet (2005). "Phagocytosis of apoptotic cells by macrophages is impaired in atherosclerosis." Arterioscler Thromb Vasc Biol **25**(6): 1256-1261.
Schrijvers, D. M., G. R. Y. De Meyer, A. G. Herman and W. Martinet (2007). "Phagocytosis in atherosclerosis: Molecular mechanisms and implications for plaque progression and stability." Cardiovascular Research **73**(3): 470-480.
Schrijvers Dorien, M., R. Y. De Meyer Guido, M. Kockx Mark, G. Herman Arnold and W. Martinet (2005). "Phagocytosis of Apoptotic Cells by Macrophages Is Impaired in Atherosclerosis." Arteriosclerosis, Thrombosis, and Vascular Biology **25**(6): 1256-1261.
Shankavaram, U. T., D. L. DeWitt, S. E. Funk, E. H. Sage and L. M. Wahl (1997). "Regulation of human monocyte matrix metalloproteinases by SPARC." J Cell Physiol **173**(3): 327-334.
Shaw, J. A., A. Bobik, A. Murphy, P. Kanellakis, P. Blombery, N. Mukhamedova, K. Woollard, S. Lyon, D. Sviridov and A. M. Dart (2008). "Infusion of reconstituted high-density lipoprotein leads to acute changes in human atherosclerotic plaque." Circ Res **103**(10): 1084-1091.
Shaw, P. X., S. Hörkkö, S. Tsimikas, M. K. Chang, W. Palinski, G. J. Silverman, P. P. Chen and J. L. Witztum (2001). "Human-derived anti-oxidized LDL autoantibody blocks uptake of oxidized LDL by macrophages and localizes to atherosclerotic lesions in vivo." Arterioscler Thromb Vasc Biol **21**(8): 1333-1339.
Shi, J. and L. Wei (2013). "Rho kinases in cardiovascular physiology and pathophysiology: the effect of fasudil." J Cardiovasc Pharmacol **62**(4): 341-354.
Singh, N. N. and D. P. Ramji (2006). "The role of transforming growth factor-β in atherosclerosis." Cytokine & Growth Factor Reviews **17**(6): 487-499.
Singh, R. B., S. A. Mengi, Y. J. Xu, A. S. Arneja and N. S. Dhalla (2002). "Pathogenesis of atherosclerosis: A multifactorial process." Exp Clin Cardiol **7**(1): 40-53.
Singh, R. K., A. S. Haka, P. Bhardwaj, X. Zha and F. R. Maxfield (2019). "Dynamic Actin Reorganization and Vav/Cdc42-Dependent Actin Polymerization Promote Macrophage Aggregated LDL (Low-Density Lipoprotein) Uptake and Catabolism." Arteriosclerosis, thrombosis, and vascular biology **39**(2): 137-149.
Smith, J. D., E. Trogan, M. Ginsberg, C. Grigaux, J. Tian and M. Miyata (1995). "Decreased atherosclerosis in mice deficient in both macrophage colony-stimulating factor (op) and apolipoprotein E." Proceedings of the National Academy of Sciences **92**(18): 8264.

Srivastava, R. A. (2011). "Evaluation of anti-atherosclerotic activities of PPAR-α, PPAR-γ, and LXR agonists in hyperlipidemic atherosclerosis-susceptible F(1)B hamsters." Atherosclerosis **214**(1): 86-93.
Stahl, P. D. and R. A. Ezekowitz (1998). "The mannose receptor is a pattern recognition receptor involved in host defense." Curr Opin Immunol **10**(1): 50-55.
Stary, H. C., A. B. Chandler, S. Glagov, J. R. Guyton, W. Insull, Jr., M. E. Rosenfeld, S. A. Schaffer, C. J. Schwartz, W. D. Wagner and R. W. Wissler (1994). "A definition of initial, fatty streak, and intermediate lesions of atherosclerosis. A report from the Committee on Vascular Lesions of the Council on Arteriosclerosis, American Heart Association." Circulation **89**(5): 2462-2478.
Stary, H. C. H. "A definition of the intima of human arteries and of its atherosclerosis-prone regions. A report from the Committee on Vascular Lesions of the Council on Arteriosclerosis, American Heart Association." Arteriosclerosis and Thrombosis: A Journal of Vascular Biology **12**(1): 120-134.
Stegemann, C., I. Drozdov, J. Shalhoub, J. Humphries, C. Ladroue, A. Didangelos, M. Baumert, M. Allen, H. Davies Alun, C. Monaco, A. Smith, Q. Xu and M. Mayr (2011). "Comparative Lipidomics Profiling of Human Atherosclerotic Plaques." Circulation: Cardiovascular Genetics **4**(3): 232-242.
Stendahl, O. I., J. H. Hartwig, E. A. Brotschi and T. P. Stossel (1980). "Distribution of actin-binding protein and myosin in macrophages during spreading and phagocytosis." Journal of Cell Biology **84**(2): 215-224.
Stewart, C. R., L. M. Stuart, K. Wilkinson, J. M. van Gils, J. Deng, A. Halle, K. J. Rayner, L. Boyer, R. Zhong, W. A. Frazier, A. Lacy-Hulbert, J. El Khoury, D. T. Golenbock and K. J. Moore (2010). "CD36 ligands promote sterile inflammation through assembly of a Toll-like receptor 4 and 6 heterodimer." Nat Immunol **11**(2): 155-161.
Stout, R. D. and J. Suttles (2004). "Functional plasticity of macrophages: reversible adaptation to changing microenvironments." Journal of Leukocyte Biology **76**(3): 509-513.
Suetsugu, S., S. Kurisu, T. Oikawa, D. Yamazaki, A. Oda and T. Takenawa (2006). "Optimization of WAVE2 complex-induced actin polymerization by membrane-bound IRSp53, PIP(3), and Rac." The Journal of cell biology **173**(4): 571-585.
Sugimoto, K., T. Ishibashi, T. Sawamura, N. Inoue, M. Kamioka, H. Uekita, H. Ohkawara, T. Sakamoto, N. Sakamoto, Y. Okamoto, Y. Takuwa, A. Kakino, Y. Fujita, T. Tanaka, T. Teramoto, Y. Maruyama and Y. Takeishi (2009). "LOX-1-MT1-MMP axis is crucial for RhoA and Rac1 activation induced by oxidized low-density lipoprotein in endothelial cells." Cardiovasc Res **84**(1): 127-136.
Suraneni, P., B. Rubinstein, J. R. Unruh, M. Durnin, D. Hanein and R. Li (2012). "The Arp2/3 complex is required for lamellipodia extension and directional fibroblast cell migration." J Cell Biol **197**(2): 239-251.
Swanson, J. A., M. T. Johnson, K. Beningo, P. Post, M. Mooseker and N. Araki (1999). "A contractile activity that closes phagosomes in macrophages." J Cell Sci **112 (Pt 3)**: 307-316.
Swirski, F. K., P. Libby, E. Aikawa, P. Alcaide, F. W. Luscinskas, R. Weissleder and M. J. Pittet (2007). "Ly-6Chi monocytes dominate hypercholesterolemia-associated monocytosis and give rise to macrophages in atheromata." J Clin Invest **117**(1): 195-205.
Tabas, I. (2010). "Macrophage death and defective inflammation resolution in atherosclerosis." Nat Rev Immunol **10**(1): 36-46.
Tabas, I., X. Zha, N. Beatini, J. N. Myers and F. R. Maxfield (1994). "The actin cytoskeleton is important for the stimulation of cholesterol esterification by atherogenic lipoproteins in macrophages." J Biol Chem **269**(36): 22547-22556.
Tacke, F., D. Alvarez, T. J. Kaplan, C. Jakubzick, R. Spanbroek, J. Llodra, A. Garin, J. Liu, M. Mack, N. van Rooijen, S. A. Lira, A. J. Habenicht and G. J. Randolph (2007). "Monocyte subsets differentially employ CCR2, CCR5, and CX3CR1 to accumulate within atherosclerotic plaques." J Clin Invest **117**(1): 185-194.
Tajbakhsh, A., M. Rezaee, P. T. Kovanen and A. Sahebkar (2018). "Efferocytosis in atherosclerotic lesions: Malfunctioning regulatory pathways and control mechanisms." Pharmacology & Therapeutics **188**: 12-25.

Takemoto, M., J. Sun, J. Hiroki, H. Shimokawa and K. Liao James (2002). "Rho-Kinase Mediates Hypoxia-Induced Downregulation of Endothelial Nitric Oxide Synthase." Circulation **106**(1): 57-62.
Talle, M. A., P. E. Rao, E. Westberg, N. Allegar, M. Makowski, R. S. Mittler and G. Goldstein (1983). "Patterns of antigenic expression on human monocytes as defined by monoclonal antibodies." Cell Immunol **78**(1): 83-99.
Tang, Y., W. Liu, W. Wang, T. Fidler, B. Woods, R. L. Levine, A. R. Tall and N. Wang (2020). "Inhibition of JAK2 Suppresses Myelopoiesis and Atherosclerosis in Apoe−/− Mice." Cardiovascular Drugs and Therapy **34**(2): 145-152.
Tavafi, M. (2013). "Complexity of diabetic nephropathy pathogenesis and design of investigations." J Renal Inj Prev **2**(2): 59-62.
Thomas, G. D., A. A. J. Hamers, C. Nakao, P. Marcovecchio, A. M. Taylor, C. McSkimming, A. T. Nguyen, C. A. McNamara and C. C. Hedrick (2017). "Human Blood Monocyte Subsets: A New Gating Strategy Defined Using Cell Surface Markers Identified by Mass Cytometry." Arterioscler Thromb Vasc Biol **37**(8): 1548-1558.
Thorp, E., G. Li, T. A. Seimon, G. Kuriakose, D. Ron and I. Tabas (2009). "Reduced apoptosis and plaque necrosis in advanced atherosclerotic lesions of Apoe-/- and Ldlr-/- mice lacking CHOP." Cell Metab **9**(5): 474-481.
Thorp, E. and I. Tabas (2009). "Mechanisms and consequences of efferocytosis in advanced atherosclerosis." J Leukoc Biol **86**(5): 1089-1095.
Thorp, E. and I. Tabas (2009). "Mechanisms and consequences of efferocytosis in advanced atherosclerosis." Journal of Leukocyte Biology **86**(5): 1089-1095.
Toba, H., L. E. de Castro Brás, C. F. Baicu, M. R. Zile, M. L. Lindsey and A. D. Bradshaw (2015). "Secreted protein acidic and rich in cysteine facilitates age-related cardiac inflammation and macrophage M1 polarization." American journal of physiology. Cell physiology **308**(12): C972-C982.
Toschi, V., R. Gallo, M. Lettino, J. T. Fallon, S. D. Gertz, A. Fernández-Ortiz, J. H. Chesebro, L. Badimon, Y. Nemerson, V. Fuster and J. J. Badimon (1997). "Tissue factor modulates the thrombogenicity of human atherosclerotic plaques." Circulation **95**(3): 594-599.
Tosello-Trampont, A.-C., K. Nakada-Tsukui and K. Ravichandran (2004). "Engulfment of Apoptotic Cells Is Negatively Regulated by Rho-mediated Signaling." The Journal of biological chemistry **278**: 49911-49919.
Tsiara, S., M. Elisaf and D. P. Mikhailidis (2003). "Early vascular benefits of statin therapy." Current Medical Research and Opinion **19**(6): 540-556.
Tsuchiya, S., M. Yamabe, Y. Yamaguchi, Y. Kobayashi, T. Konno and K. Tada (1980). "Establishment and characterization of a human acute monocytic leukemia cell line (THP-1)." Int J Cancer **26**(2): 171-176.
Umetani, N., Y. Kanayama, M. Okamura, N. Negoro and T. Takeda (1996). "Lovastatin inhibits gene expression of type-I scavenger receptor in THP-1 human macrophages." Biochimica et Biophysica Acta (BBA) - Lipids and Lipid Metabolism **1303**(3): 199-206.
Van Aelst, L. and C. D'Souza-Schorey (1997). "Rho GTPases and signaling networks." Genes Dev **11**(18): 2295-2322.
van der Meij, E., G. G. Koning, P. W. Vriens, M. F. Peeters, C. A. Meijer, K. E. Kortekaas, R. L. Dalman, J. H. van Bockel, R. Hanemaaijer, T. Kooistra, R. Kleemann and J. H. N. Lindeman (2013). "A clinical evaluation of statin pleiotropy: statins selectively and dose-dependently reduce vascular inflammation." PloS one **8**(1): e53882-e53882.
van der Wal, A. C. and A. E. Becker (1999). "Atherosclerotic plaque rupture – pathologic basis of plaque stability and instability." Cardiovascular Research **41**(2): 334-344.
van Furth, R. and H. Beekhuizen (1998). Monocytes. Encyclopedia of Immunology (Second Edition). P. J. Delves. Oxford, Elsevier**:** 1750-1754.
VanderLaan Paul, A., A. Reardon Catherine and S. Getz Godfrey (2004). "Site Specificity of Atherosclerosis." Arteriosclerosis, Thrombosis, and Vascular Biology **24**(1): 12-22.

Vedham, V., H. Phee and K. M. Coggeshall (2005). "Vav activation and function as a rac guanine nucleotide exchange factor in macrophage colony-stimulating factor-induced macrophage chemotaxis." Mol Cell Biol **25**(10): 4211-4220.
Vengrenyuk, Y., H. Nishi, X. Long, M. Ouimet, N. Savji, F. O. Martinez, C. P. Cassella, K. J. Moore, S. A. Ramsey, J. M. Miano and E. A. Fisher (2015). "Cholesterol loading reprograms the microRNA-143/145-myocardin axis to convert aortic smooth muscle cells to a dysfunctional macrophage-like phenotype." Arterioscler Thromb Vasc Biol **35**(3): 535-546.
Verreck, F. A., T. de Boer, D. M. Langenberg, M. A. Hoeve, M. Kramer, E. Vaisberg, R. Kastelein, A. Kolk, R. de Waal-Malefyt and T. H. Ottenhoff (2004). "Human IL-23-producing type 1 macrophages promote but IL-10-producing type 2 macrophages subvert immunity to (myco)bacteria." Proc Natl Acad Sci U S A **101**(13): 4560-4565.
Virmani, R., A. P. Burke, A. Farb and F. D. Kolodgie (2006). "Pathology of the Vulnerable Plaque." Journal of the American College of Cardiology **47**(8, Supplement): C13-C18.
Virmani, R., F. D. Kolodgie, A. P. Burke, A. Farb and S. M. Schwartz (2000). "Lessons from sudden coronary death: a comprehensive morphological classification scheme for atherosclerotic lesions." Arterioscler Thromb Vasc Biol **20**(5): 1262-1275.
Waldo, S. W., Y. Li, C. Buono, B. Zhao, E. M. Billings, J. Chang and H. S. Kruth (2008). "Heterogeneity of Human Macrophages in Culture and in Atherosclerotic Plaques." The American Journal of Pathology **172**(4): 1112-1126.
Waldo, S. W., Y. Li, C. Buono, B. Zhao, E. M. Billings, J. Chang and H. S. Kruth (2008). "Heterogeneity of human macrophages in culture and in atherosclerotic plaques." Am J Pathol **172**(4): 1112-1126.
Wang, D., W. Wang, L. Weiqun, W. Yang, P. Zhang, M. Chen, D. Ding, C. Liu, J. Zheng and W. Ling (2018). "Apoptotic cell induction of miR-10b in macrophages contributes to advanced atherosclerosis progression in ApoE-/- mice." Cardiovascular research **114**.
Wang, H.-W., P.-Y. Liu, N. Oyama, Y. Rikitake, S. Kitamoto, J. Gitlin, J. K. Liao and W. A. Boisvert (2008). "Deficiency of ROCK1 in bone marrow-derived cells protects against atherosclerosis in LDLR-/- mice." FASEB journal : official publication of the Federation of American Societies for Experimental Biology **22**(10): 3561-3570.
Wang, X., M. Tanaka, S. Krstin, H. S. Peixoto, C. C. d. M. Moura and M. Wink (2016). "Cytoskeletal interference – A new mode of action for the anticancer drugs camptothecin and topotecan." European Journal of Pharmacology **789**: 265-274.
Wang, Y.-X., B. Martin-McNulty, V. Cunha, J. Vincelette, X. Lu, Q. Feng, M. Halks-Miller, M. Mahmoudi, M. Schroeder, B. Subramanyam, J.-L. Tseng, G. Deng, S. Schirm, A. Johns, K. Kauser, W. Dole and D. Light (2005). "Fasudil, a Rho-Kinase Inhibitor, Attenuates Angiotensin II–Induced Abdominal Aortic Aneurysm in Apolipoprotein E–Deficient Mice by Inhibiting Apoptosis and Proteolysis." Circulation **111**: 2219-2226.
Wang, Z., J. Chen, J. Hu, H. Zhang, F. Xu, W. He, X. Wang, M. Li, W. Lu, G. Zeng, P. Zhou, P. Huang, S. Chen, W. Li, L. P. Xia and X. Xia (2019). "cGAS/STING axis mediates a topoisomerase II inhibitor-induced tumor immunogenicity." J Clin Invest **129**(11): 4850-4862.
Wassmann, S., U. Laufs, K. Müller, C. Konkol, K. Ahlbory, A. T. Bäumer, W. Linz, M. Böhm and G. Nickenig (2002). "Cellular antioxidant effects of atorvastatin in vitro and in vivo." Arterioscler Thromb Vasc Biol **22**(2): 300-305.
Wei, Y., J. Corbalán-Campos, R. Gurung, L. Natarelli, M. Zhu, N. Exner, F. Erhard, F. Greulich, C. Geißler, N. H. Uhlenhaut, R. Zimmer and A. Schober (2018). "Dicer in Macrophages Prevents Atherosclerosis by Promoting Mitochondrial Oxidative Metabolism." Circulation **138**(18): 2007-2020.
Weibel, G. L., M. R. Joshi, W. G. Jerome, S. R. Bates, K. J. Yu, M. C. Phillips and G. H. Rothblat (2012). "Cytoskeleton disruption in J774 macrophages: consequences for lipid droplet formation and cholesterol flux." Biochimica et biophysica acta **1821**(3): 464-472.
Wheeler, A. P. and A. J. Ridley (2007). "RhoB affects macrophage adhesion, integrin expression and migration." Exp Cell Res **313**(16): 3505-3516.

Wheeler, A. P., S. D. Smith and A. J. Ridley (2006). "CSF-1 and PI 3-kinase regulate podosome distribution and assembly in macrophages." Cell Motil Cytoskeleton **63**(3): 132-140.
Wolfs, I. M., M. M. Donners and M. P. de Winther (2011). "Differentiation factors and cytokines in the atherosclerotic plaque micro-environment as a trigger for macrophage polarisation." Thromb Haemost **106**(5): 763-771.
Wolfs, I. M. J., M. M. P. C. Donners and M. P. J. de Winther (2011). "Differentiation factors and cytokines in the atherosclerotic plaque micro-environment as a trigger for macrophage polarisation." Thromb Haemost **106**(11): 763-771.
Woollard, K. J. and F. Geissmann (2010). "Monocytes in atherosclerosis: subsets and functions." Nature reviews. Cardiology **7**(2): 77-86.
Wu, D.-J., J.-Z. Xu, Y.-J. Wu, L. Jean-Charles, B. Xiao, P.-J. Gao and D.-L. Zhu (2009). "Effects of fasudil on early atherosclerotic plaque formation and established lesion progression in apolipoprotein E-knockout mice." Atherosclerosis **207**(1): 68-73.
Wu, D.-J., J.-Z. Xu, Y.-J. Wu, J.-C. Lafarge, B. Xiao, P.-J. Gao and D.-L. Zhu (2009). "Effects of fasudil on early atherosclerotic plaque formation and established lesion progression in apolipoprotein E-knockout mice." Atherosclerosis **207**: 68-73.
Wu, D. J., J. Z. Xu, Y. J. Wu, L. Jean-Charles, B. Xiao, P. J. Gao and D. L. Zhu (2009). "Effects of fasudil on early atherosclerotic plaque formation and established lesion progression in apolipoprotein E-knockout mice." Atherosclerosis **207**(1): 68-73.
Xiao, L., Y. Liu and N. Wang (2013). "New paradigms in inflammatory signaling in vascular endothelial cells." American Journal of Physiology-Heart and Circulatory Physiology **306**(3): H317-H325.
Xu, F., Y. Xu, L. Zhu, P. Rao, J. Wen, Y. Sang, F. Shang and Y. Liu (2016). "Fasudil inhibits LPS-induced migration of retinal microglial cells via regulating p38-MAPK signaling pathway." Molecular vision **22**: 836-846.
Xu, H., J. Jiang, W. Chen, W. Li and Z. Chen (2019). "Vascular Macrophages in Atherosclerosis." Journal of immunology research **2019**: 4354786-4354786.
Xu, L., X. Dai Perrard, J. L. Perrard, D. Yang, X. Xiao, B. B. Teng, S. I. Simon, C. M. Ballantyne and H. Wu (2015). "Foamy monocytes form early and contribute to nascent atherosclerosis in mice with hypercholesterolemia." Arterioscler Thromb Vasc Biol **35**(8): 1787-1797.
Xu, S., S. Ogura, J. Chen, P. J. Little, J. Moss and P. Liu (2013). "LOX-1 in atherosclerosis: biological functions and pharmacological modifiers." Cell Mol Life Sci **70**(16): 2859-2872.
Xu, X. H., P. K. Shah, E. Faure, O. Equils, L. Thomas, M. C. Fishbein, D. Luthringer, X. P. Xu, T. B. Rajavashisth, J. Yano, S. Kaul and M. Arditi (2001). "Toll-like receptor-4 is expressed by macrophages in murine and human lipid-rich atherosclerotic plaques and upregulated by oxidized LDL." Circulation **104**(25): 3103-3108.
Yamada, Y., T. Doi, T. Hamakubo and T. Kodama (1998). "Scavenger receptor family proteins: roles for atherosclerosis, host defence and disorders of the central nervous system." Cell Mol Life Sci **54**(7): 628-640.
Yamaguchi, H. and J. Condeelis (2007). "Regulation of the actin cytoskeleton in cancer cell migration and invasion." Biochim Biophys Acta **1773**(5): 642-652.
Yamamoto, S., P. G. Yancey, Y. Zuo, L. J. Ma, R. Kaseda, A. B. Fogo, I. Ichikawa, M. F. Linton, S. Fazio and V. Kon (2011). "Macrophage polarization by angiotensin II-type 1 receptor aggravates renal injury-acceleration of atherosclerosis." Arterioscler Thromb Vasc Biol **31**(12): 2856-2864.
Yu, J., D. Zhang, J. Liu, J. Li, Y. Yu, X.-R. Wu and C. Huang (2012). "RhoGDI SUMOylation at Lys-138 increases its binding activity to Rho GTPase and its inhibiting cancer cell motility." The Journal of biological chemistry **287**(17): 13752-13760.
Yu, X. H., Y. C. Fu, D. W. Zhang, K. Yin and C. K. Tang (2013). "Foam cells in atherosclerosis." Clin Chim Acta **424**: 245-252.
Yu, X. H., H. L. Jiang, W. J. Chen, K. Yin, G. J. Zhao, Z. C. Mo, X. P. Ouyang, Y. C. Lv, Z. S. Jiang, D. W. Zhang and C. K. Tang (2012). "Interleukin-18 and interleukin-12 together downregulate ATP-binding

cassette transporter A1 expression through the interleukin-18R/nuclear factor-kappaB signaling pathway in THP-1 macrophage-derived foam cells." Circ J **76**(7): 1780-1791.
Yuasa-Kawase, M., D. Masuda, T. Yamashita, R. Kawase, H. Nakaoka, M. Inagaki, K. Nakatani, K. Tsubakio-Yamamoto, T. Ohama, A. Matsuyama, M. Nishida, M. Ishigami, T. Kawamoto, I. Komuro and S. Yamashita (2012). "Patients with CD36 deficiency are associated with enhanced atherosclerotic cardiovascular diseases." J Atheroscler Thromb **19**(3): 263-275.
Yurdagul, A., A. C. Doran, B. Cai, G. Fredman and I. A. Tabas (2018). "Mechanisms and Consequences of Defective Efferocytosis in Atherosclerosis." Frontiers in Cardiovascular Medicine **4**(86).
Yurdagul, A., Jr., A. C. Doran, B. Cai, G. Fredman and I. A. Tabas (2017). "Mechanisms and Consequences of Defective Efferocytosis in Atherosclerosis." Front Cardiovasc Med **4**: 86.
Zandi, S., S. Nakao, K. H. Chun, P. Fiorina, D. Sun, R. Arita, M. Zhao, E. Kim, O. Schueller, S. Campbell, M. Taher, M. I. Melhorn, A. Schering, F. Gatti, S. Tezza, F. Xie, A. Vergani, S. Yoshida, K. Ishikawa, M. Yamaguchi, F. Sasaki, R. Schmidt-Ullrich, Y. Hata, H. Enaida, M. Yuzawa, T. Yokomizo, Y. B. Kim, P. Sweetnam, T. Ishibashi and A. Hafezi-Moghadam (2015). "ROCK-isoform-specific polarization of macrophages associated with age-related macular degeneration." Cell Rep **10**(7): 1173-1186.
Zanin-Zhorov, A., R. Flynn, S. D. Waksal and B. R. Blazar (2016). "Isoform-specific targeting of ROCK proteins in immune cells." Small GTPases **7**(3): 173-177.
Zhang, L., M. Jiang, Y. Shui, Y. Chen, Q. Wang, W. Hu, X. Ma, X. Li, X. Liu, X. Cao, M. Liu, Y. Duan and J. Han (2013). "DNA topoisomerase II inhibitors induce macrophage ABCA1 expression and cholesterol efflux—An LXR-dependent mechanism." Biochimica et Biophysica Acta (BBA) - Molecular and Cell Biology of Lipids **1831**(6): 1134-1145.
Zhang, W., P. G. Yancey, Y. R. Su, V. R. Babaev, Y. Zhang, S. Fazio and M. F. Linton (2003). "Inactivation of macrophage scavenger receptor class B type I promotes atherosclerotic lesion development in apolipoprotein E-deficient mice." Circulation **108**(18): 2258-2263.
Zhou, Q., Y. Mei, T. Shoji, X. Han, K. Kaminski, G. T. Oh, P. P. Ongusaha, K. Zhang, H. Schmitt, M. Moser, C. Bode and J. K. Liao (2012). "Rho-associated coiled-coil-containing kinase 2 deficiency in bone marrow-derived cells leads to increased cholesterol efflux and decreased atherosclerosis." Circulation **126**(18): 2236-2247.
Zhou, Q., Y. Mei, T. Shoji, X. Han, K. Kaminski, G. T. Oh, P. P. Ongusaha, K. Zhang, H. Schmitt, M. Moser, C. Bode and J. K. Liao (2012). "Rho-associated coiled-coil-containing kinase 2 deficiency in bone marrow-derived cells leads to increased cholesterol efflux and decreased atherosclerosis." Circulation **126**(18): 2236-2247.
Ziegler-Heitbrock, L., P. Ancuta, S. Crowe, M. Dalod, V. Grau, D. N. Hart, P. J. Leenen, Y. J. Liu, G. MacPherson, G. J. Randolph, J. Scherberich, J. Schmitz, K. Shortman, S. Sozzani, H. Strobl, M. Zembala, J. M. Austyn and M. B. Lutz (2010). "Nomenclature of monocytes and dendritic cells in blood." Blood **116**(16): e74-80.
Zigmond, S. H. (2004). "Formin-induced nucleation of actin filaments." Curr Opin Cell Biol **16**(1): 99-105.